"IRON-TITANIUM OXIDE MINERALS IN SOME IGNEOUS ROCKS OF ARRAN"

A Thesis submitted for the degree of Doctor of Philosophy
in the University of Durham

by

A.R.Ramsden

April 1964.

ABSTRACT

Examination of the opaque minerals in an intrusive sheet of analcite dolerite shows that they consist partly of a cubic solid solution, referred to for brevity as 'magnetite', and partly of a rhombohedral solid solution referred to as 'ilmenite'

Systematic variation of the properties of the 'magnetites' indicates an increase in titanium dontent towards the more slowly cooled central part of the sheet.

'Ilmenite' usually occurs as oriented intergrowths in 'magnetite' crystals and contains 10-20% ferric oxide in solid solution. Less commonly, 'ilmenite' also occurs as a discrete phase believed to have crystallised before the formation of the 'magnetite'-'ilmenite' intergrowths, and this seems not to contain ferric oxide in solid solution.

'Magnetite'-'ilmenite' relationships are considered in terms of an Fe_3O_4-$FeTiO_3$ phase diagram constructed from the experimental data of previous workers.

The content of opaque minerals decreases regularly from 9% in the marginal rocks to less than 1% at the centre of the intrusion.

The intensity of natural remanent magnetization decreases systematically away from the margins of the sheet and is clearly dependent on the content of 'magnetite' in the intrusion.

The intrusion is reversely magnetized and has a mean direction of magnetization that confirms its age as Tertiary in agreement with geological data. However, there is considerable variation in the palaeomagnetic directions within the sheet due to the multiple nature of the intrusive processes. This is especially clear in the inclinations.

The contact relations of the intrusion suggest that the reverse magnetization is a primary feature although the possibility of self-reversal cannot be ruled out entirely.

Constructional details are given of instruments designed for the accurate automatic measurement of the Curie temperature of a minute ferromagnetic sample, and for the determination of the saturation magnetization of such samples at room temperature.

CONTENTS

.....

List of Figures

.....

List of Plates

.....

List of Tables

.....

Introduction

The chief iron-titanium oxide minerals are magnetite, hematite, ilmenite and ulvöspinel. Solid-solution relationships exist between these, and the present investigation is concerned mainly with those minerals known as the titaniferous magnetites or titanomagnetites. The term titaniferous magnetite is applied to minerals intermediate in composition between magnetite and ulvospinel and also to non-stoichiometric phases which may be regarded as the oxidised equivalents of these solid-solutions.

Previous investigations of naturally occurring titaniferous magnetites have concentrated either on those which exist in plutonic rocks or in lavas, and so far as is known, there have been no detailed studies of those phases which crystallise under hypabyssal conditions. An important objective of the present research, therefore, has been to study the mineralogy of these intermediate phases, and in particular, the nature of the magnetite-ilmenite relationship.

Since, however, titanomagnetites are ferrimagnetic and are the main carriers of rock magnetism, it has been considered not unreasonable to combine this mineralogical investigation with a study of the palaeomagnetism of the parent rock.

Titaniferous magnetites are normally associated with basic or ultrabasic igneous rocks, and for the purposes of the present study, a basic hypabyssal intrusion has been chosen as the source of material.

The so-called Clauchlands "sill" in the Isle of Arran, Scotland, is particularly suitable in this connection. It has the form of an inclined

sheet about 130 feet thick and a continuous section from top to bottom is exposed at Clauchlands Point, north of Lamlash Bay. In general, the rock is a coarse-grained analcite-dolerite, but nevertheless, there is a wide variety of material which ranges from the fine-grained marginal rocks to very coarse segregations of dolerite-pegmatite.

The Clauchlands "sill", however, is but one of three intrusions of analcite-dolerite which outcrop around Lamlash Bay and which together probably form a cone-sheet with a focus beneath the bay. Therefore, strictly speaking, the "sill" is best regarded as the Clauchlands sheet since this emphasizes the nature of its origin.

Material for the present studies has been obtained from the Clauchlands sheet at Clauchlands Point and it forms a collection representing a vertical section through the intrusion, with an average of about 4 feet vertically between each sample. This collection has been examined petrographically and episcopically and the iron-titanium oxide minerals have been analysed by X-rays and by magnetic methods.

A vertical section has been chosen for these investigations since this gives a cross-section of the crystallization history of the minerals, those at the margins having formed earlier and cooled more rapidly than those at the centre of the sheet. This method of examination, therefore, should indicate the nature of any exsolution relationships.

Oriented samples have also been obtained from Clauchlands Point and these form a collection which closely parallels that used for the mineralogical investigations. The direction and the intensity of magnetization in these samples has been measured and in this way it has been possible to study the palaeomagnetism at different levels within the sheet.

As a part of the mineralogical investigations it has been necessary to measure two magnetic properties of the titaniferous magnetites, namely the Curie point and the intensity of saturation magnetization, since these give a useful indication of the chemical composition.

Two instruments have been built in order to measure these properties. One, a thermomagnetic balance for the accurate and automatic measurement of Curie points, incorporates a number of features hitherto not included in instruments of this type. The construction and calibration data for this instrument are presented fully in Part II of the present work. The other for the measurement of saturation magnetization at room temperature is described in Part III of this work and essentially follows a design of Chevallier and Mathieu (1943).

ACKNOWLEDGEMENTS

The present research has been supported by a NATO Science Research Studentship which is here gratefully acknowledged. The Royal Society of London awarded a grant to finance the construction of the thermomagnetic equipment and the saturation magnetization equipment, and this also is gratefully acknowledged.

I would like to express sincere appreciation to R. Phillips Esq. for supervising the present work and to Professor K.C. Dunham for making available facilities in the Department of Geology. I would also like to thank Dr. R.W. Girdler for advice and much helpful guidance with the palaeomagnetic aspects of the work.

My thanks are due to many other people but in particular to the following:-

Professor G.D. Rochester - for making available a laboratory in the Department of Physics at Durham in order to house the thermomagnetic equipment.

Dr. A. Apostolakis and Dr. W.D. Corner of the Department of Physics in Durham - for much help with the physical aspects involved during the design and construction of the equipment.

Mr. G.R. Martin of the Department of Radiochemistry in Durham - for the circuit design used in the Temperature Recording System of the thermomagnetic equipment and for guidance when assembling this.

Professor S.K. Runcorn - for the use of the workshop facilities in the Department of Physics, The University, Newcastle upon Tyne, during coring of palaeomagnetic samples and for the use of a magnetometer during their subsequent measurement.

Mr. R. Boult and the staff of the Electron Microscopy Laboratory, The University, Newcastle upon Tyne - for the preparation of replicated surfaces and assistance during their examination.

Mr. C. Chaplin and the technical staff of the Department of Geology, Durham - for the preparation of many thin-sections, polished-sections and photographs.

Mr. F. Venmore and the technical staff in the laboratory workshops at Durham for the construction of many parts of the thermomagnetic and saturation magnetization equipment.

Miss V. Shepherd, Secretary in the Department of Geology - for typing the text.

Part I.

Iron-Titanium Oxide Minerals in some Igneous Rocks of Arran

Chapter I. Field Relations

A. Introduction

Material for the present investigations has been obtained from an intrusive sheet of analcite-dolerite in the Isle of Arran, Buteshire, Scotland. This, somewhat rare, rock-type outcrops around Lamlash Bay as three inclined sheets which are referred to by Tyrrel (1928) as the Clauchlands sill, Monamore sill and Kingscross sill, and are considered by him to have originated from an inferred focus or foci lying somewhere to the east under the Firth of Clyde. The annular outcrop pattern of these rocks, however, immediately suggests that they belong to a single ring intrusion which may have originated under Lamlash Bay.

Surprisingly, however, it is only recently that the concept of a Lamlash cone-sheet complex has been put forward. Tomkeieff (1961) recognises two sets of cone sheets around Lamlash, an earlier basic set consisting of the analcite-dolerites which is intersected by a later set of acid sheets with foci somewhat further to the north.

The present study, however, is concerned only with the basic sheets, and more especially with their functions as carriers of the iron-titanium oxide minerals and their rock magnetic properties.

Material for the present research project has been obtained exclusively from the Clauchlands sill, and since this intrusion has the superficial form of a sill, it has been considered necessary to undertake a general field survey of the analcite-dolerites in order to decide whether they are indeed sills or whether, as Tomkeieff has proposed, they belong to a single intrusion of cone-sheet type.

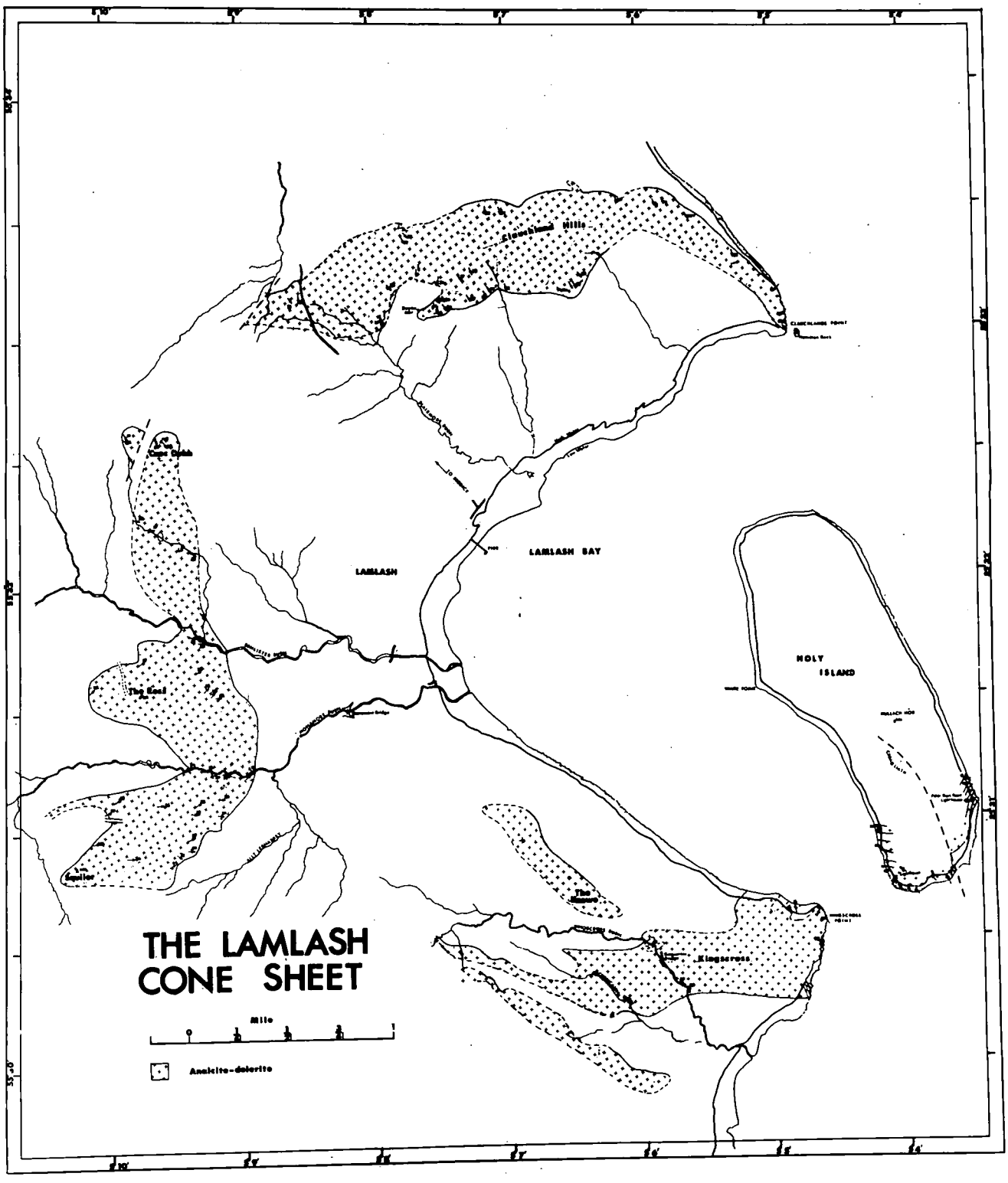
THE LAMLASH
CONE SHEET
Miles
Analcite-dolerite
LAMLASH
LAMLASH BAY
HOLY
ISLAND
Kingscross

Figure 1.

Figure 1.

Map showing the general field relations of the Lamlash Cone-Sheet. The Claudhlands Sheet in the north, the Monamore Sheet in the west and the Kingscross Sheet in the south.

B. General Field Relations

The general field relations are summarised in Figure 1 and they show how the analcite-dolerites form inclined sheets which appear to originate from beneath Lamlash Bay.

The sheets are about 100 feet thick and dip on average at about 30° into the bay. They, therefore, form a saucer shaped intrusion which is best described as a cone sheet.

Cone sheets were first described from Skye, Mull and Ardnamurchan, respectively, by Harker (1904), Bailey et al (1924) and Richey (1930). In these areas the sheets are generally 30 - 40 feet thick and dip 45° towards a common centre. The present intrusion, therefore, is considerably thicker than these but is comparable in size to some cone sheets of Northern Nigeria, examples of which are up to 200 feet thick. (Jacobson, Macleod and Black 1958).

The form of the intrusion is not due to any structural basin in this region, for the Permo-Triassic sediments (Lamlash - Machrie Sandstone) into which it is intruded have a regional dip which is consistently to the south; hence, although the Clauchlands "sill" is more or less concordant with the strata, the Kingscross "sill" and especially the Monamore "sill" are undoubtedly transgressive.

It appears, therefore, that the analcite-dolerites were emplaced from a common magma chamber somewhere beneath Lamlash Bay. Hence, in the present work, these intrusions are referred to as the Clauchlands sheet, Monamore sheet and Kingscross sheet, and it is proposed that, together, they form the Lamlash cone sheet.

The Kingscross sheet is the southern member of the cone sheet and reaches

its maximum development on the Kingscross peninsula. Here, it consists of three sheets, each about thirty feet thick, dipping about 20° to the north and separated from each other by sandstones which are dipping gently in the opposite direction.

The same three sheets must continue across the bay for they also appear on the southern shore of Holy Island where, likewise, they are intruded into sandstones.

Exposures of the upper two sheets, however, are very poor on the Kingscross shore and are not particularly good on Holy Island. As a consequence, the lowest of the three sheets is the most important for it is well exposed on both shores.

The top of this sheet is exposed on Holy Island where isolated patches of hard sandstone lie on top of the dolerite and are all that remains of the original cover. The base of the sheet, however, is not exposed on the Island although the dense nature of the rock at the strand line indicates that the contact cannot be far below water level.

The base of the sheet, however, is well exposed on the Kingscross shore along that stretch of the coast line which extends southwards for about a quarter of a mile from the Point. Along this section, hard baked sandstone outcrops beneath the dolerite and also appears as rafts within the lower layers of the intrusion. Although the dolerite dips north and the sandstone dip south there is no marked discordance because the angles are small in both cases.

The Kingscross sheet can be traced westwards by means of exposures in the Kingscross burn and Knockenkelly burn, but it then appears to fray out into a number of thin sheets at its western extremity and does not connect with the Monamore sheet further to the west.

Exposures of analcite-dolerite also occur along the ridge known as the Knowe which runs slightly north of the main exposures of the Kingscross sheet. The Knowe appears to be formed of a horizontal sheet which, although now isolated from the main intrusion, is clearly related to it and may, in fact be the equivalent of the uppermost of the three sheets exposed on the shore.

The Kingscross sheet is cut in a number of places by basalt dykes of the Arran dyke swarm, which are Tertiary in age, and these are well exposed in the shore sections and in Kingscross burn. Rarely, thin sheets of quartz dolerite also cut the sheet on the Kingscross and Holy Island shores.

A prominent felsite dyke cuts the sheets on the Holy Island shore, and felsite also cuts the intrusion towards its western extremity, where in this case they probably belong to the system of acid cone sheets postulated by Tomkeieff.

Holy Island itself is formed largely of a mass of riebeckite trachyte (Tyrrel 1928) which overlies a basement formed of the Lamlash - Machrie Sandstone Group. In the south this basement is intruded by the Kingscross sheet(s) and by the Tertiary dykes. It is clear, however, that all these intrusions are earlier than the trachyte for none of them penetrate it. It is therefore generally considered that the riebeckite trachyte represents the last phase of igneous activity in the area, and indeed probably in Arran as a whole. (Tyrrel 1928).

Radioactive dating (potassium - argon) by Miller and Harland (1963) has suggested that the whole range of later igneous activity in Arran took place within Palaeocene and Eocene times, (55 - 65 million years ago). The age of the Kingscross sheet (and hence of the Lamlash cone sheet) is, therefore, probably early Tertiary, for it intrudes sediments of Permo-Triassic age and is, itself, cut by rocks of Tertiary age.

The Monamore sheet is the western member of the Lamlash cone sheet and its outcrop extends northwards from Squiler to Cnoc Dubh. This intrusion takes its name from the Monamore burn along which a reasonably complete section is exposed.

The average dip appears to be some 20° to 30° to the east and since the regional dip of the country rocks is to the south there must clearly be a marked discordance. Unfortunately, although the contacts of the Monamore sheet can be delimited for mapping purposes, they are never well exposed and such a discordance cannot be seen.

Unlike the Kingscross sheet, this member of the cone sheet consists only of one intrusion which in many places is cut by sheets of felsite. These felsites are well exposed in the Monamore burn and belong to the acid cone sheets proposed by Tomkeieff.

The southern boundary of the intrusion runs along the southern flanks of Squiler and the top can be traced around until it merges with the base. Likewise at the northern boundary the top and bottom coincide around the summit of Cnoc Dubh. This must mean, therefore, that the sheet is lenticular in cross section.

The exposures at the summit of Cnoc Dubh are also cut in many places by numerous fine whitish veins (Plate I c.) which by analogy with similar sections in the Clauchlands sheet (see later) indicate that they lie close to the base of the intrusion.

A subsidiary summit some 300 yards west of Cnoc Dubh is also formed of extensively veined analcite dolerite and appears to be a small downfaulted section of the intrusion which now lies isolated as a result of erosion. The Monamore sheet is responsible for the high ground which lies to the west of Lamlash and which has Squiler (1300'). The Ross (992') and Cnoc Dubh

Plate I

a) Segregation of dolerite pegmatite in the Clauchlands sheet at Clauchlands Point.

b) Basaltic xenolith in the Clauchlands sheet at Clauchlands Point.

c) Zeolitic veins cutting analcite-dolerite near the base of the Monamore sheet at the summit of Cnoc Dubh.

Plate I.

a.

b.

c.

(1003') as its prominent summits and is dissected by the Monamore and Benlister burns.

The summits of Squiler and Cnoc Dubh are formed of analcite dolerite which can be readily recognised in the field, but although analcite-dolerite also clearly makes up most of the Ross, the nature of material exposed at the summit cannot be identified in situ. Even in thin section, Tyrrel (1928) was unable to say whether this material really was a continuation of the Monamore sheet.

Petrographic examination of material collected from this locality in the present survey, shows however, that it is part of the same intrusion which in this region (Chapter II Petrography) has been severely attacked by hydrothermal agencies.

The Clauchlands sheet is the northern member of the cone sheet and is probably the best known of the three. It takes its name from the Clauchland Hills which rise to about 800 feet above Lamlash, and separate Lamlash Bay from Brodick Bay.

Analcite dolerite outcrops along the top of these hills and the base of the sheet, although rarely seen in this region, can be readily traced along the Clauchland escarpment westwards from Dun Fionn as far as the main Lamlash-Brodick road. The relationships to the west of this road are obscure but the sheet may be terminated by a fault.

The top of the sheet can be traced along the southern flanks of the Clauchland Hills and may be seen in some of the streams which drain these slopes.

Both top and bottom are exposed on the shore at Clauchlands point with a continuous section between them. A detailed description of these exposures

is given under C, below, since it is from this section that all the geological and palaeomagnetic samples have been collected.

Like the Monamore sheet, this intrusion forms a single sheet and is cut by a number of basalt dykes and also, on Dun Fionn, by felsite. It has been intruded more or less parallel to the strata and hence has many of the aspects of a sill. The contacts, however, are generally slightly transgressive and, moreover, it is now apparent that the Clauchlands sheet cannot be considered in isolation from the other analcite-dolerites of the area, which are decidedly transgressive.

C. The Field Relations at Clauchlands Point

A complete section through the Clauchlands sheet is exposed along the shore for a quarter of a mile north of Clauchlands point, and analcite-dolerite is also seen in the Hamilton Rock just off the point.

The sheet is intruded into sandstones which dip, on average, about 40° to the south west. The sandstones immediately overlying the intrusion are grey in colour, hard and laminated. The country rocks, however, which here form the Lamlash Sandstone, are generally dull-red flaggy sandstones and form a scarp six foot high above the contact.

The upper contact is exposed opposite the Hamilton Rock and is slightly transgressive, plunging at 50° beneath the sandstones. The chilled margin is basaltic and a xenolith of sandstone, one foot thick, is incorporated in the upper layers. These relations are illustrated in Figure 2.

The dolerite coarsens rapidly away from the contact and develops prominent jointing parallel to the margins of the intrusion. These joint planes, which are characteristic of all members of the cone sheet, provide excellent surfaces on which to make dip measurements.

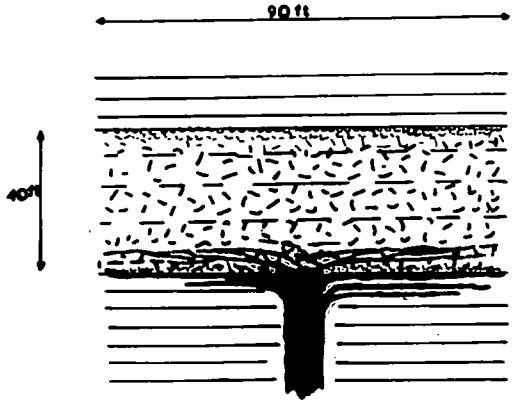

Figure 4.

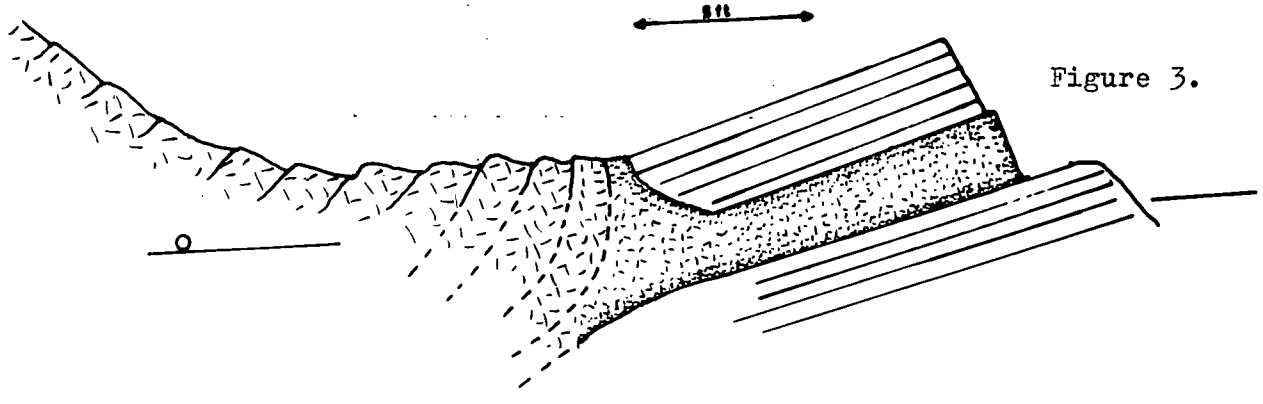

Figure 3.

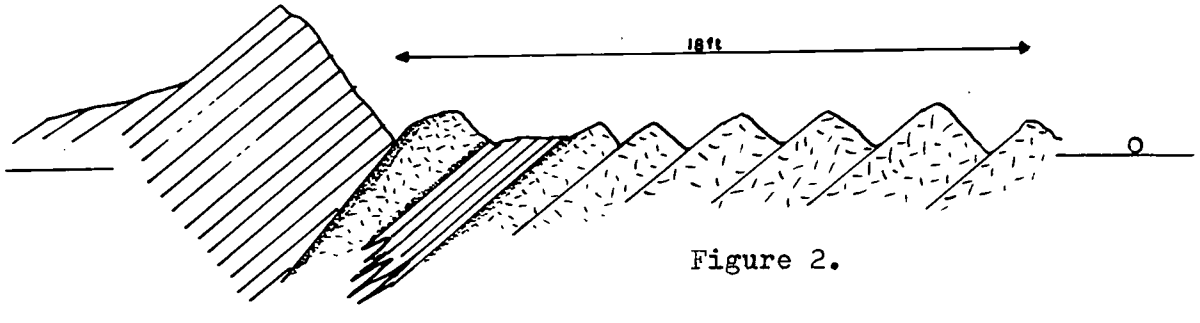

Figure 2.

Figure 2.

Sketch of the upper contact of the Clauchlands Sheet at Clauchlands point.

Figure 3.

Sketch of the lower contact of the Clauchlands Sheet at Clauchlands point.

Figure 4.

Sketch interpretation of the basalt/dolerite relationships at Kingscross point. A basalt dyke (black), having failed to penetrate the dolerite (stipled), has spread laterally along prominent joint planes in the lower layers of the sheet.

Towards the base of the sheet the dips steepen abruptly and at the contact, which is exposed on the shore, they appear to be overturned as shown in Figure 3. This, however, is not the true base but is the contact against an exposed xenolith of sandstone. Below this xenolith lies a sheet of basalt two feet thick and more or less concordant with the underlying country rock, which represents the real base of the intrusion.

The lower margins of the intrusion are traversed by a large number of white, zeolitic, veins which also extend into the underlying sandstones. Away from the margin, the intensity of such veining decreases rapidly and dies out some thirty feet above the base.

The formation of these veins, which also appear at the top margin, although on a much reduced scale, is interpreted as the result of a build up of volatiles within the cooling intrusion.

The very coarse, almost gabbroic, texture of much of the analcite-dolerite also indicates that the cooling intrusion contained a large proportion of volatile material, and the existence of segregations of dolerite-pegmatite further supports this.

These segregations are conspicuous for their large, black crystals of augite (Plate I/b.), and they appear at a limited horizon some forty feet above the base. Apart from indicating a high volatile content within the intrusion they also represent the final solidification products and thus establish where consolidation last took place.

A final important relationship seen in the Clauchlands section is exposed in the lower thirty feet of the intrusion. Here are found rounded xenoliths of basalt surrounded by the coarse analcite-dolerite. These xenoliths are generally oval in shape and have a marked preferred orientation such that their long axes lie parallel to the margins of the intrusion. They are quite

Plate II

Basalt/dolerite relationships exposed at Kingscross Point.

Plate II.

large towards the base of the sheet, some being three feet long, but decrease in size away from the margin until they are only a few inches long and then disappear (Plate I b.)

The xenoliths have clearly been caught up within the intruding magma and have acquired their preferred orientation under the influence of the intrusive pressures, and possibly also to some extent as a result of settling.

Petrographic examination (Chapter II Petrography) has shown that the xenoliths are related to the main intrusion and hence this leads to the conclusion that the Clauchlands sheet is multiple. Thus after the initial magma had chilled against the country rock, more magma was intruded with sufficient force to dislodge portions of the solidified margins.

The history of the Clauchlands sheet, therefore, is well preserved in this area and hence this section forms an excellent source of material for the work to be described in the following pages.

D. The Field Relations at Kingscross Point

About sixty yards south of Kingscross Point, the coarse analcite-dolerite is extensively penetrated by thin sheets, anastomosing veins and shreds of basalt, (Plate II), and a number of thin sills of what appear to be the samematerial are exposed slightly to the north of this place, outcropping from beneath the analcite-dolerite.

Tyrrel (1928) interpreted these relationships as showing veining of the dolerite by the basalt, and this indeed is the most obvious explanation, especially as many of the veins have tachylitic rims in contact with the dolerite.

Recently, however, Tomkeieff and Longstaff (1960) have concluded that the reverse relationship is in fact the true one and that the basalt exists as relicts within a later dolerite, while the tachylitic contacts are the

result of rheomorphic melting of the basalt.

This interpretation, however, appears to be unneccessarily complicated and, moreover, fails to account for the restricted distribution of the basalt.

The zone in which the veining occurs is only about thirty yards wide, and veining is most intense only at the centre of this zone and then fades laterally. Likewise, the veins are restricted to the immediate base of the sheet and do not extend more than a few feet vertically within it.

Further, the basalt tends to be distributed more or less horizontally along the joint planes within the analcite-dolerite. This evidence together with the existence of the thin sills beneath the sheet suggests the following interpretation for the origin of these relationships.

It seems probable that basalt has been intruded vertically beneath this zone to form one of the many dykes of the Arran swarm, except that in this particular case the intrusion has failed to cut the analcite-dolerite, and instead the magma has squirted out laterally, taking the lines of least resistance, which are namely beneath the sheet and along the joint planes (Figure 4).

Further evidence is discussed briefly in Chapter II (Petrography) which supports Tyrrel's original interpretation that the basalt veins are later than the dolerite, although in the context of the present study, this is but a digression to consider an intriguing observation.

E. Summary

The Clauchlands analcite-dolerite sheet has been selected as the source of material for the present research project because it is well exposed and its geological history can be ascertained.

Although superficially it has the form of a sill it has been shown, in fact, to be but one member of a single conical or saucer-shaped, intrusion which is best described as the Lamlash cone sheet.

The age of the intrusion is considered to be early Tertiary because it is intruded into Permo-Triassic sediments and is itself cut by dykes and felsite sheets of undoubted Tertiary age.

It is considered that the failure of one such basalt dyke to cut the Kingscross sheet has resulted in the complex basalt-dolerite relationships at Kingscross Point.

Chapter II Petrography

A. Introduction

Tyrrel (1928) in describing the rocks which are now included in the Lamlash cone-sheet refers to them as crinanite. However, the two terms crinanite and teschenite are often loosely applied in order to describe basic igneous rocks containing analcite. Various aspects of the use of these terms have been discussed by Wilkinson (1955) and he concluded that ".. the retention of the term crinanite is fundamentally misleading inasmuch as the terms teschenite and crinanite as used by many writers are virtually synonymous". He favoured retention of the term teschenite, because:

"a) It has priority of definition.

b) In general its chemical and mineralogical affinities are such that it constitutes a well recognised and widespread rock species.

c) Uniform designation as teschenite of hypabyssal or plutonic basic rocks of alkaline character carrying analcite as an essential constituent lends true emphasis to the frequent field association picrite-teschenite and focusses attention on an important petrogenetic problem."

The term teschenite was first used in 1861 by Hohenegger who applied it in a very general sense to certain igneous rocks intrusive into Cretaceous strata in the neighbourhood of Paskau, Moravia. Tschermak (1869) used the same term to describe a crystalline granular rock composed essentially of feldspar, hornblende, augite and analcite. Walker (1923) proposed the definition that "teschenites are rocks consisting of plagioclase feldspar (which is partly or wholly analcitized), titanaugite and analcite. Barkevikite is often present, sometimes in greater abundance than the titanaugite, and

olivine is a frequent constituent". Wilkinson (1955) has recommended that the usage of this term be continued and has suggested that intrusive alkaline basic rocks with minor analcite (2-3% by volume) are adequately covered by the term 'analcite-bearing olivine-dolerites'.

Using the above criteria, then, the rocks of the Lamlash cone-sheet cannot be described strictly as teschenites because analcite is a minor constituent, being a late stage interprecipitate that has crystallised in the available spaces which remained, and it rarely forms more than a few percent of the whole rock. The term analcite-dolerite, however, is considered to be fully descriptive of these rocks and is used throughout this work. The term olivine-analcite-dolerite is not used because frequently olivine is not abundant and then titanaugite forms the major mafic mineral.

B. General Petrography of the Lamlash Cone-Sheet

The bulk of the cone-sheet consists of a coarse analcite-dolerite in which the major minerals are plagioclase, olivine, titanaugite and ore minerals. (Plate III a.). Analcite is ubiquitous but generally is present in only small amounts forming wedge-shaped or irregular "infillings" in the spaces between plagioclase laths. Apatite is always present as minute crystals but is quantitatively unimportant, and other minor constituents are biotite and amphibole.

An important feature of these rocks is that the analcite has all the appearance of a primary mineral which has crystallized at a late stage. The lath-like habit of the plagioclase crystals results naturally in the formation of wedge-shaped cavities between them, and it is in these cavities that the analcite has generally crystallized.

In fresh material the analcite is clear and colourless, isotropic or

feebly birefrigent, and is clearly not derived by zeolitization of the plagioclase. In the more usual sections, however, where alteration has taken place, then the analcite tends to be replaced by radiate fibrous aggregates showing brilliant interference colours. Such aggregates also appear to invade crystals of plagioclase and they are considered to be zeolites formed at a deuteric stage of activity as distinct from the slightly earlier stage at which analcite appeared as a primary mineral. Tyrrel (1928) reports that these aggregates have been identified as natrolite and scolecite.

Frequently the olivine constituent of the rocks is partly or even wholly replaced by a heterogeneous assemblage of chlorite-serpentine minerals, and such alterations are also regarded as the products of a deuteric stage of activity.

The textures of the rocks are typically ophitic or sub-ophitic, with relatively large platey crystals of purplish titanaugite containing many laths of plagioclase.

Polysynthetic twinning is strongly developed in the plagioclase crystals, and extinction angles of about 30° measured on albite twins suggests that the composition is that of labradorite. (Rogers and Kerr 1942 p.242). However, since zoning is strongly developed as well as twinning, such an estimate must be only an average indication of the plagioclase composition.

A modal analysis (Table 1) shows a sample from the Clauchlands sheet, to consist of 57.59% plagioclase, 24.47% olivine, 8.81% titanaugite, 2.88% ore minerals, 3.59% chlorite-serpentine minerals derived from the olivine 0.36% biotite and 2.28% zeolites. This figure for the zeolites includes secondary fibrous zeolites and in fact the content of primary analcite is probably less than one percent. This mode, however, shows that over 90%

Table 1.

Modal Analysis of Sample A/C/3/37 from 54ft above the Base of the Clauchlands Sheet

Mineral	Counts	Percentage	Error
Plagioclase	2882	57.59	± 1.4
Olivine	1225	24.47	± 1.3
Titanaugite	441	8.81	± 0.7
Opaques	144	2.88	± 0.4
Chlorites	180)		
Biotite	18)	6.23	± 0.6
Zeolites	114		
	5004	99.98	

Errors estimated after Barringer (1953).

of the rock consists of plagioclase, olivine and titanaugite. The qualitative examination of other slides has shown that the relative amounts of olivine and titanaugite are highly variable.

C. Detailed Petrography of the Clauchlands Sheet

A detailed collection of material has been obtained from the section through the Clauchlands Sheet at Clauchlands Point. Samples from this collection have been polished and sectioned, and the remaining material has been crushed and separated for the purposes of the further analysis of the ores. It has thus been possible to correlate detailed petrographic variations with the episcopic, X-ray, thermomagnetic and other data which have a bearing on the nature of the ore minerals.

The value of such a petrographic investigation is not only that it establishes firmer foundations on which to interpret the field relations but also that it provides important information as to the relations of the ores to the rest of the crystallizing magma, and also as to the nature of the environment in which the ores formed and cooled.

An immediate observation is that the chilled material is a microcrystalline basalt and that it contains only a few sporadically ~~disturbed~~ distributed phenocrysts of plagioclase. This indicates, therefore, that the magma was in an essentially liquid form when intruded and that crystallization had barely started.

Sample S25 is representative of this chilled material and comes from two feet below the top of the intrusion where it is in contact with a xenolith of sandstone. In thin-section the rock is seen to be a dense porphyritic basalt. (Plate III b.). Isolated phenocrysts of broad plagioclase laths are partially replaced by calcite and occur in a dark microcrystalline matrix which is composed almost exclusively of a plexus of minute plagioclase laths

Plate III

a) Thin section of analcite dolerite from the Clauchlands sheet. Twinned plagioclase laths occur intergrown sub-ophitically with titanaugite (top left). Subhedral crystals of olivine and euhedral opaque crystals are also visible. Magnification X32. Crossed nicols.

b) Thin section of chilled material from the Clauchlands sheet showing the abundance of the opaque minerals. Magnification X32. Plane-polarised light.

c) Thin section of analcite dolerite from the Clauchlands sheet showing amphibole (light-grey) moulded round a euhedral opaque crystal. Magnification X32. Plane-polarised light.

Plate III.

a.

b.

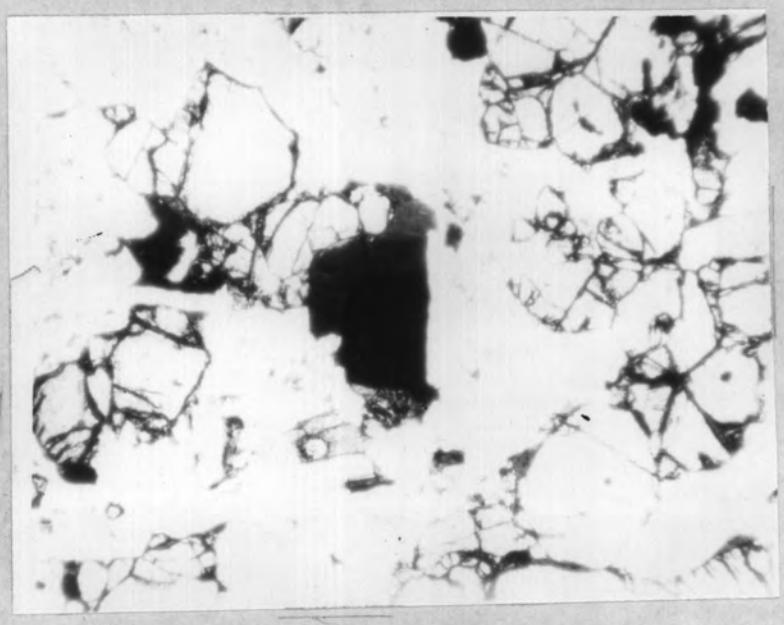

c.

and abundant minute crystals of the ore minerals together with green chlorite, probably after olivine. Relatively large flakes of biotite are also distributed through this section.

The large amount of ore minerals in this material is significant in that (1) it shows that the ores are an early crystalline phase appearing at more or less the same time as plagioclase and olivine, and (2) Since pyroxene is apparently absent at this stage it suggests [redacted] that the subsequent appearance of pyroxene in the dolerite may be the result of reactions between the ores and the magma.

The rock coarsens rapidly away from the margins of the sheet passing through fine to a coarse grained analcite-dolerite which characterizes most of the intrusion. Although this transition is rapid at both margins, it is more rapid from the bottom than from the top; the zone of fine-grained dolerite extending for a distance of only five feet above the base of the sheet whereas the corresponding zone at the top extends for twelve feet into the intrusion. This observation indicates that the sheet cooled asymmetrically, most of the heat having been lost from the upper margins.

Analcite has the general formula $Na_2O.Al_2O_3.4SiO_2.2H_2O$. (Dana 1958), and its presence as a primary mineral in igneous rocks is generally taken as evidence that the magma retained considerable amounts of soda and water vapour.

From a detailed examination of the thin-sections, it is clear that as crystallization proceeded, an association developed between the ore minerals and a reddish-brown amphibole. This association first appears about seventeen feet above the base of the sheet and continues throughout much of the intrusion, althogh it is absent at the margins.

The presence of the amphibole, combined with the existence of primary analcite must, therefore, be further evidence that the crystallizing magma

retained its water vapour and other volatiles.

The amphibole first appears as thin tenuous rims moulded onto the opaque crystals and it is difficult to distinguish from the flakes of biotite which are nearly always present in the rocks. Towards the centre of the intrusion, however, it becomes more conspicuous and forms platey crystals although still crystallizing against or close to the ore minerals (Plate III)

The mineral is deep reddish-brown in colour is distinctly pleochroic to a straw-yellow colour, and hence strongly resembles sections of biotite. However, rare sections are present which have the amphibole cleavage, and when this is absent, the distinction can usually be made in terms of the 2V which is large for the amphibole and very small for biotite. The straight extinction of biotite and oblique extinction of amphibole sections is not a safe criterion for distinction because the extinction angle of the amphibole is very small. However, a distinguishing feature which is of some value is the fact that the interference colours of biotite invariably show a characteristic schillerization effect which is not shown by the amphibole.

As mentioned earlier, the high concentration of opaque minerals in the chilled magma is evidence that the ore minerals are an early crystallization phase. Examination of the dolerite sections supports this conclusion, for, on textural evidence, it is clear that the ores crystallized generally later than olivine and plagioclase because these latter minerals tend to show idiomorphic outlines against the ores; but, using this same criterion, it is apparent that the ores crystallized before the titanaugite for the opaque crystals tend to show idiomorphic outlines against the pyroxene (Plate IV a)

The modal content of the ore minerals has been determined by point counting and the results are summarized in Table 2 and plotted in Figure 5.

Plate IV

a) Thin section of analcite-dolerite from the Clauchlands sheet. A large crystal of titanaugite (light grey) contains sub-ophitically intergrown laths of plagioclase. The plagioclase laths show euhedral boundaries against the opaque mineral (top centre) indicating that they formed earlier. The opaque mineral is euhedral against the pyroxene indicating that the pyroxene is the later mineral. Magnification X32. Crossed nicols.

b) Thin section of material from the Ross. The dolerite texture can be recognised. The rock is much altered (especially at left of the field of view) with the introduction of hydrothermal calcite. Magnification X32. Crossed nicols.

Plate IV.

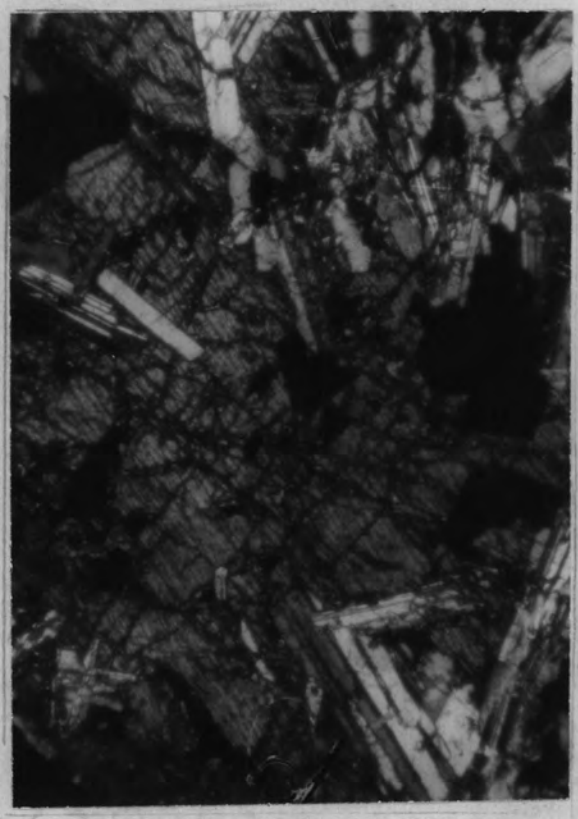

a.

b.

Table 2.

Percentage of Opaque Minerals in the Clauchlands Sheet

Sample.	Horizon. (feet)	Number of Points Counted. Opaque	Rest	Total	% Opaques	Error ±
S 1	Top	268	3333	3601	7.4	0.8
S 2	126	415	5383	5798	7.1	0.6
S 3	122	285	5163	5448	5.2	0.5
S 4	118	244	3781	4025	6.1	0.6
S 5	114	188	4927	5115	3.7	0.5
S 6	110	179	4806	4985	3.6	0.5
S 7	106	278	7252	7530	3.7	0.4
S 8	102	240	7506	7746	3.1	0.4
S 9	98	154	4708	4862	3.2	0.5
S10	94	120	5219	5339	2.2	0.3
S11	90	253	8084	8337	3.0	0.4
S12	86	50	3472	3522	1.4	0.3
S30	82	36	3502	3538	1.0	0.3
S31	78	147	8004	8151	1.8	0.2
S32	74	128	4990	5118	2.5	0.3
S33	70	196	7304	7500	2.6	0.2
S34	66	168	7080	7248	2.3	0.2
S35	62	103	3324	3427	3.0	0.4
S36	58	159	6784	6943	2.3	0.2
S37	54	204	5530	5734	3.5	0.3
S38	50	96	3898	3994	2.4	0.3
S39	46	139	3391	3530	3.9	0.4
S40	42	154	4261	4415	3.5	0.3
S41	20	339	6358	6697	5.1	0.5
S42	17	267	3956	4223	6.3	0.6
S43	14	208	7429	7637	2.7	0.3
S44	11	231	4437	4668	4.9	0.3
S45	8	494	5237	5731	8.6	0.5
S46	5	258	5071	5329	4.8	0.3
S13	40	Pegmatite segregation			8.6	
S14	30	Basalt xenolith			4.2	
S15	26	Basalt xenolith			4.1	

Errors estimated after Barringer (1953).

Figure 5.

DISTRIBUTION OF THE ORE MINERALS WITHIN THE CLAUCHLANDS SHEET

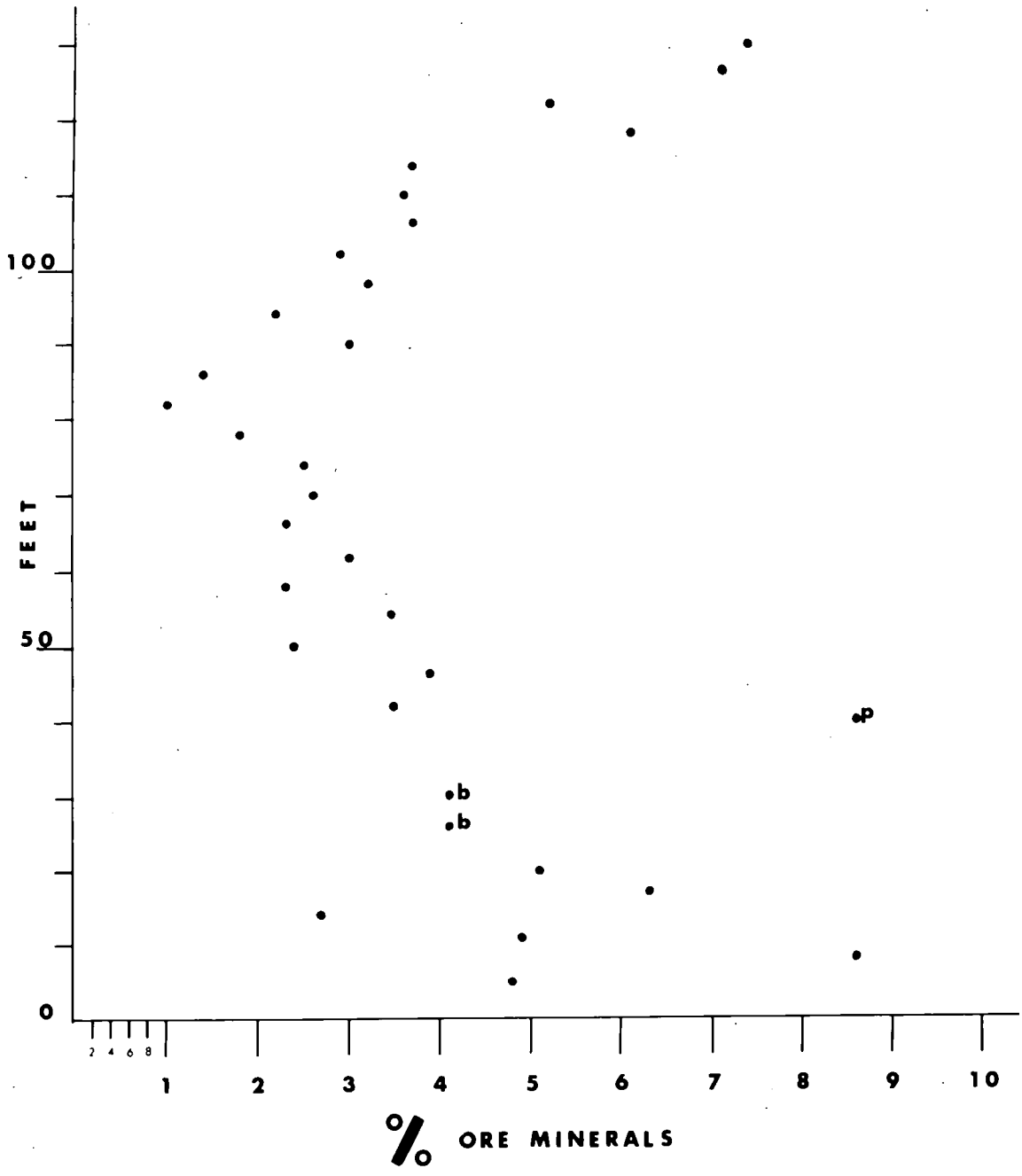

p Dolerite-pegmatite Segregation

b Basalt Xenoliths

From this it can be seen that the amount of ore minerals in the rock decreases fairly regularly away from the margins of the sheet. Whatever the origin of this variation, however, its effect on the palaeomagnetism of the sheet is strikingly shown in Fig. 8 (Chapter VI Palaeomagnetism) which summarizes the variations in the intensity of magnetization through the sheet. It is clear that the intensity is controlled in large part by the amount of "magnetite" in the rock.

Petrographic examination of the 'basaltic' xenoliths mentioned in Chapter I show that they are fine-grained dolerites consisting of ophitically intergrown plagioclase and titanaugite with chloritised pseudomorphs of olivine and abundant ore minerals. Rarely, the ores are rimmed with amphibole, and hence these rocks are essentially similar to the material of the sheet itself, except that analcite cannot be certainly identified. It seems clear that the xenoliths are portions of the intrusion which have been caught up from slightly lower horizons as a result of later intrusive pulses.

Thin-sections of the country rock above and below the sheet show that whereas the sandstone immediately above the intrusion contains a high percentage of ore minerals, the sandstone immediately below the intrusion contains no ore minerals but consists essentially of quartz cemented by carbonate and showing little evidence of recrystallization.

Episcopic observations (Chapter III) show that the ores in the sandstone are not related to those of the intrusion but consist largely of hematite derived by recrystallization of a ferriferous cement. The absence of such ores at the lower contact is probably due to the different lithology of the underlying sandstones for they belong to the top of the Brodick Breccia Group and do not have the characteristic reddish colouration of the Lamlash Sandstone above the intrusion.

D. The Nature of Material from the Ross

The Ross is a prominent hill (992 ft.) which rises on the north side of Monamore Glen between the Monamore and Benlister valleys (See Chapter I). The nature of material from the Ross has been in some doubt and Tyrrel (1928) concludes that "without fresh material it is hard to say whether this mass is really a continuation of the Monamore crinanite (as it is mapped on the One-Inch Geological Map), or a member of the quartz-dolerite suite."

Two samples have been investigated in the present work, both of them from high up on the southern flanks of the Ross, and both of them, although extensively altered, can be recognised as having originally been analcite-dolerite.

A description of Sample S65 is representative of both samples. In thin-section it is seen to be fundamentally an analcite-dolerite which has suffered extensive alteration as a result of hydrothermal activity (Plate IV b.). The basic ophitic texture between plagioclase laths and titanaugite remains but both the plagioclase crystals and the titanaugite have been extensively replaced by calcite, and calcite also forms prominent wedge-shaped masses between the plagioclase laths. Fibrous zeolites are also present and have probably replaced original analcite. The olivine constituent is entirely pseudomorphed by green chlorite (penninite) and, in fact, the only unaltered material appears to be the abundant euhedral crystals of the ore minerals.

Material from the Ross, therefore, is petrographically similar to the fresh analcite-dolerite of the cone-sheet found in the Monamore and Benlister and hence, the map (Figure I - Chapter I) shows the outcrop of the Monamore Sheet extending north-south across the Ross.

E. Relationships at Kingscross Point

The field relationships at Kingscross Point have been discussed earlier (Chapter I Field Relations), when it was pointed out that according to Tyrrel (1928) the basalt is the later rock type and occurs as veins in the analcite-dolerite whilst Tomkeieff and Longstaff (1960) hold the opposite view and consider that the basalt is the earler rock and that it occurs as remnants within the later analcite-dolerite. The field evidence which is used by Tyrrel to indicate chilling of basalt against dolerite is considered by Tomkeieff and Longstaff to indicate zones of remelting and intrusion of rheomorphic basalt into the dolerite.

As a result of the present observations it is considered that the view of Tyrrel is more likely to be correct, namely that the basalt is the later rock, and its origin has been tentatively explained as arising from a dyke beneath the sheet of analcite-dolerite (See Chapter I Field Relations).

Three sections of the basalt/dolerite contact have been examined. Two of these are from the Petrographical Collection in the Department of Geology at Durham, Nos. 4336A and 4336B, and the third Sample S17 was collected during the course of the present work. All three show essentially the same features and a description of S17 is typical.

The two rocks represented are a coarse holocrystalline dolerite and a dense microcrystalline porphyritic basalt which is tachylitic at the actual contact.

The dolerite consists essentially of plagioclase and titanaugite with some olivine and ore minerals. The texture is crudely sub-ophitic, but much of the rock, especially near the contact, shows marked granulation. Minor amounts of biotite are present, associated with the ores and typically occurring between a crystal of ore and titanaugite. Although analcite cannot

be recognised this may simply be due to the effects of granulation, for in its general mineralogy the rock is similar to other material from the cone-sheet.

The contact between the basalt and the dolerite is sharp and irregular, and the basalt appears as a black tachylite. Large phenocrysts of distorted laths of plagioclase occur in the basalt and are clearly derived from the dolerite margins. Granulation of the dolerite is extreme close to the contact but the rock rapidly coarsens away from the contact.

The basalt also coarsens away from the contact and becomes microcrystalline. It consists essentially of a dense plexus of minute laths of plagioclase and abundant minute euhedral crystals of the ore minerals together with minute anhedral crystals of pyroxene which are straw in colour. Yoder and Tilley (1962 p.373) have described yellow to lemon-yellow clinopyroxenes that have developed on heating basalts under oxidising conditions and state that the colour is indicative of the presence of ferric iron.

The dense tachylitic contact and the extreme granulation of the dolerite is considered to be clear evidence that the basalt is later than the dolerite and that it intruded the dolerite in fully liquid form which would argue against it being rheomorphic in origin.

F. Summary

The term analcite-dolerite fully describes the rocks of the Lamlash Cone-Sheet.

Detailed investigations of the Clauchlands Sheet indicate that the magma retained its volatiles to a late stage of cooling. The ore minerals, however, crystallized at an early stage, between the plagioclase-olivine

phase and the titanaugite stage.

The modal content of the ore minerals has been found to decrease fairly regularly away from the margins of the sheet, and this variation is reflected in the intensity of magnetization of the rocks.

The 'basaltic' xenoliths described in Chapter I are petrographically similar to material from the intrusion proper.

The material forming the summit of the Ross has been shown to belong to the cone-sheet and hence the outcrop on the map has been drawn across this hill.

It is considered that Tyrrel's explanation for the complex basalt-dolerite relationship at Kingscross Point are more likely to be correct than that of Tomkeieff and Longstaff.

Chapter III. Ore-Microscopy

A. Introduction

The work of Newhouse (1936) has shown that the commonest opaque minerals in igneous rocks are oriented intergrowths of magnetite and ilmenite. Subsequent work, however, has shown that these minerals are more complex than was realised by Newhouse, and that these terms, as used by him, are best regarded as general terms to describe isotropic minerals having properties similar to those of natural magnetite (Fe_3O_4), and anisotropic minerals having properties similar to those of natural ilmenite ($FeTiO_3$).

In the present investigation it has been found that in general the opaque minerals in the Clauchlands sheet also consist of such oriented intergrowths between an isotropic mineral resembling magnetite and an anisotropic mineral resembling ilmenite. However, the X-ray data and the magnetic data discussed in Chapters IV and V have shown that these minerals are of variable composition and are not pure Fe_3O_4 and pure $FeTiO_3$. Therefore they cannot be described as magnetite and ilmenite except in the imprecise sense used by Newhouse, and so in the present work it is proposed, for convenience, to describe them as 'magnetite' and 'ilmenite'.

B. Iron-Titanium Oxide Minerals in the System $FeO-Fe_2O_3-TiO_2$

Pouillard (1950) first represented the compositions of the iron-titanium oxides in terms of the system $FeO-Fe_2O_3-TiO_2$ (Figure 6). The important minerals in this system are magnetite (Fe_3O_4), ilmenite ($FeTiO_3$), hematite (Fe_2O_3) and ulvöspinel (Fe_2TiO_4). Rutile (TiO_2) may occur in acid igneous rocks but is apparently absent from basic igneous rocks (Newhouse 1936), and pseudobrookite (Fe_2TiO_5) is a rare mineral which is unstable below about 500°C

Figure 6.

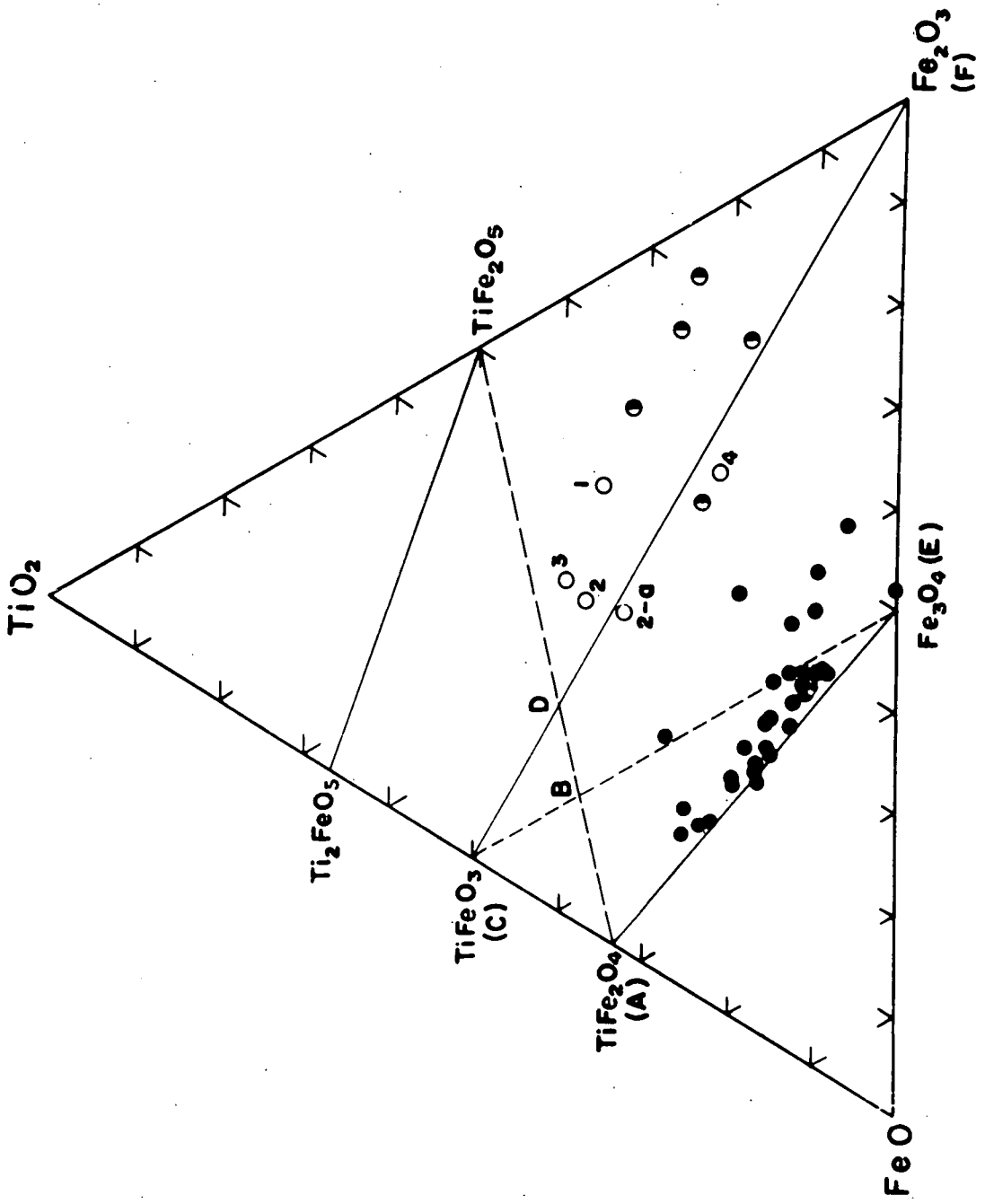
TiO2
TiFe2O5
Fe2O3 (F)
Ti2FeO5
TiFeO3 (C)
TiFe2O4 (A)
Fe3O4 (E)
FeO
D
B
1
2
3
2-a
4

Figure 6.

The System $FeO-Fe_2O_3-TiO_2$ (after Katsura and Kushiro 1961) illustrating the range in composition of γ-spinels.
Solid circles represent titanomagnetites.
Open and half solid circles represent titanomaghemites from Japanese rocks and from South Africa respectively.

(Taylor 1961). The compound $FeTi_2O_5$ does not occur naturally and is unstable below 1000°C (Taylor 1961).

The important characteristics of these minerals are described below:

Magnetite (Fe_3O_4) appears light greyish brown in polished section (Uytenbogaardt 1951), has a reflectivity in air of 21.1% (Bowie and Taylor 1958), and a Vickers hardness number in the range 530 - 599 (Bowie and Taylor 1958). It is isotropic.

Ilmenite ($FeTiO_3$) is light to dark brown in polished section sometimes with a faint pinkish or violet tint, and exhibits reflection pleochroism from light pinkish brown (O) to dark brown (E) (Uytenbogaardt 1951). It has a reflectivity in air of 19.4% (Folinsbee 1949; Bowie and Taylor 1958) and a Vickers hardness number within the range 519 - 703 (Bowie and Taylor 1958). It is strongly anisotropic and exhibits light greenish grey or brownish grey colours between crossed nicols (Uytenbogaardt 1951). Ilmenite is a rhombohedral mineral.

Hematite (α -Fe_2O_3) appears whiter than ilmenite in polished section and is grey-white in colour with a bluish tint (Uytenbogaardt 1951). It has a reflectivity in air of 27.5% (Bowie and Taylor 1958) and a highly variable Vickers hardness number within the range 739 - 1062 (Bowie and Taylor 1958). This variation in hardness appears to depend on the degree of crystallinity, ranging from 739 - 822 for microcrystalline samples, and from 920 - 1062 for coarsely crystalline samples. (Bowie and Taylor 1958). Hematite is distinctly anisotropic and exhibits greyish blue or greyish yellow colours

between crossed nicols. Deep red internal reflections are also very common when the specimen is not well polished (Uytenbogaardt 1951). Hematite is also a rhombohedral mineral.

It has long been known that there also exists a cubic form of Fe_2O_3 which is distinguished as maghemite (γ-Fe_2O_3). By means of X-rays, Hägg (1935) determined its structure and Verwey (1935) showed that, compared with magnetite, it exhibits a lattice defect, 1 in 9 of the iron ions being absent. Maghemite is metastable and on heating inverts to α-Fe_2O_3, the inversion probably being monotropic (Mason 1943). Basta (1953) has demonstrated the existence in nature of all stages in the oxidation of magnetite to maghemite.

Maghemite (γ-Fe_2O_3) appears bluish-grey in polished section and is isotropic (Ödman 1932). It has a reflectivity in air of 25.0% (Bowie and Taylor 1958) and a Vickers hardness number within the range 894 - 988 (Bowie and Taylor 1958).

Ulvöspinel (Fe_2TiO_4) may be difficult to identify in reflected light. It is cubic, and the natural mineral is only known to occur as fine intergrowths within magnetite. (Mogensen 1946; Ramdohr 1953; Basta 1953; Vincent and Phillips 1954). In polished section it appears darker brown than magnetite, although colour is apparently not a safe criterion for its recognition (Ramdohr 1953), and it forms a characteristic cloth or 'petit-point' texture (Plate V) in which minute lamellae of ulvöspinel are oriented along the (100) planes of the magnetite.

Rutile (TiO_2) appears grey, sometimes with a bluish tint, in polished

Plate V

Ulvöspinel (dark grey) intergrown with magnetite (light grey) in a characteristic 'petit-point' texture. The large transparent blades (black) are spinel. Polished section. Plane polarised light. Magnification X 400. Sample from Lac de la Blache, Saguenay Co., Quebec, Canada.

Plate V.

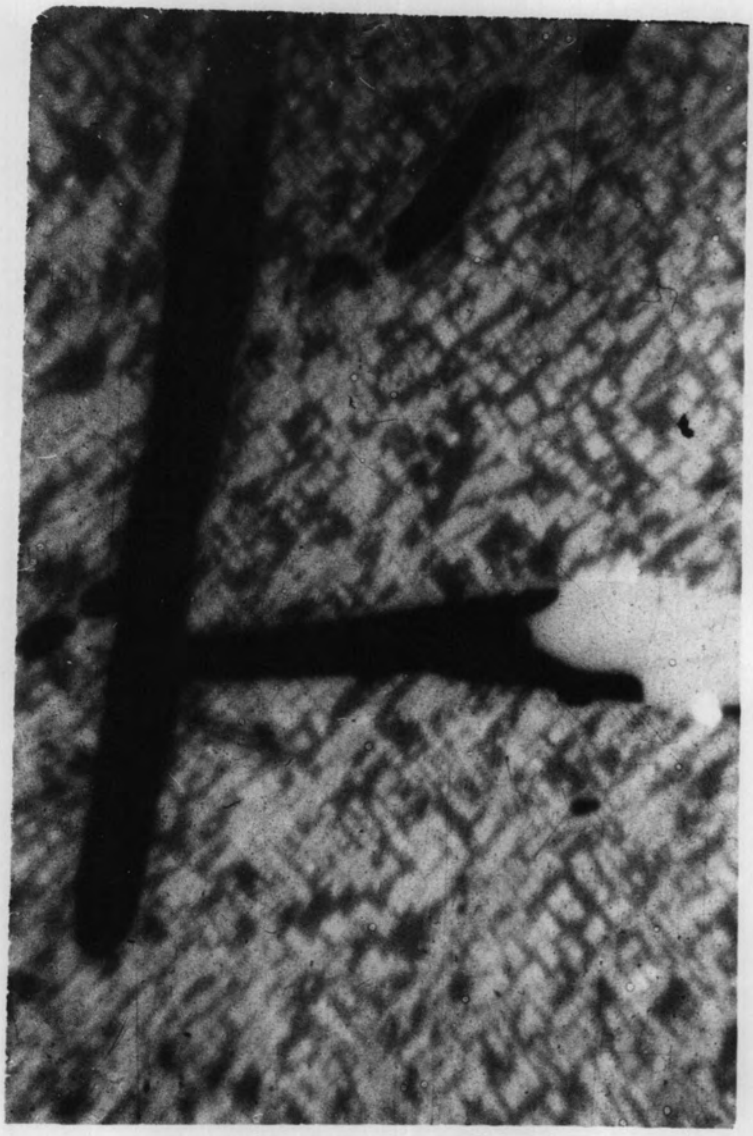

section (Uytenbogaardt 1951) and has a reflectivity in air of 20.2% (Bowie and Taylor 1958). Therefore, in colour and reflectivity it resembles magnetite. Rutile, however, is a strongly anisotropic mineral, although the anisotropy is usually masked by strong yellow to brown internal reflections (Uytenbogaardt 1951), and it is also much harder than magnetite, having a Vickers hardness number within the range 1074 - 1210 (Bowie and Taylor 1958).

Pseudobrookite (Fe_2TiO_5) closely resembles rutile in polished section, both as regards its colour and its yellow or brown internal reflections. (Uytenbogaardt 1951). Values for reflectivity and microhardness are not known but it appears to have a lower reflectivity than rutile (Uytenbogaardt 1951).

Three solid-solution series are known to exist in the system $FeO-Fe_2O_3-TiO_2$. Solid solutions between magnetite and ulvöspinel are cubic, solid-solutions between hematite and ilmenite are rhombohedral, and solid solutions between pseudobrookite and $FeTi_2O_5$ are orthorhombic.

Pouillard (1950) first demonstrated the existence of extensive solid-solution between magnetite and ulvöspinel to form cubic titanomagnetites having properties intermediate between those of magnetite and ulvöspinel. Later workers have shown that there also exists a wide variety of cubic minerals having properties similar to those of the titanomagnetites, but whose compositions cannot be expressed simply in terms of magnetite-ulvöspinel solid-solutions. (Basta 1953; 1959; Akimoto, Katsura and Yoshida 1957; Katsura and Kushiro 1961). Figure 6 shows the known range of compositions of these cubic minerals. It can be seen that these extend beyond the $FeTiO_3-Fe_2O_3$ join of the rhombohedral

minerals.

Frequently those minerals having compositions close to the magnetite-ulvöspinel join have been called titanomagnetites (Akimoto, Katsura and Yoshida 1957) whilst those minerals having compositions close to the hematite-ilmenite join have been called titanomaghemites (Basta 1953; 1959; Katsura and Kushiro 1961). This, however, would appear to be an arbitrary and unsatisfactory distinction.

Verhoogen (1962) has proposed that hematite, ilmenite and the rhombohedral solid-solutions be called α-phases, and that the cubic iron-titanium oxides be distinguished as β- phases in the case of magnetite, ulvöspinel and their solid solutions, or as γ-phases in the case of maghemite and those cubic minerals which are not simply solid-solutions between magnetite and ulvöspinel. Using this classification, then the term γ-phase would include all those cubic minerals shown to the right of the magnetite-ulvöspinel join in Figure 6 and would, therefore, avoid any confusion between the terms titanomagnetite and titanomaghemite.

It is known that these phases may be formed by oxidation of titanomagneties (β-phases) whose compositions lie on the magnetite-ulvöspinel join (Akimoto, Katsura and Yoshida 1957; Katsura and Kushiro 1961), although it is not known whether this is the only way that they may form. It seems preferable to refer to these minerals as γ-phases, rather than to apply arbitrary divisions of terminology.

It has long been known that solid-solution is continuous between hematite (α-Fe_2O_3) and ilmenite ($FeTiO_3$) at temperatures above 1050°C (Ramdohr 1926; Posnjak and Barth 1934). Pouillard (1950) first demonstrated the existence of a gap in the solid solution series at 950°C, which extends from about 33%

$FeTiO_3$ to 66% $FeTiO_3$, and at normal temperatures, solid solution is much more restricted. Edwards (1938) has reported hematites containing approximately 20% $FeTiO_3$, and ilmenites containing up to 6% Fe_2O_3, and Basta (1953) has reported ilmenite containing up to 18% ~~$FeTiO_3$~~. Fe_2O_3.

Edwards (1938) has called the hematite-rich solid-solutions titan-hematites. They are more grey-white than pure hematite in reflected light, have a lower reflectivity and show strong anisotropy. They lack the deep red internal reflections of hematite and are more resistant to hydrofluoric acid or mixtures of hydrofluoric and sulphuric acids. (Edwards 1938).

The ilmenite-rich solid-solutions are also strongly anisotropic but are brown compared to the titanhematites, and are pleochroic in brownish tints (Edwards 1938). Such minerals have been called ferri-ilmenites by Basta (1953).

The rhombohedral solid-solutions between pseudobrookite and $FeTi_2O_5$ are, as yet, imperfectly known, Taylor (1961) refers to them collectively as pseudobrookite and has found that they are rare in nature because they decompose at low temperatures. $FeTi_2O_5$ decomposes to rutile and ilmenite below 1000°C, and Fe_2TiO_5 decomposes to hematite and $Fe_2O_3 \cdot 3TiO_2$ below about 500°C. According to Basta (1953), $Fe_2O_3 \cdot 3TiO_2$ (arizonite) is not a mineral but is really a mixture of hematite and anatase with some rutile.

C. The Opaque Minerals in the Clauchlands Sheet

Apart from minor amounts of pyrite and chalcopyrite, the opaque minerals in the Clauchlands sheet consist of an isotropic phase resembling magnetite and an anisotropic phase resembling ilmenite. Data obtained from the X-ray analyses and the magnetic analyses (Chapters IV and V) indicate that these

minerals are not pure Fe_3O_4 and pure $FeTiO_3$ and therefore, in the present work it is proposed to refer to them, for convenience, as 'magnetite' and 'ilmenite'.

Throughout most of the intrusion, the 'magnetite' and 'ilmenite' occur as oriented intergrowths (see later) but towards the centre of the sheet 'ilmenite' appears also as a separate phase. Before these relationships are considered, however, some episcopic properties of the 'magnetite' and the separate 'ilmenite' are presented below.

D. Some Episcopic Properties of the 'Magnetites'

a) Microhardness.

A G.K.N. micro-indentation hardness tester has been used to obtain hardness measurements on ten samples of the 'magnetite' in the Clauchlands sheet.

This instrument, which has been described by Bowie and Taylor (1958), has a square diamond pyramid indentor with a 136° included angle between opposite faces producing square indentations.

The hardness value, which is a function of load over area, can be calculated from the length of the diagonals by use of the formula:

$$H = \frac{2P\sin\theta}{D^2}$$

where H is the diamond pyramid hardness number, P the load in kilograms, D the length of the diagonal in millimeters and θ is half the included angle between opposite pyramid faces.

In practice the hardness numbers for different values of the load P

have been tabulated against the diagonal length, and thus are readily determined from measurements of the diagonals. However, since the hardness of most surfaces tends to be anisotropic, both diagonals are usually measured and the hardness obtained as a function of the mean diagonal length.

The hardness values obtained with this instrument are Vickers Hardness Numbers and must be distinguished from Knoop Hardness Numbers which are obtained from a diamond indentor in which one diagonal is about seven times the length of the other, (Cameron 1959), thus producing a diamond-shaped indentation. The sources of error associated with microhardness determination have been discussed by Nicholl (1962).

Measurements have been made using a 100g load in order to investigate (a) the variation in hardness within an individual grain and (b) the variation in mean hardness of the 'magnetite' throughout the intrusion. The results are summarized in Table 3 and plotted graphically in Figure 7.

The mean hardness values are higher than those of magnetite and lie intermediate between the values quoted for magnetite and those given for maghemite. (Bowie and Taylor 1958). This might indicate that the minerals are γ-phases but the presence of impurities such as Al^{+++} within the 'magnetite' might also result in hardness values higher than those of magnetite, so that firm conclusions are not justified.

Hardness measurements made within individual grains do not show significant variations which could be interpreted as inhomogeneity nor do the means for single grains differ significantly from those obtained from different grains.

b) Reflectivity

The reflectivity of a mineral is defined as the percentage of normally incident light that is reflected from the surface, and it is a property which

Table 3.

Microhardness Values of the 'Magnetites'

Sample	Horizon (feet)	Hardness Values			Mean	
S 2	126	1048	1115	1064	1076	...three measurements on a single grain.
		1097	1115	1033	1082	...single measurements on three different grains
S 3	122	698	707	649	685	...three measurements on a single grain.
		724	554	835	704	...single measurements on three different grains
S 6	110	657	772	988	806	...three measurements on a single grain.
		813	1048	519	793	...single measurements on three different grains
S30	82	870	847	920	879	...three measurements on a single grain.
		894	920	858	891	...single measurements on three different grains
S31	78	824	803	946	858	...three measurements on a single grain.
		858	920	642	807	...single measurements on three different grains.
S34	66	673	642	566	627	...single measurements on three different grains
S36	58	690	792	858	780	...three measurements on a single grain.
		724	803	824	784	...single measurements on three different grains
S40	42	762	858	613	744	...single measurements on three different grains
C41	14	762	882	907	850	...three measurements on a single grain.
		673	762	792	742	...single measurements on three different grains
S47	$2\frac{1}{2}$	782	835	824	814	...single measurements on three different grains

Microhardness range for :

Magnetite = 540-600

Maghemite = 890-990 (Bowie and Taylor 1958).

Figure 7.

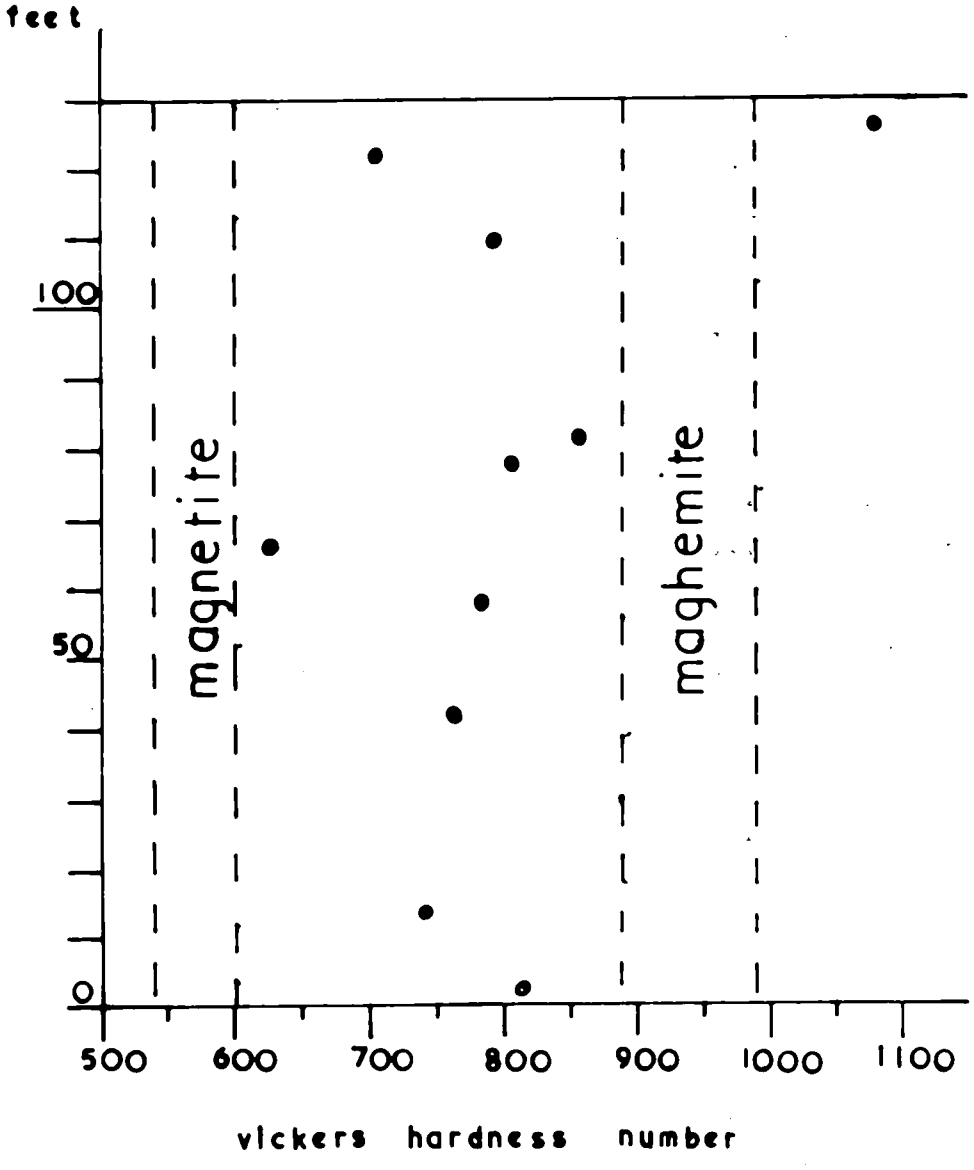
feet
100
50
0
magnetite
maghemite
500
600
700
800
900
1000
1100
vickers hardness number

Figure 7.

Microhardness (VHN) of some 'magnetites' in the Clauchlands Sheet. The ranges for magnetite and maghemite (according to Bowie and Taylor 1958) are shown for comparison.

may be measured accurately ($\pm$ 1%), by photoelectric methods. (Bowie and Taylor 1958; Nicholl 1962; Gray and Millman 1962). It is the most fundamental property of an isotropic mineral that can be determined by reflection microscopy. (Cameron 1959).

The equipment used in the present investigation has been described by Nicholl (1962) and consists of an eleven-stage photomultiplier, E.M.I. type 6094B, powered from a 2Kv stabilized power pack, the current from the collector being recorded directly on a spot galvanometer (Cambridge Instrument Co. Ltd.) having an internal resistance of 450 ohms.

The reflectivity in white light has been determined for 'magnetite' from eight samples, by comparison with a pyrite standard of 54% (Bowie and Taylor 1958), and these results are given in Table 4.

The variation in reflectivity within an individual sample does not exceed about 2% and, indeed there appears to be no appreciable variation in reflectivity within the intrusion as a whole. The values obtained, however, are much lower than would be expected for magnetite. (Bowie and Taylor 1958).

The white colour of a mineral, however, depends on the nature and distribution of its absorption bands, the medium of observation, and the spectral response of the observer's eye. (Gray and Millman 1962). If, therefore, the reflectivity is determined for incident light of different wavelengths, a spectral reflectivity profile may be constructed which is characteristic of the mineral.

Only cubic minerals, however, show a single spectral reflectivity profile that is constant in shape regardless of orientation. Minerals of lower symmetry are bireflecting and hence the character of the spectral reflectivity profile changes with orientation.

The spectral reflectivity profiles of the 'magnetite' in four samples

Table 4.

Reflectivity Values of the 'Magnetites'

1. Reflectivity in white light using pyrite as standard at 54%.

Sample	R% Different Grains			R% Mean
S 2	17.0	16.5	16.5	16.7
S 7	19.5	17.0	16.5	17.2
S11	20.5	20.0	18.0	19.5
S32	16.5	18.0	17.0	19.5
S34	16.5	19.0	17.0	17.8
S36	19.5	17.0	19.0	18.5
S39	17.5	17.0	17.0	17.2
S47	18.5	19.0	18.5	18.7

2. Dispersion of the reflectivity.

Sample	610mμ	470mμ blue.	520mμ green.	575mμ yellow.	600mμ orange.	700mμ red.
Pyrite*	54.8	46.0	52.0	54.5	54.8	56.0
S 7	16.8	15.7	17.4	16.0	16.3	18.0
S11	17.3	15.2	15.1	17.3	17.8	17.5
S32	16.8	15.5	15.6	16.5	15.8	17.5
S39	17.8	17.5	17.4	16.3	17.8	17.7
3439**	16.5	15.0	15.1	15.3	16.3	17.5
Magnetite**	20.0	24.7	22.3	18.6	18.9	18.4
Magnetite***	21.1	27.6	25.0	22.1	21.9	19.5

* Pyrite reflectivity as given by the National Physical Laboratory. (via Bowie 1963).

** Magnetite/ulvöspinel ore from Lac de la Blache, Quebec Canada.

*** Data from Gray and Millman (1962).

have been determined by measuring the reflectivity at wavelengths of 470mμ, (blue), 520mμ (green), 575mμ (yellow) 600mμ (orange), 700mμ (red) and 610mμ, using a Schott continuous band interference filter, with a half value width of 250Å supplied by Bellingham and Stanley, London.

The reflectivities have been measured against a pyrite standard, taking values of the reflectivity of pyrite in light of various wavelengths as listed in Table 5. These values have been supplied by the National Physical Laboratory (via Bowie 1963), and represent the most recent data on the reflectivity of pyrite.

The profiles are shown in Figure 8 and may be compared with the spectral reflectivity profiles of magnetite which have been drawn from the data of Gray and Millman (1962).

Figure 8 also includes the spectral reflectivity profile of a magnetite/ulvöspinel ore from Lac de la Blache, Quebec (Departmental Collection No.3439) which has been measured as part of the present investigation. This ore is brown in colour and the intergrown ulvöspinel can be clearly seen (Plate Va).

It is apparent that the reflection characteristics of the Clauchlands 'magnetites' resemble those of the magnetite/ulvöspinel ore. However, the existence of an 'ulvospinel'-type intergrowth in these minerals has not been confirmed although there is indirect evidence which indicates that they may be present in some samples. This evidence is discussed below.

c) Deuteric Alteration of 'magnetite'

Sample S5 is unique in the present collection in that it has suffered extensively from the action of deuteric solutions. This activity has resulted in the selective etching of the 'magnetite' whilst leaving the 'ilmenite' lamellae unattacked (Plate VI). These structures clearly develop inwards

Table 5.

Pyrite Reflectivity as given by the National Physical Laboratory (via Bowie 1963)

mμ	R%
440	41.2
460	44.3
480	47.5
500	50.2
520	52.0
540	53.2
560	54.0
580	54.7
600	54.8
620	55.0
640	55.2
660	55.7
680	56.0
700	56.0

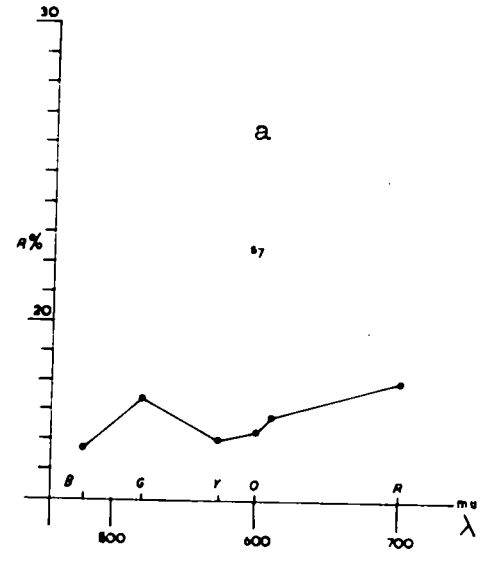
30
a
A%
20
B
G
Y
O
R
mu
λ
500
600
700

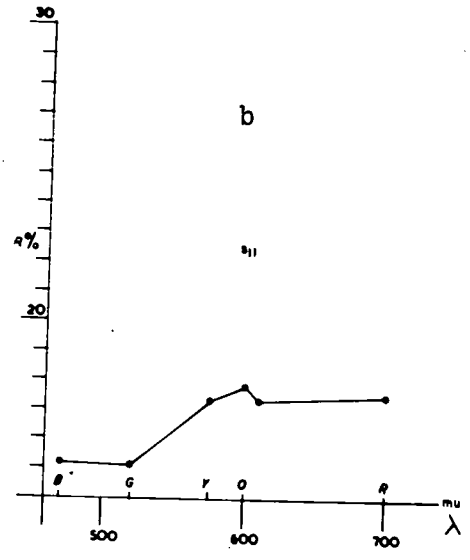
30
b
A%
20
B
G
Y
O
R
mu
λ
500
600
700

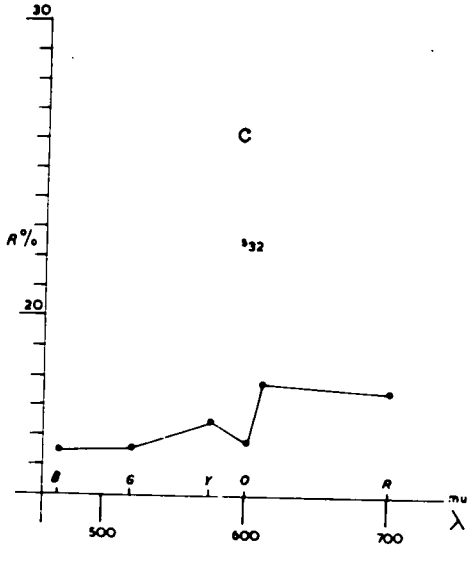
30
c
A%
20
B
G
Y
O
R
mu
λ
500
600
700

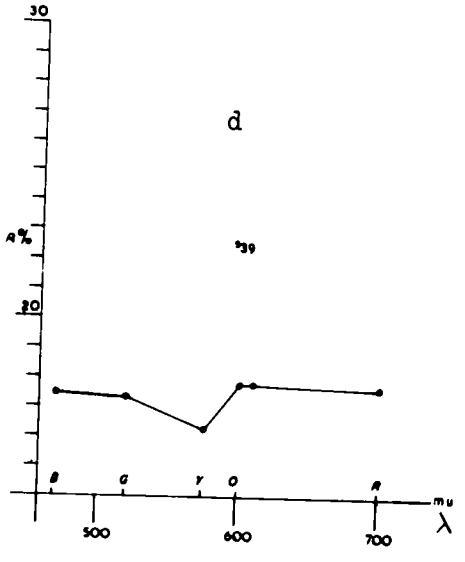
30
d
A%
20
B
G
Y
O
R
mu
λ
500
600
700

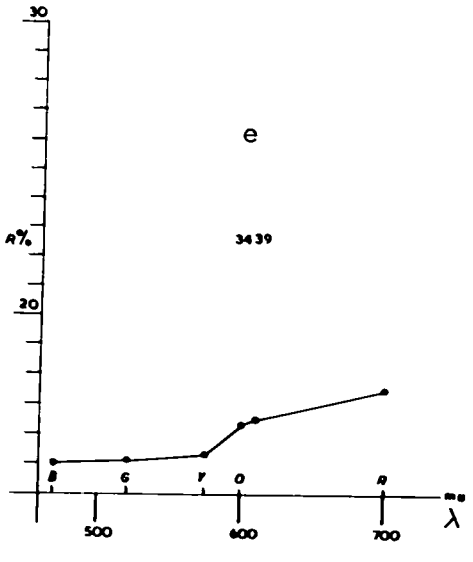
30
e
A%
20
B
G
Y
O
R
mu
λ
500
600
700

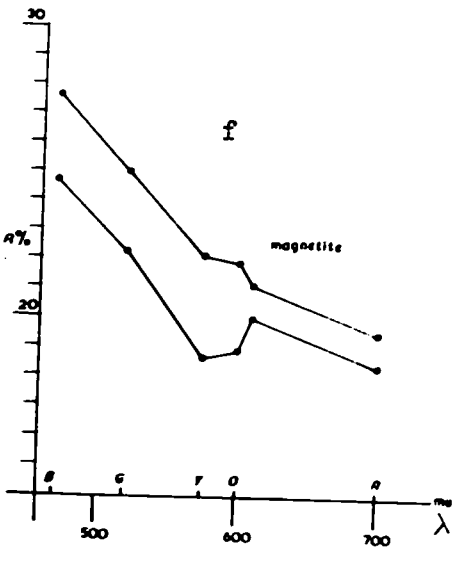
30
f
A%
magnetite
20
B
G
Y
O
R
mu
λ
500
600
700

Figure 8.

Spectral reflectivity profiles

a) 'Magnetite' in sample S7 from the Clauchlands Sheet

b) 'Magnetite' in sample S11 " " " "

c) 'Magnetite' in sample S32 " " " "

d) 'Magnetite' in sample S39 " " " "

e) Magnetite/ulvöspinel intergrowth from Lac de la Blache, Canada. (Departmental Collection No 3439).

f) Magnetite (two sets of data) after Gray and Millman 1962.

Plate VI

a) 'Magnetite' from the Clauchlands sheet (Sample S5) that has been etched by natural agencies, (probably deuteric solutions). Polished section. Plane polarised light. Magnification X100.

b) Detail of the etched structure. Plane polarised light. Magnification X400.

a.

Plate VI.

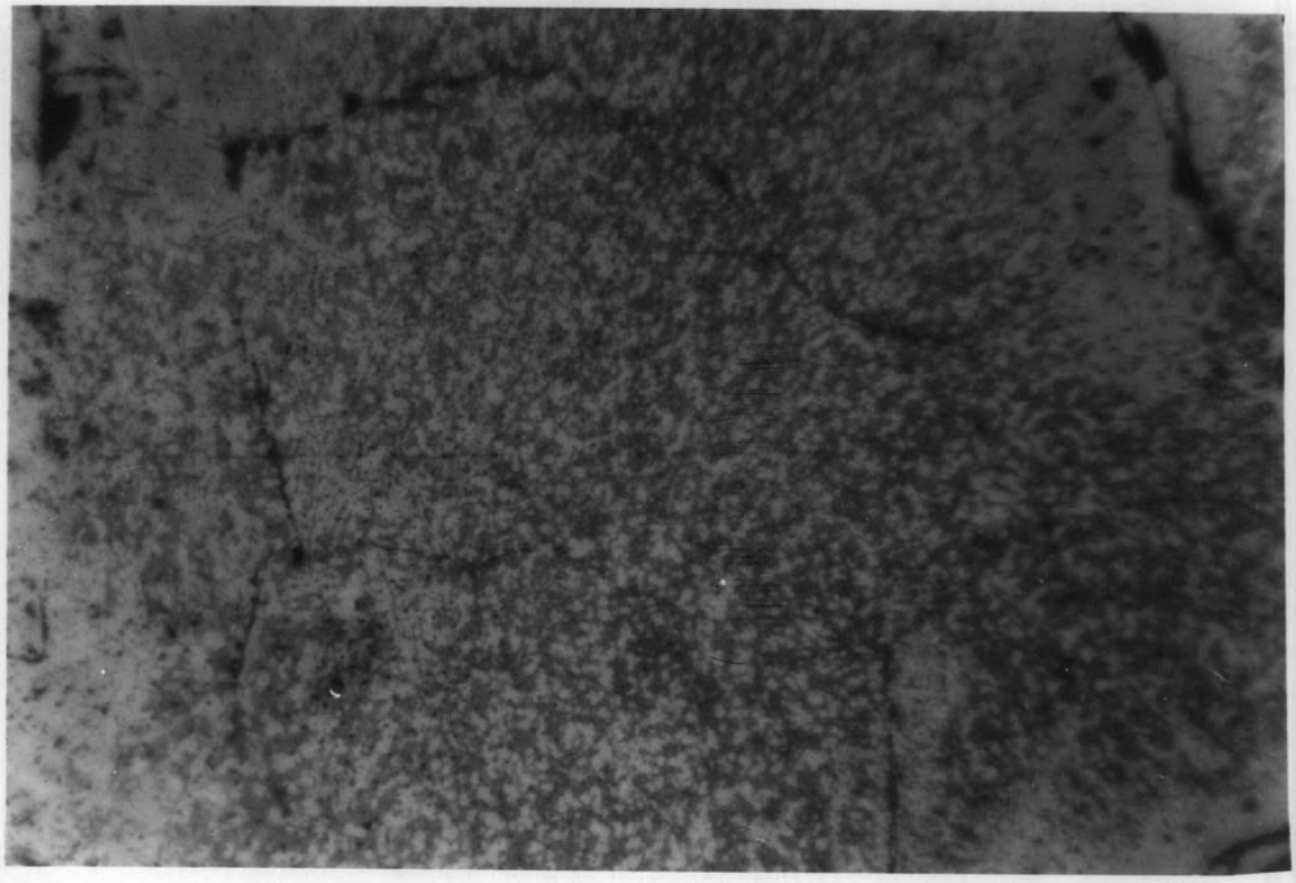

b.

from the margins of the crystals and there can be no doubt but that they have been produced deuterically.

The etched 'magnetite' has a cellular texture that closely resembles an intergrowth of two cubic phases, and since X-ray analysis shows that two spinels are present in this sample (a_o = 8·394A) it is concluded that they are intergrown in this manner.

A number of other samples are known to contain more than one spinel phase, and hence this result is of particular value because it indicates that these spinels are probably intergrown, rather than occurring as separate crystals or as zoned crystals.

E. Some Episcopic Properties of the 'Ilmenites'

a) Microhardness

Microhardness measurements have been made on the separate 'ilmenite' crystals from four samples within the Clauchlands sheet. The measurements have been made using a 100g load in order to investigate (a) the variation in hardness within individual grains and (b) the variation in mean hardness from one sample to the next.

The results are summarized in Table 6 and they show that the mean values do not differ appreciably from those given for ilmenite by Bowie and Taylor (1958) and that there is no significant variation within individual grains.

b) Reflectivity

The spectral reflectivity profiles of the separate 'ilmenite' from four samples have been determined against a pyrite standard, and these results are summarized in Table 7.

Table 6.

Microhardness Values of the Separate 'Ilmenites'

Sample	Horizon (feet)	Hardness Values			Mean	
S36	58	724	673	772	723	...three measurements on a single grain.
		690	752	715	719	...single measurements on three different grains
C39	46	642	690	620	651	...three measurements on a single grain.
		734	634	715	694	...single measurements on three different grains
C42	32	673	634	649	655	...three measurements on a single grain.
		698	536	716	650	...single measurements on three different grains
C43	28	724	835	824	794	...three measurements on a single grain.

Microhardness range for ilmenite : 536-703 (Bowie and Taylor 1958).

Table 7.

a) Reflectivity Values of the Separate 'Ilmenites'

Sample	610mu	470mμ blue	520mμ green	575mμ yellow	600mμ orange	700mμ red
Pyrite*	54.8	46.0	52.0	54.5	54.8	56.0
S12	18.3	19.5	16.3	15.3	16.8	17.5
S30	17.3	20.5	18.3	17.3	15.2	18.0
S36'	17.3	17.0	17.7	14.8	14.2	17.5
C42'	18.8	18.5	18.2	17.3	16.2	18.5
Ilmenite a)**	19.3	28.3	26.1	21.3	20.0	19.5
b)	22.2	30.0	28.2	23.7	22.1	21.7

* Pyrite reflectivity as given by the National Physical Laboratory (via Bowie 1963).

' C42 is abbreviation for sample number A/C/3/42.

**Data from Gray and Millman (1962)
a) Section perpendicular to (0001).
b) Section parallel tp (0001).

b) Reflectivity of the Opaque Minerals in the Sandstone above the Clauchlands Sheet. Sample A/C/3/13.

Sample	610mμ	470mμ blue	520mμ green	575mμ yellow	600mμ orange	700mμ red
Pyrite*	54.8	46.0	52.0	54.5	54.8	56.0
'Hematite'	23.9	23.0	25.0	19.9	20.8	22.2
'Magnetite'	17.3	19.5	17.2	14.8	15.7	15.9
Hematite a)***	22.8	30.3	28.0	25.3	22.4	21.0
b)	26.4	31.6	30.3	28.2	25.7	24.3

* Pyrite reflectivity as given by the National Physical Laboratory (via Bowie 1963).

***Data from Gray and Millman (1962).
a) Section perpendicular to (0001).
b) Section parallel to (0001).

The spectral reflectivity profiles are shown in Figure 9 where they may be compared with profiles for ilmenite sections cut parallel to (0001) and perpendicular to (0001) which have been drawn from the data of Gray and Millman (1962).

The present measurements have been made on unoriented sections and hence differ from the profiles of oriented sections. The profiles, however, are surprisingly similar amongst themselves considering the random nature of the ilmenite sections.

F. The Opaque Minerals in the Sandstones above the Intrusion

The sandstones immediately above the intrusion contain abundant opaque minerals, and these rocks have been found to have the same reversed direction of magnetization as found within the intrusion itself (See later). Therefore, it is important to investigate such material in order to determine whether the ores have originated within the sandstone or whether they have been introduced from the intruding magma.

In polished section the opaque minerals occur as abundant anhedral grains and as minute specks disseminated throughout the rock. They are white in colour with a reflectivity of about 23·5% in white light and a microhardness of about 790, and at high magnification (400 diameters) a faint reflection pleochroism is clearly visible in which the colour varies from white to a delicate mauve. Between crossed nicols they show greyish-blue anisotropy colours and a complex recrystallised texture (Plate VII). X-ray analysis confirms that the mineral is hematite although the 'characteristic' red internal reflections are absent.

A spectral profile is shown in Figure 9 where it may be compared with profiles for oriented sections of hematite drawn from the data of Gray and

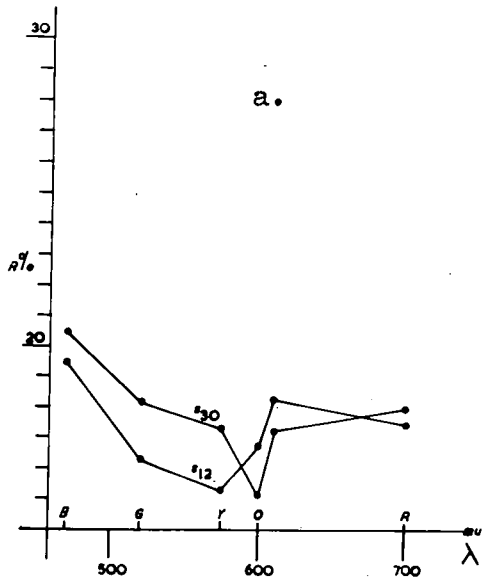
a.
30
20
R%
S30
S12
B
G
Y
O
R
500
600
700
λ

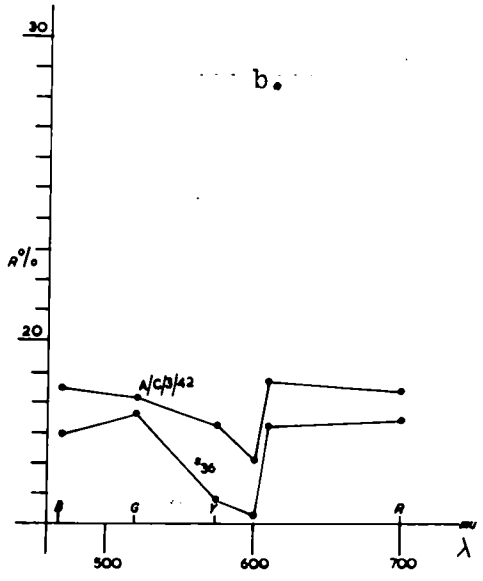
b.
30
20
R%
A/C/3/42
S36
B
G
Y
O
R
500
600
700
λ

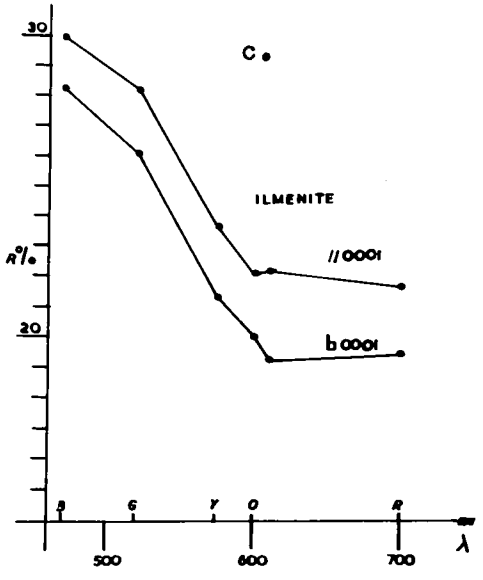
c.
30
20
R%
ILMENITE
//0001
b 0001
B
G
Y
O
R
500
600
700
λ

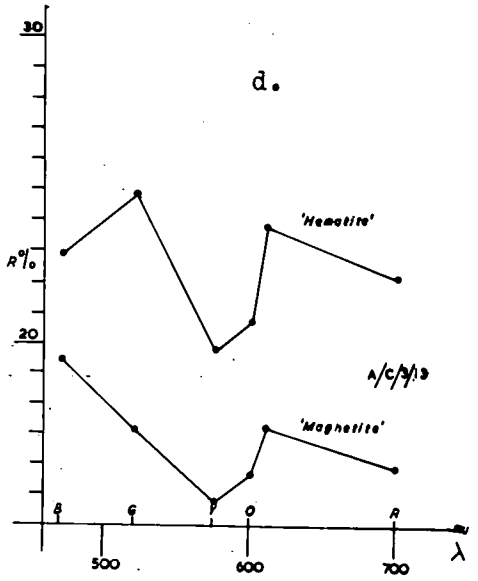
d.
30
20
R%
'Hematite'
A/C/3/13
'Magnetite'
B
G
Y
O
R
500
600
700
λ

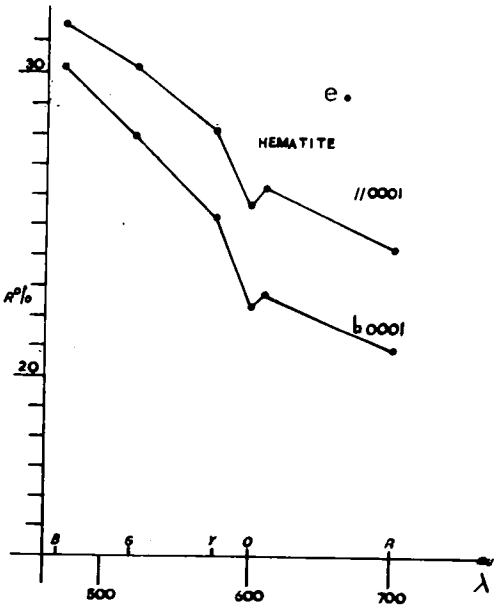
e.
30
20
R%
HEMATITE
//0001
b 0001
B
G
Y
O
R
500
600
700
λ

Figure 9.

Spectral reflectivity profiles.

a) Separate 'ilmenite' in samples S12 and S30 from the Clauchlands Sheet.

b) Separate 'ilmenite' in samples S36 and A/C/3/42 from the Clauchlands Sheet.

c) Ilmenite (oriented sections) after Gray and Millman 1962.

d) 'Hematite' and 'magnetite' in sample A/C/3/13 from sandstone at top contact of the Clauchlands Sheet.

e) 'Hematite' (oriented sections) after Gray and Millman 1962.

Plate VII

a) Polished section of the baked sandstone above the Clauchlands sheet. The opaque minerals are mostly 'hematite' (white). 'Magnetite' (light grey) is visible at the centre of the field, rimmed by 'hematite'. Dark areas are quartz and the black areas are pits in the polished surface. Plane-polarised light. Magnification X100.

b) As above but viewed between crossed nicols to show the complex granular texture of the 'hematite' grains.

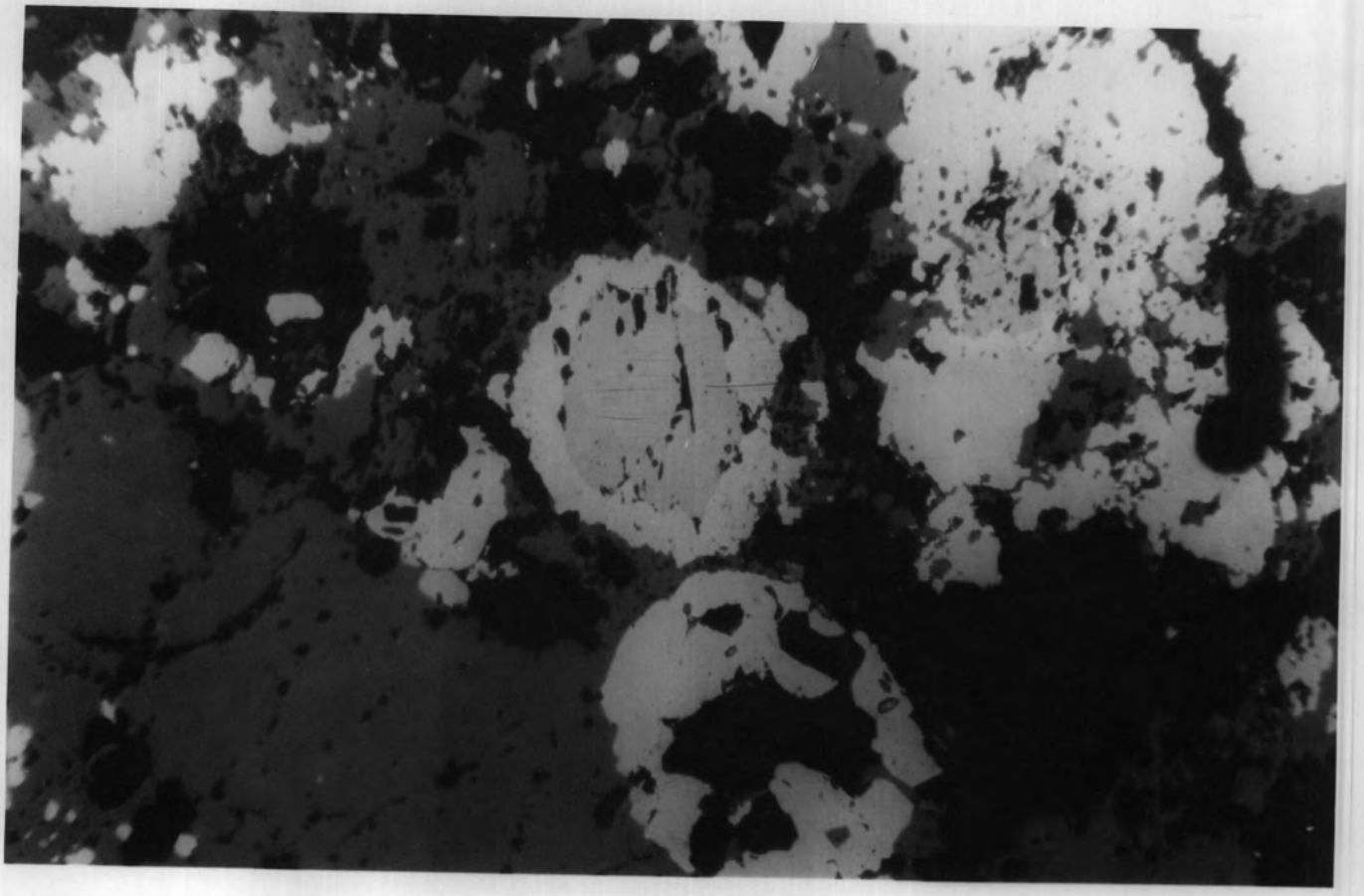

a.

Plate VII.

b.

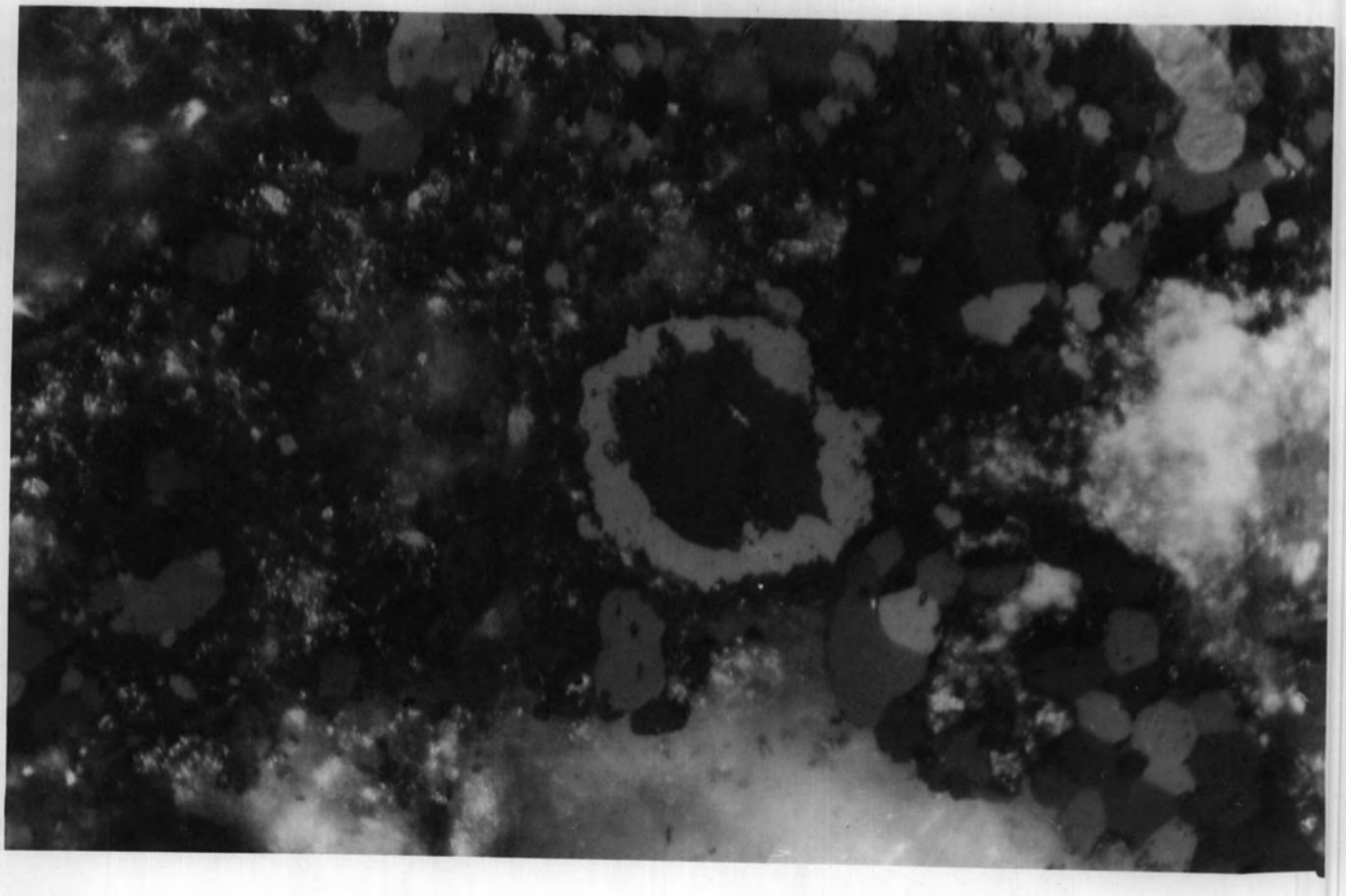

and Millman (1962). This profile probably has little meaning since the hematite crystals are composed of complex granular aggregates which are randomly oriented.

However, a small amount of 'magnetite' is also present among the ores, and its spectral reflectivity profile is also given in Figure 9. Compared with the hematite, the 'magnetite' has an appreciably lower reflectivity and the shape of the profile is closely similar to that shown in Figure 8 for the magnetites investigated by Gray and Millman (1962).

The mineral is distinctly blue when compared with the hematite, and with a microhardness of 776 it is appreciably harder than magnetite so that it might be an oxidised γ-phase (see earlier). It is isotropic and apparently homogeneous and occurs typically as the core within hematite grains (Plate VII).

Its presence in this environment may be interpreted as being relict crystals of unoxidised 'magnetite' or, in view of the recrystallized nature of the hematite it may represent localised dissociation of hematite to magnetite. Similar textures are known to form in hematite ores that have been sintered at 1100°C - 1300°C (R. Phillips personal communication).

The sandstones above the intrusion, belong to the Lamlash-Machrie Sandstone Group in which the rocks have a characteristic dull reddish colour. Immediately above the intrusion, however, these sandstones are dark grey, hard and laminated, and contain the hematite/magnetite assemblage described above.

The X-ray data (Chapter IV) indicates that the hematite contains about 35 mol % $FeTiO_3$ in solid-solution. Detrital hematite grains in red sandstones commonly contain intergrown 'ilmenite' (R. Phillips Personal Communication) and, therefore, it seems probably that this assemblage has been derived from the sandstone.

G. The 'Magnetite' - 'Ilmenite' Relationships in the Clauchlands Sheet

a) Statement of Problem

Oriented intergrowth textures of the type illustrated in Plate IX are considered in metallography to be the normal result of unmixing from solid solution and, indeed, are taken as a definite indication that unmixing has occurred. (Mehl and Barret 1930). Therefore, it is natural when such textures are observed in ores that they also should be interpreted as of exsolution origin.

Moreover, since oriented intergrowths of 'magnetite' and 'ilmenite' are the commonest opaque oxides in igneous rocks (Newhouse 1936), they are frequently figured in the literature as the typical examples of an exsolution texture. (Schwartz 1931; Edwards 1947; Bastin 1950; Schwartz 1951).

However, similar textures are known that are undoubtedly the result of replacement. For example, Lindsley (1962) has produced the 'magnetite' - 'ilmenite' intergrowth illustrated in Plate VIII, by oxidation of ulvöspinel. There can be no doubt, therefore, that such 'magnetite' - 'ilmenite' intergrowths can be produced by the oxidation of a β-spinel.

Gruner (1929) has shown by examining polished sections cut parallel to the (111) planes that the ilmenite lamellae lie in the (111) planes of the 'magnetite'. He found that in such sections the 'ilmenite' occurs as a more or less complete network of equilateral triangles.

Gruner (1929) has also shown the structural reason for the occurrence of these intergrowths. Every third and seventh (111) plane in magnetite consists of oxygen ions only, whilst in ilmenite, every third (0001) plane also consists of oxygen ions. Therefore, the intergrowths are made possible by the sharing of a common plane of oxygen ions.

Thus the textures of 'magnetite' - 'ilmenite' intergrowths generally

Plate VIII

A triangular intergrowth between magnetite solid-solution and ilmenite solid-solution produced by oxidation of synthetic ulvöspinel.

Polished section. Plane polarised light. Magnification X 2200.

Taken from Lindsley (1962).

Plate VIII.

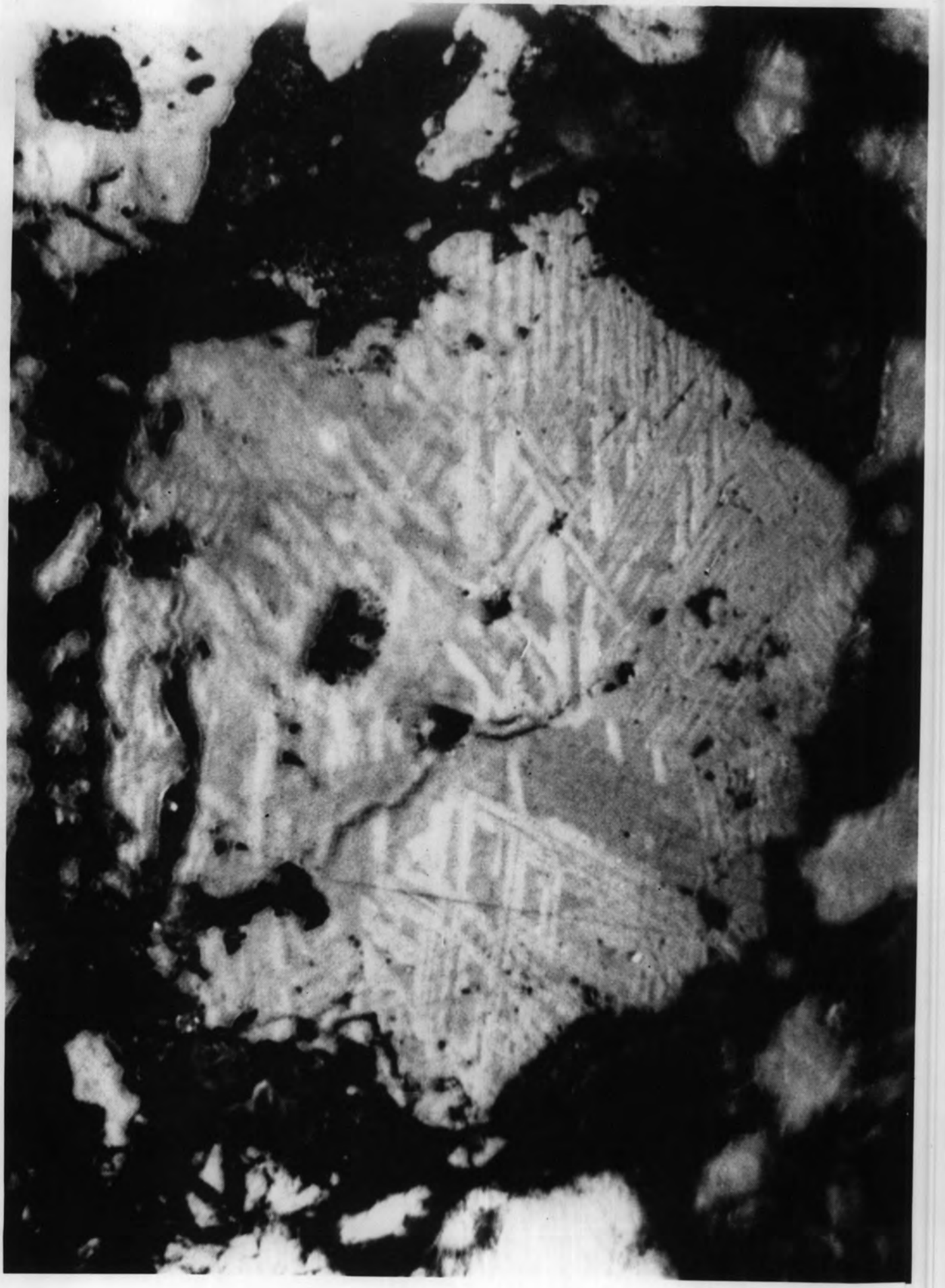

are of a type which would be regarded in metallography as being of exsolution origin and, moreover, there appear to be satisfactory structural reasons to account for such intergrowths between a cubic and rhombohedral phase.

However, in recent years reliable data on the synthetic system FeO-Fe_2O_3-TiO_2 has accumulated which leaves little doubt but that even at high temperatures there is only limited miscibility between Fe_3O_4 and $FeTiO_3$ (Schmahl and Meyer 1959; Webster and Bright 1961; Taylor 1961) and that the maximum amount of 'ilmenite' in such intergrowths should not exceed about 21 wt% if it is solely the result of exsolution (Taylor 1961).

b) The evidence from the Clauchlands sheet

In the present investigation a collection of material has been examined which represents a complete section through the Clauchlands sheet, the average interval between samples being of the order of four feet. If exsolution has taken place, then it might be expected to show up in this section since it includes samples ranging from the rapidly chilled marginal facies to slowly cooled material from within the body of the intrusion.

The ore minerals in the marginal facies appear to be homogeneous 'magnetites'. They are bluish grey or brownish in colour, have a moderate reflectivity and are isotropic. Some are oxidised to 'hematite' showing strong red internal reflections and such martitization is especially common at the lower margin where it is associated with the introduction of abundant hydrothermal calcite.

The homogeneous 'magnetites', however, rapidly become oriented intergrowths of 'magnetite and 'ilmenite', and in sample S46 five feet above the base, all crystals are of this type, and many contain a large amount of 'ilmenite'.

This transition appears to be less rapid at the top margin for in sample

S2, from four feet below the top, the majority of the crystals are still homogeneous 'magnetites' although with pronounced anomalous anisotropy, and where 'ilmenite' does appear it forms broad irregular lamellar intergrowths. However, twelve feet below the top in sample S4, all the crystals contain oriented intergrowths of 'ilmenite' in which the (ilmenite occurs as lamellae parallel to (111) and also as irregular segregations. It is an abundant component, and in some cases, forms at least half of the crystal.

Apart from the narrow marginal zones, the opaque minerals through most of the intrusion consist predominantly of these oriented intergrowths. The proportion of 'ilmenite' varies considerably and the intergrowths may form well defined triangular textures (Plate IX) in which the 'ilmenite' occurs as fine incipient lamellae or as well developed lamellae, or in which the lamellae may show a seriate distribution. The 'ilmenite' may also occur as broad laths oriented predominantly in one direction and frequently showing a seriate distribution (Plate X), or the intergrowths may contain irregular blebs and segregations of 'ilmenite' often distributed near to the crystal margins, (Plate XI). Less commonly, the intergrowths may be of a complex character as illustrated in Plate XII.

However, 'ilmenite' also exists within the body of the intrusion as crystals which are clearly of primary origin. Such 'ilmenite' forms homogeneous anhedral crystals which may occur quite separately from the 'magnetite' or they may occur in intimate association with 'magnetite' - 'ilmenite' intergrowths (Plate XIII), and indeed the irregular 'ilmenite' illustrated in Plate XI is probably of this type.

'Ilmenite' of this type first appears about thirty feet above the base of the intrusion. 46ft. above the base (sample S39) it appears as but a few discrete crystals in association with 'magnetite' - 'ilmenite' intergrowths

Plate IX

'Magnetite'-'Ilmenite' Intergrowths in the Clauchlands Sheet

a) Incipient lamellae of 'ilmenite' (light grey) oriented in triangular texture within 'magnetite', (medium grey). The dark grey area at top left is a silicate mineral showing internal reflections is also visible to the right of the field. Polished section. Crossed nicols. Magnification X100.

b) 'Ilmenite' lamellae (light grey) intergrown with 'magnetite' (dark) and forming a well developed Widmanstätten texture. Polished section. Crossed nicols. Magnification 100.

c) Abundant 'ilmenite' (light grey to white) intergrown with 'magnetite' (dark). The lamellae vary in size from fine to coarse, thus forming a seriate texture. Polished section. Crossed nicols. Magnification X100.

Plate IX.

a.

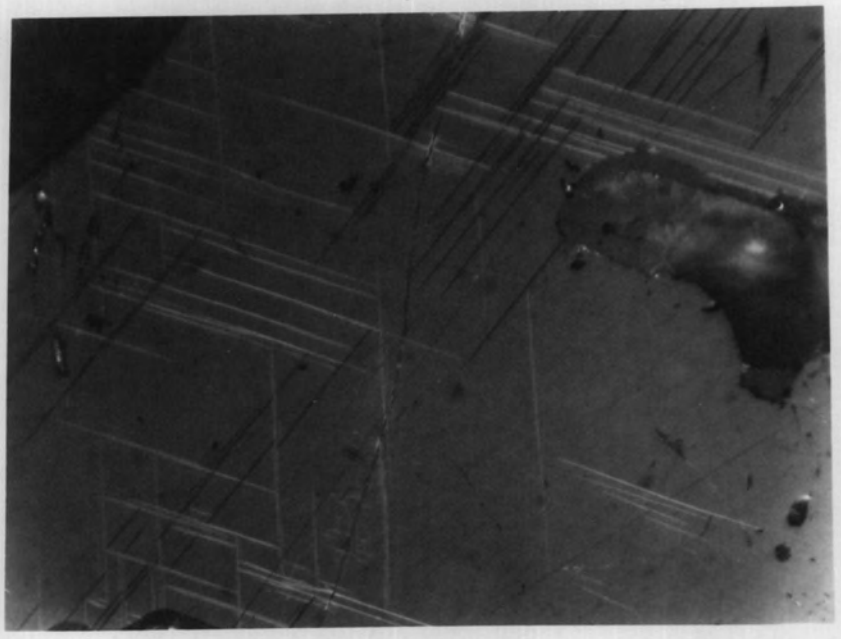

b.

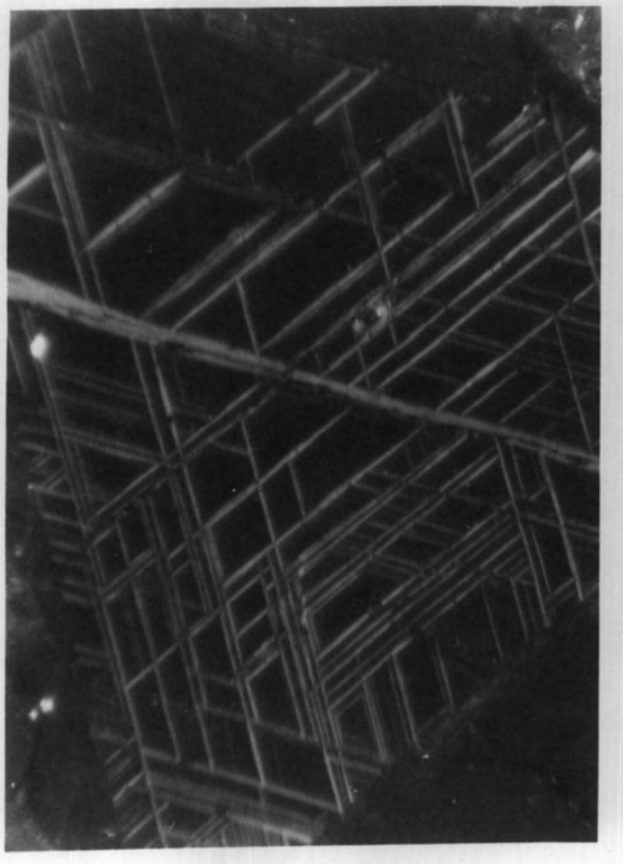

c.

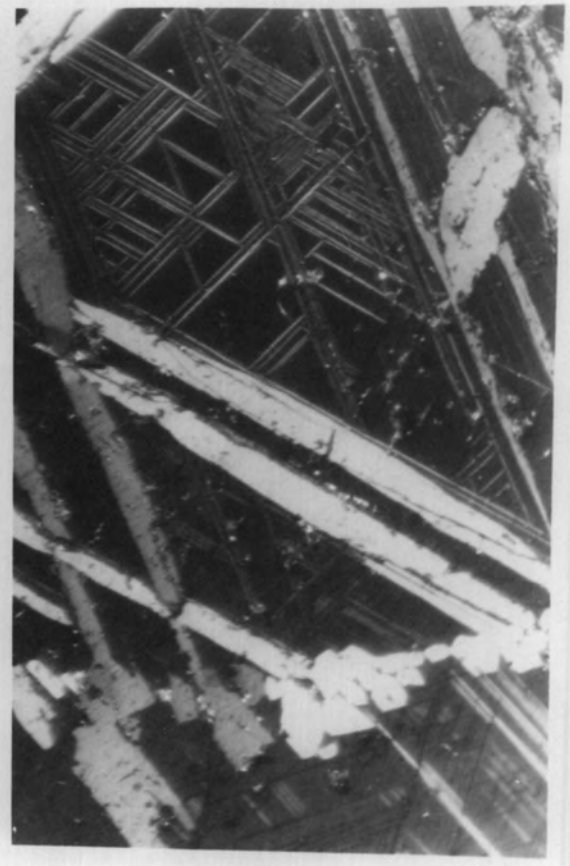

Plate X

'Magnetite'-'Ilmenite' Intergrowths in the Clauchlands Sheet

a) Coarse lamellae of 'ilmenite' (light grey) intergrown predominantly in one direction in 'magnetite' (black). A few fine lamellae of 'ilmenite' are also present. Silicates, showing internal reflections are visible at top left. Polished section. Crossed nicols. Magnification X100.

b) Lamellae of 'ilmenite' (light grey) intergrown predominantly in one direction in 'magnetite' (black). Polished section. Crossed nicols. Magnification X100.

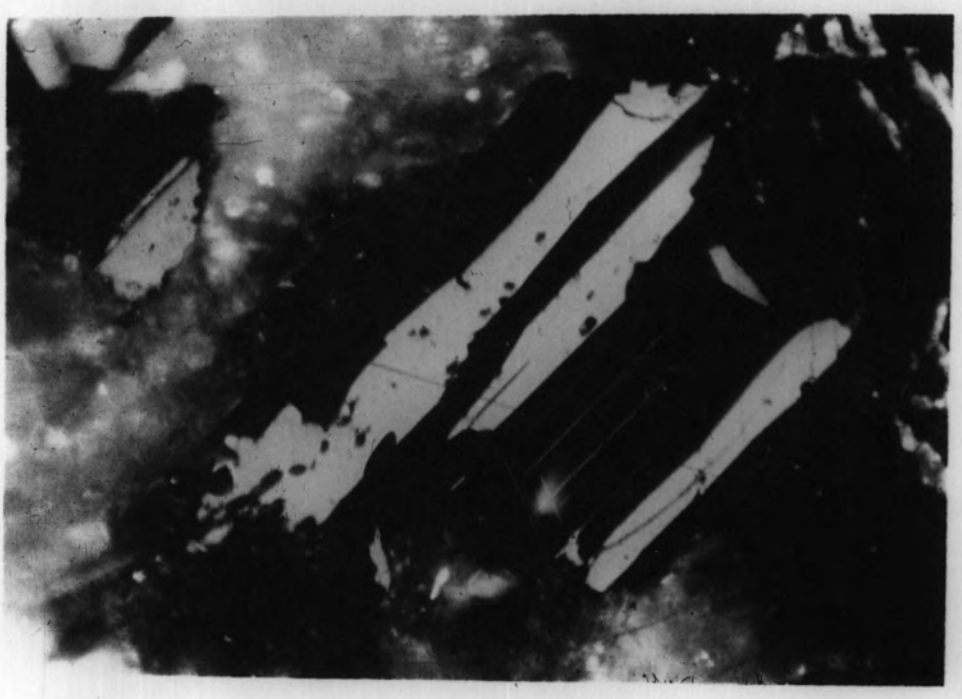

a.

Plate X.

b.

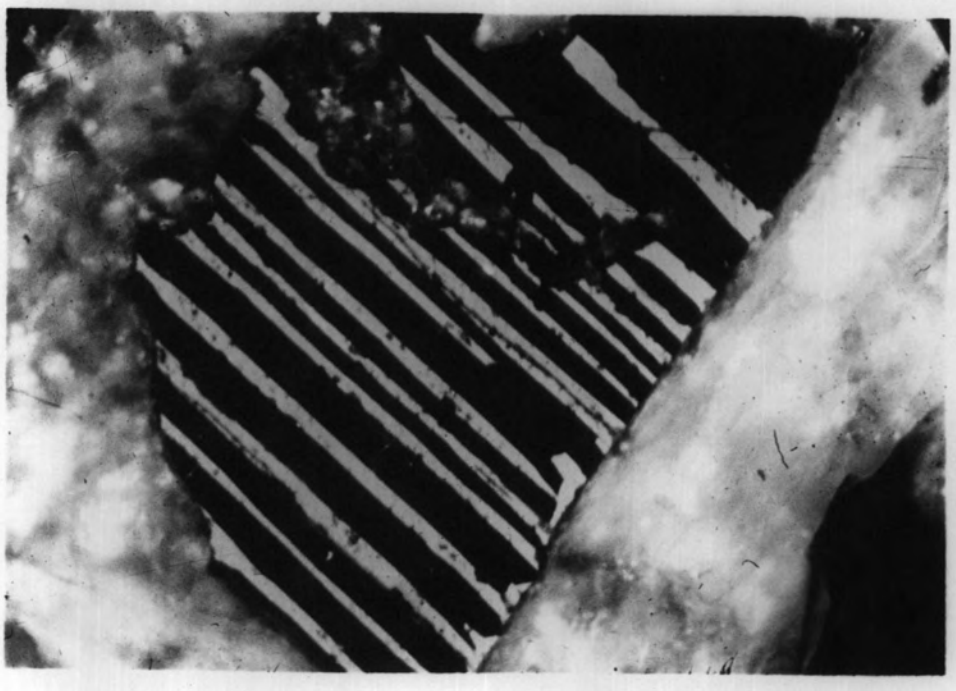

Plate XI

'Magnetite'-'Ilmenite' Intergrowths in the Clauchlands Sheet

a) 'Ilmenite' (white and medium grey) occurring as coarse blebs and incipient lamellae in 'magnetite' (black). Silicates, showing internal reflections are visible at top right. Polished section. Crossed nicols. Magnification X100.

b) Coarse 'ilmenite' (grey) concentrated at the margins of a 'magnetite' crystal containing intergrown 'ilmenite' lamellae. Polished section. Crossed nicols. Magnification X100.

c) Coarse 'ilmenite' (grey and white) occurring in 'magnetite' containing a seriate intergrowth of 'ilmenite' lamellae. Polished section. Crossed nicols. Magnification X100.

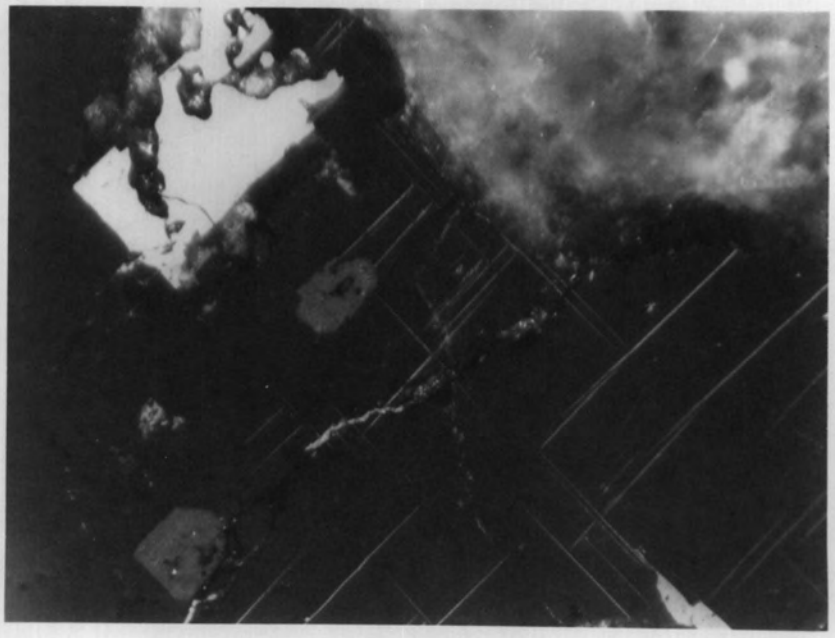

a.

Plate XI.

b.

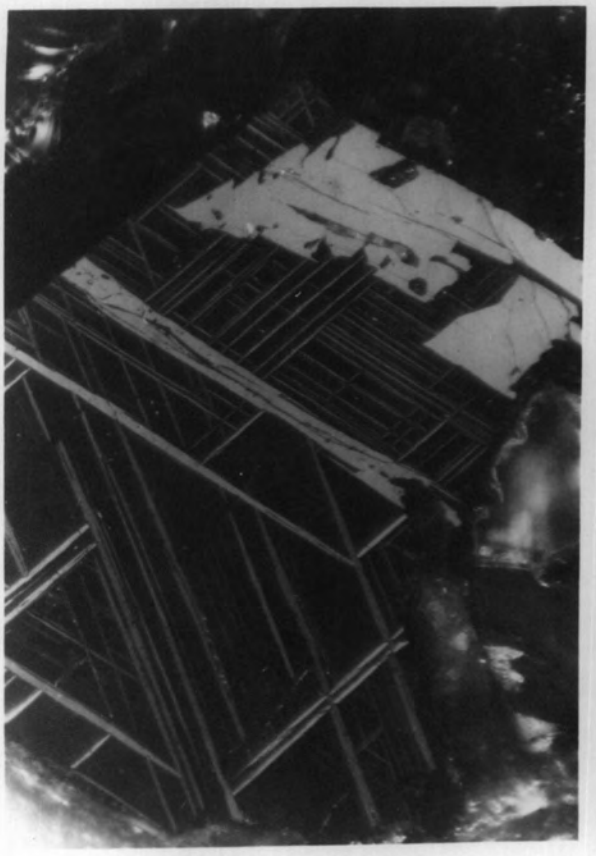

c.

Plate XII

'Magnetite'-'Ilmenite' Intergrowths in the Clauchlands Sheet.

A complex intergrowth between 'magnetite' and 'ilmenite'. 'Ilmenite' forms a large part of this intergrowth. Polished section. Crossed nicols. Magnification X100.

Plate XII.

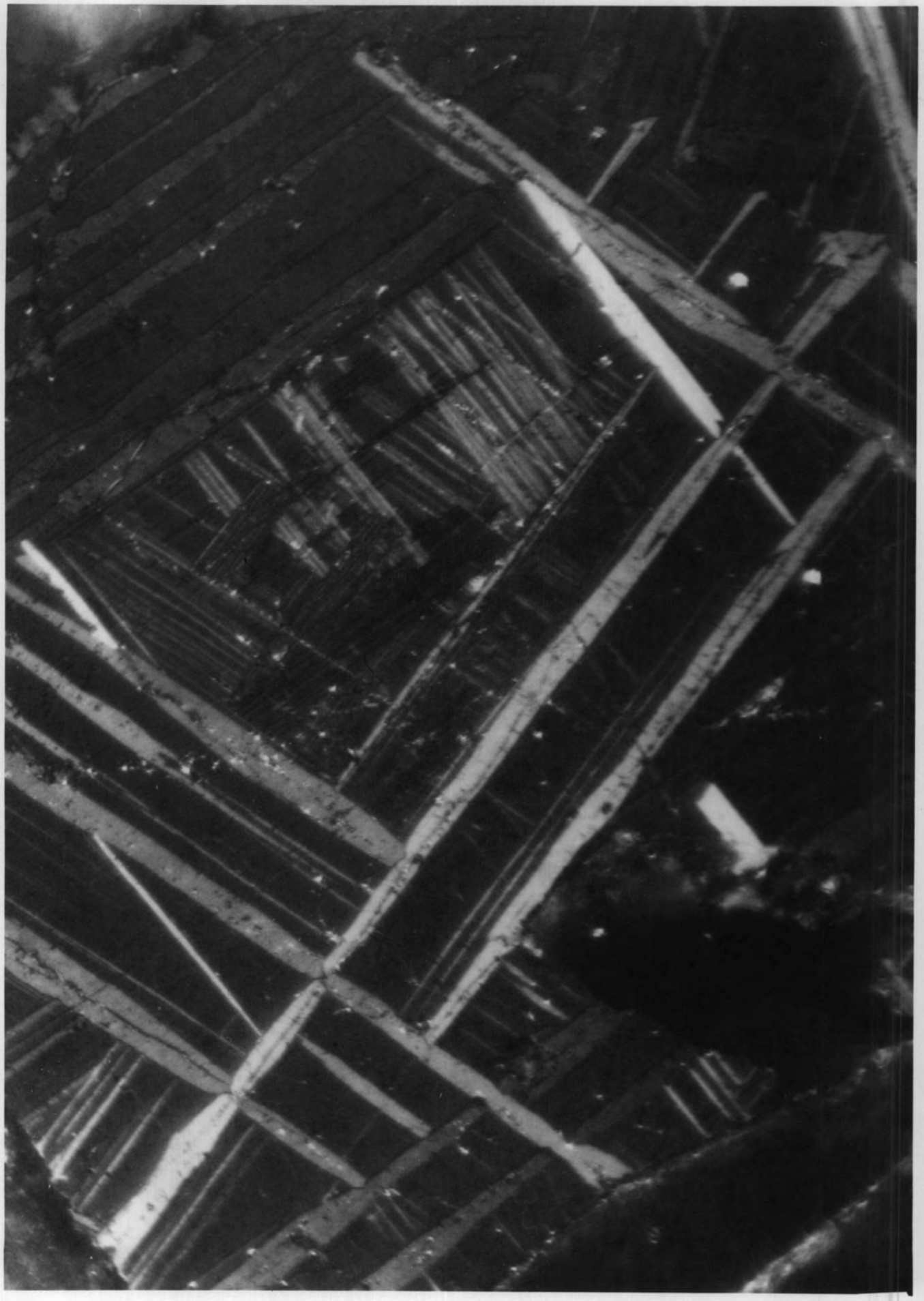

but at 54ft (sample S37), it forms the principal ore mineral together with only minor amounts of 'magnetite' - 'ilmenite' intergrowths, whilst at 58ft (sample S36), there are no intergrowths and the opaque minerals consist of homogeneous 'ilmenite' and apparently homogeneous 'magnetite' as separate crystals with 'magnetite' in excess. However, the presence of ilmenite as a fine intergrown phase is indicated by the results of X-ray analysis in (sample S34).

This association of separate 'magnetite' and 'ilmenite' persists up to at least 66ft (sample S34) but at 74 ft, (sample S32), the 'magnetite' - 'ilmenite' intergrowths are once more dominant with only minor amounts of discrete 'magnetite' and 'ilmenite'.

Ascending the next twenty feet of the intrusion, the ore minerals consist of the association intergrown 'magnetite' - 'ilmenite', separate 'ilmenite', and rarely some separate 'magnetite', often with the separate 'ilmenite' present in appreciable amounts.

Above 106ft (sample S7), however, the separate 'ilmenite' crystals disappear and the ores consist only of 'magnetite' - 'ilmenite' intergrowths, which at the top margin are replaced by homogeneous 'magnetite'.

These relationships are summarized in Figure 10. It is tempting at first to interpret them as indicating the exsolution of 'ilmenite' from a homogeneous 'magnetite' in order to form the 'magnetite' - 'ilmenite' intergrowths, and then to carry this process one step further in order to obtain the association separate 'magnetite' separate 'ilmenite' which appears in the slowly cooled centre of the sheet. This, however, cannot be the correct explanation for the separate 'ilmenites' are clearly earlier than the 'magnetite' - 'ilmenite' intergrowths as can be seen in Plate XIII.

Figure 10.

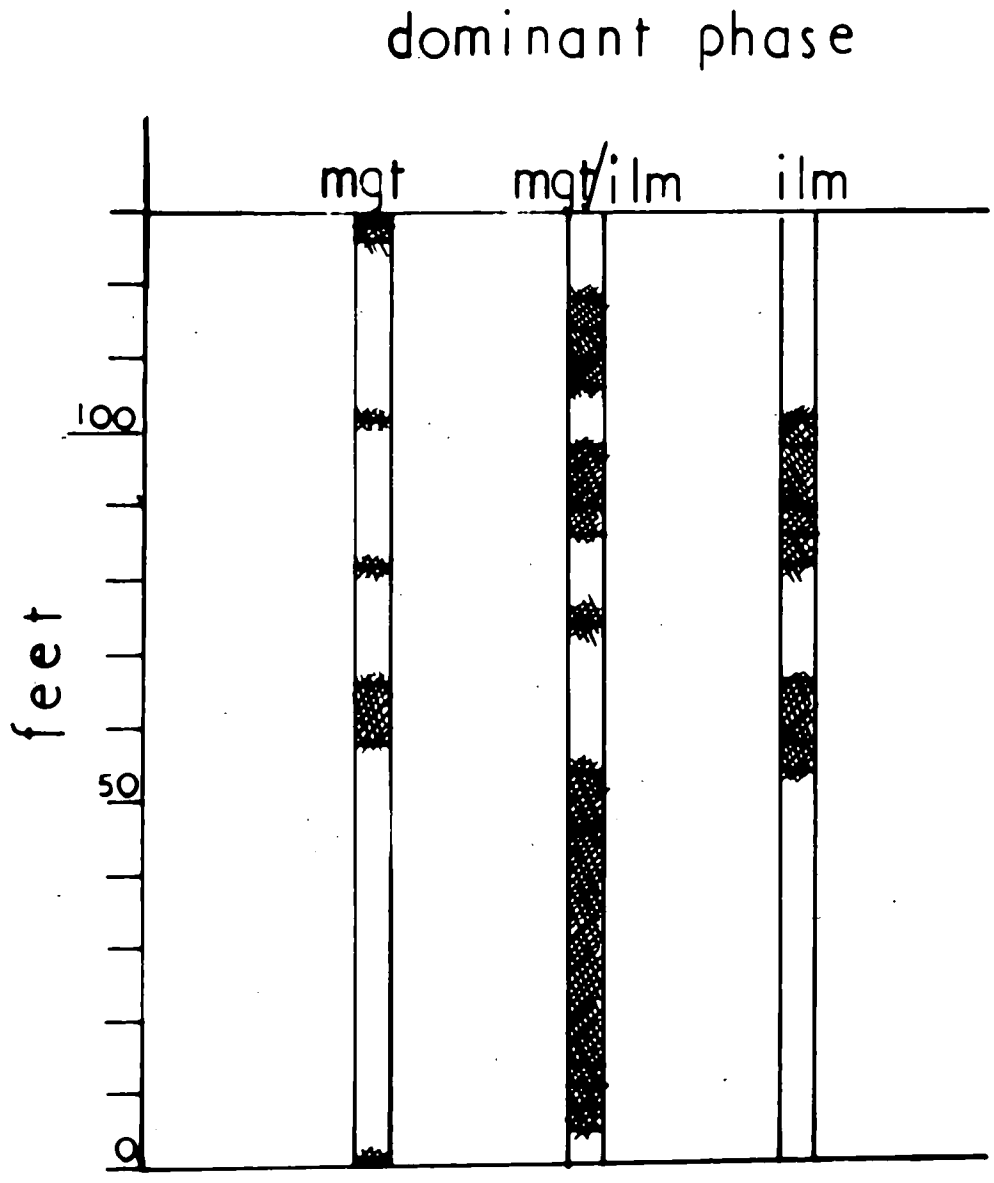

Figure 10.

Changes in the relative importance of the phases 'magnetite', 'magnetite'-'ilmenite' intergrowth and separate 'ilmenite' in a vertical section of the Clauchlands Sheet; shown diagrammatically.

Plate XIII

'Magnetite'-'Ilmenite' Intergrowths in the Clauchlands Sheet

a) Separate 'ilmenite' (light grey) associated with 'magnetite' containing an oriented intergrowth of 'ilmenite' lamellae. The black area at the lower part of the field of view is silicate. The euhedral margin of the intergrown crystal is seen where the 'ilmenite' lamellae are terminated. Polished section. Crossed nicols. Magnification X100.

b) Separate 'ilmenite' (grey) and silicate minerals. The latter show internal reflections. Polished section. Crossed nicols. Magnification X100.

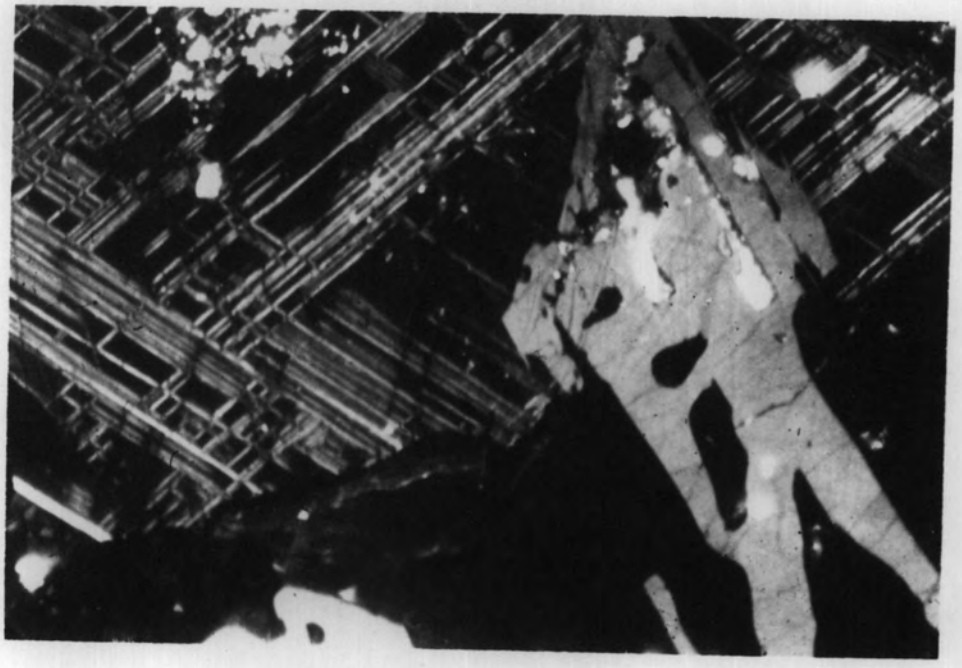

a.

Plate XIII.

b.

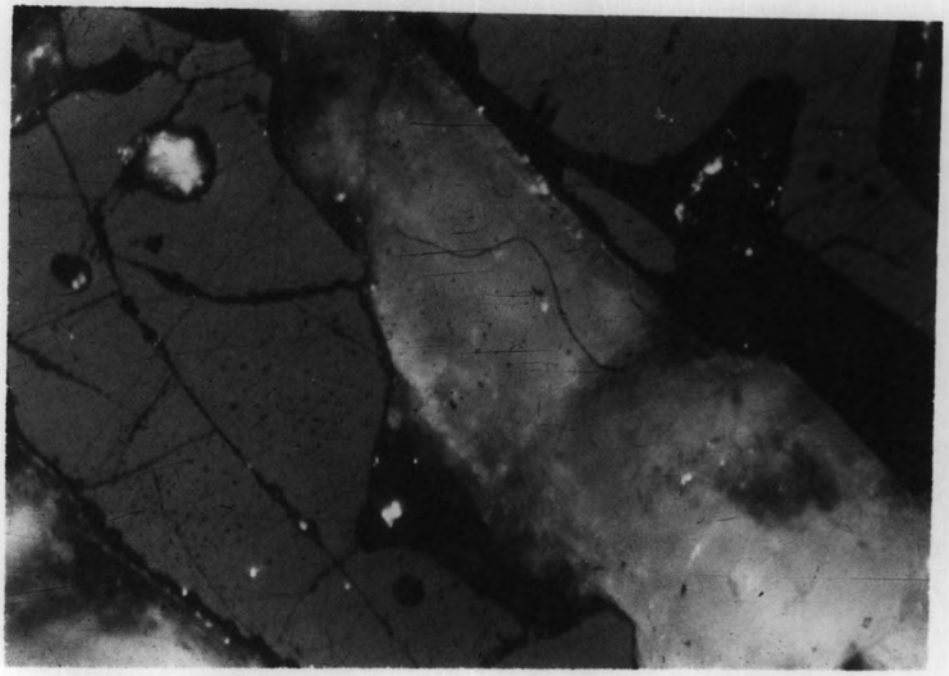

The 'magnetite' - 'ilmenite' relationships, therefore, cannot be explained simply as the results of an exsolution process. However, in the light of the present data and also that of the subsequent Chapters, an interpretation of these relationships is attempted in Chapter VI.

H. Examination by Replica Electron Microscopy

The 'magnetites' in the Clauchlands sheet are generally brown in colour, and as described earlier, there are some indications that where more than one cubic phase is present then these may be intergrown in the magnetite/ulvöspinel manner. Such intergrowths, however, have not been resolved optically at magnifications up to 1500 diameters, but this may be due to the relatively fine grained nature of the host rock as compared with the plutonic rocks in which such intergrowths have been reported previously. However, by means of replica electron microscopy it is possible to extend the range of investigation to much higher magnifications.

The techniques for obtaining surface replicas are to be found in standard textbooks on electron microscopy such as Wyckoff (1949). In the present investigations collodion or cellulose acetate replicas have been obtained from etched surfaces and then shadowed with a Au-Pd mixture. The resulting replicas are negatives so that elevations on the etched surface appear as hollows and vice versa.

The results of such an examination carried out on known magnetite/ulvöspinel intergrowths are illustrated in Plate XV. These results were obtained with sample E.G. 2308, an ore-rich hypersthene-olivine gabbro from the Skaergaard intrusion of East Greenland, which had been etched momentarily in HF. (Vincent and Phillips 1954). The appearance of this etched surface

Plate XIV

Sample EG2308 from the Skaergaard intrusion of East Greenland, after momentary etching with HF. (Phillips and Vincent 1954). The rhomb shaped crystallites are thought to be ulvöspinel (Phillips and Vincent 1954). The electron micrographs illustrated in Plate XV refer to the areas between these crystallites. Polished section. Plane polarised light. X100.

Plate XIV.

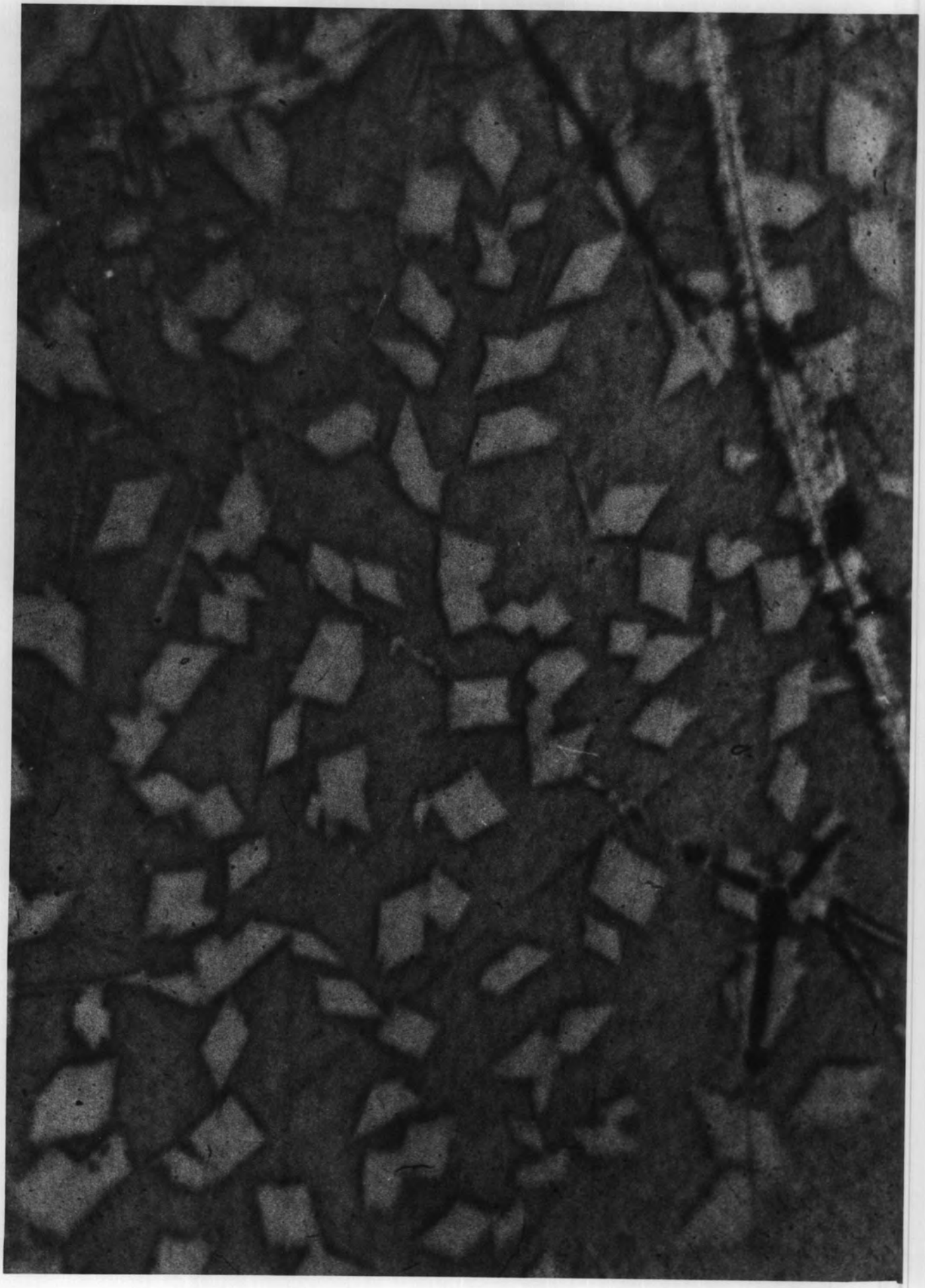

Plate XV

Electron Micrographs of Sample EG2308

a) Intergrowth of magnetite, ulvöspinel and ilmenite. The ilmenite lamellae appear as smooth troughs and magnetite-ulvöspinel intergrowths form the intervening areas. Surface replica of polished section. Magnification X4000.

b) Intergrowth of magnetite, ulvöspinel and ilmenite. Surface replica of polished section. Magnification X6000.

c) Intergrowth of magnetite and ulvöspinel, showing that the two phases are present in roughly equal proportions. Surface replica of polished section. Magnification X8000.

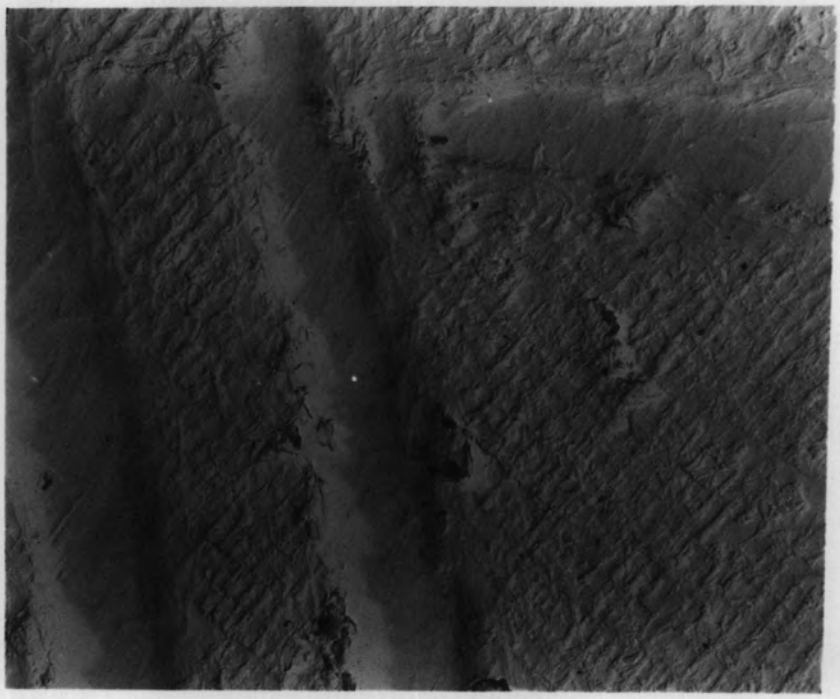

a.

Plate XV.

b.

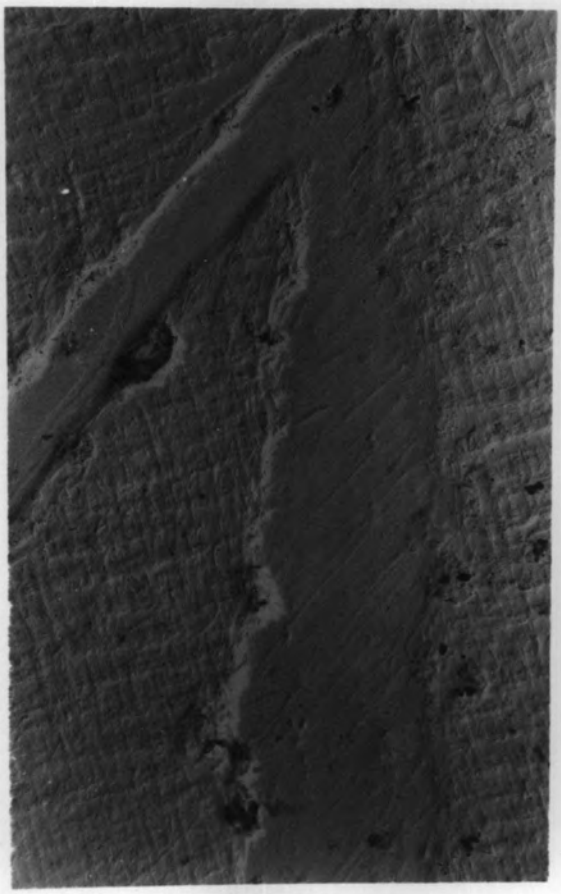

c.

at a magnification of 100 diameters is shown in Plate XIV. Apart from the prominent rhomb shaped crystallites, which are possibly ulvöspinel (Vincent and Phillips 1954), the surface is also intersected by a few fine ilmenite lamellae. In polished section, the 'magnetite' between the ilmenite lamellae is seen to consist of two constituents intergrown on a fine scale so that at a magnification of 770 diameters it has the appearance of a closely woven piece of cloth (Vincent and Phillips 1954). Plate XV shows this texture at magnifications ranging from 4000 diameters up to 8000 diameters and it can be seen that the areas between the ilmenite lamellae consists of a regular intergrowth of two phases at right angles and in roughly equal proportions. This result, therefore, confirms the earlier investigations and, in agreement with the published chemical analysis (Vincent and Phillips 1954), indicates that the two phases are present in roughly equal amounts.

Plate XVI shows the results of a similar investigation carried out on samples from the Clauchlands sheet which on the basis of X-ray and thermo-magnetic data were likely to contain intergrown cubic phases. Although the ilmenite lamellae can be clearly recognised in these sections there does not appear to be any significant microstructure in the 'magnetite' areas.

A similar investigation was attempted with the deuterically altered sample (S5), but it was found that even after momentary etching with HF the resultant texture was too coarse to be satisfactorily identified with the electron microscope at its minium magnification of 3500 diameters.

In terms of the Clauchlands sheet, therefore, these results do not indicate the presence of sub-microscopic intergrowths within the magnetites. However the results with the Skaergaard sample have shown that this method of investigation is capable of detecting such intergrowths.

Plate XVI

Electron Micrographs of 'Magnetite' in the Clauchlands Sheet

a) Sample S 12. The oriented 'ilmenite' lamellae appear as smooth troughs. The 'magnetite' between the lamellae has been etched by conc. HCl but shows no regular microstructure. Surface replica of polished section. Magnification X4000.

b) Sample S37 . The oriented 'ilmenite' lamellae appear as smooth troughs. The fact that the lamellae are intergrown at right angles indicates that this is a section parallel to (100) of the 'magnetite' host. The 'magnetite' between the lamellae has been etched by conc. HCl but shows no regular microstructure. Surface replica of polished section. Magnification X8000.

Plate XVI.

a.

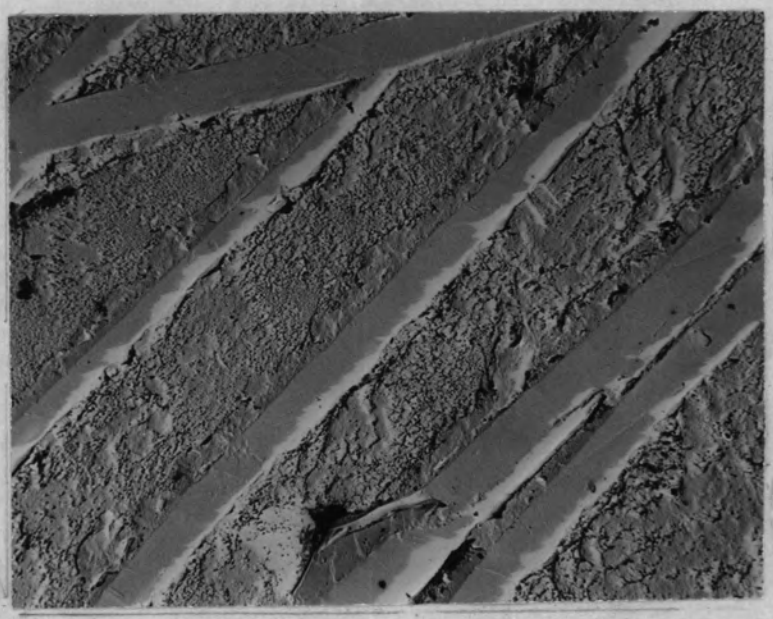

b.

I. Summary

The opaque minerals in the Clauchlands sheet have been found to consist mainly of 'magnetite' and 'ilmenite', these terms being used to describe isotropic minerals having properties similar to those of natural magnetite (Fe_3O_4) and anisotropic minerals having properties similar to those of natural ilmenite ($FeTiO_3$). Parentheses have been used since these minerals may have variable compositions which cannot be determined in reflected light.

The 'magnetites' are generally brown in colour and their spectral reflectivity profiles closely resemble that obtained from a 'magnetite'/'ulvöspinel' intergrowth.

This result indicates how brown the 'magnetites' are and suggests that the colour may be due to intergrowths similar to the 'magnetite'/ulvöspinel sample. Such intergrowths are not visible in reflected light nor have they been seen using the electron microscope, and therefore, it is concluded that the 'magnetites' are generally homogeneous. However, in one sample that has been etched deuterically, and in which X-ray analysis has shown there is more than one cubic phase, the resultant cellular texture would suggest that such an intergrowth is present.

Microhardness measurements on the 'magnetites' have shown them to have hardness values intermediate between those of magnetite and maghemite. This may indicate that the 'magnetites' are γ-phases although impurities such as Al^{3+} would also increase the hardness of the minerals.

The reflectivity profiles of the separate 'ilmenites' have been found to be similar amongst themselves and the microhardness values do not differ significantly from those of natural ilmenite.

Examination of a vertical section through the Clauchlands sheet has shown that the 'magnetite' and 'ilmenite' commonly occur as oriented intergrowths. Homogeneous 'magnetite' occurs at the margins of the intrusion, however, with no 'ilmenite' whilst in the centre of the sheet a separate 'ilmenite' phase coexists with the 'magnetite' - 'ilmenite' intergrowths and can be shown to be earlier than the intergrowths. These relationships, therefore, cannot be explained simply in terms of the exsolution of 'ilmenite' from an originally homogeneous high temperature 'magnetite'.

The sandstones above the intrusion have been found to contain abundant opaque minerals but these are mainly 'hematite' grains showing complex recrystallized textures. The 'hematite' has probably been derived from the sandstones. Subordinate amounts of 'magnetite' are also present but it is unlikely to have been introduced from the magma.

Chapter IV. X-Ray Analyses

A. Introduction

Material for the present analyses has been obtained from the Clauchlands sheet, and the magnetic fraction has been extracted on a Cook separator, as described in Appendix 1. Although this fraction consists largely of 'magnetite', some admixed 'ilmenite' is usually present as well, since it occurs as a fine intergrowth in the 'magnetite' (Chapter III) and cannot be separated.

The samples have been X-rayed using a Phillips PW1010 X-ray generator in conjunction with a wide angle goniometer PW1050 and diffractometer unit PW1051. Copper Radiation (K_α = ~~1.54178Å~~ 1.54046Å has been used) and, therefore, a discriminator unit PW4082 has been included to minimise the effect of the resultant fluorescent radiation.

Where possible normal cavity mounts have been prepared in the standard aluminium holders which are supplied with the above equipment. However, such mounts require a relatively large amount of material (about 1-2 grms) and when such quantities were not available, smear mounts have been prepared on glass slides. In both cases, however, a small amount of pure silicon has been added to act as an internal standard.

As described in Chapter III, a separate 'ilmenite' phase appears towards the centre of the Clauchlands sheet as well as the 'magnetite/'ilmenite' intergrowths. Such 'ilmenite' is not magnetic and, therefore, is not retained with the magnetic fraction, and since it forms less than 1% of the residue, its extraction would be very difficult. However, this phase has been X-rayed by drilling small amounts of powder directly from a polished sample and

Figure 11.

a.

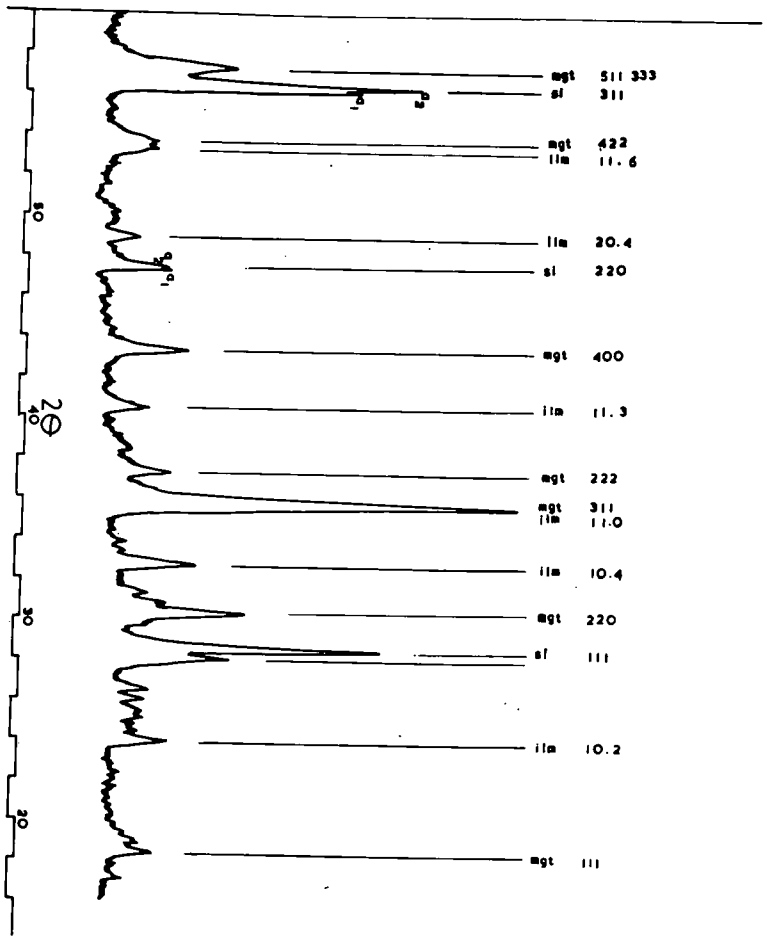
mgt 511 333
sl 311
mgt 422
ilm 11.6
ilm 20.4
sl 220
mgt 400
ilm 11.3
mgt 222
mgt 311
ilm 11.0
ilm 10.4
mgt 220
sl 111
ilm 10.2
mgt 111
50
40
30
20
2Θ

b.

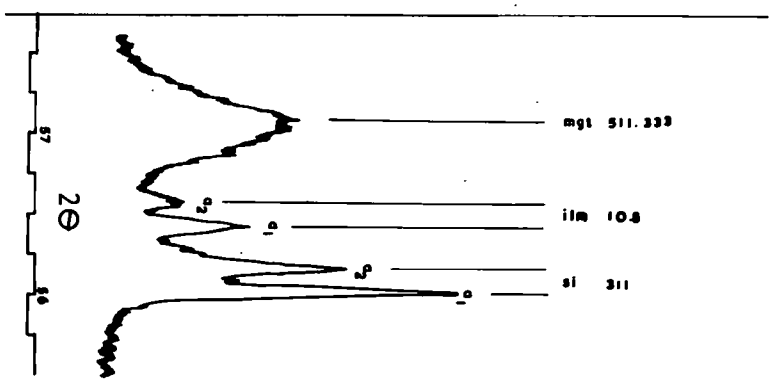
mgt 511.333
ilm 10.8
sl 311
57
56
2Θ

Figure 11.

Diffractometer record of 'magnetite' (sample S2) from the Clauchlands Sheet.

a) Record from $2\theta = 16°$ to $2\theta = 60°$ made at a scanning rate of 2°/min., with a chart speed of 800 mm/hr, using CuK_α radiation with a discriminator. 'Magnetite', intergrown 'ilmenite' and silicon peaks are present.

b) Record from $2\theta = 55.5°$ to $2\theta = 57.75°$ made at a scanning rate of 1/8° /min., with a chart speed of 400 mm/hr, using CuK_α radiation with discriminator. Silicon internal standard.

obtaining a powder photograph.

This technique has been described by Sorem (1960), and although long exposures (up to 70 hrs) are required the method has the advantage of giving results which apply unambiguously to the separate 'ilmenite' phase and not to the intergrown 'ilmenites'.

These results and also those for the 'magnetite'/'ilmenite' intergrowths are discussed in the following sections.

B. 'Magnetites' and Intergrown 'Ilmenites'

The reflections for both these phases appear on the same diffractometer record (Figure 11), and after correction with reference to the silicon internal standard, they may be used to determine the cell parameters.

a) 'Magnetites'

Twenty one samples have been analysed and the results represent the unit cell edges of the 'magnetites' throughout the Clauchlands sheet.

The unit cell edge has been determined from the 511/333 reflection which for pure magnetite appears at $2\theta = 57.06^{\circ}$ Table 8) and thus may be corrected with reference to the 311 reflection of the silicon standard which appears at 56.174° . (Table 9).

The position of the 511/333 reflection changes with variation in the unit cell edge as can be seen in Figure 12 and the unit cell edge can readily be calculated from the corresponding d-spacing, since there is a simple relationship between d_{333} and a_o as shown in Figure 13.

The results, which are summarized in Table 10 and shown graphically in Figure 4, indicate a regular increase in the unit cell edge away from the margins of the intrusion reaching a maximum value of $a_o = 8.4855\text{Å} \pm 0.002\text{Å}$ at approximately the centre of the sheet.

Table 8.

X-Ray Data for Magnetite from Bisperg, S. Sweden. (Basta 1953). CoK_{α} Radiation.

I	d Å	2θ °	hkl
30	4.847	18.31	111
70	2.966	30.13	220
100	2.530	35.48	311
10	2.419	37.16	222
60	2.096	43.16	400
40	1.712	53.53	422
80	1.614	57.06	511/333
90	1.483	62.64	440
15	1.327	71.02	620
20	1.279	74.14	533
10	1.264	75.17	622
15	1.2112	79.05	444
20	1.1214	86.76	642
40	1.0922	89.79	731/553
25	1.0498	94.52 α_1	800
		94.65 α	
		94.85 α_2	
10	0.9890	102.29 α_1	822/660
5		102.66 α_2	
30	0.9692	105.28 α_1	752/555
20		105.66 α_2	
20	0.9386	110.38 α_1	840
15		110.73 α_2	
25*	0.8794	122.30 α_1	931
		122.81 α_2	
35*	0.8565	128.14 α_1	844
20*		128.74 α_2	
30*	0.8113	143.42 α_1	951
15*		144.32 α_2	

* These values obtained from powder photograph using CuK_{α} radiation.

Table 9.

X-Ray Reflection Data for Silicon - Phillips Labs. Inc. N.Y.

$\frac{I}{I_o}$	d Å	2θ	hkl
100	3.13537	25.654 β_1 28.445 α_1 28.466 α 28.514 α_2	111
60	1.92001	42.512 β_1 47.302 α_1 47.344 α 47.428 α_2	220
35	1.63739	50.316 β_1 56.122 α_1 56.174 α 56.275 α_2	311
8	1.35766	61.290 β_1 69.130 α_1 69.196 α 69.326 α_2	400
13	1.24587	67.934 β_1 76.376 α_1 76.452 α 76.600 α_2	331
17	1.10852	77.796 β_1 88.030 α_1 88.124 α 88.306 α_2	
9	1.04512	83.524 β_1 94.952 α_1 95.058 α 95.264 α_2	511/333
5	0.96001	92.952 β_1 106.708 α_1 106.838 α 107.092 α_2	440
11	0.87194	98.630 β_1 114.092 α_1 114.240 α 114.534 α_2	531
9	0.85866	108.322 β_1 127.544 α_1 127.740 α 128.126 α_2	620
5	0.82816	144.390 β_1 136.892 α_1 137.138 α 137.622 α_2	533
	0.78384	125.256 β_1 158.628 α_1 159.146 α 160.200 α_2	444

Figure 12

333 DIFFRACTION PEAKS FOR TWO TITANOMAGNETITE SAMPLES WITH SILICON AS STANDARD

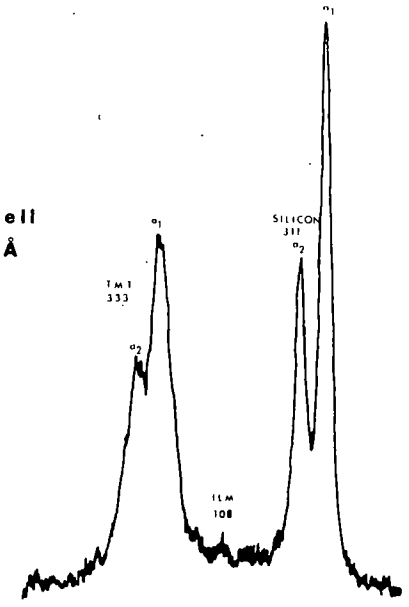

$\frac{1}{8}^{\circ}$ / min 400mm/hr

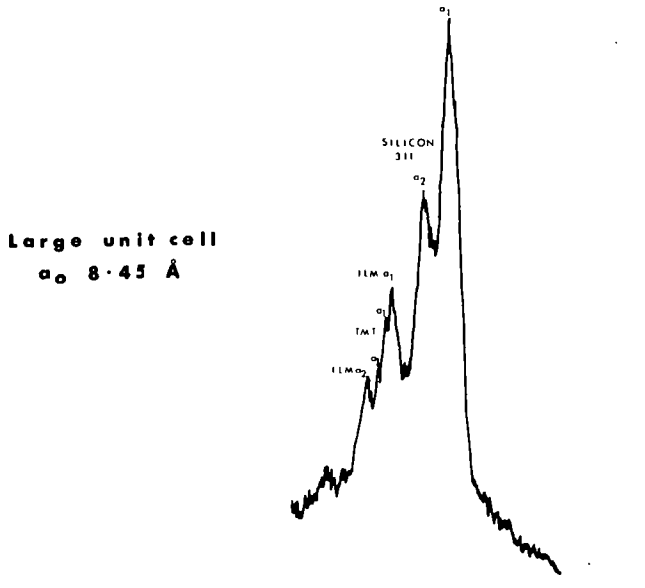

Figure 12.

Variation in the position of the 333 peak of 'magnetite' according to the size of the unit cell. Scanning rate 1/8° /min., with a chart speed of 400 mm/hr, using CuK_{α} radiation. Silicon internal standard.

Figure 13.

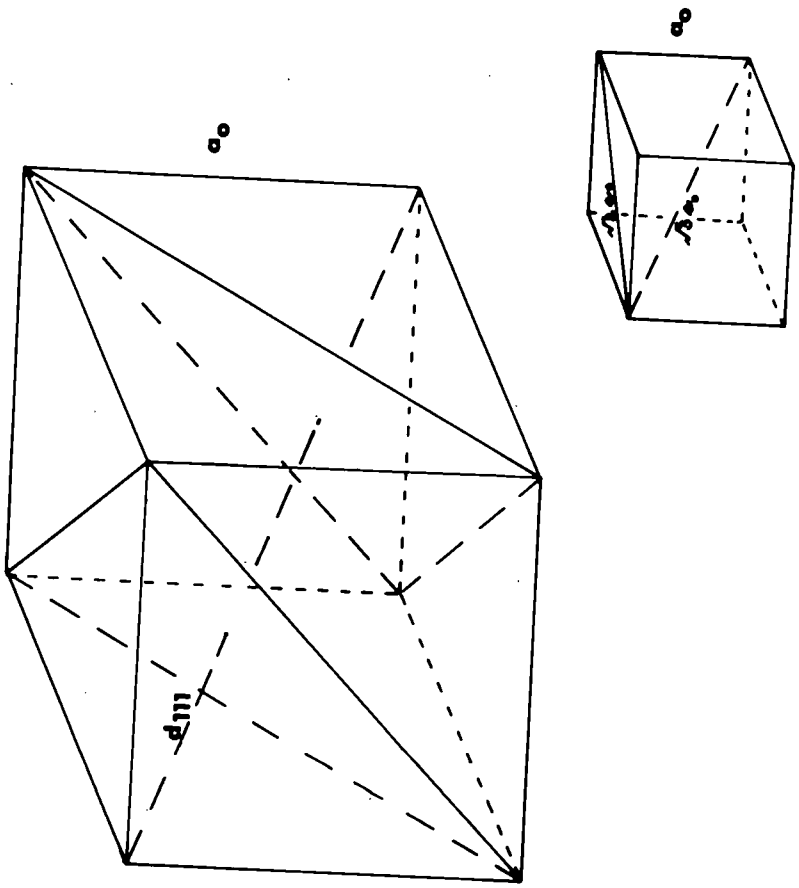

Figure 13.

Relationship between the d-spacing obtained from the 333 peak of 'magnetite' (d_{333}) and the unit cell edge a_o.

Table 10.

Unit Cell Edges of 'Magnetites' in the Clauchlands Sheet

Sample	Horizon (feet)	Unit Cell Edges Å		
S 1	Top	8.3716	8.3774	
S 2	126	8.3641		
S 3	122	8.4085	8.4139	
S 4	118	8.3900		
S 5	114	8.3861	8.3940	
S6	110	8.4033	8.4139	
S 7	106	8.4085		
S 9	98	8.4595		
S10	94	8.4314		
S12	86	8.4232	8.4310	8.4378
S31	78	8.4569		
S34	66	8.4491	8.4543	
S35	62	8.4855		
S36	58	8.4543		
S40	40	8.4320		
S41	20	8.3660	8.3764	8.3816
S43	14	8.3894		
S45	8	8.3993		
S46	5	8.3904		
S47	$2\frac{1}{2}$	8.3920		
S13	40 pegmatite.	8.3868		

Figure 14.

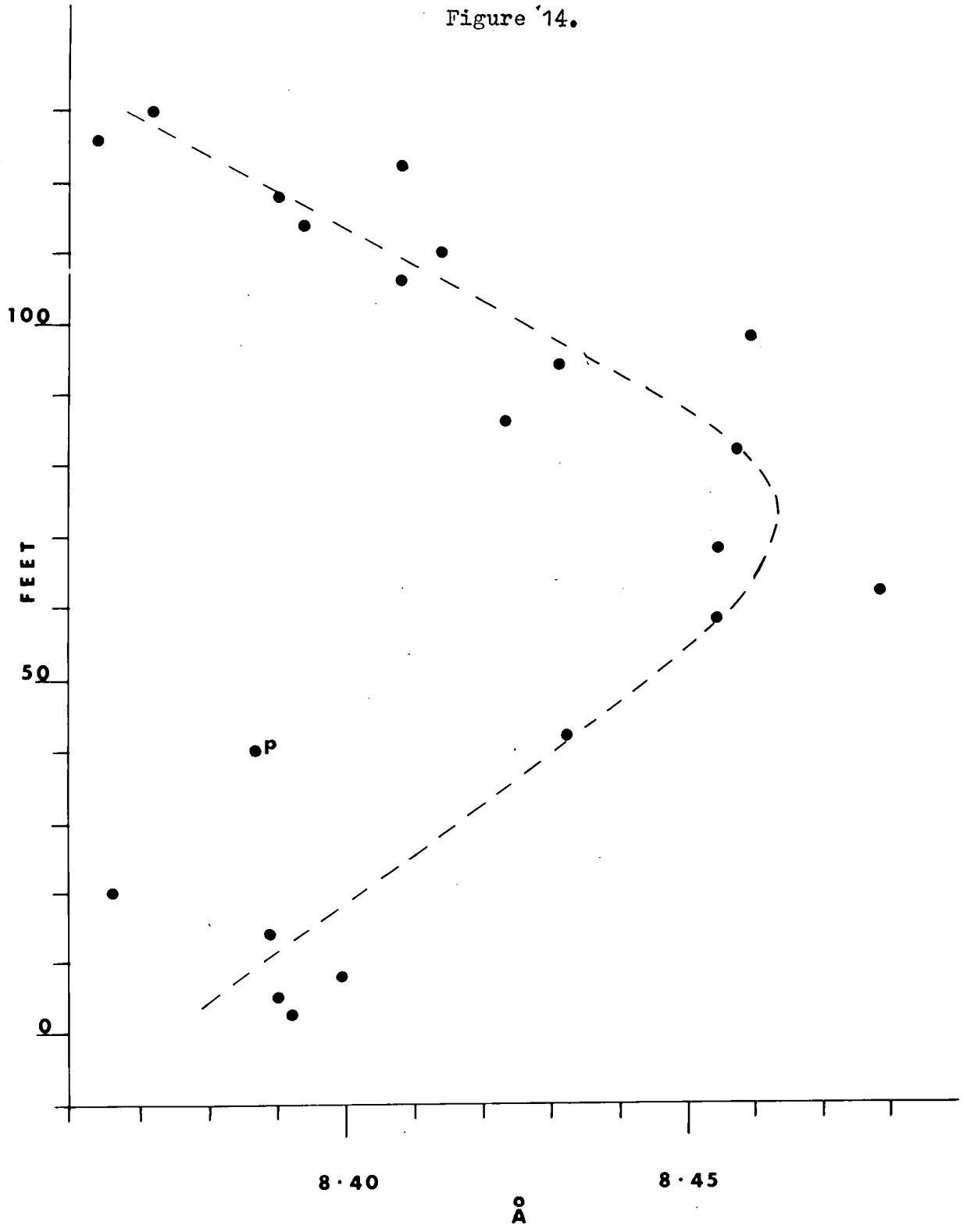

Seven samples contain more than one 'magnetite'. In these samples, a_o has been plotted for the principal component only.

Figure 14.

Variation in a_o of the 'magnetites' in the Clauchlands Sheet.

If the 'magnetites' were simple solid solutions between magnetite and ulvöspinel (i.e. β -spinels Chapter III) this would indicate increased substitution of TiO_2 away from the intrusive margins up to a maximum content corresponding to a composition of 27%Fe_3O_4 - 63%Fe_2TiO_4 (applying Vegard's law:- linear change in lattice parameter with composition), since the unit cell edge of 'magnetite' is 8.396Å (Basta 1953) and the unit cell edge of ulvospinel is 8.534Å (Pouillard 1950). However, these 'magnetites' are unlikely to have such simple compositions, and in particular, the existence of samples with cell edges less than that of magnetite may indicate the presence of Al_2O_3 and Cr_2O_3 or of oxidation to γ -spinels.

The X-ray analysis of 'magnetites', however, does not, by itself, provide unique solutions as to their compositions (see later). Nevertheless, the marked increase in the unit cell edge towards the centre of the intrusion when considered in conjunction with a sympathetic decrease in the Curie points (see Chapter V) is an indication that the substitution of TiO_2 is greater within the sheet than at the margins, although in view of the unknown extent of substitution by other cations and/or the possible effects due to oxidation, it is not possible to define any precise limits to such changes.

Of the 21 samples analysed, only seven clearly contain more than one 'magnetite' phase and only in one such case, S5, is there any evidence to indicate that such phases are intergrown. (Chapter III).

The minimum difference between the unit cell edges of the coexisting magnetites is 0.0052Å and the maximum is 0.0154Å. When it is considered that in terms of even the simple system Fe_3O_4-Fe_2TiO_4 a change in the unit cell edge of 0.014Å indicates a change in composition of only 10 mol%, it can be seen that the compositional differences between these coexisting magnetites will only be very small.

b) Intergrown 'Ilmenites'

Of the 21 samples analysed, 11 contain 'ilmenite' in quantities sufficient to appear on the diffractometer records.

In terms of a hexagonal unit cell the lattice parameters a and c are related to the Bragg angle by the equation:

$$\sin^2\theta_{hk.l} = \frac{\lambda^2}{4c^2}\left[\frac{4c^2}{3a^2}(h^2 + hk + l^2)\right]$$ Peiser, Rooksby Wilson (1955)

and they may be determined by solving simultaneous equations.

Reflections having indices 10.4; 10.8 and 20.4 have been used in the present analysis and the appropriate equations for these reflections are:

$$c^2 = \frac{60\lambda^2}{4\sin^2\theta_{10.8} - \sin^2\theta_{20.4}} \quad \ldots\ldots\ldots\ldots\ldots\ldots 1$$

$$c^2 = \frac{12\lambda^2}{\sin^2\theta_{10.8} - \sin^2\theta_{10.4}} \quad \ldots\ldots\ldots\ldots\ldots\ldots 2$$

$$a^2 = \frac{c^2\lambda^2}{3(c^2\sin^2\theta_{10.8} - 16^2)} \quad \ldots\ldots\ldots\ldots\ldots\ldots 3$$

These results are summarized in Table 11 where the lattice parameters are also given on the basis of a rhombohedral unit cell. The conversion from hexagonal parameters to rhombohedral parameters was acheived by using the relations:

Table 11.

Lattice Parameters of the Intergrown 'Ilmenites'.

Sample	Horizon (feet)	Hexagonal Cell			Rhombohedral Cell		Mole%
		a	c	$\frac{a}{c}$	a_{rh}	α	$FeTiO_3$
S 2	126	5.069	14.01	2.76	5.511	54°46'	80
S 3	122	5.093	14.01	2.75	5.518	54°58'	87
S 5	114	4.968	14.09	2.84	5.503	54°40'	72
S 6	110	5.043	14.05	2.79	5.514	54°25'	80
S10	94	5.020	14.09	2.80	5.520	54°06'	87
S34	66	5.091	14.02	2.76	5.521	54°57'	87
S43	14	5.076	14.01	2.77	5.513	54°49'	80
S45	8	5.069	14.02	2.77	5.514	54°38'	80
S47	$2\frac{1}{2}$	5.076	14.02	2.76	5.516	54°47'	87
S13	40 pegmatite	5.090	14.01	2.76	5.518	54°56'	87

Hexagonal and rhombohedral lattice parameters are related by the following equations :

$$a_{rh} = \frac{1}{3}\sqrt{3a^2 + c^2} \quad \ldots\ldots 1$$

$$\sin\frac{\alpha}{2} = \frac{3a}{2\sqrt{3a^2 + c^2}} \quad \ldots\ldots 2$$

Mole% $FeTiO_3$ has been determined from a_{rh} (see Figure 15), after Akimoto (1957).

$$a_{rh} = \frac{1}{3}\sqrt{3a^2 + c^2} \qquad \ldots\ldots\ldots\ldots 4$$

Henry, Lipson and Wooster 1951.

$$\sin\frac{\alpha}{2} = \frac{3a}{2\sqrt{3a^2 + c^2}} \qquad \ldots\ldots\ldots\ldots 5$$

The composition of the ilmenite has been determined from a_{rh} using the a_{rh}/ composition curve of Akimoto (1957) which is shown in Figure 15. These compositions are plotted in Figure 16 and it can be seen that, in contrast to the 'magnetites' with which they are associated, they show no systematic variation through the intrusion, but in general contain about 10-20mol% Fe_2O_3 in solid solution, so far as reference to Akimoto's curve is concerned.

C. Separate 'Ilmenite'

'Ilmenite' appears as a separate phase within the central part of the intrusion, occurring in association with the 'magnetite'/'ilmenite' intergrowths. Powder samples have been drilled out from the polished samples and mounted on gelatin fibres following the method described by Soren (1960).

Gelatin is a particularly suitable mounting medium because the powder readily adheres to the fibre without the need of an adhesive, the fibre can be prepared with a very fine point, and it produces virtually no amorphous scattering of the X-rays.

Such samples have been mounted in a 57 cm diameter powder camera and X-rayed with CoK_α radiation (λ =1.7902Å). However, because of the small size of the samples it has been necessary to make long exposures of up to 70 hours before the powder photographs showed measurable lines in the back reflection region.

Figure 15.

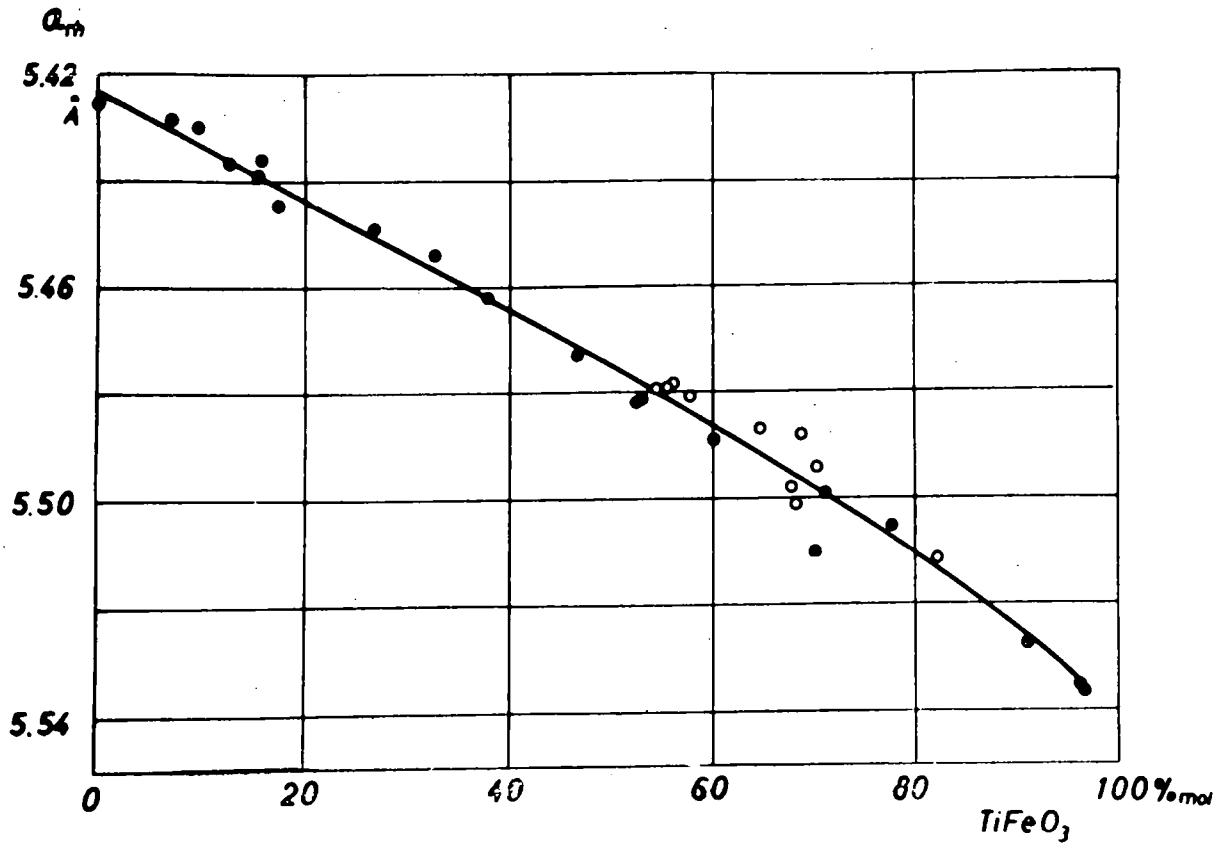

Figure 15.

The relationship between the composition of the rhombohedral solid solutions $FeTiO_3$-Fe_2O_3 and a_{rh}. (after Akimoto 1957).

Figure 16.

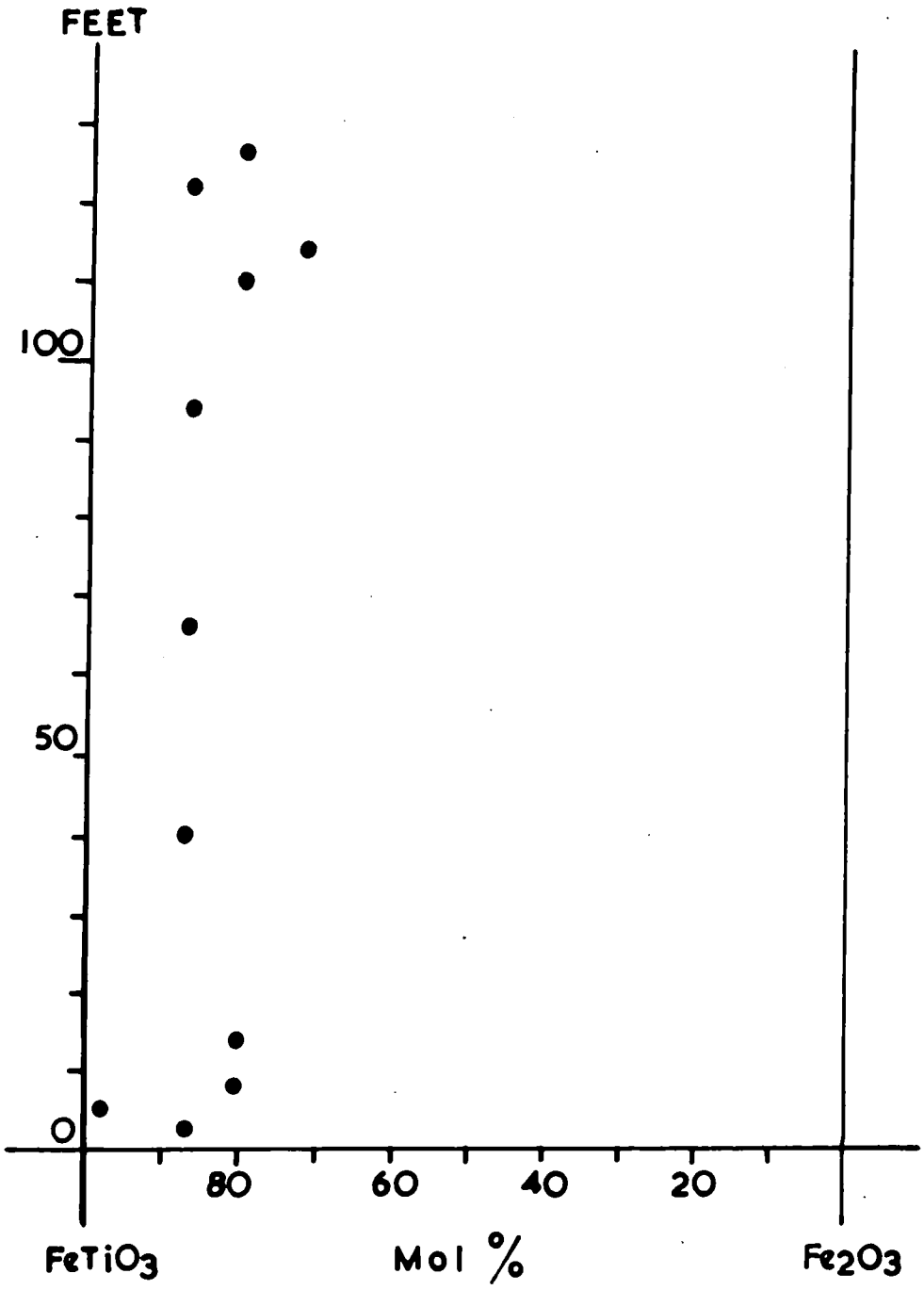

Figure 16.

Compositions of the intergrown 'ilmenites' in the Clauchlands Sheet, determined from Figure 15.

Four samples have been analysed in this way and their diffraction patterns are shown in Plate XVII, with the corresponding d-spacings listed in Table 12. In each case, these patterns confirm that the mineral is 'ilmenite'.

On the basis of an hexagonal unit cell, the lattice parameters a_o and c_o have been determined graphically following the method of successive approximations described by Klug and Alexander (1954 p481).

This method, which requires a preliminary knowledge of the approximate axial ratio a/c, utilizes the quadratic form of the Bragg equation, which for the hexagonal system is either:

$$a_o = \frac{\lambda}{2\sin\theta}\left(\frac{4}{3}s + \left(\frac{a}{c}\right)^2 l^2\right) \qquad \ldots\ldots 6$$

or

$$c_o = \frac{\lambda}{2\sin\theta}\left(\frac{4}{3}\left(\frac{c}{a}\right)^2 s + l^2\right) \qquad \ldots\ldots 7$$

where $s = (h^2 + hk + k^2)$

Lines with relatively large h and k indices are used to extrapolate to a preliminary value of a, and lines with relatively large l index are used to extrapolate to a preliminary value of c. A new axial ratio a/c is thus defined which can be used in equations 6 and 7 to obtain new values for a and c, and the process of successive approximations is continued until these extrapolated values become constant.

The extrapolation data for the four samples have been summarized in Table 13 and the calculations from which these have been derived have been included in Appendix 2. In the case of the samples, however, the value

Table 12.

X-Ray Data for the Separate 'Ilmenites'
CoK_{α} Radiation = 1.7902Å

Sample S36.

θ	d	hk.l	I
14.097	3.67	10.2	s
19.264	2.71	10.4	vvs
20.819	2.519	11.0	vvs
23.804	2,218	11.3	s
28.946	1.818	20.4	s
31.555	1.170	11.6	vs
33.562	1.619	10.8	w
36.722	1.534	21.4	s
37.776	1.461	30.0	s
42.240	1.331	101.0	m
45.000	1.266	22.0	vw
47.886	1.206	31.2	vw
49.190	1.181 α_1	20.10	vw
50.946	1.152 α_1	31.4	vw
53.203	1.117 α_1	22.6	vw
56.539	1.072 α_1	21.10	vw
58.345	1.051	-	vw
63.111	1.003 α_1	31.8	vw
66.021	0.979 α_1	101.4	vw
67.124	0.971 α_1	32.4	vw
68.404	0.962 α_1	41.0	vw
75.929	0.922 α_1	31.10	vw

Sample S34.

θ	d	hk.l	I
19.290	2.71	10.4	vvs
20.969	2.52	11.0	s
23.877	2.212	11.3	m
28.911	1.851 α_1	20.4	ms
31.541	1.711 α_1	11.6	ms
33.596	1.618 α_1	10.8	w
36.727	1.497 α_1	21.4	m
37.755	1.462 α_1	30.0	m
			vvw
not measurable			w
			vvw
			vvw
50.700	1.156 α_1	31.4	vvw
53.197	1.117 α_1	22.6	vvw
56.379	1.074 α_1	21.10	vvw

Sample A/C/3/42

θ	d	hk.l	I
17.305	3.01	[illegible]	w
19.258	2.715	10.4	s
20.811	2.52	11.0	ms
23.819	2.217	11.3	wm
25.494	2.08		vvw
28.825	1.857 α_1	20.4	m
31.479	1.714 α_1	11.6	m
36.739	1.496 α_1	21.4	w
37.790	1.461 α_1	30.0	w
not measurable			vvw
			vvw
50.782	1.155 α_1	31.4	vvw
53.318	1.116 α_1	22.6	vvw
56.317	1.075 α_1	21.10	vvw

Sample A/C/3/39

θ	d	hk.l	I
14.019	3.69	10.2	s
19.626	2.665	10.4	vs
20.728	2.529	11.0	s
23.732	2.223	11.3	ms
23.802	2.218		ms
31.392	1.718 α_1	11.6	ms
33.414	1.625 α_1	10.8	w
36.699	1.498 α_1	21.4	wm
37.720	1.463 α_1	30.0	m
			w
not measurable			vvw
			vvw
			vvw
50.878	1.153 α_1	31.4	vvw
53.201	1.117 α_1	22.6	vvw
56.435	1.073 α_1	21.10	vvw

Table 13.

Determination of the Lattice Parameters of the Separate 'Ilmenites' by Successive Extrapolations.- Summarised Results.

Sample A/C/3/42

	a	c
Assumed values.	5.0791	14.1350
	(ASTM Card 3-0799)	
Extrap. 1	5.130	14.167
Extrap. 2	"	14.120
Extrap. 3	"	14.090
Extrap. 4	"	14.076
Extrap. 5	"	14.076

Sample A/C/3/39

	a	c
Assumed values.	5.0791	14.1350
	(ASTM Card 3-0799)	
Extrap. 1	5.1005	14.182
Extrap. 2	"	14.173
Extrap. 3	"	14.170
Extrap. 4	"	14.170

Sample S36

	a	c
Assumed values.	5.0791	14.1350
	(ASTM Card 3-0799)	
Extrap. 1	5.1034	14.1685
Extrap. 2	"	14.1235
Extrap. 3	"	14.1035
Extrap. 4	"	14.0956
Extrap. 5	"	14.0730
Extrap. 6	"	14.0730

Sample S34

	a	c
Assumed values.	5.0791	14.1350
	(ASTM Card 3-0799)	
Extrap. 1	5.150	14.180
Extrap. 2	5.119	14.152
Extrap. 3	5.123	14.152
Extrap. 4	5.121*	14.150

*Mean of Extraps.2 and 3.

Plate XVII

X-Ray Powder Patterns

a) Separate 'ilmenite' in sample S36.

CoK_{α} . radiation.

b) Separate 'ilmenite' in sample A/C/3/39.

CoK_{α} . radiation.

c) Separate 'ilmenite' in sample S34.

CoK_{α} . radiation.

d) Separate 'ilmenite' in sample A/C/3/42.

CoK_{α} . radiation.

e) 'Hematite' from the baked sandstone above the Clauchlands sheet. CoK_{α} . radiation.

Plate XVII.

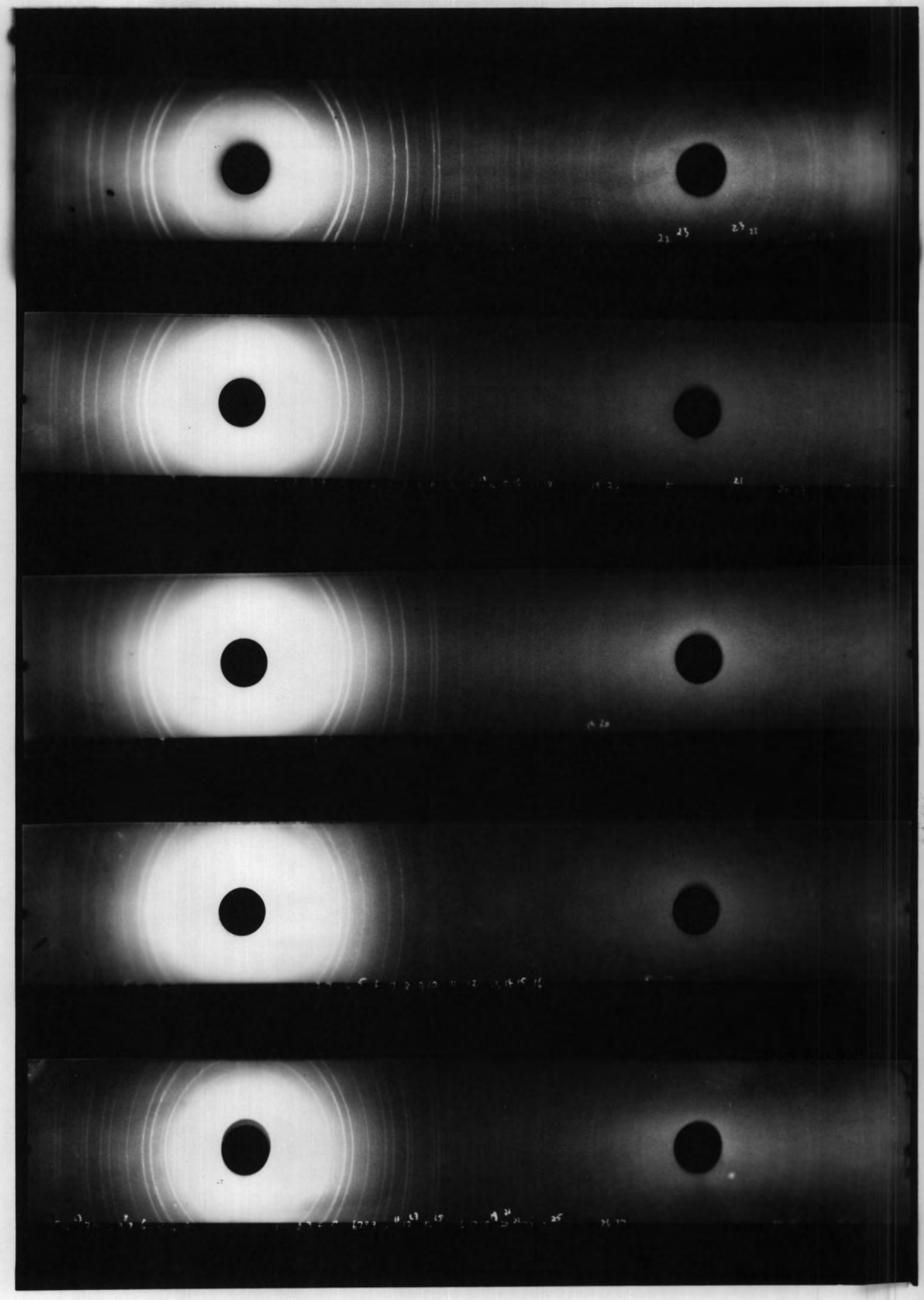

of a has been obtained directly by using lines with indices 30.0, 22.0 and 41.0, since in equation 6, $(\frac{a}{c})^2$ is zero, so that the initial extrapolation requires no further refinement, and therefore the further extrapolations apply only to c.

The lattice parameters are summarized in Table 14 where they are given for both the hexagonal and rhombohedral unit cells. The values of a_{rh} are consistently higher for the separate 'ilmenites' than for the intergrown 'ilmenites', and by reference to the a_{rh}/ composition curve of Akimoto (1957), Figure 15, it can be seen that the separate 'ilmenites' appear to be free of dissolved Fe_2O_3.

However, it has been noted that ilmenites which occur in association with magnetites tend to be preferentially enriched in Mn^{2+} (Deer, Howie and Zussman 1962). Such substituted ilmenites will have larger values for a_{rh} and smaller values for α depending on the amount of substitution, since the lattice parameters of pyrophanite ($MnTiO_3$) are $a_{rh} = 5.62\text{Å}$; $\alpha = 54^\circ 16'$ (Barth and Posnjak 1934). Hence the results of the present investigation may indicate that the separate ilmenites contain some Mn^{2+}, whereas the lattice parameters of the intergrown ilmenites would indicate that they are solid solutions between $FeTiO_3$ and Fe_2O_3.

D. Opaque Minerals in the Sandstones above the Intrusion

As described in Chapter III, the opaque minerals in the sandstones above the intrusion appear to consist largely of 'hematite'. In polished section, however, the mineral does not show the red internal reflections which are characteristic of 'hematite' and hence confirmation of its identity

Table 14.

Lattice Parameters of the Separate 'Ilmenites'

Sample	Horizon (feet)	Hexagonal Cell			Rhombohedral Cell		Mol%
		a	c	$\frac{a}{c}$	a_{rh}	α	$FeTiO_3$
S34	66	5.121	14.15	2.76	5.57	54°46'	?100
S36	58	5.103	14.07	2.75	5.54	54°52'	98
S39*	46	5.100	14.17	2.77	5.57	54°32'	?100
CC42*	32	5.130	14.08	2.74	5.55	55°04'	?100

* Abbreviations for samples A/C/3/39 and A/C/3/42.

Table 15.

X-Ray Data for 'Hematite' in Sandstone above the Sheet

θ	d	hk.l	
14.216	3.64	10.2	'hematite'
16.518	3.15	-	?
17.294	3.015	-	calcite
19.421	2.69	10.4	'hematite'
20.898	2.58	11.0	'hematite'
23.976	2.203	11.3	'hematite'
27.530	1.937	-	calcite
29.107	1.840	20.4	'hematite'
31.895	1.690	11.6	'hematite'
32.711	1.657	12.1	'hematite'
34.037	1.599	10.8	'hematite' + calcite
36.966	1.489	21.4	'hematite' + calcite
37.992	1.454	30.0	'hematite' + calcite
43.197	1.308	11.9	'hematite' + calcite
44.975	1.267	22.0	'hematite'
46.427	1.234	30.6	'hematite' + calcite
52.434	1.128	-	calcite
53.735	1.109	22.6	'hematite'
57.364	1.062	-	?
67.851	0.966	-	calcite

CoK_α radiation. $= 1.7902\text{Å}$

$a_{rh} = 5.47\text{Å}$. $\alpha = 55°23'$

is dependent upon X-ray examination.

Material has been drilled out of the polished sample following the same procedure used for the separate 'ilmenites', and this has been X-rayed using CoK_{α} radiation. The powder pattern is shown in Plate XVII and the d-spacings are given in Table 15. The results confirm that the mineral is 'hematite' and the powder pattern also includes lines attributed to calcite of hydrothermal origin which is known to be present in these rocks. (Chapter II).

The hexagonal lattice parameters of the 'hematite' have been determined by the method of successive approximations and then converted to rhombohedral lattice parameters. The relevant data are summarized below and the calculations on which they are based have been included in Appendix 2.

a) Extrapolation Data:

		a	c	
Assumed value		5.039	13.76	(Berry and Thompson 1962)
Extrap.	1	5.081	13.824	
	2		13.836	
	3		13.839	
	4		13.838	

b) Lattice Parameters:

Hexagonal Unit Cell - $a = 5.081\text{Å}$; $c = 13.84\text{Å}$; $c/a = 2.72$

Rhombohedral " " - $a_{rh} = 5.47 \pm 0.01\text{Å}$

$\alpha = 55^{\circ}23'$

In terms of Akimoto's a_{rh}/ composition curve, this result would suggest that about 35mol% $FeTiO_3$ may be present in the mineral.

E. The Effects of Substitution on the Lattice Parameters of Magnetite and Ilmenite

X-ray analysis by Bragg (1915) first showed magnetite to have the spinel type structure in which the unit cell is based on a cubic face centered lattice and contains 32 oxygen ions and 24 cations. 8 cations occur in 4-fold co-ordination on A-sites and 16 in 6-fold co-ordination on B-sites, as illustrated in Figure 17.

In magnetite, two thirds of the cations are Fe^{3+} and one third are Fe^{2+} - ($FeO.Fe_2O_3$) - Barth and Posnjak (1932) have shown that half the Fe^{3+} and all the Fe^{2+} ions occur on the B-sites whilst the A-sites are occupied by the remaining Fe^{3+}. This structure, therefore, is to be distinguished from the normal spinel structure, as found in $MgAl_2O_4$, in which the divalent ions restricted to the A-sites and the trivalent ions to the B-sites, and hence it is known as the inverse spinel structure (Figure 17).

In terms of the general formula $R_8^{2+}.R_{16}^{3+}.O_{32}$ these two structures are characterised by the following distribution of the cations:

$8R^{2+}$ in A-sites; $16R^{3+}$ in B-sites. .....Normal

$8R^{3+}$ in A-sites; $8R^{2+}$, $8R^{3+}$ in B-sites .....Inverse

However, many cations may substitute for the Fe^{2+} and Fe^{3+} in magnetite resulting in a wide variety of substituted magnetites. Such magnetites may contain monovalent ions such as Na^+ and K^+ (Michel 1937), divalent ions such as Mn^{2+}, Mg^{2+}, Ni^{2+} and Co^{2+} (Benard and Chaudron 1937), trivalent ions such as Al^{3+} and Cr^{3+} (Pouillard 1950) or the tetravalent ion Ti^{4+} (Pouillard 1950). A given unit cell size may result from more than one

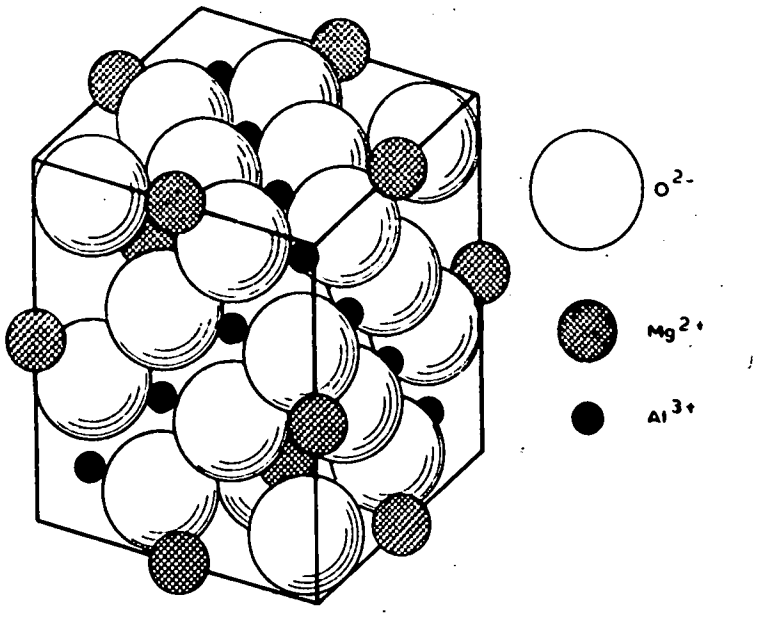

Fig. 15.

a.

Figure 17

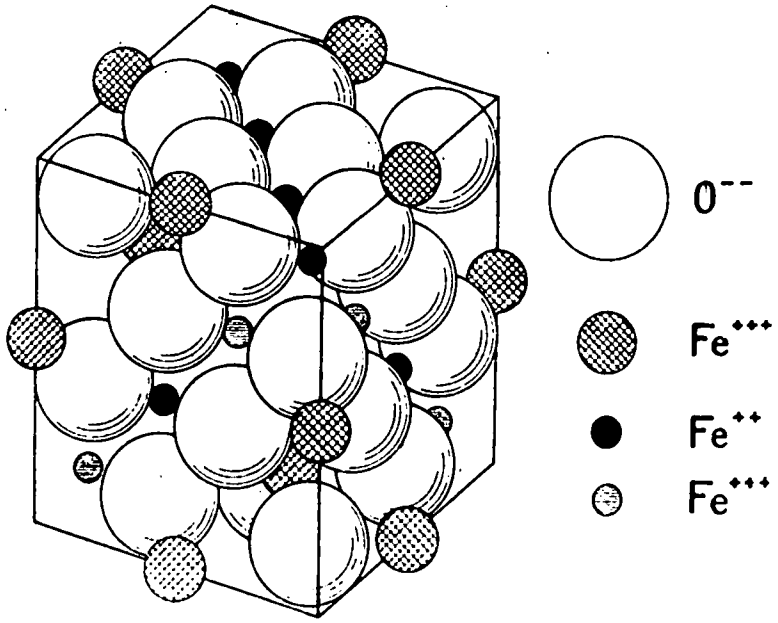

Fig. 15.

b.

Figure 17.

Spinel structures

a) Normal spinel - $MgAl_2O_4$.

b) Inverse spinel- $FeFe_2O_4$.

combination of substituting elements.

Hence, although the unit cell edge of a magnetite is known accurately (8.3963 ± 0.0005Å Basta 1953; 1957), the unit cell edge of most natural magnetites will differ from this depending on the amount and type of substitution so that no simple relation exists between lattice parameter and composition.

Data on the unit cell edge, and the Curie point, of various substituted magnetites are summarized in Table 16, and it can be seen that substitution by MnO or TiO_2 appreciably increases the unit cell edge and decreases the Curie point, substitution by MgO has little effect on the cell edge but decreases the Curie point, and substitution by Al_2O_3 or, Cr_2O_3 appreciably lowers the unit cell edge and also lowers the Curie point slightly. Substitution by V_2O_3 probably also decreases the cell edge (Table 17).

Substituted magnetites containing Na^+, K^+ or Co^{2+} can be prepared in the laboratory, but these elements do not seem to appear in natural magnetites. (Table 17). Similarly, although Ni^{2+} can readily be substituted experimentally into magnetite, the iron-nickel spinel trevorite ($NiFe_2O_4$) - Table 17 No. ~~14~~ 11 is only known from the Scotia talc mine, Transvaal, South Africa. (Deer, Howie and Zussman 1962), and Ni^{2+} is generally absent from natural magnetites. Likewise, franklinite ($ZnFe_2O_4$) is known only from the one locality, in association with zinc ore deposits, at Franklin and Sterling Hill, New Jersey, and Zn^{2+} is generally absent from natural magnetites.

Most natural magnetites, however, are titaniferous, and as can be seen in Table 17, they contain such large amounts of TiO_2 relative to the other cations, that the variation in unit cell edge and Curie point may generally be correlated with the TiO_2 content, with probably only minor modifications

Table 16.

Substituted Magnetites

Natural Fe_3O_4 - a_o = 8.3963 ± 0.0005Å. (Basta 1953).

Synthetic " - θ_c = 585°C (Brailsford 1960).

Substitution by Divalent Ions. (Benard and Chaudron 1937).

Oxide Added	Parameters of the Limiting Solid Solution	
	a_o	c
CoO	8.38Å	520°C
NiO	8.35	600
MgO	8.40	420
MnO	8.54	140

Substitution by Al_2O_3 :- $(Fe^{3+}_{2-y}Al^{3+}_{y}Fe^{2+})O_4$ (Pouillard 1950).

y =	0.00	0.03	0.09	0.15	0.21	0.30	0.30
a_c =	575	571	560	548	545	535	535
a_o =	8.413	8.403	8.390	8.381	8.375	8.365	8.365

Substitution by Cr_2O_3 :- $(Fe^{3+}_{2-y}Cr^{3+}_{y}Fe^{2+})O_4$ (Pouillard 1950).

y =	0.00	0.135	0.30	0.36
a_c =	575	569	563	560
a_o =	8.41	8.38	8.34	8.31

Substitution by TiO_2 (Pouillard 1950).

Mol% $TiFe_2O_4$	0	8	10	18	25	42	100
a_c =	575	524	485	475	468	230	-
a_o =	8.413	8.420	8.428	8.43	8.44	8.46	8.534

Table 17.*

Magnetite Analyses

	1	2	3	4	5	6	7	8	9	10	11	12**	13**	
SiO_2	0.03	0.27	0.73	1.55	0.48	0.38	0.10	0.33	0.72	-	1.40	-	-	SiO_2
TiO_2	-	tr	0.05	0.05	2.98	6.98	19.42	26.76	-	0.09	-	-	-	TiO_2
Al_2O_3	0.19	0.21	0.04	0.14	0.02	3.62	1.39	2.31	-	-	-	-	-	Al_2O_3
Cr_2O_3	-	-	0.02	0.00	-	0.01	0.07	0.38	-	-	-	-	-	Cr_2O_3
V_2O_3	-	-	0.01	0.00	-	0.10	1.97	0.37	-	-	-	68.41	72.04	V_2O_3
Fe_2O_3	68.95	68.85	67.55	67.57	63.40	57.11	28.37	21.10	66.58	73.69	66.24	0.52	0.24	Fe_2O_3
FeO	30.82	30.78	31.43	28.40	32.25	21.83	46.06	45.22	-	2.57	1.96	30.75	27.92	FeO
MnO	-	-	0.05	0.06	0.00	1.82	0.33	0.61	9.96	13.94	-	-	-	MnO
MgO	-	tr	0.18	1.85	0.39	7.18	2.29	1.93	0.34	9.26	0.24	-	-	MgO
ZnO	-	-	-	-	-	-	-	-	20.77	-	-	-	-	ZnO
NiO	-	-	-	-	-	-	-	-	-	-	29.71	-	-	NiO
CaO	0.02	tr	0.01	0.00	0.23	0.94	0.06	0.59	0.43	-	-	-	-	CaO
H_2O	0.04	-	-	-	-	-	-	-	0.71	-	0.36	-	-	H_2O
Total	100.05	100.11	100.07	99.62	99.75	99.97	100.06	99.60	99.51	99.82	99.91	99.68	100.20	Total
a_o Å		8.395 ;	8.3963;	8.3955;		8.396;	8.450;	8.48;	8.45;	8.394;	8.386;	8.297;		

1. Magnetite, contact metasomatic deposit, Takanokura mine, Fukushima Prefecture, Japan (Takeuchi and Nambu 1958).

2. Magnetite, Lover's Pit, Mineville New York. (Newhouse and Glass 1936). Anal. M.G.Keyes.

3. Magnetite, Bisperg, Sater, Dalecarlia, Sweden. (Basta 1957). Anal. H.B.Milner.

4. Magnesiomagnetite, Kropferberg, Saxony. (Basta 1959). Anal. H.B.Milner.

5. Titaniferous magnetite, basic two-pyroxene granulite of the Charnockite Series, Nagaramalai, Salem, Madesa. (Howie 1955).

6. Titanomagnetite, Magnet Cove, Arkansas, U.S.A. (Basta 1957). Anal. H.B.Milner.

7. Titaniferous magnetite, hypersthene-olivine gabbro, Skaergaard intrusion, East Greenland. (Vincent et al 1957). Anal. Vincent and Wright.

8. Titanomagnetite, teschenite, Black Hack Sill, Gunnedah, N.S.W. Australia. (Wilkinson 1957). Anal. J.F.G.Wilkinson.

9. Franklinite, ($ZnFe_2O_4$), Franklin, New Jersey, U.S.A. (Palache 1910). Anal. W.T.Schaller.

10. Jacobsite, ($MnFe_2O_4$), in calcite, Jacobsberg, Wermland, Sweden. (Johansson 1928). Anal. K.Johansson.

11. Trevorite, ($NiFe_2O_4$), phyllite, Barberton district, Transvaal. (Walker 1923). Anal. E.W.Todd.

12. Coulsonite, (FeV_2O_4), Buena Vista Hills, Nevada, U.S.A. (Radtke 1962). Sample 1. Anal. A.S.Radtke.

13. Coulsonite, (FeV_2O_4), Buena Vista Hills, Nevada, U.S.A. (Radtke 1962). Sample 2. Anal. A.S.Radtke.

* Analyses 1 to 11 have been taken from Deer, Howie and Zussman. (1962).

**Taken from Radtke (1962).

due to substitution by other cations such as Mg^{2+}, Al^{3+} V^{3+}.

However, although it is known that substitution by TiO_2 increases the unit cell edge (and decreases the Curie point) of magnetite (Pouillard 1950), Akimoto, Katsura and Yoshida (1957) have shown that a knowledge of the unit cell edge does not lead to a unique solution for the composition and that, in fact, as can be seen in Figure 18, there remains considerable ambiguity.

Such ambiguities arise because titaniferous magnetites may oxidise in varying degrees to form spinels with a defect lattice structure similar to that of maghemite, γFe_2O_3, and hence their compositions may plot over a large part of the system $FeO-Fe_2O_3-TiO_2$.

Maghemite is cubic with $a_o = 8.322$ (Hägg 1935). Like magnetite it is an inverse spinel, but exhibits a defect structure such that 1 in 9 of the iron ions are absent. (Verwey 1935). Both Basta (1959) and Katsura and Kushiro (1961) have shown that there exists a series of similar minerals in the system $FeO-Fe_2O_3-TiO_2$, which they have called titanomaghemites and such minerals have been designated as γ-phases by Verhoogen (1962).

Both hematite and ilmenite are rhombohedral minerals and they have closely similar structures (Barth and Posnjak 1934; Posnjak and Barth 1934). The lattice parameters of hematite are $a_{rh} = 5.431$Å; $\alpha = 55°16'$, and the lattice parameters for ilmenite are $a_{rh} = 5.53$Å; $\alpha = 54°48.5'$ (Berry and Thompson 1962).

Solid-solution is complete between hematite and ilmenite at temperatures above 1050°C (Ramdohr 1926; Posnjak and Barth 1934), although at 950°C there is a gap in the solid-solution series which extends from 33% $FeTiO_3$ (Pouillard 1950), and at normal temperatures the solid-solutions are even more limited (see Chapter III).

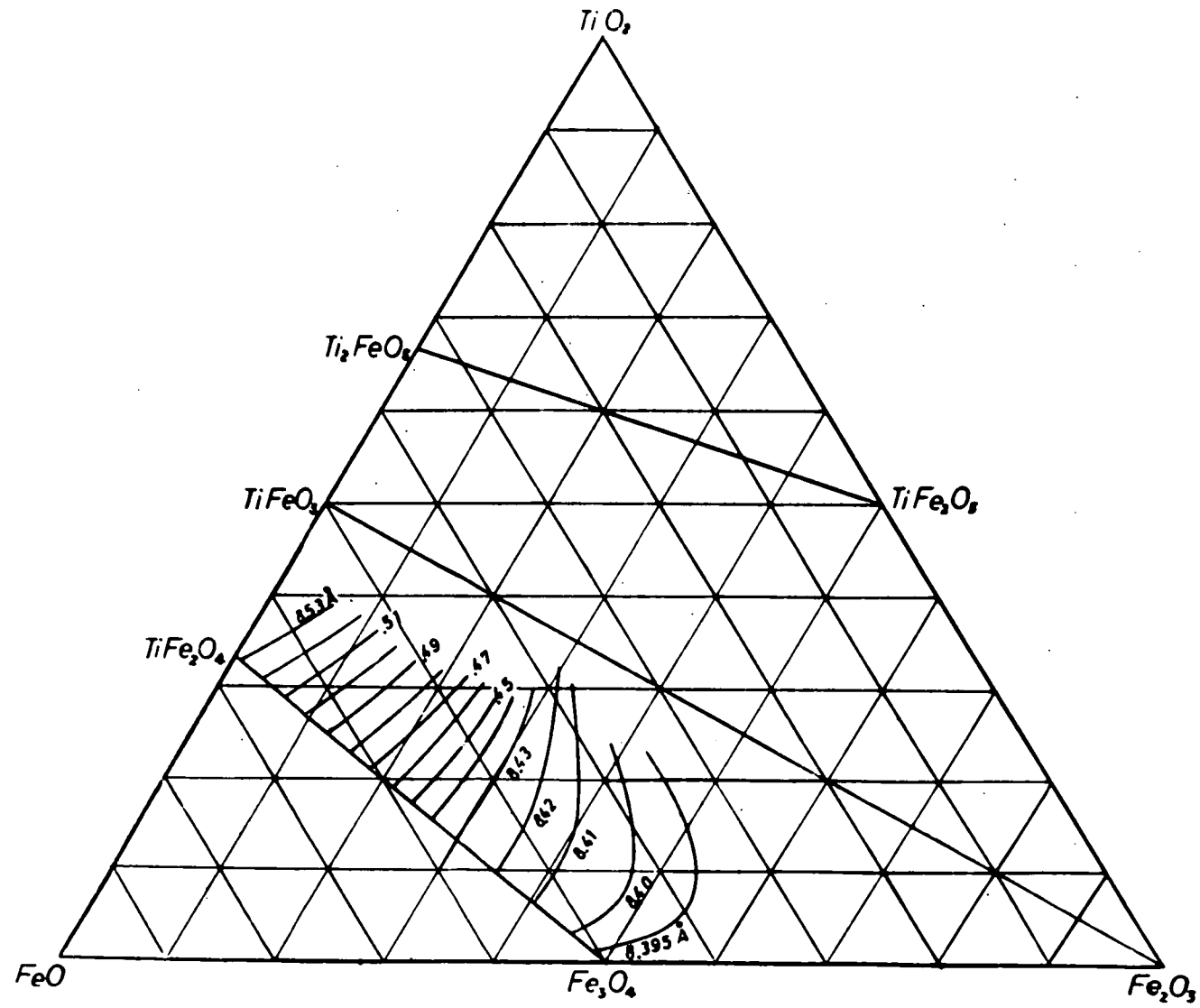

Figure 18.

Fig. 6 Lines of equal lattice parameter of the generalized titanomagnetite in a FeO–Fe_2O_3–TiO_2 system.

Figure 18.

The system FeO-Fe_2O_3-TiO_2 showing lines of equal a_o as determined by Akimoto, Katsura and Yoshida (1957).

Akimoto (1957) has demonstrated a continuous change in the lattice parameters (a_{rh}) of such solid-solutions (Figure 15) and, therefore, it is possible to estimate the composition of the 'ilmenites' on the basis of their lattice parameters. Although Mg^{2+} and Mn^{2+} may substitute for Fe^{2+} in ilmenite, it is more usual to find only small amounts of these cations occurring in natural ilmenites so that the effects of such substitution are likely to be small.

It is clear, therefore, that the relations between the X-ray data and the compsoitions of natural 'magnetites' are complex and that although the unit cell edge is probably largely a function of the TiO_2 content, substitution by other cations may sometimes have an appreciable effect. Even when such cations are absent, however, the unit cell edge is not uniquely related to composition since it is known that titanomagnetites (β-phases) can oxidise, in varying degrees to give γ-phases, and that γ-phases with the same unit cell edge can represent different degrees of oxidation according to the TiO_2-content.

In the case of the rhombohedral α-phases it does appear possible to estimate their compositions in terms of the X-ray data since the complex relationships characteristic of the cubic phases are absent.

F. Summary

The lattice parameters of 21 titaniferous magnetites have been determined and the results represent a cross-section through the Clauchlands sheet.

The unit cell edge has been found to increase systematically away from the margins of the intrusion and this result indicates an overall increase in the TiO_2 content within the body of the sheet.

However, the existence of 'magnetites' with unit cell edges less than 8.396Å indicates that other ions, especially Al^{3+}, are likely to be present in the lattice, although oxidation to γ-spinels may also decrease the cell edge.

Of the analysed samples, only seven contain more than one cubic phase and in view of the small differences in the unit cell edges of these 'magnetites' they probably differ only slightly in composition.

The lattice parameters of the 'ilmenites' intergrown with the 'magnetites' have been determined and although they do not show any systematic variation through the intrusion, the results do indicate that the minerals contain about 10-20mol% Fe_2O_3.

The lattice parameters of the separate 'ilmenites' have also been determined and the results would indicate that little or no Fe_2O_3 is present in these minerals but suggest that Mn^{2+} may be present.

X-ray examination of the opaque minerals in the sandstone above the intrusion have confirmed that the predominant mineral is 'hematite', and on the evidence of the rhombohedral lattice parameters it is concluded that the mineral contains about 35mol% $FeTiO_3$ in solid solution.

Chapter V. Magnetic Analyses

A. Introduction

As discussed in Chapter IV, the X-ray analysis of the iron-titanium oxide minerals is of only limited value when investigating their compositions owing to the effects of substitution and/or oxidation. These effects are particularly serious in the titaniferous magnetites and Akimoto, Katsura and Yoshida (1957) have shown that considerable ambiguity remains as to their compositions even when the unit cell edge is known (see Figure 18 Chapter IV).

Natural magnetites, however, are generally strongly magnetic and, their magnetic properties form the basis of the study of rock magnetism. Of these properties the Curie point and the saturation magnetization are two of the most important for they depend on the chemical composition of the mineral. Their measurement, therefore, provides data that is complementary to that obtained from the unit cell edge (NB. The exact significance of some of the terms used in this Chapter is explained later, p 67).

Although ilmenite is common in igneous rocks it is not usually ferrimagnetic and even when present the amounts of ferrimagnetic ilmenite are usually very small as compared with the amounts of titaniferous magnetites and maghemites. In volcanic rocks from Japan, for example, the amounts of ferrimagnetic ilmenite are less than one tenth the amounts of the ferrimagnetic spinels (Nagata 1961).

Thus the magnetic analysis of igneous rocks, or their ferromagnetic mineral fraction, may generally be expected to yield information on the nature of the spinels. Ferrimagnetic ilmenites, where these are present, may be

distinguished by their lower Curie points and smaller saturation magnetizations, whilst hematite or titanhematites may be distinguished by their high Curie points and weak ferromagnetism (see later).

As with other methods of investigation, of course, the results of these analyses may not be considered in isolation but must be related to X-ray, chemical and microscopic data in order to be fully exploited.

Thermomagnetic analysis is a particularly useful method of investigation at the qualitative level for it provides information as to the number of magnetic phases present and their approximate compositions which cannot be obtained in any other way.

Thermomagnetic curves showing the variation in magnetic moment of a sample as a function of temperature in constant field H may be expected to have the general forms shown in Figure 19. (after Chevallier, Mathieu and Vincent 1954).

The presence of a single homogeneous 'magnetite' will give rise to an abrupt change in the slope of the curve at the Curie point, whilst if more than one 'magnetite' is present the curve will either have a step-wise appearance, or will show a gradual slope if the composition varies continuously.

On the other hand, the thermomagnetic curves of ferri-ilmenites may be expected to change more or less linearly with temperature (Nagata 1961), provided that their presence is not masked by the more intensely magnetized spinels.

A further advantage of these analyses is that they may be carried out on unseparated rock samples since the results are independent of the non-magnetic minerals in the rock.

A measure of the saturation magnetization, is in general, less easily obtained than the Curie point and requires that the ferromagnetic material

Figure 19.

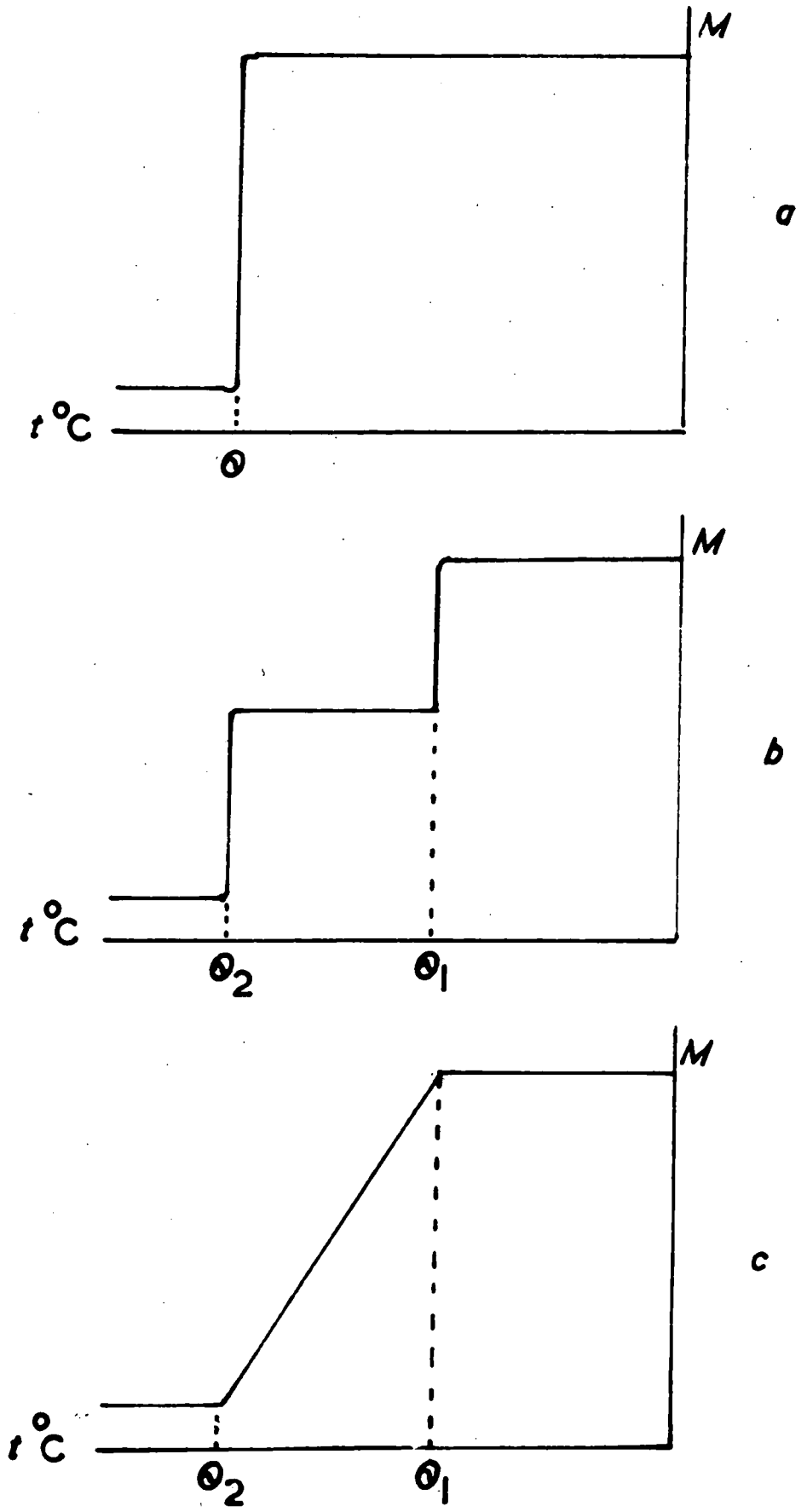

Figure 19.

Idealised thermomagnetic curves of 'magnetites' (after Chevallier, Mathieu and Vincent 1954).

a) Single phase with Curie point of θ .

b) Two separate phases with Curie points of θ_1 and θ_2 .

c) Continuous change in composition between solid solutions having the Curie points θ_1 and θ_2 .

be separated from the rock.

It has been found (Akimoto, Katsura and Yoshida 1957) that if the ferromagnetic mineral is a homogeneous cubic phase with a composition in the system $FeO-Fe_2O_3-TiO_2$ then knowledge of the Curie point and saturation magnetization together enables this composition to be determined, since lines of equal Curie point in this system intersect lines of equal saturation magnetization. (Figures 20 and 21).

Chevallier, Mathieu and Vincent (1954) also state that the measured saturation magnetization, σ_1, of a heterogeneous 'magnetite' sample (at 20°C), can be used in conjunction with the Curie point in order to determine the amount of Fe_3O_4 in the 'magnetite', whatever the nature of the other oxides in solid solution.

Their results show that, knowing the Curie point, it is possible to evaluate the concentration, f, and the saturation magnetization σ_∞ of the spinel responsible for the ferromagnetism. Further, the expression $100\ \frac{\sigma_1}{\sigma_\infty}$ gives the proportion of the ferromagnetic spinel present in the titaniferous magnetite and the expression $f\ \frac{\sigma_1}{\sigma_\infty}$ gives the percentage of Fe_3O_4 in the mineral as a whole.

Using this method, Chevallier, Mathieu and Vincent have found that there is good agreement between the % Fe_3O_4 calculated and that obtained by chemical analysis (Table 18) in the case of magnetites from the Skaergaard intrusion.

B. Thermomagnetic Analysis

Curie points have been determined for separated ferromagnetic fractions of the rocks extracted on a Cook magnetic separator as described in Appendix 1, but in some cases, unseparated rock fragments have been used.

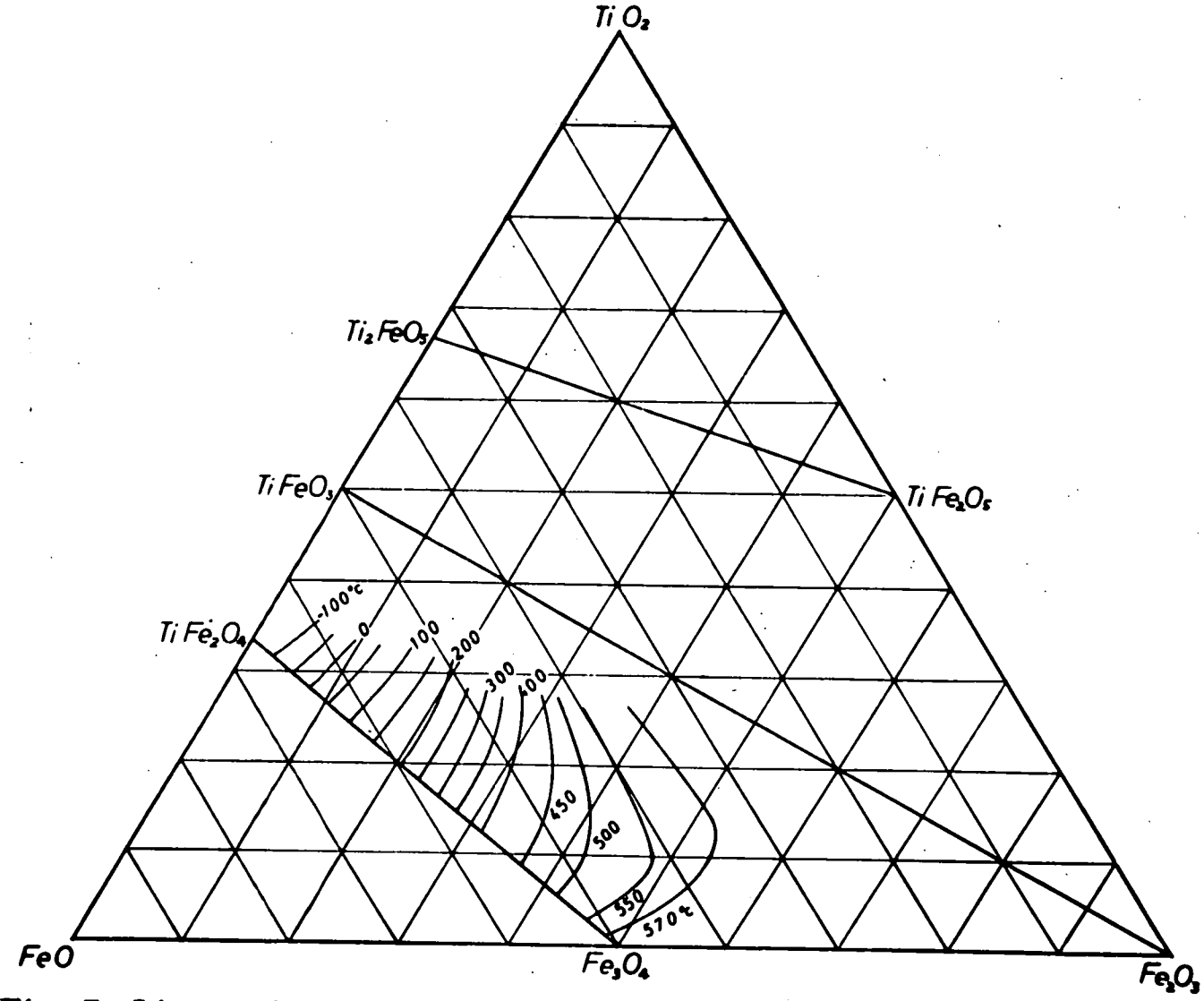

Figure 20.

Fig. 7 Lines of equal Curie temperature of the generalized titanomagnetite in a FeO–Fe_2O_3–TiO_2 system.

Figure 20.

The system FeO-Fe_2O_3-TiO_2 showing lines of equal Curie temperature of 'magnetites' as determined by Akimoto, Katsura and Yoshida (1957).

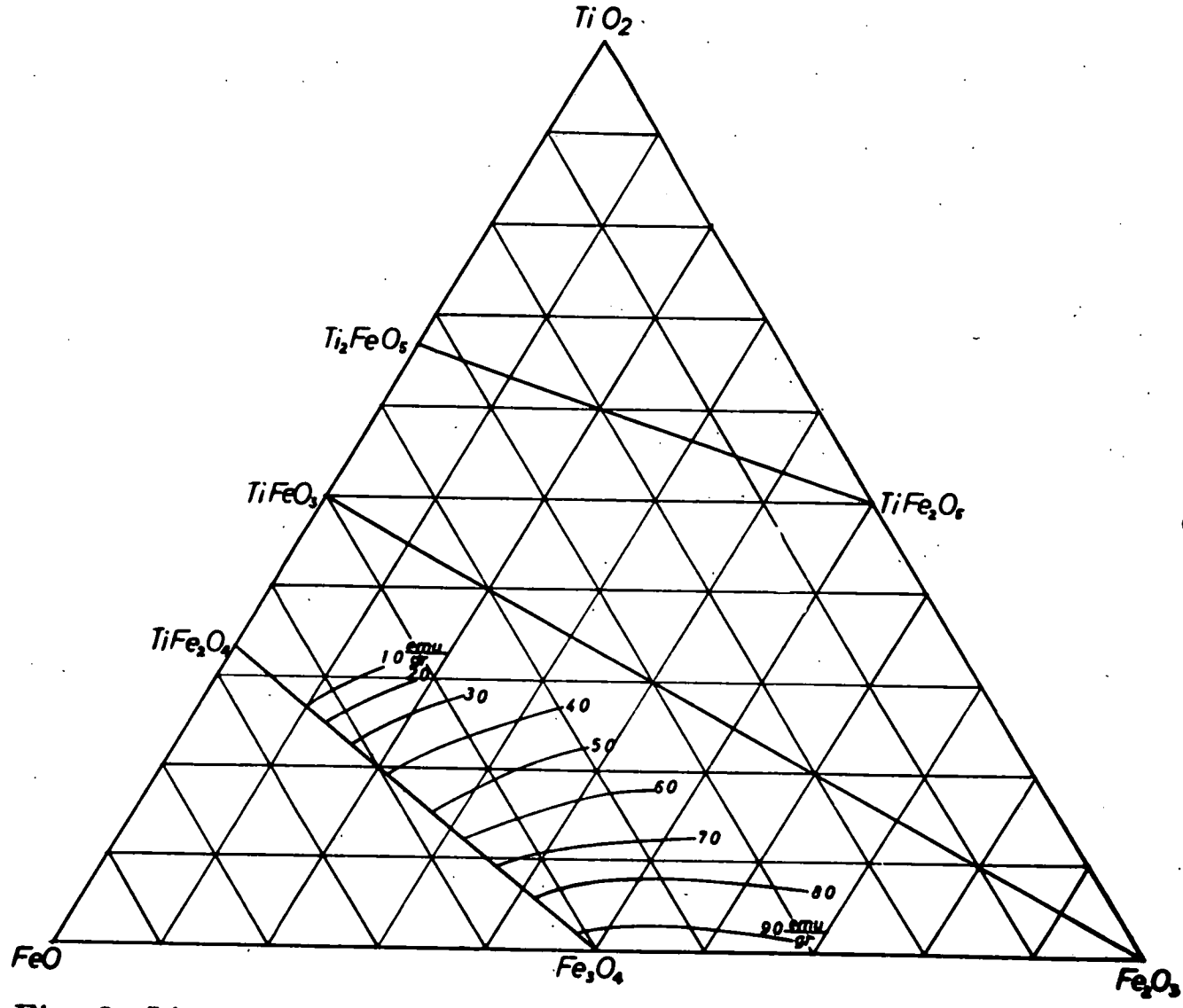

Figure 21.

Fig. 8 Lines of equal saturation moment at the room temperature of the generalized titanomagnetite in a FeO–Fe_2O_3–TiO_2 system.

Figure 21.

The system $FeO-Fe_2O_3-TiO_2$ showing lines of equal saturation magnetization at room temperature of 'magnetites' as determined by Akimoto,Katsura and Yoshida (1957).

Table 18.

The Composition of some Skaergaard 'Magnetites' as determined by Chemical Analyses and deduced from Magnetic Analyses

Rock Number EG	Magnetic Analysis % Fe_3O_4	Chemical Analysis
2307	51.5*	56.0
2308	37.2*	35.3
3661	55.3*	57.3
2574	60.0*	59.7
2569	40.5*	39.9
4147	63.1*	61.5
1974	37.6*	41.8
4142	54.2*	55.3

* Calculated as $f\ \sigma_1 / \sigma_\infty$

Data from Chevallier, Mathieu and Vincent (1954).

The analyses have been made with an automatically recording thermomagnetic balance the construction and calibration data for which form Part II of this thesis. This instrument can measure accurately the Curie point of about 1 mgm of powder.

The accuracy has been checked using samples of pure synthetic Fe_3O_4 prepared by M. Guillaud at Bellevue, France. The results indicate that an accuracy of $\pm$ 1°C may be expected for the Curie points of titaniferous magnetites.

The results of the present investigation are summarized in Table 19 and show graphically in Figure 22. In general, the Curie point is sharp and marked by an abrupt change of slope in the thermomagnetic curve as shown in Figure 23. The results show that the Curie points are highest towards the margins of the intrusion and decrease towards the centre. This variation correlates well with that shown by the unit cell edge of the 'magnetites' (Chapter IV).

However, Figure 24 shows the relationship between the Curie points and the unit cell edges and it is clear that although an inverse relationship exists between them this cannot be explained in terms of simple solid-solutions between Fe_3O_4 (a_o = 8.39 Å; T_c = 585°C) and $TiFe_2O_4$ (a_o = 8.53 Å; T_c = about - 150°C, although theoretically paramagnetic). Instead, the Curie point decreases much less rapidly with increase in a_o, thus indicating that spinels with unit cell edges less than 8.39 Å are also present in solid-solution (see later).

The sandstone at the top contact of the intrusion has a single Curie point of 519°C (measured on a rock fragment). This is almost certainly due to the small amount of 'magnetite' contained in this rock. However, investigations with the ore microscope have shown that 'hematite' is the major ore

Table 19.

Magnetic Properties of Clauchlands 'Magnetites'

Sample	Horizon (feet)	Measured		Calculated			
		θ_c °C	σ_1 emu/g	σ_∞ emu/g	f %	$100\frac{\sigma_1}{\sigma_\infty}$ %	$f\frac{\sigma_1}{\sigma_\infty}$ %
S21	130	537	-	-	-	-	-
S 1	130	547	-	-	-	-	-
S22	129	577	-	-	-	-	-
S25	127	526	-	-	-	-	-
S 2	126	549	31.73	81.5	91.5	38.93	35.6
S 3	122	516	-	-	-	-	-
S 4	118	556	23.19	83.0	92.5	27.94	25.8
S 5	114	470*	-	-	-	-	-
S 6	110	510 526	-	-	-	-	-
S 7	106	472	-	-	-	-	-
S 9	98	488	22.31	67.0	80.5	33.30	26.8
S10	94	467	-	-	-	-	-
S11	90	488	18.75	67.0	80.5	27.98	22.5
S12	86	503 464 443 397	-	-	-	-	-
S30	82	445*	-	-	-	-	-
S31	78	474	11.71	64.0	78.5	18.30	14.4
S34	66	468	-	-	-	-	-
S35	62	332*	-	-	-	-	-
S36	58	405*	-	-	-	-	-
S40	42	509	43.24	71.5	84.0	60.60	50.8
S41	20	533	-	-	-	-	-
C 7**	16	509	-	-	-	-	-
S43	14	495	32.22	68.0	81.5	47.40	38.6
C 6**	12	502*	-	-	-	-	-
S45	8	512 363	-	-	-	-	-
S46	5	522	-	-	-	-	-
S47	$2\frac{1}{2}$	495	26.62	68.0	81.5	39.20	32.0
S13	40 (pegmatite)	589 536	-	-	-	-	-

* Samples showing a range of Curie points - lowest value recorded.

** Abbreviations for samples A/C/1/7 and A/C/1/6.

Addendum :

Sample	Horizon	θ_c	
S14	30	483	) basalt xenoliths.
S15	26	484	

Figure 22.

Curie-Points of the Titanomagnetites
in the Clauchlands Sheet

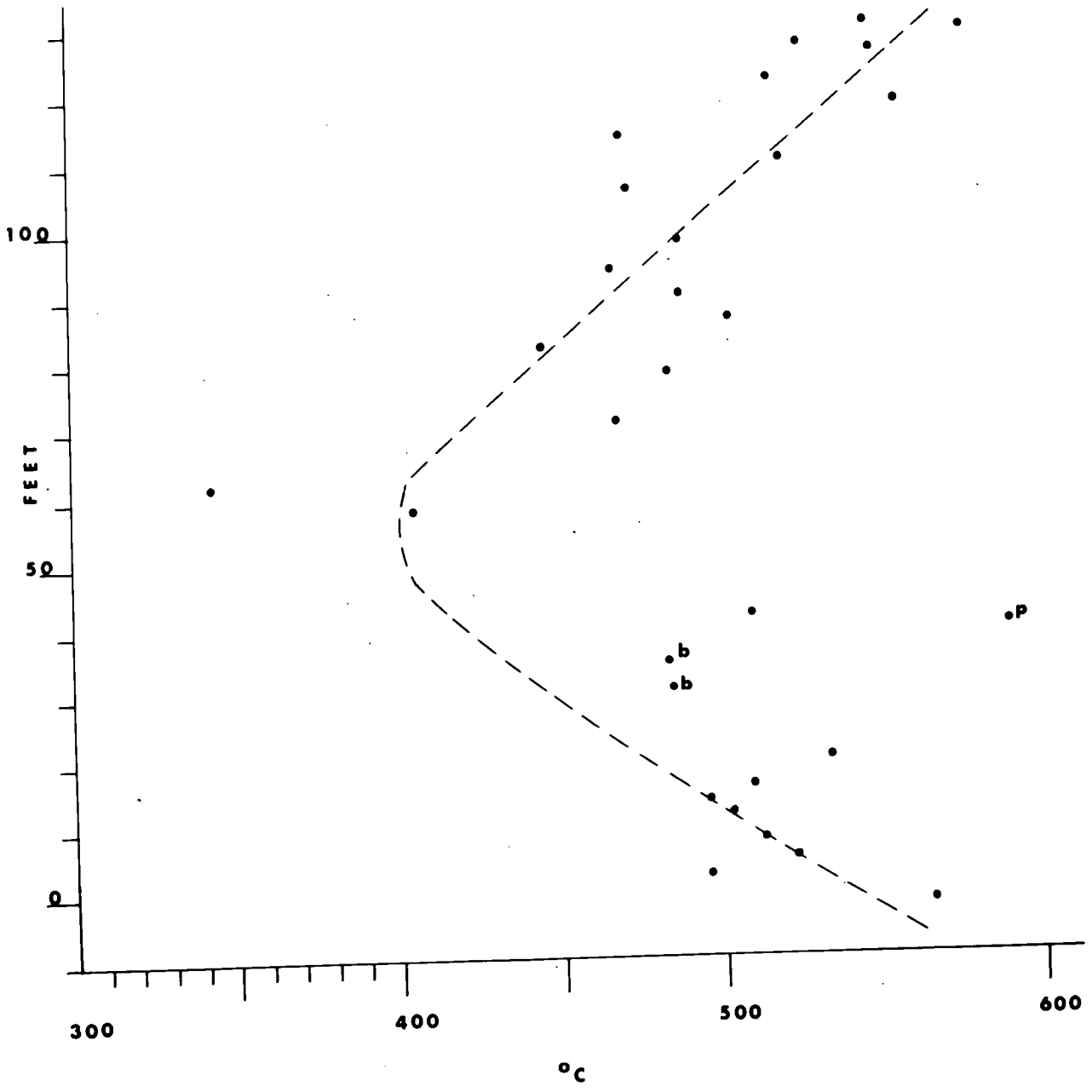

Four samples show more than one Curie point.
Only the highest θ_c has been plotted for these.

Figure 22.

Variation in θ_c of the 'magnetites' in the Clauchlands Sheet.

Figure 23.

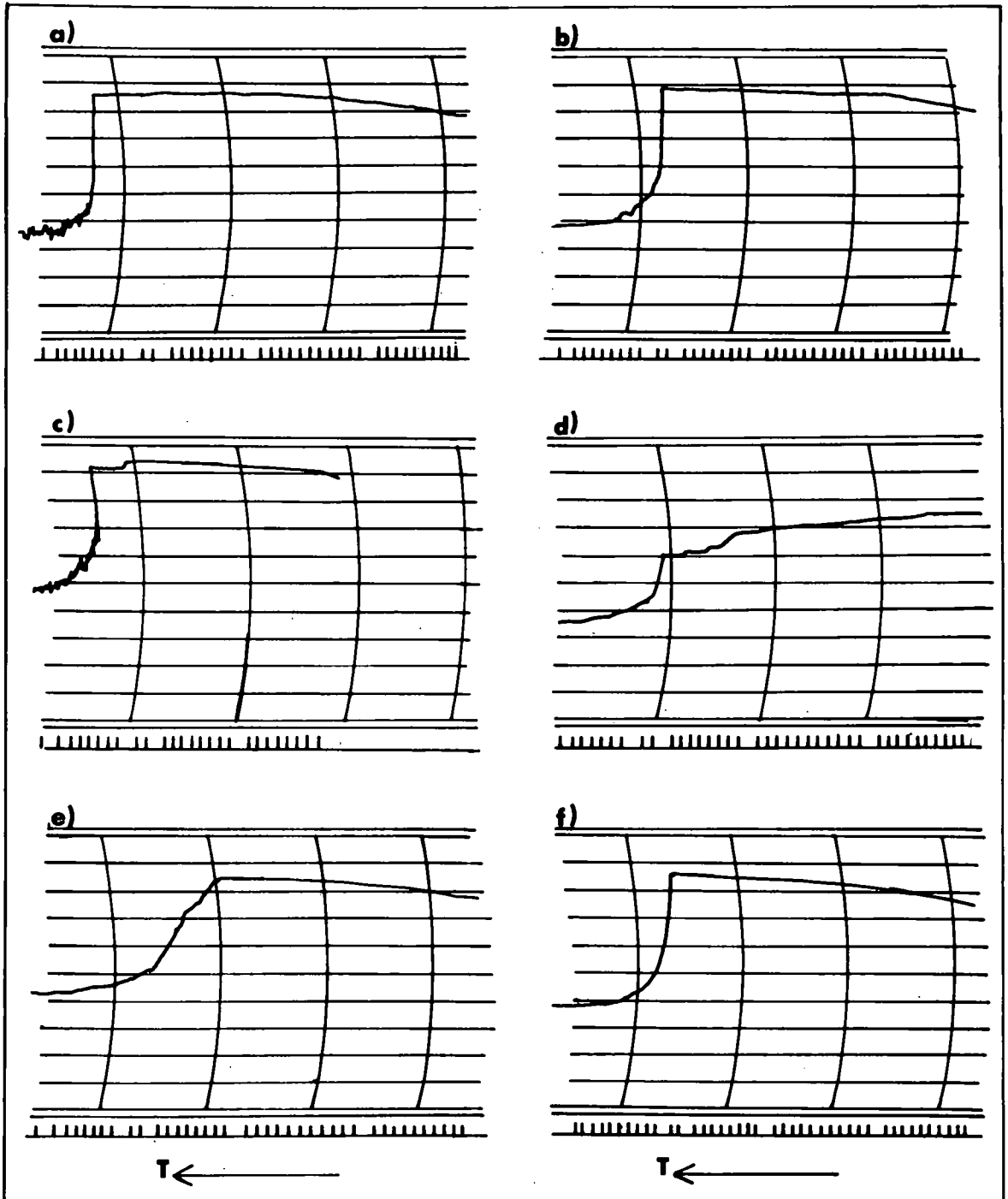

THERMOMAGNETIC CURVES

a) Pure Fe_3O_4 θ = 585°C

b) S3 θ = 516°C

c) S 13 θ = 589°C ; 536°C

d) S 12 θ = 503°C; 464°C; 443°C; 397°C.

e) S 36 θ = 405°C

f) S 25 θ = 526°C

Figure 23.

Examples of thermomagnetic curves obtained with 'magnetites' from the Clauchlands Sheet.

Figure 24.

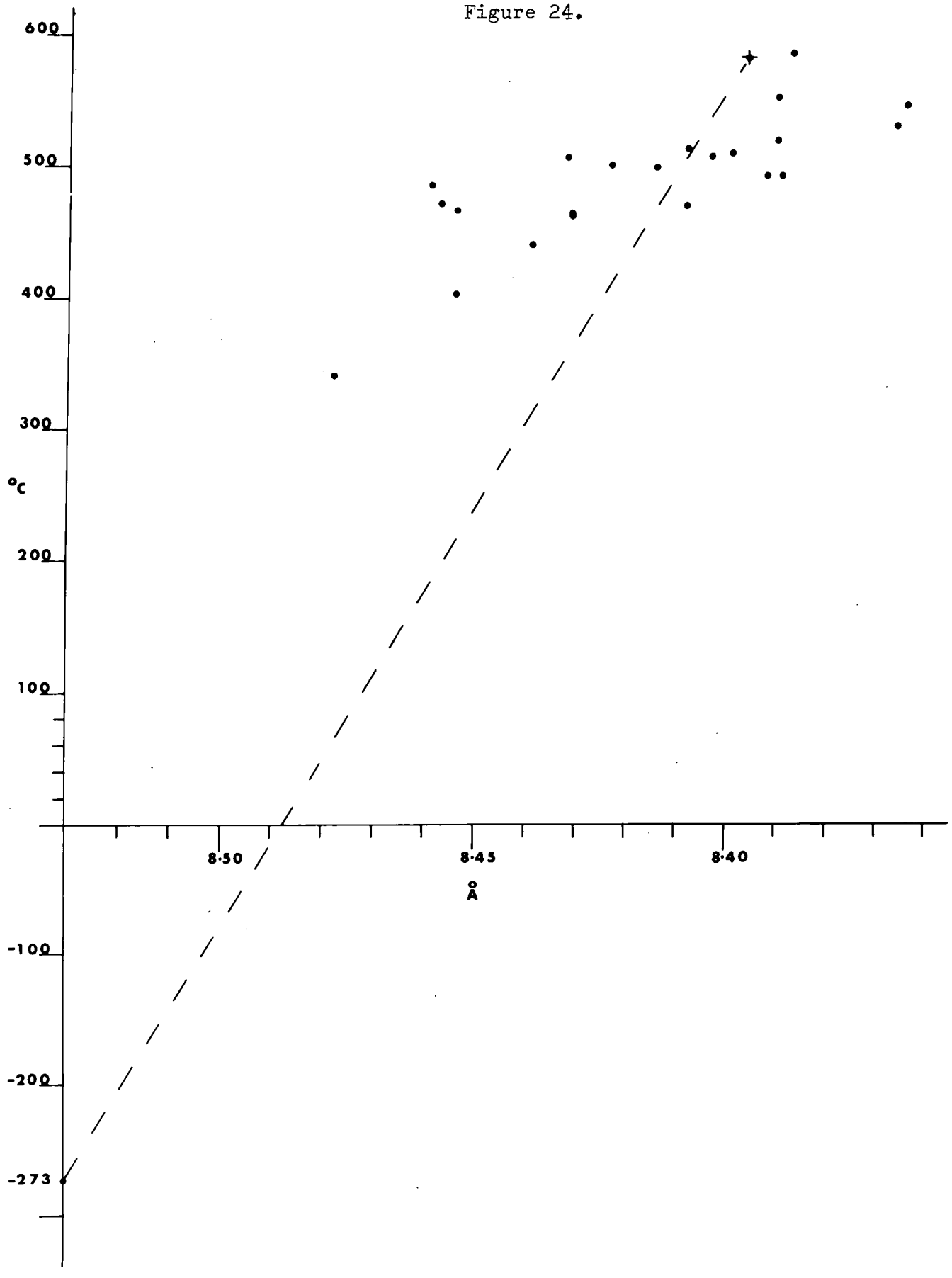

Figure 24.

Relationship between the Curie points and the unit cell edges of 'magnetites' from the Clauchlands Sheet. The dashed line extends from pure Fe_3O_4 with a Curie point of 585°C to pure Fe_2TiO_4 which, ideally, should have no Curie point.

mineral in this rock (Chapter III), and X-ray analysis has indicated that it probably contains about 35 mol% $FeTiO_3$ in solid-solution (Chapter IV) and, therefore, should exhibit a parasitic ferromagnetism (Nagata 1961). Further, according to Akimoto (1957) the Curie point of the hematite-ilmenite solid-solutions varies linearly with composition (Figure 25) and a Curie point of 520°C would correspond to hematite containing about 20 mol% $FeTiO_3$. Therefore, the possibility exists that the measured Curie point is due to the 'hematite'. This is considered unlikely to be the case, because although the 'magnetite' is only present in small amounts, it will have a spontaneous magnetization about 100 times that of the 'hematite' and may be expected to dominate the magnetic properties of the rock. Further, the abrupt loss of magnetization at the Curie point is characteristic of 'magnetites' whereas it is known that the magnetization of the hematite-ilmenite solid-solutions decrease more or less linearly with increase in temperature.

C. Saturation Magnetization at Room Temperature.

Measurement of the saturation magnetization at room temperature has been carried out on 8 of the ferromagnetic powders, but time has been insufficient to allow this to be done on all.

The analyses have been made with a magnetic balance of the translation type the construction and calibration data of which form Part III of this thesis. The accuracy of the measurements have been checked using samples of pure synthetic Fe_3O_4 prepared by M. Guillaud, and these results indicate that errors of $\pm$ 1% to 2% may be expected.

Measurements have been made on two specimens from each sample and the mean values recorded. The results are summarized in Table 19 and the data

Figure 25.

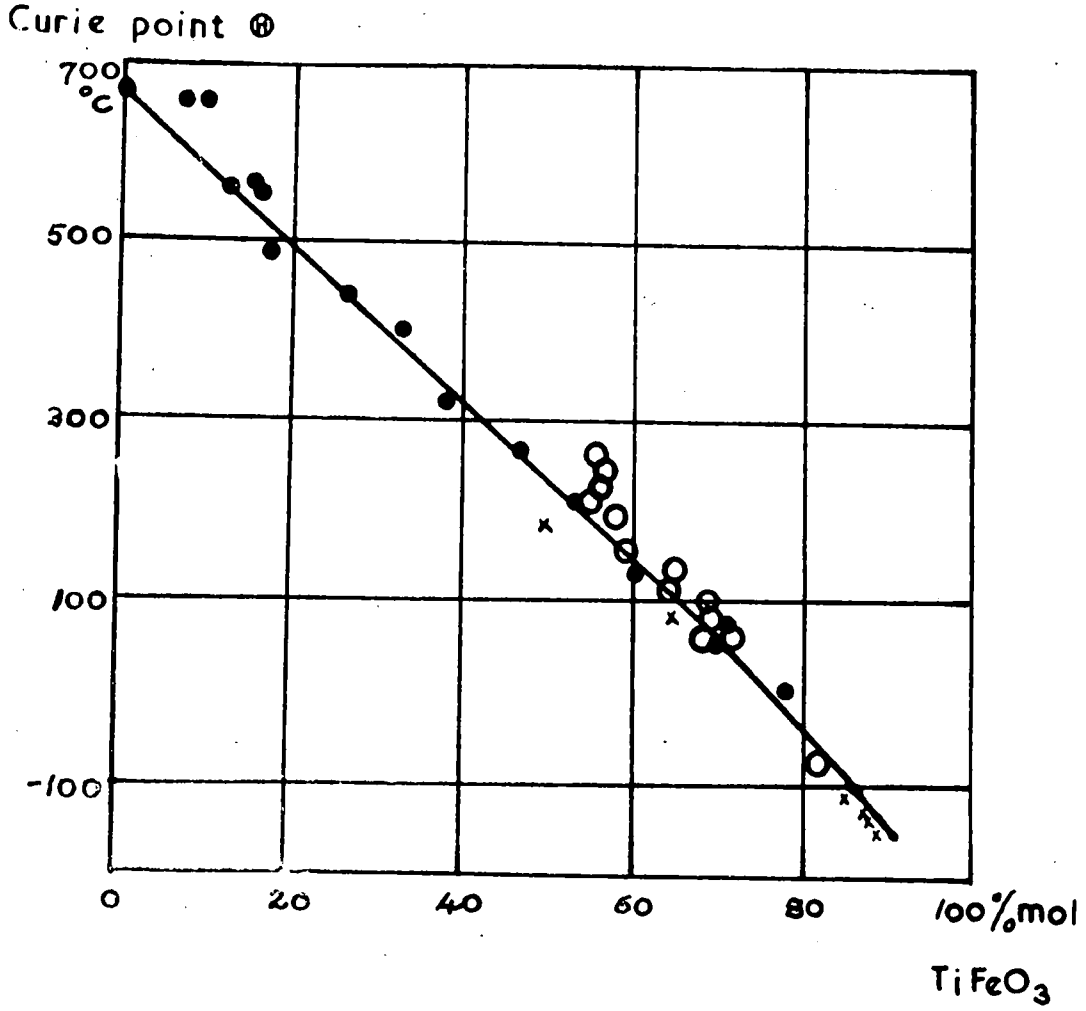

Figure 25.

The relationship between the composition of the rhombohedral $FeTiO_3$-Fe_2O_3 solid solutions and the Curie point.

on which they are based have been included in Appendix 3 .

The % Fe_3O_4 in the 'magnetites' has been calculated from the Curie points (Figure 26a) following the method used by Chevallier, Mathieu and Vincent, and these results are given in Table 19 . They show a general decrease in the Fe_3O_4 -content away from the margins of the intrusion.

Knowing the content of Fe_3O_4 in the 'magnetite', the value of the saturation magnetization corresponding to this composition has been obtained from Figure 26b. The percentage of 'magnetite' in the inhomogeneous 'magnetite'-'ilmenite' sample has then been calculated as $100\frac{\sigma_1}{\sigma_\infty}$ where σ_1 is the measured saturation magnetization. It has been assumed that the remainder of the sample consists of intergrown 'ilmenite'.

These results are given in Table 19 and they show that the amount of 'ilmenite' in the 'magnetite'-'ilmenite' intergrowths is in the range 40 - 80%. There is a clear increase in the amount of intergrown 'ilmenite' away from the top margin of the intrusion, but in view of the limited data it is not certain whether this same trend takes place from the bottom margin.

The %Fe_3O_4 in the 'magnetites' expressed as a percentage of the 'magnetite'-'ilmenite' intergrowths, has been calculated as $f\frac{\sigma_1}{\sigma_\infty}$ and these results are given in Table 19. These values have been plotted against Curie point in Figure 27 and, taking the Curie point of 100% Fe_3O_4 as 585°C, the results show that even for 0% Fe_3O_4 there still remains a magnetic constituent of the intergrowths having a Curie point in the limits 440°C to 530°C.

The intergrown 'ilmenites' are known to contain 10 - 20 mol% Fe_2O_3 in solid-solution (Chaper IV) and according to Akimoto (1957), these would have Curie points in the region of -100°C (Figure 25). Therefore, this other magnetic constituent cannot be the 'ilmenite'.

Figure 26.

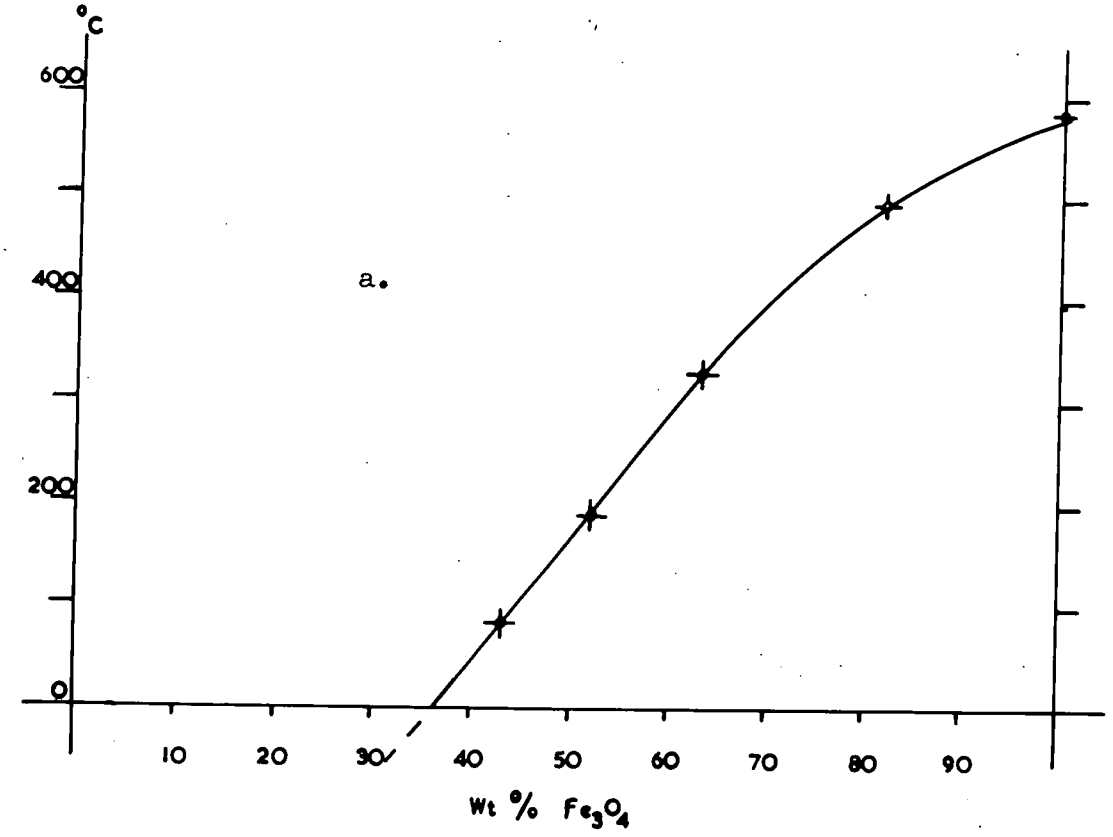
°C
600
400
200
0
a.
10
20
30
40
50
60
70
80
90
Wt % Fe_3O_4

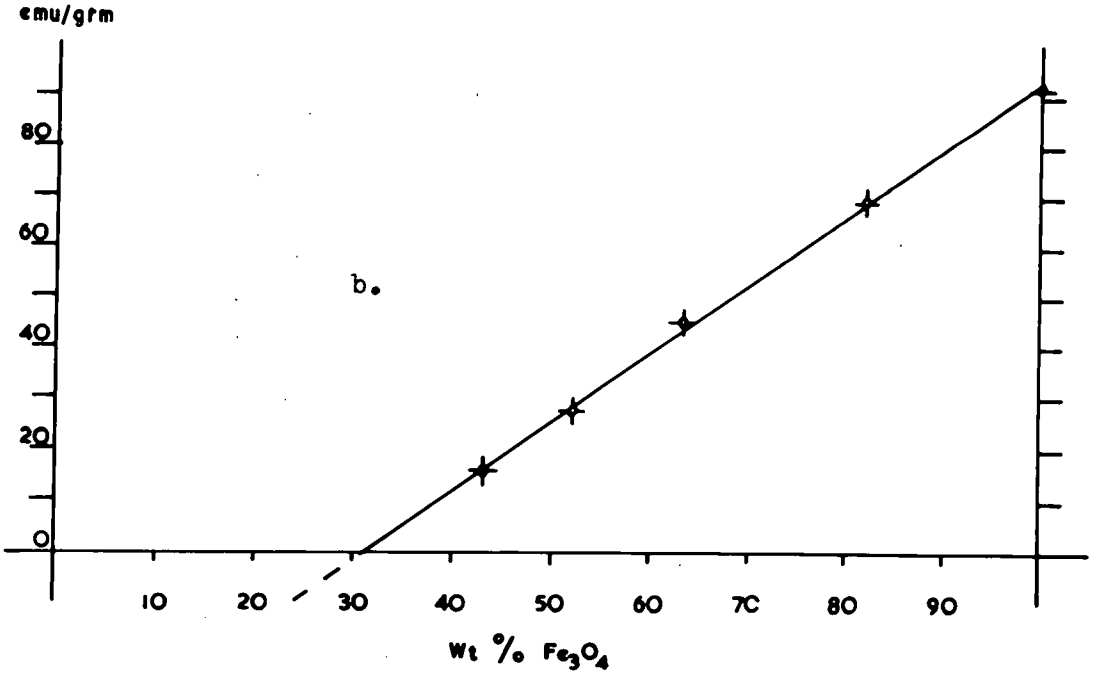
emu/grm
80
60
40
20
0
b.
10
20
30
40
50
60
70
80
90
Wt % Fe_3O_4

Figure 26.

a) The Curie point as a function of $\%Fe_3O_4$ in natural 'magnetites', plotted from the data of Chevallier, Bolfa et Mathieu (1955), but modified slightly by taking the Curie point of pure Fe_3O_4 as 585°C not 578°C.

b) The saturation magnetization at room temperature as a function of $\%Fe_3O_4$ in natural 'magnetites', plotted from the data of Chevallier, Bolfa et Mathieu (1955).

Figure 27.

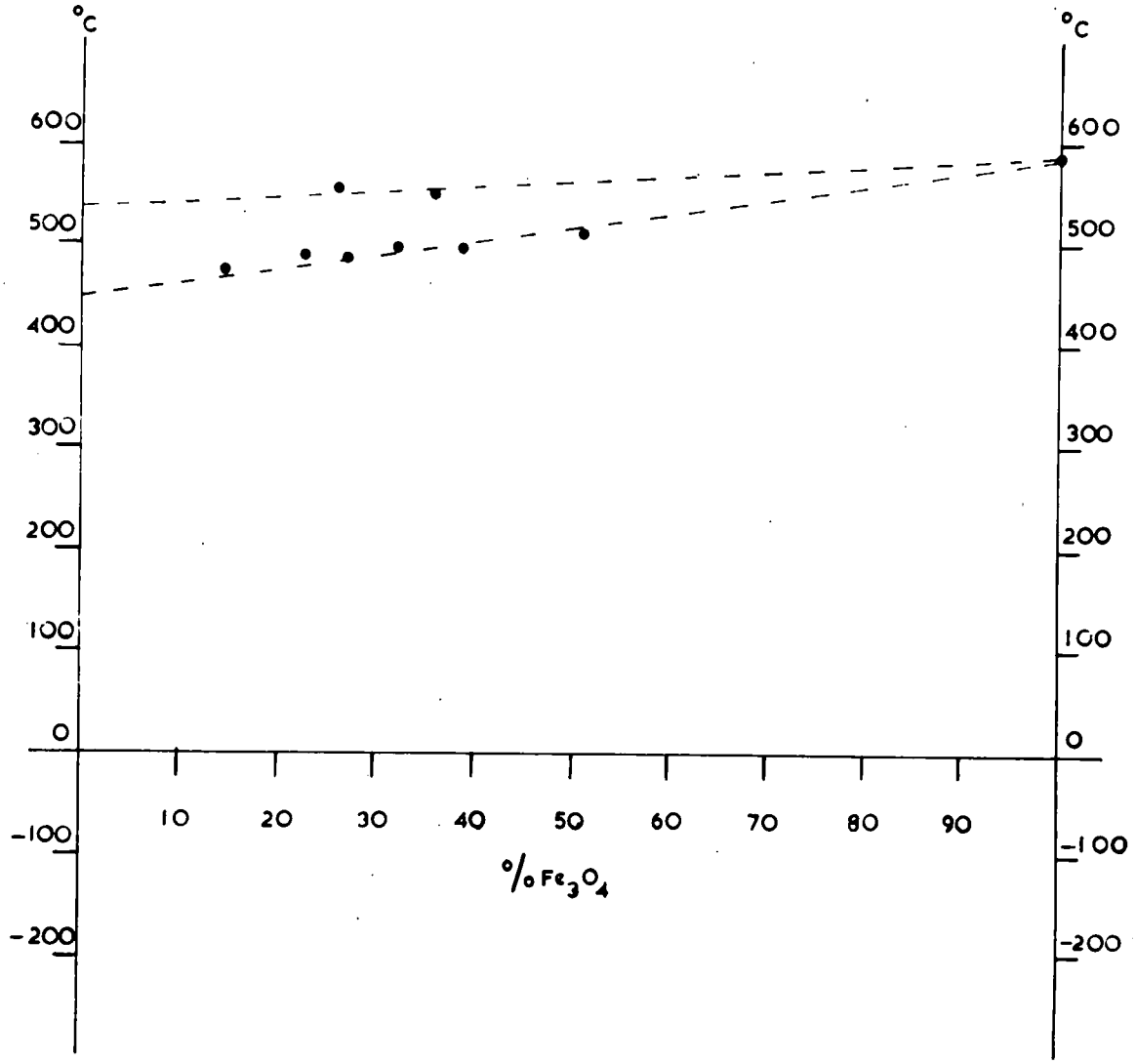

Figure 27.

The $\%Fe_3O_4$ in the 'magnetite' samples from the Clauchlands Sheet, calculated from the magnetic constants, plotted against the Curie points of these samples.

It is known that $MgFe_2O_4$ has a Curie point of 440°C (Brailsford 1960), so that is suggested that this may be the other constituent present in solid-solution in the 'magnetite'.

D. Magnetic Nature of the Iron-Titanium Oxide Minerals

Since a clear understanding of the magnetic nature of the iron-titanium oxide minerals is essential to an understanding of the above results and also to the discussion in the following Chapters, some fundamental aspects of this magnetization are reviewed below.

1) The Origin of Magnetic Moment (Ref. Brailsford 1960; Nagata 1961)

Magnetism in its most elementary form is due to electrons. The magnetic moment of an atom is cause either by the orbital motion or the spin of its electrons or by a combination of both.

An orbiting electron is equivalent to a circular current and this in turn is equivalent to a magnetic shell having a magnetic moment m. The value of m corresponding to this orbital motion is given by:-

$$m = l\frac{eh}{4\pi m_o c} \qquad \text{.....1)}$$

where e = the charge of the electron.

m_o = the rest mass of the electron.

c = velocity of light

h = Planck's constant

l = the asimuthal quantum number, which gives the orbital angular momentum of the electron and indicates its sub-shell in the Bohr atomic model.

The ratio of the angular momentum N of the orbiting electron to the

magnetic moment m is given by:-

$$r_o = \frac{N}{m} = \frac{2m_o c}{e} \qquad \ldots\ldots\ldots\ldots 2)$$

whilst the ratio of the angular momentum of the spinning electron to the magnetic moment is given by:-

$$r_s = \frac{m_o c}{e} \qquad \ldots\ldots\ldots\ldots 3)$$

and thus half that due to the orbital motion.

The relative contributions to the magnetic moment of an atom made by the spin and the orbital motions are given by Landé's factor, g, which appears in the expression:-

$$r = \frac{2m_o c}{e} \cdot \frac{1}{g} \qquad \ldots\ldots\ldots\ldots 4)$$

where $1 \leqslant g \leqslant 2$, and r is the ratio of the magnetic moment of the atom to the angular momentum of the electrons within it.

According to the classical atomic theory of Bohr (1913), electrons can only revolve around a nucleus in certain definite orbits, or shells, corresponding to certain allowed energy states.

These shells are shown in Table 20 for the ferromagnetic elements Mn, Fe, Co and Ni together with the electron configuration for the corresponding ions. They may be compared with the non-magnetic elements Mg, Al, Ti, Cu and Zn.

In copper, for example, the 3d sub-shell is complete with 10 electrons

Table 20.

The Electron Configurations of some Common Magnetic and Non-Magnetic Atoms and Ions.

Shell		K	L			M		N
Sub-shell		1s	2s	2p	3s	3p	3d	4s
Z.								
12	Mg	2	2	6	2			
	Mg^{2+}	2	2	6	-			
13	Al	2	2	6	2	1		
	Al^{3+}	2	2	6	-	-		
22	Ti	2	2	6	2	6	2	2
	Ti^{4+}	2	2	6	2	6	-	-
25	Mn	2	2	6	2	6	5	2
	Mn^{2+}	2	2	6	2	6	5	-
26	Fe	2	2	6	2	6	6	2
	Fe^{2+}	2	2	6	2	6	6	-
	Fe^{3+}	2	2	6	2	6	5	-
27	Co	2	2	6	2	6	7	2
	Co^{2+}	2	2	6	2	6	7	-
28	Ni	2	2	6	2	6	8	2
	Ni^{2+}	2	2	6	2	6	8	-
29	Cu	2	2	6	2	6	10	1
	Cu^{+}	2	2	6	2	6	10	-
30	Zn	2	2	6	2	6	10	2
	Zn^{2+}	2	2	6	2	6	10	-

but in Mn, Fe, Co and Ni, this subshell is incomplete to the extent of 5, 4, 3 and 2 electrons respectively and hence the atoms have uncompensated spins. These uncompensated spins give rise to atomic magnetic moments of 5, 4, 3 and 2μ_B respectively, where 1μ_B is the magnetic moment due to a single spinning electron and is known as the Bohr magneton. From equation 1), the value of the Bohr magneton is given as:-

$$1\,\mu_B = \frac{eh}{4\pi m_o c} = 0.9274 \quad 10^{-20} \text{emu} \qquad \ldots\ldots\ldots 5)$$

Similarly, the ions Mn^{2+}, Fe^{2+}, Fe^{3+}, Co^{2+} and Ni^{2+}, have spin magnetic moments of 5, 4, 5, 3 and 2μ_B respectively, whereas the ions Mg^{2+}, Al^{3+}, Ti^{4+}, Cu^{+} and Zn^{2+} are non-magnetic.

Experiments have shown that the Landé factor for these atoms is nearly 2 thus indicating that their magnetic moments are due largely to the spin of the electrons rather than to their orbital motions (Greenwald, Pickart & Grannis 1954).

For elements coming higher in the periodic table than nickel, the M shell is complete with 18 electrons and since a completed shell is magnetically neutral the atoms have no net magnetic moment. Thus, only atoms with incomplete electron shells can have a magnetic moment.

2) Diamagnetism, Paramagnetism and Ferromagnetism.

Diamagnetism is a property fundamental to all substances although its effects may be hidden when the substance contains atoms having magnetic moments.

If a field H is applied at some angle to the plane in which an electron is orbiting, then Larmor has shown that the whole orbit precesses with the direction of H as axis, and that the direction of the precessional rotation

is such as to set up an opposing field to that applied.

This is the phenomenon which gives diamagnetic substances a negative susceptibility:-

$$k = -N \frac{e^2}{6m_o c^2} \sum \overline{r_{oi}^2} \qquad \ldots\ldots\ldots\ldots 6)$$

where N = the number of atoms in unit volume.

r_{oi} = the radius of the orbit of an electron from the centre of the nucleus.

Paramagnetic substances, on the other hand, contain a large number of atoms having a magnetic moment, such as Fe, Mn, Ni, Co, but since the interaction among them is very small these moments are randomly oriented and hence the substance has no net magnetic moment.

However, under the effect of a field H, the substance takes on a magnetic moment M which, at temperature T, is given approximately by:-

$$\frac{M}{M_o} = \frac{M_o H}{3RT} \qquad \ldots\ldots\ldots\ldots 7)$$

where M_o = the sum of the magnetic moments of all the atoms in unit volume.

R = Boltzmann's universal gas constant.

The paramagnetic susceptibility per mol is thus given by:-

$$\chi_{mol} = \frac{M}{H} = \frac{M_o^2}{3RT} = \frac{C}{T} \qquad \ldots\ldots\ldots\ldots 8)$$

and this relation is known as Curie's law. It states that for a paramagnetic

substance χ_{mol} is inversely proportional to the absolute temperature. The constant $C = M_o^2 / 3R$ is called the Curie constant; it should not, however, be confused with the Curie temperature (or Curie point) of ferromagnetic substances.

In a ferromagnetic substance the interaction among neighbouring atoms is so strong that the magnetic moments of all the atoms tend to be parallel and a magnetization (J_s per unit volume) exists even when there is no external field. This magnetization is known as the spontaneous magnetization.

The spontaneous magnetization decreases with increasing temperature according to the Curie-Weiss law:-

$$\chi_{mol} = \frac{M_o^2}{3R} \frac{1}{T - T_c} \qquad \ldots\ldots\ldots\ldots 9)$$

and becomes zero at the Curie temperature T_c, above which the substance behaves as a paramagnetic and follows Curie's law (Equation 8). It can thus be seen that Curie's law corresponds to the extreme case where T_c is absolute zero.

3) Antiferromagnetism and Ferrimagnetism

Some magnetic substances have properties which cannot be classified as either ferromagnetic or paramagnetic. Although they have susceptibilities of the order of 10^{-3} emu which would indicate that they are paramagnetic they do not follow Curie's law. Instead, the susceptibility takes a maximum value at a temperature known as the λ-point, or Néel temperature, and at higher temperatures it varies according to the Curie-Weiss law:-

$$\chi = \frac{C}{T + \theta} \qquad \ldots\ldots\ldots\ldots 10)$$

where θ, the Curie point, is generally positive.

The magnetic state at temperatures below the Néel temperature can be attributed to the condition that the spins of the neighbouring atoms are antiparallel to one another owing to a negative exchange reaction (cp positive exchange reaction in ferromagnetic substances), and hence this phenomenon is known as antiferromagnetism (Van Vleck 1945).

When an antiferromagnetic coupling occurs between atoms having different magnetic moments, then the substance exhibits a net magnetic moment, as with ferromagnetic substances, and has a spontaneous magnetization, J_s, due to the difference between the opposing magnetic moments.

The magnetic properties of such substances are, therefore, very like those of ferromagnetic substances and hence this special case of antiferromagnetism has been called ferrimagnetism (Néel 1948).

Ferrimagnetic substances have a Curie temperature, as with ferromagnetic substances, at which the spontaneous magnetization becomes zero, but above this temperature their paramagnetic susceptibilities do not follow Curie's law (Equation 8) but vary according to a hyperbolic function:-

$$\frac{1}{\chi} = \frac{T}{C} + \frac{1}{\chi_o} - \frac{\sigma}{T - \theta} \qquad \ldots\ldots\ldots 11)$$

where C = the theoretical Curie constant of the ions present.

θ = the Curie temperature.

σ = the saturation magnetic moment at absolute zero.

The values of χ_o, σ and θ depend on the magnitude of the magnetic interactions.

4) The Ferrimagnetic Iron-Titanium Oxide Minerals

The silicate minerals which form the greater part of most rocks are either paramagnetic or diamagnetic depending on the presence or absence of

magnetic ions such as Fe^{2+}, Fe^{3+} and Mn^{2+}. Thus quartz and the feldspars are typically diamagnetic minerals whereas, olivine, pyroxenes and biotite, are paramagnetic.

Certain of the iron-titanium oxide minerals, however, are ferrimagnetic and have properties analogous to those of the ferrites MFe_2O_4, where M is a divalent ion such as Mn, Fe, Co, Ni, Zn, Mg.

The magnetic ferrites are generally cubic and have an inverse spinel structure (Chapter IV) so that, ideally, the M ion occupies one of the B-sites and the two Fe^{3+} ions are divided between the A-site and the remaining B-site:-

$$\underset{A}{Fe^{3+}} \quad \underset{B}{(M^{2+} \; Fe^{3+})} \quad O_4$$

Three sets of interatomic forces exist in such a structure those between ions on A-sites, those between ions on B-sites and those between ions on the A- and B-sites, that is A-A, B-B, and A-B interactions.

The interaction in these ionic compounds occurs via the adjoining anions (oxygen). A theory of this so-called super-exchange has been given by Anderson (1950), whose calculations show that for Fe^{3+} and other ions with five or more 3d electrons, these interactions are negative and the two metal ions have antiparallel spin, whereas for Cr^{3+} or other ions with less than five 3d electrons these interactions are positive and the two metal ions have parallel spin. The theory also indicates that the interaction is strongest for a collinear configuration M - O - M and weakest for a right-angle configuration $\begin{matrix} M - O \\ \quad\quad | \\ \quad\quad M \end{matrix}$.

In the spinel structure the A- and B-sites are relatively close together and make an angle A-O-B of about 125°, whereas adjacent A-sites and B-sites are much further apart and make angles A-O-A and B-O-B of about 80° and 93° respectively (Gorter 1957). Therefore A-A and B-B interactions are weak as compared with the strong A-B interactions. The theory of super-exchange also indicates that the A-B interactions are negative in the ferrites.

This result was postulated independently by Néel in order to explain the magnetic properties of ferrites and it has been confirmed by neutron diffraction studies on a number of ferrites (Shull et al 1951; Hastings and Corliss 1953; Corliss et al 1953).

Thus at low temperatures, when the thermal disturbance of the ions is small, the magnetic lattice of a ferrite may be regarded as divided into two sublattices A and B whose spontaneous magnetizations J_A and J_B are oriented in opposite directions. (Néel 1955). The net magnetic moment is then the difference between the moments on the A- and B-sites:-

$$\underset{J_A}{\overrightarrow{Fe^{3+}}} \quad (\underset{J_B}{\overleftarrow{M^{2+}} \; \overleftarrow{Fe^{3+}}}) \; O_4$$

and since the moments of the Fe^{3+} ions cancel out, the magnetic moment of the ferrite is given by the moment of the M ion.

Data on the magnetic properties of some common ferrites have been summarized in Table 21 and it can be seen that there is in general a close agreement between the measured magnetic moments and those calculated from the theory. Thus for M $= Ni^{2+}$, Co^{2+}, Fe^{2+} and Mn^{2+} the molecular magnetic moments of the corresponding ferrites are close to 2, 3, 4 and 5 μ_B which are

Table 21.

Properties of some Ferrites : after Brailsford 1960.

Ferrite	Structure $\rightarrow$ A $\leftarrow$ B $\leftarrow$	Magnetic Moment Theoretical	Magnetic Moment Measured	Curie Temperature
$MnFe_2O_4$	$Fe^{3+}.(Mn^{2+}\ Fe^{3+}).O_4$	$5\mu_B$	$4.6\mu_B$	300°C
$FeFe_2O_4$	$Fe^{3+}.(Fe^{2+}\ Fe^{3+}).O_4$	$4\mu_B$	$4.1\mu_B$	585°C
$CoFe_2O_4$	$Fe^{3+}.(Co^{2+}\ Fe^{3+}).O_4$	$3\mu_B$	$3.7\mu_B$	520°C
$NiFe_2O_4$	$Fe^{3+}.(Ni^{2+}\ Fe^{3+}).O_4$	$2\mu_B$	$2.3\mu_B$	585°C
$CuFe_2O_4$	$Fe^{3+}.(Cu^{2+}\ Fe^{3+}).O_4$	$1\mu_B$	$1.3\mu_B$	455°C
$MgFe_2O_4$	$Fe^{3+}.(Mg^{2+}\ Fe^{3+}).O_4$	0	$1.1\mu_B$	440°C
$ZnFe_2O_4$	$Zn^{2+}.(Fe^{3+}\ Fe^{3+}).O_4$	0	0	-

the values of the spin magnetic moments of these ions (Table 20). The slight remaining differences are probably due to residual orbital moments (Néel 1955).

Natural magnetites, however, rarely contain appreciable amounts of Co^{2+}, Ni^{2+} or Mn^{2+} (Chapter IV) so that these ferrites are unlikely to contribute significantly to the magnetic properties of substituted magnetites. On the other hand, Mg^{2+}, may sometimes occur in appreciable amounts and although magnesioferrite should ideally, be non-magnetic:-

$$\underset{J_A}{Fe^{3+}} \quad (\underset{J_B}{Mg^{2+}} \quad \underset{J_B}{Fe^{3+}}) \quad O_4$$

it generally has a molecular moment of about $1.1\mu_B$ which can be explained by a formula $Fe_{1-x}Mg_x\ (Mg_{1-x}Fe_x)\ O_4$ with $x = 0.11$ (Gorter 1957). Hence, the presence of $MgFe_2O_4$ may sometimes influence the magnetic properties of magnetite.

The great majority of natural magnetites, however, are titaniferous and are either solid solutions between $FeFe_2O_4$-$TiFe_2O_4$ or their oxidised equivalents. Thus, it is the magnetic effects associated with the substitution of Ti^{4+} that are of primary interest.

These effects have been investigated by a number of research workers, Barth and Posnjak 1932; Ernst 1943; Pouillard 1950; Chevallier and Girard 1950; Chevallier, Bolfa et Mathieu 1955; Akimoto 1954, 1955, 1957, 1962; Akimoto, Katsura and Yoshida 1957; Akimoto and Katsura 1959; Katsura and Kushiro 1961.

Ti^{4+} is a non-magnetic ion with the electron configuration:-

Shell	K	L		M		
	1s	2s	2p	3s	3p	3d
	2	2	6	2	6	-

it therefore acts as a diluent to the magnetic properties of magnetite and causes a decrease in the saturation magnetization and Curie temperature as the substitution of Ti^{4+} increases.

Ulvöspinel $TiFe_2O_4$ is paramagnetic at room temperatures and at lower temperatures it should be antiferromagnetic (Nagata 1961):-

$$\underset{J_A}{Fe^{2+}} \quad (\ Ti^{4+} \quad \underset{J_B}{Fe^{2+}}\ ) \quad O_4$$

According to Akimoto (1962), the Curie points of the synthetic solid-solutions between Fe_3O_4 and $TiFe_2O_4$ decrease with increasing $TiFe_2O_4$ content as shown in Figure 28 and reach room temperature at a composition of 20% Fe_3O_4. The extrapolation of this curve indicates that pure $TiFe_2O_4$ has a Curie point of about $-150^{\circ}C$, and therefore the ideal antiferromagnetic arrangement shown above does not hold.

Chevallier, Bolfa and Mathieu (1955) have shown that the Curie points of natural titaniferous magnetites decrease with Fe_3O_4 content as shown in Figure 26a. For compositions in the range 60 - 100% Fe_3O_4, this curve agrees with that given by Akimoto for the synthetic solid-solutions. For compositions less than 60% Fe_3O_4, however, the results diverge increasingly from those given for the synthetic solid-solutions and at room temperature there is a difference of about 16% Fe_3O_4 between the composition given by Akimoto's curve and that given for the natural minerals. It would seem, therefore, that the relationship between the Curie point and the composition of natural magnetites

Figure 28.

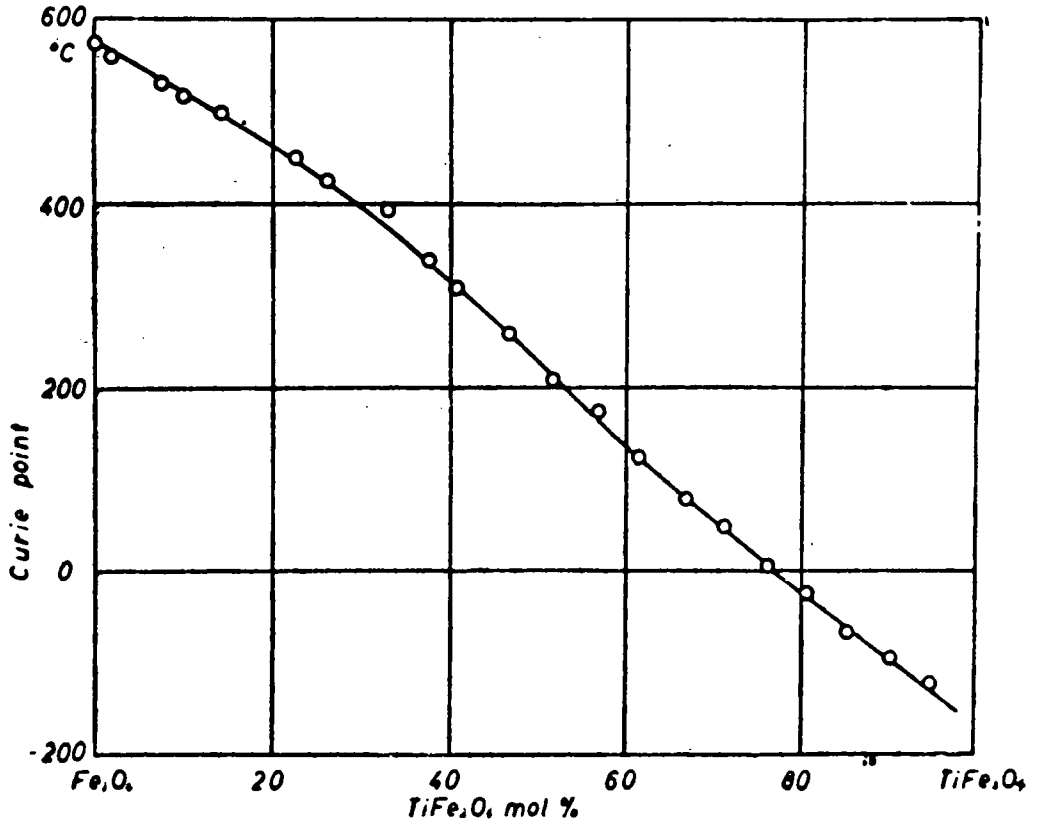

Figure 29.

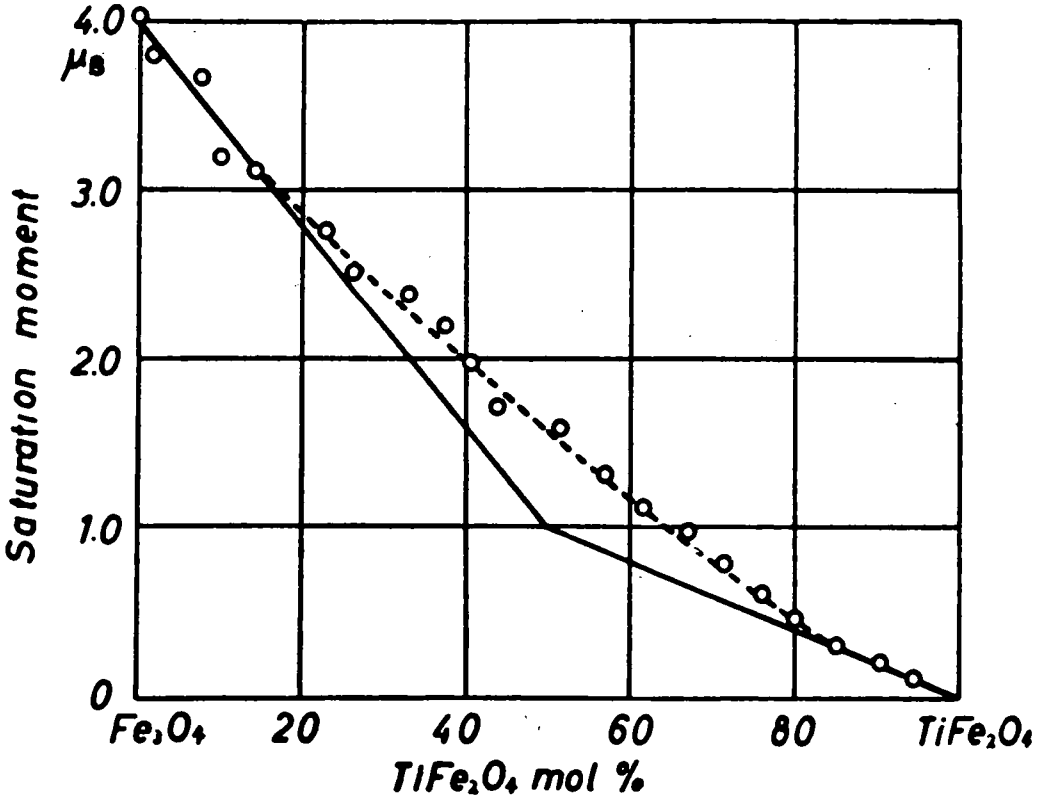

Figure 28.

The Curie point as a function of composition in the cubic Fe_3O_4-Fe_2TiO_4 solid solutions. (after Akimoto 1957).

Figure 29.

The saturation magnetization at absolute zero as a function of composition in the cubic Fe_3O_4-Fe_2TiO_4 solid solutions. (after Akimoto 1957).

(which contain other oxides such as MgO, Al_2O_3, V_2O_3 etc.) are somewhat different from those for the synthetic solid-solutions, although these differences are apparently not great for minerals having Curie points higher than about 300°C.

The saturation magnetization at absolute zero of synthetic Fe_3O_4-$TiFe_2O_4$ solid-solutions decreases more or less linearly with increase in $TiFe_2O_4$ from about $4\mu_B$ for Fe_3O_4 to zero for $TiFe_2O_4$ as shown in Figure 29 (Akimoto 1962). Both Nicholls (1955) and Gorter (1957) have suggested that this variation indicates one or other of the following cation distributions in these solid-solutions:-

$$Fe^{3+}_{1-a}Ti^{4+}_{a}.\ (Fe^{2+}_{1+x}Fe^{3+}_{1-2x+a}Ti^{4+}_{x-a}).\ O^{2-}_{4}$$

with a saturation moment of $4 - 6x + 10a$ or:-

$$Fe^{3+}_{2-2x}Fe^{2+}_{2x-1-a}Ti^{4+}_{a};\ (Fe^{2+}_{2-x+a}Ti^{4+}_{x-a}).\ O^{2-}_{4}$$

with a saturation moment of $2 - 2x + 8a$.

Thus, if titaniferous magnetites were simply solid-solutions between magnetite and ulvöspinel, then measurement of the Curie point would give the chemical composition and a determination of the saturation magnetization would indicate the probable distribution of the cations.

However, natural 'magnetites' are not such simple compounds and rarely do they have compositions that plot directly on the Fe_3O_4-$TiFe_2O_4$ join in the system FeO-Fe_2O_3-TiO_2, but instead, they may have compositions that plot well to the right of this join as shown in Figure 6 (Chapter IV). It is known that

such γ-phases may form by oxidation of Fe_3O_4-$TiFe_2O_4$ solid-solutions (β-phases) (see Chapter III), and Akimoto, Katsura and Yoshida (1957) have shown that as oxidation proceeds, the Curie points become higher (Figure 20), while for magnetites having a low content of $TiFe_2O_4$ the saturation moment decreases, and for magnetites having a high content of $TiFe_2O_4$, the saturation moment increases as oxidation proceeds (Figure 21).

5) Magnetic Properties of the Rhombohedral Iron-Titanium Oxide Minerals

Ilmenite is antiferromagnetic at very low temperatures, below the liquid nitrogen temperature, and has a Néel temperature of 55°K. (Ishikawa and Akimoto 1957). Shirane et al (1959), have demonstrated this antiferromagnetic structure by means of neutron diffraction studies. Above the temperature of liquid nitrogen, ilmenite becomes paramagnetic.

However, the magnetization of some antiferromagnetic substances at temperature T in a field H can be represented by the formula:-

$$\sigma = \sigma_0 + \chi H \qquad \text{.....12)}$$

where the specific susceptibility has a maximum value as with ordinary antiferromagnetics, but the substance also has a weak spontaneous magnetization σ_0 of about 10^{-1}-10^{-2} μ_B /mol which is much less than that of ordinary ferrimagnetic substances. This spontaneous magnetization disappears at the Curie point and this phenomenon has been called parasitic ferromagnetism. (Néel 1953).

Hematite Fe_2O_3 is a typical example of a substance with parasitic ferromagnetism (Néel and Pauthenet 1952; Néel 1953), and it has a Curie point of 677°C at which the weak ferromagnetism disappears.

The magnetic properties of the ilmenite-hematite solid-solutions $xFeTiO_3 \cdot (1-x)Fe_2O_3$ vary according to composition. Pure ilmenite ($x = 1.0$) is antiferromagnetic, below the Néel temperature, solid solutions in the range $1 > x \geqslant 0.45$ (i.e. ferri-ilmenites) are ferrimagnetic, and solid-solutions in the range $0.5 \geqslant x > 0$ (i.e. titanhematites and hematite) have a parasitic ferromagnetism superimposed on antiferromagnetism (Akimoto 1962).

X-ray analysis (Ishikawa and Akimoto 1958) and neutron diffraction studies (Shirane et al 1959) have shown that the ferrimagnetic ferri-ilmenites have an ordered structure and that the transition to the antiferromagnetic titanhematites is accompanied by a change to a disordered structure.

Ilmenite with symmetry $R\bar{3}$ corresponds to an ordered hematite structure, with symmetry $R\bar{3}C$ (Posnjak and Barth 1934). In the ordered state the Ti^{4+} ions selectively occupy every other cation layer perpendicular to the triad axis whilst in the disordered state the Ti^{4+} and Fe^{2+} ions are distributed equally through all the layers. Therefore, in the ferri-ilmenites a net magnetic moment appears due to the presence of Fe^{3+} (from Fe_2O_3) distributed in the ordered structure.

Akimoto (1957) has shown that the Curie point of the ilmenite-hematite solid-solutions decreases almost linearly with composition from 680°C for hematite, and reaches room temperature for a composition of about 75 mol% $FeTiO_3$ (Figure 25). Chevallier Bolfa and Mathieu (1955) have found that naturally occurring titanhematites generally have Curie points in the range 680°C to 600°C while the naturally occurring ferri-ilmenites have Curie points below about 250°C.

E. Summary

The Curie points and saturation magnetization of samples from the Clauchlands

sheet have been measured.

The Curie points have been found to vary systematically through the intrusion. They are highest towards the margins ($\theta_c \sim 500^{\circ}C$) and decrease towards the centre of the sheet where they fall as low as $332^{\circ}C$.

The relationship between the Curie points and the unit cell edges of the 'magnetites' has been found to be an inverse one. However, the rate of change of Curie point with unit cell edge is much less than would be expected if the 'magnetites' were simple solid-solutions between Fe_3O_4 and $TiFe_2O_4$.

The % Fe_3O_4 in the 'magnetites' has been calculated from the Curie points and the saturation magnetization values following the method used by Chevallier and Mathieu and Vincent (1954). In general, the Fe_3O_4-content has been found to decrease away from the margins of the intrusion.

The % Fe_3O_4 in the 'magnetites' has been calculated from the Curie points and has been found to decrease by about 10% towards the centre of the intrusion.

Knowing the %Fe_3O_4 in the 'magnetites', the values of σ_ω have been calculated and the ratios $100\frac{\sigma_1}{\sigma_\omega}$ have been calculted to give the percentage of 'magnetite' in the 'magnetite'-'ilmenite' intergrowths.

The ratio $f\frac{\sigma_1}{\sigma_\omega}$ has been calculted to give the %Fe_3O_4 expressed as a percentage of the intergrowths. A plot of these values against Curie point has indicated that a magnetic constituent other than Fe_3O_4 is also present in these intergrowths, and it is thought that this may be as $MgFe_2O_4$ in solid-solution in the 'magnetites'.

Chapter VI. Summary and Discussion of the Mineralogical Data

A. Introduction

Examination of thin-sections of material from the Clauchlands sheet has shown that the rock is best described as an analcite-dolerite. Opaque minerals form an important constituent of this rock and appear to have crystallised after the formation of plagioclase and olivine but before precipitation of the pyroxene which latter, in view of its purplish brown colours, is considered to be titaniferous augite.

Samples representing a vertical cross-section of the intrusion have been investigated in thin-section and the results have revealed a systematic variation in the content of opaque minerals within the sheet such that whereas the marginal rocks contain more than 9% of opaque constituents, less than 1% is present in rocks at the centre of the sheet (Figure 5). There is no evidence to suggest that crystal settling has occurred towards the base of the sheet.

In polished sections the opaque minerals consist largely of an isotropic mineral resembling magnetite (Fe_3O_4) and an anisotropic mineral resembling ilmenite ($FeTiO_3$) (Chapter III). However, measurement of reflectivity, microhardness, unit cell parameters and magnetic properties has indicated that the minerals are not pure Fe_3O_4 or pure $FeTiO_3$ and hence they have been described as 'magnetite' and 'ilmenite' respectively.

The opaque minerals in the sandstones at the top contact of the intrusion consist predominantly of 'hematite' and subordinate 'magnetite' that appear to have formed from an original ferriferous cement (Chapter III). They have a distinctive recrystallised texture (Plate VII) which is similar to those observed in sintered hematite ores and a temperature of formation in the

range 1100°C to 1300°C is suggested (Chapter III). This was probably the temperature of the magma on intrusion. The 'hematite' is not pure α-Fe_2O_3 but contains about 35 mol% $FeTiO_3$ in solid-solution (Chapter IV).

B. Properties of the 'Magnetites'

The properties of the 'magnetites' indicate that they have compositions that are significantly different from those of pure Fe_3O_4. The values for the unit cell edges (a_o) and the Curie points (T_c) - Tables 10 and 19 - are in general agreement with those reported for naturally occurring minerals that are known, from chemical analyses, to be titaniferous magnetites, i.e. essentially solid-solutions between Fe_3O_4 and Fe_2TiO_4 (Figure 6). It seems probable, therefore, that the 'magnetites' in the Clauchland sheet are also titaniferous, especially as the pyroxene appears to be titaniferous augite.

It is known that substitution of TiO_2 in magnetite (Fe_3O_4) has the effect of increasing the unit cell edge and decreasing the Curie point (Chapters IV and V). For solid-solutions between Fe_3O_4 and Fe_2TiO_4 there should be a simple inverse linear relationship between these two properties varying from a_o = 8.396Å, T_c = 585°C for pure Fe_3O_4 to a_o = 8.53Å, T_c = about -150°C for pure Fe_2TiO_4. The present investigation has shown that this simple relationship does not hold for the 'magnetites' in the Clauchlands sheet. Although there is an inverse relationship between a_o and T_c (Figure 24), it cannot be explained simply in terms of solid-solution between Fe_3O_4 and Fe_2TiO_4 and, therefore, it is concluded that other constituents are present in solid solution as well as TiO_2.

It is known that many cations may substitute in the spinel lattice of magnetite (Tables 16 and 17) but, apart from TiO_2, those found in greatest abundance in natural 'magnetites' are Al_2O_3, V_2O_3 MgO and MnO. Of these,

Al_2O_3 and V_2O_3 cause a decrease in the unit cell edge of the substituted 'magnetite', MgO has no appreciable effect and MnO, like TiO_2, causes an increase in the unit cell edge. Substitution by these cations (with the exception of V_2O_3 for which no data is available) is known to decrease the Curie point of the substituted 'magnetite'.

The relationship between a_o and T_c shown in Figure 24 can be understood if the assumption is made that constituents such as those mentioned above are present in the minerals; i.e. if it is considered that the minerals are essentially titaniferous 'magnetites' whose properties have been modified by these other constituents. In such a situation, the effects due to substitution by TiO_2 are partly counteracted by the effects due to substitution of the other cations. Assuming that T_c is determined largely by the concentration of Fe_3O_4 in the mineral, then Figure 24 shows that the measured cell size corresponding to a measured Curie point is smaller than would be the case if the mineral were simply a Fe_3O_4-Fe_2TiO_4 solid-solution. This requires, therefore, that components are present which tend to reduce the unit cell edge of the substituted 'magnetite'.

A few of the 'magnetites' have unit cell edges that are less than that of pure Fe_3O_4 (Table 10). Since TiO_2 is normally the dominant substituent in natural 'magnetites' (Table 10) it seems improbable that there would be a concentration of components such as Al_2O_3 and V_2O_3 sufficient to reduce the cell size to this extent because the effect of the TiO_2 is to increase the cell edge. However, such components may be expected to be present in the minerals and therefore to contribute to the reduction of the cell edge.

It is known that the low temperature oxidation of titaniferous magnetites results in the formation of cubic phases of variable composition (Figure 6) having smaller unit cell edges than the corresponding stoichiometric phase

(Figure 18), and that such phases can have cell sizes less than that of pure Fe_3O_4 even though they contain TiO_2. Verhoogen (1962) has called such minerals γ-phases since they have defect lattices similar to that of maghemite, γ-Fe_2O_3, (for which $a_o = 8.32\text{Å}$). It is possible, therefore, that the 'magnetites' in the Clauchland sheet are γ-phases of this type. However, this is not to say that they have formed by oxidation for, although it is known that they may form in this way, it is not certain that this is the only mode of formation. In view of the complex relationships in the FeO-Fe_2O_3-TiO_2 system, it seems not impossible that such phases might have formed metastably without the advent of oxidising conditions, as is discussed in Section F.

Measurement of the microhardness of some of the Clauchlands 'magnetites' has shown that they have values that are intermediate between those of magnetite and those of maghemite (Figure 7); i.e. they are harder than magnetite but softer than maghemite. This result tends to support the identification of these minerals as γ-phases. However, little is known about the hardness of substituted 'magnetites' and it may well be the case that the presence of such molecules as $MgAl_2O_4$ also tends to increase the hardness of the minerals since it is well known that spinel is considerably harder than magnetite. Hence this data should be treated with caution.

There is indirect evidence indicating that MgO is present in the Clauchlands 'magnetites'. This is tentatively based on the results of a few magnetic measurements. The Curie point and the saturation magnetization at room temperature of samples of the 'magnetites' have been determined and from these values the $\%Fe_3O_4$ in the samples has been calculated using the method of Chevallier, Mathieu and Vincent (1954) described in Chapter V. A good inverse relationship has been found to hold when the $\%Fe_3O_4$ so determined is plotted against the Curie point (Figure 27).

If Fe_3O_4 were the only magnetic constituent of the samples, then for a composition of 0 %Fe_3O_4 the above relationship should give a Curie point of absolute zero. However, it is clear that this is not the case and, taking the Curie point of pure Fe_3O_4 as 585°C, that Figure 27 indicates a Curie point in the range 440°C to 530°C even when no Fe_3O_4 is present. It is concluded, therefore, that another magnetic constituent is also present in the samples.

X-ray examination of such samples has shown that 'ilmenite' is normally present, this having been retained as a fine intergrowth with the 'magnetites'. However, the lattice parameters of such 'ilmenite' indicate that the minerals contain about 10-20 mol% Fe_2O_3 in solid-solution (Chapter IV) and, according to Akimoto (1957), such minerals would have Curie points of about -100°C (Figure 25) and therefore, would be non-magnetic at room temperatures. Hence, this 'ilmenite' cannot be the other magnetic constituent of the samples.

X-ray examination of the 'magnetites' has shown that a number of samples contain more than one 'magnetite' but that in such cases the coexisting minerals are likely to have closely similar compositions (Table 10). As measurements of the Curie points (determined on very small samples) have rarely shown more than one phase to be present and these results show no good correlation with the X-ray data, it is concluded that the co-existing phases represent slight variations in composition within the powder samples, and are not intergrowths. This seems especially likely when it is considered that the powders have been concentrated from fairly large hand-sized rock specimens.

Thus, the data does not indicate the presence of an intergrown magnetic phase within the 'magnetite' samples, and therefore it is concluded that the unknown magnetic constituent is present in solid-solution in the 'magnetites'.

MgO is normally found in natural 'magnetites' where it may be regarded as occurring as $MgFe_2O_4$ (magnesioferrite) in solid-solution with the 'magnetite'.

It is known that magnesioferrite is a ferromagnetic spinel with a Curie point of 440°C so that its presence in the Clauchlands 'magnetites' might account for the results shown in Figure 27, hence it is concluded that MgO is a component of the 'magnetites'.

However, the above result can give no indication as to the amount of MgO in the 'magnetites'. The relationship shown in Figure 27 indicates only the presence of a magnetic constituent, probably $MgFe_2O_4$, having a Curie point in the range 440°C to 530°C. This Curie point has been obtained by making an extrapolation to the unlikely condition that the minerals contained no Fe_3O_4. The Curie point, however, is independent of the amount of the constituent. Indeed, it is probable that the concentration of MgO (present as $MgFe_2O_4$) is quite small judging by recorded chemical analyses of natural 'magnetites'.

Summarizing, it is concluded that the 'magnetites' in the Clauchlands sheet are essentially titaniferous, in common with other naturally occurring 'magnetites'. However, the properties of these minerals are not those of simple solid-solutions between Fe_3O_4 and Fe_2TiO_4 but may be explained if it is considered that the properties of the simple minerals have been modified by other components. Al_2O_3, V_2O_3 and MgO may be expected to be present and to contribute to such modifications of the properties. However, it is also concluded that the 'magnetites' may be non-stoichiometric γ-phases (i.e. the oxygen content may be variable) and it seems probable that this factor may be more effective than the others in determining the properties of the 'magnetites'. However, it is not implied, nor considered necessary to consider that the minerals have been oxidised at low temperatures.

C. Systematic Variations in the Properties of the 'Magnetites'

Both the Curie points and the lattice parameters of the 'magnetites'

have been found to vary systematically within a vertical section of the intrusion. As the Curie points decrease towards the centre of the sheet (Figure 22), the unit cell edges increase (Figure 14). Thus the composition of the 'magnetites' is not uniform but varies systematically. Since the minerals at the centre of the sheet have crystallised later, and cooled more slowly, than those at the margins, this variation in composition is presumably related to the rate of cooling and indicates changes in composition as equilibrium is approached.

It has been concluded that the 'magnetites' are essentially titaniferous, albeit with their properties modified by other constituents, and therefore it seems probable that the observed variations indicate changes in the TiO_2 content of the minerals, such that there is an increase in the TiO_2 content towards the centre of the sheet. Thus the trend of crystallisation is one of increasing TiO_2 content as equilibrium is approached. As is discussed in Section F below, this trend is to be expected during the development of the 'magnetite'-'ilmenite' relationships in the sheet.

It is not possible to state the variations in TiO_2 content within the sheet, although the variations in a_o and T_c would indicate that it is appreciable. This is because the 'magnetites' are clearly not simple minerals formed by solid-solutions between Fe_3O_4 and Fe_2TiO_4.

There is, however, an alternative mechanism which could cause a_o and T_c to vary. It has been concluded earlier that the minerals are non-stoichiometric γ-phases. Thus, the variations might indicate that the 'magnetites' have a constant titanium content throughout the sheet but that the Fe^{2+}/Fe^{3+} ratio increases within the sheet so that the composition changes towards a stoichiometric composition represented on the Fe_3O_4-Fe_2TiO_4 join in the FeO-Fe_2O_3-TiO_2 system (Figure 6).

The unit cell edge of the 'magnetites' varies from 8.364Å to 8.485Å (Table 10), and the Curie point varies from 577°C to 332°C (Table 19). Although there is no data on the values of these parameters in the Fe_3O_4-Fe_2O_3 region (Figures 18 and 20) of the system, it would seem possible for minerals containing about 20% TiO_2 to show the above range in parameters simply by a change in the Fe^{2+}/Fe^{3+} ratio, assuming that the lines of equal a_o and T_c ($=\theta_c$) continue the indicated trend of increasing curvature into the Fe_3O_4-Fe_2O_3 regions of Figures 18 and 20.

Such a mechanism, however, does not account for the observed 'magnetite'-'ilmenite' relationships in the Clauchlands sheet, whereas if the variations in properties are taken to indicate a trend of increasing TiO_2 content in the 'magnetites' then it is possible to understand how these relationships might have developed (see Section F). For this reason, therefore, it is considered that the data indicate changes in TiO_2, rather than a varying Fe^{2+}/Fe^{3+} ratio with constant TiO_2.

D. Exsolution of "Ulvöspinel" in the 'Magnetites'?

In polished sections the 'magnetites' generally have a brownish colour similar to that of known magnetite-ulvöspinel intergrowths. This colour has been demonstrated by measuring the spectral reflectivities of the minerals, and the results have shown that the spectral reflectivity profiles are closely similar to that obtained from a magnetite-ulvöspinel intergrowth but are totally different from that of pure magnetite (Figure 8). However, no such intergrowths have been seen in the Clauchlands 'magnetites', and although it has been found possible to examine known intergrowths of this type by means of replica electron microscopy, the application of this technique to the Clauchlands minerals did not reveal an intergrown cubic phase. It has

been concluded, therefore, that exsolution of ulvöspinel-type has not occurred in the Clauchlands 'magnetites', even on a sub-microscopic scale.

This conclusion is supported by the X-ray results which, although indicating the presence of more than one 'magnetite' in some samples, in general only reveal one such phase. Where more than one 'magnetite' is present the lattice parameters are very similar (Table 10) and indicate that the minerals have similar compositions. Thermomagnetic analyses of such samples (using much less material than for an X-ray examination) in general do not correlate with the X-ray results in indicating the presence of two 'magnetite' phases. As suggested earlier, therefore, it seems probable that where coexisting 'magnetites' are indicated in a sample, this is due to slight variations in composition within the sample caused by the concentration of the 'magnetite' fraction from relatively large rock specimens. It is not considered that the 'magnetites' occur as intergrowths.

E. Properties of the 'Ilmenites'

The 'ilmenite' in the Clauchlands sheet has been found to occur in two forms. Most commonly it occurs as fine to coarse oriented intergrowths within crystals of 'magnetite'. Such 'ilmenite' occurs throughout most of the intrusion except at the extreme contacts of the sheet. However, towards the centre of the sheet 'ilmenite' crystals, comparable in size to the 'magnetite'-'ilmenite' intergrowths, appear as well as the intergrowths. The mode of occurrence of such 'ilmenite' is quite distinct from that of the intergrown 'ilmenite' and it appears towards the slowly cooled centre of the intrusion. It may occur either as separate crystals or appear as irregular segregations intergrown with the 'magnetite'-'ilmenite' intergrowths, and it can be shown to be earlier than such intergrowths.

X-ray examination of the intergrown 'ilmenites' has shown no systematic variation in properties (cp. the marked variations in the 'magnetites'). The composition of the minerals has been determined from the curve relating a_{rh} to composition (Figure 15) as given by Akimoto (1957), and the results indicate that 10-20 mol% Fe_2O_3 is present in them. With such compositions the 'ilmenites' would have Curie points of about -100°C (Figure 25). The results of the thermomagnetic analyses support this conclusion since the thermomagnetic records show no Curie points attributable to an 'ilmenite' phase.

The composition of the discrete 'ilmenite' has also been determined from the X-ray data. Using a_{rh} as an indicator (Figure 15), this data suggests that the minerals contain little or no Fe_2O_3 in solution but may contain some $MnTiO_3$. There appears to be no systematic variation in composition.

F. Interpretation of the 'Magnetite'-'Ilmenite' Relationships

Since the samples examined in the present investigation form a vertical section through the Clauchlands sheet ranging from rapidly chilled contact rocks to slowly cooled pegmatitic facies, the data obtained from these should reflect the crystallisation trends in the minerals under consideration and from this it should be possible to derive information as to the nature of the 'magnetite'-'ilmenite' system.

Recently, experimental data has become available on the synthetic system $FeO-Fe_2O_3-TiO_2$ from which it is possible to construct the probable form of the $Fe_3O_4-FeTiO_3$ diagram. This diagram is shown in Figure 30. The liquidus has been drawn from the data of Taylor (1961). Taylor has also shown that the solubility of $FeTiO_3$ in Fe_3O_4 is limited to about 24 mol% $FeTiO_3$ (21 wt%) at 1300°C and that the solubility of Fe_3O_4 in $FeTiO_3$ is probably only about 2 wt%

Figure 30.

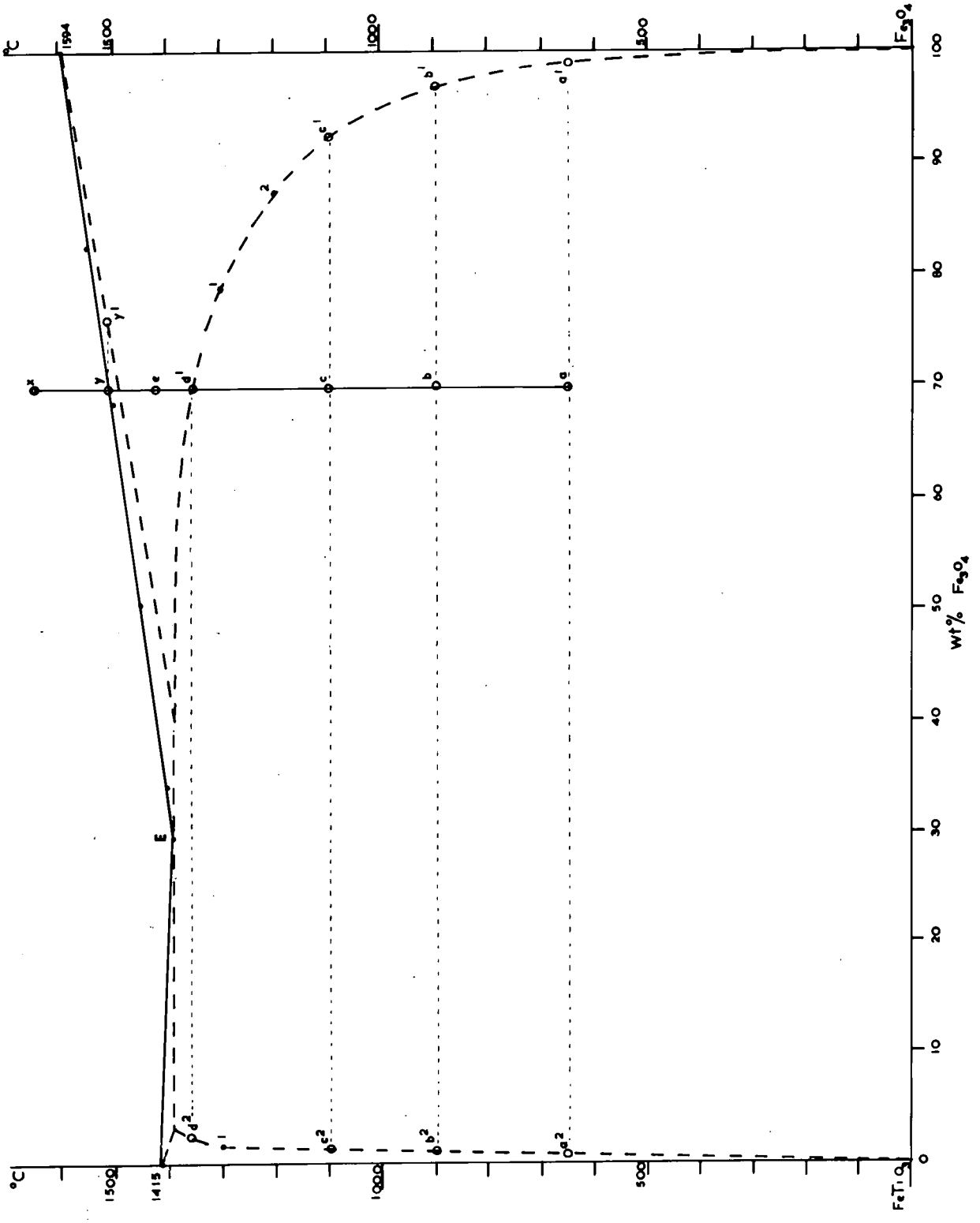
°C
1594
1500
1000
500
0
Fe_3O_4
100
90
80
70
60
50
40
30
20
10
0
Wt% Fe_3O_4
°C
1500
1415
1000
500
$FeTiO_3$
E
x
y
e
d
c
b
a
y^1
d^1
c^1
b^1
a^1
d^2
c^2
b^2
a^2

Figure 30.

Probable phase diagram for the Fe_3O_4-$FeTiO_3$ system, based on the experimental data of Taylor (1962) and Webster and Bright (1962).

at this temperature. These points have been represented as solid circles in Figure 30 and labelled 1. Data for a temperature of 1200°C has been obtained from Webster and Bright (1961) who have found that the solubility of $FeTiO_3$ in Fe_3O_4 at this temperature is about 16 mol% (13 wt%) and this point has been labelled 2 in Figure 30. The data of Webster and Bright also indicate that the solubility of Fe_3O_4 in $FeTiO_3$ at 1200°C is negligible. Below about 1000°C the solubility of $FeTiO_3$ in Fe_3O_4 is also probably negligible.

The most interesting feature of the Fe_3O_4-$FeTiO_3$ diagram constructed from this data is that the solvus is markedly assymetric, and it is thus possible to account for the existence of 'ilmenite' in two modes of occurrence in the Clauchlands sheet and also for the fact that the 'magnetites' are probably γ-phases.

Consider the conditions of cooling and crystallization that are likely to exist in an intrusion such as the Clauchlands sheet. Jaeger (1956) has shown that on intrusion of a sill, the margins chill rapidly to about 650°C (see Chapter VII) and thereafter, the intrusion cools slowly over an extended period. The composition of any solid-solution minerals crystallizing in the marginal rocks, therefore, will bear no relation to their true equilibrium compositions owing to their having been precipitated from a supercooled melt. However, the extent of such supercooling will decrease away from the margins and, therefore, the composition of these minerals will tend to change towards the equilibrium composition as the centre of the intrusion is approached. In an intrusion of the size of the Clauchlands sheet, however, it is unlikely that the rate of cooling even at the centre of the sheet was ever slow enough for true equilibrium cooling to occur, so that the minerals throughout the sheet may be regarded as non-equilibrium assemblages.

Consider, therefore, how the 'magnetite'-'ilmenite' relations might develop within the sheet, assuming that Figure 30 is valid. For the sake of argument, let the melt from which the ores crystallize have some arbitrary composition X.

On intrusion of the sheet, the liquid is supercooled to about 650°C at the contacts with the country rock and a metastable phase -a- is precipitated. Liquid further from the margins will not cool to such a low temperature and, therefore, metastable phases such as -b- and -c- will precipitate towards the centre of the sheet.

After the initial act of intrusion and rapid fall in temperature throughout the sheet, the rock then cools slowly down to normal temperatures. These conditions will favour the breakdown of such metastable phases as -a-, -b- and -c- into the assemblages a^1-a^2, b^1-b^2, c^1-c^2 etc., where a^1, b^1 and c^1 are cubic phases resembling magnetite, and a^2, b^2 and c^2 are rhombohedral phases close to $FeTiO_3$ in composition. Thus examination of a cross-section of the intrusion will show a nearly pure ilmenite phase associated with a 'magnetite' phase, and that the 'magnetite' becomes increasingly titaniferous towards the centre of the sheet. However, this association might not be expected at the extreme contacts of the intrusion where the metastable phase initially precipitated is unable to dissociate due to the low temperature to which it was quenched.

Consider now the composition of the 'magnetites' that form with the almost pure $FeTiO_3$ in the above association. In terms of the system FeO-Fe_2O_3-TiO_2 these minerals appear in the area between the Fe_3O_4-Fe_2TiO_4 join and the Fe_2O_3-$FeTiO_3$ join since, in fact, they are located on the $FeTiO_3$-Fe_3O_4 join. Cubic minerals in this area, however, are non-stoichiometric γ-phases. (Figure 6), and Verhoogen (1962) has shown theoretically that such γ-phases

should be metastable to the association α-phase/β-phase, where the α-phase is a rhombohedral $FeTiO_3$-Fe_2O_3 solid-solution, and the β-phase is a cubic Fe_2TiO_4-Fe_3O_4 solid-solution. Therefore, the 'magnetites' should themselves breakdown to an α-β association.

Lindsley (1962) has shown experimentally that the oxidation of ulvöspinel can give rise to an oriented intergrowth between an ilmenite solid-solution (α-phase) and a magnetite solid-solution (β-phase) typical of those observed in nature (Plate VIII), this presumably taking place by way of an intermediate γ-phase. It seems probable, therefore, that the 'magnetite'-'ilmenite' intergrowths in the Clauchlands sheet have developed by the breakdown of such γ-phases, with the 'ilmenite' in these intergrowths being $FeTiO_3$-Fe_2O_3 solid-solutions in contrast to the almost pure $FeTiO_3$ of the discrete 'ilménite'.

The 'magnetites' in these intergrowths should become more titaniferous towards the centre of the sheet since this trend is shown by the initial γ-phases from which they are derived. Ideally, the 'magnetites' should also be β-phases, i.e. have compositions on the Fe_2TiO_4-Fe_3O_4 join. It is conceivable, however, that in an intrusion such as the Clauchlands sheet, the rate of cooling after emplacement of the sheet might yet be too rapid for the dissociation of the γ-phases to go completely to the association α-phase - β-phase, so that in the final assemblage the spinel-phase might not have reached the composition of β-phases but might still have compositions that plot away from the Fe_2TiO_4-Fe_3O_4 join. Thus the 'magnetites' might still remain as γ-phases, albeit not of the same composition as the initial γ-phases.

It has been concluded that the 'magnetites' in the Clauchlands sheet are probably γ-phases and that these become increasingly titaniferous towards the centre of the intrusion. It has also been found that 'ilmenite' occurring intergrown with the 'magnetite' is a solid-solution containing Fe_2O_3 whereas a

separate 'ilmenite' phase associated with the intergrowths is almost pure. Further, the pure 'ilmenite' has crystallized before formation of the intergrowths. In broad outline, therefore, these relations agree with those indicated in Figure 30.

It should be noted, however, that the experimental data of Taylor (1961) obtained at 1300°C indicate that, under conditions of equilibrium, the system Fe_3O_4-$FeTiO_3$ is not binary. Thus, a melt of composition X would not split into a pure ilmenite phase and a γ-phase lying on the $FeTiO_3$-Fe_3O_4 join as considered here, but would split into an α-phase (on the $FeTiO_3$-Fe_2O_3 join) and a β-phase (on the Fe_2TiO_4-Fe_3O_4 join) with compositions determined by the line of constant oxygen pressure passing through X. (see Figure 9 of Taylor -1961-).

Such experimental data, however, refers to assemblages in equilibrium, whereas the minerals in the Clauchlands sheet are considered to be manifestly the products of non-equilibrium. It seems probable, therefore, that crystallization under the non-equilibrium conditions found in the Clauchlands sheet is responsible for the development of the observed mineral assemblage due to the initial formation of metastable phases of varying composition throughout the sheet.

According to the results of the magnetic measurements, the amount of 'ilmenite' in the intergrown crystals varies from about 40 wt% to as much as 80 wt% (Table 19), there being an apparent increase in content towards the centre of the sheet. This trend is to be expected since, according to Figure 30, the amount of $FeTiO_3$ present in the original γ-phase is greater at the centre of the sheet. However, Figure 30 also indicates that amount of intergrown $FeTiO_3$ should not exceed about 60 wt%. Only one sample gives a result as high as 80 wt% 'ilmenite' (Table 19), and this may, therefore, be an error

caused by impurities in this sample.

Petrographic examination of the chilled contacts of the Clauchlands sheet indicate that the magma was almost entirely liquid on intrusion. However, the presence of recrystallised 'hematite' grains in the sandstones at the top contact has been taken to indicate that the temperature of the intruding magma was of the order of 1100°C to 1300°C (Chapter III), which is appreciably lower than the liquidus shown in Figure 30 for the Fe_3O_4-$FeTiO_3$ system. Clearly, therefore, the simple relations suggested in Figure 30 must be considerably modified in the magma itself such that the liquidus is depressed, and presumably the solvus is also affected, but to an unknown extent.

The field evidence (Chapter I) has indicated that the Clauchlands sheet is a multiple intrusion and this may therefore account for the complex seriate nature of many of the 'magnetite'-'ilmenite' intergrowths (Plates IX to XII). In such intergrowths the 'ilmenite' may vary fromminute incipient lamellae to broad laths within a single grain. Such textures may have developed during the alternating 'hot' and 'cold' phases through which the intrusion must have passed as it cooled to normal temperatures. Under these conditions, the fine lamellae may have formed during periods of relatively rapid cooling whilst the coarser laths may be the products of long continued growth when the rate of cooling was slow.

G. Conclusions

Conclusions based on the mineralogical data are that:-

1. The properties of the 'magnetites' are essentially those of titaniferous magnetites, although with modifications due to the presence of cations other than TiO_2.

2. The relationship between the Curie point and the lattice parameter indicates the presence of components that tend to reduce the unit cell edge of the substituted magnetite. Al_2O_3 and V_2O_3 probably contribute to this effect although the fact that some of the 'magnetites' have cell edges less than that of pure Fe_3O_4 suggests that the minerals are also γ-phases.

3. The fact that the 'magnetites' are harder than pure magnetite (Fe_3O_4) but softer than maghemite (γ-Fe_2O_3) also suggests that they are γ-phases. However, the presence of components such as $MgAl_2O_4$ might also account for this result.

4. The relationship between $\%Fe_3O_4$ in the 'magnetites' (deduced from magnetic measurements) and the Curie point suggest that MgO may be present (in the form of $MgFe_2O_4$).

5. 'Ilmenite' occurs in two forms in the intrusion. Most commonly it forms oriented intergrowths with 'magnetite'. Such 'ilmenite' is a solid-solution containing 10-20 mol% Fe_2O_3. However, a separate 'ilmenite' phase also exists that is earlier than formation of the intergrowths. This 'ilmenite' appears not to contain Fe_2O_3 in solution.

6. The variation in properties of the 'magnetites' indicates that they become more titaniferous towards the centre of the sheet. This trend and also the observed 'magnetite'-'ilmenite' relationships may be understood in terms of the system Fe_3O_4-$FeTiO_3$ when this is considered in relation to the non-equilibrium conditions likely to exist within the Clauchlands sheet.

7. The complex seriate nature of the 'magnetite'-'ilmenite' intergrowths may be due to fluctuations in the rate of cooling, since the Clauchlands sheet is a multiple intrusion.

Although it is possible to account for the 'magnetite'-'ilmenite' relationships in the above general sense, this is clearly only a superficial

explanation of a complex mineralogy. However, the results do point the way for future investigations of this nature in that measurable variations are to be found in intrusions of this size. It is clearly desirable that future work be accompanied by chemical analyses. Unfortunately this has not been possible in the present examination owing to, lack of time.

Chapter VII The Palaeomagnetism of the Clauchlands Sheet

A. Introduction

Many rocks possess a measurable permanent magnetization known as the natural remanent magnetization (NRM) due to the presence of ferromagnetic minerals within them. Titaniferous magnetites and the rhombohedral ilmenite-hematite minerals are the principal carriers of this magnetization, although rarely, pyrrhotite (FeS_{1+x}) may be responsible. (Almond, Clegg and Jaeger 1956a; Fuller 1960; Nagata and Yama-ai 1961; Kawai and Yong-Ho Kang 1962).

Seven types of natural remanence have been recognised (Nagata 1961) but of these, only thermoremanent magnetization (TRM) and, to a lesser extent, chemical remanent magnetization (CRM) are of importance when dealing with igneous rocks.

Chemical remanent magnetization is produced when a ferromagnetic substance is formed chemically or by crystallization under the influence of an external magnetic field H_{ex}. It is magnetization that may be acquired below the Curie point and is probably an important component of the natural remanence of altered, weathered and metamorphic rocks.

Thermoremanent magnetization, on the other hand, is acquired when a ferromagnetic substance is cooled under the influence of an external magnetic field H_{ex}. If the substance is cooled from above its Curie point then it acquires over 90% of its total TRM at a temperature, known as the blocking temperature, just below the Curie point, and only 10% is acquired during subsequent cooling. Such magnetization, therefore, is the dominant component of the natural remanence of igneous rocks.

The magnitude of both CRM and TRM is generally much larger than that of the induced magnetization in the present geomagnetic field H_o and it may

be expressed as a ratio Q_n (Königsberger 1938) where:

$$Q_n = \frac{J_n}{kH_o} > 1$$

J_n = Intensity of remanent magnetization

k = susceptibility

Q_n is generally about 2 - 10 for igneous rocks, but values of up to 100 have been reported from 'lodestone' partially altered to maghemite (Nagata 1961).

The development of such an intense magnetization in an external field of only about 0.5 Oe (the geomagnetic field) is a remarkable phenomenon and its origins have been discussed theoretically by Néel (1949; 1955), Stacey (1958) and Verhoogen (1959) in relation to TRM and by Haigh (1958) and Kobayashi (1961) in relation to CRM.

Nagata (1943) demonstrated that the natural remanent magnetization of fresh igneous material is largely of thermoremanent origins since in volcanic rocks of historical age, the ratio $\frac{NRM}{TRM}$ is very nearly unity. Thus, in general, the NRM of igneous rocks can be equated with the TRM acquired as the rocks cooled.

Nagata (1961) has also summarized several important characteristics of TRM of which the most fundamental is the fact that the direction of TRM is generally parallel to that of the applied field during cooling. This, of course, is the basis for the interpretation of the palaeomagnetism of igneous rocks.

TRM is also very stable and tends to resist demagnetization whether by AC demagnetization, thermal demagnetization or by applying a reverse field to destroy it.

Some igneous rocks, however, have an unstable natural remanence, which can probably be explained in terms of CRM rather than TRM. For example, Akimoto and Kushiro (1960) found that the unstable magnetization of some dolerites in Japan was restricted exclusively to those rocks which had been altered hydrothermally so that the titanogmagnetite had been partly replaced by titanomaghemite. In unaltered dolerites nearby which contained fresh titanomagnetite, the magnetization was stable.

It may be concluded, therefore, that fresh igneous material is the most likely to possess a stable natural remanence and that this will be largely of thermoremanent origin. It is on the basis of this conclusion that the present investigations are founded.

The study of palaeomagnetism deals with the measurement of the directions of such natural remanence in rocks and the interpretation of these measurements in terms of geological history. Lavas are frequently used as the source rocks for such studies but occasionally intrusive rocks have been used (Almond Clegg and Jaeger 1956; Creer, Irving and Nairn 1959), and often sedimentary rocks are used, (in which case the remanence is a depositional remanent magnetization, DRM, with properties not directly related to TRM).

The basic assumption underlying all such studies is that the NRM formed parallel to the direction of the geomagnetic field at the time of the formation of the materials and that it has been preserved stably against the later changes of the magnetic field.

In the case of lava flows, this assumption is probably justified because the rocks cool rapidly and hence should 'freeze-in' the direction of the magnetic field. The rapid cooling also results in the formation of homogeneous titaniferous magnetites rather than heterogeneous magnetite-ilmenite inter-

growths and hence a complicated mineralogical (and magnetic?) sequence tends to be absent.

In intrusive rocks, however, this assumption is probably not justified because the material cools slowly and hence the magnetic field may change during the process of acquiring TRM (secular variation), or the NRM may change as a result of changes in the ferromagnetic minerals. Such material, therefore, is probably unsuitable as a basis for palaeomagnetic measurements.

The present investigation, however, has not been undertaken in order to determine the palaeomagnetic field direction at the time of instrusion.

The primary purpose of the present investigation has been to study the natural remanent magnetization of the sheet in relation to its mineralogy and known intrusive history.

B. The NRM of the Clauchlands Sheet

Thirty oriented samples have been collected from the Clauchlands sheet, at Clauchlands Point (localities 1, 2 and 3), and from the cliffs one quarter of a mile to the north (locality 4) using the method described in Appendix 4. This forms a collection which represents a vertical section through the intrusion with a sampling interval of about 4ft. and it closely parallels that used for the petrological and mineralogical investigations described in Chapters II to V.

Ten samples have been selected from this collection so as to represent a cross-section of the intrusion. These samples have been cored (Collinson and Nairn 1960) and the resulting cylinders measured with the Newcastle magnetometer (see Appendix 4). The intensity of magnetization as well as the direction of the NRM of these samples has been measured and the results

are summarized in Table 22.

At a later stage, the Durham magnetometer became available (see Appendix 4) and Table 22 also includes the directions of NRM in the twenty samples measured with this instrument. However, the intensity of magnetization has not been determined for these samples since the magnetometer is not calibrated for such measurements.

Figure 31 shows how the intensity of magnetization decreases away from the margins of the intrusion. This trend is caused by a decrease in the amount of 'magnetite' towards the centre of the intrusion (cp Figure 5).

The values of J_n are of the same order of magnitude (10^{-3} Oe) as have been recorded from other igneous rocks. For example the Great Whin Sill (Creer, Irving and Nairn 1959), the Deccan Traps and the Rajmahal Traps (Deutsch, Radakrishnamurty and Sahasrabudhe 1958a; 1958b) and the Midland Basalts (Everitt 1960).

The high value of J_n may be taken as indirect evidence of the stability of the NRM, for Akimoto and Kushiro (1960) have found that in unstable dolerites (containing titanomaghemites) the intensity, J_n, is of the order of 10^{-5} Oe, whilst in adjacent stable dolerites (containing fresh titanomagnetite), J_n is of the order of 10^{-4} Oe.

The directions of the NRM (Table 22) have been plotted on a Schmidt net and are shown in Figure 32. Twenty three samples have a reverse magnetization and eight are normally magnetized; the directions, however, show a wide scatter.

The direction of magnetization of three of the normally magnetized samples is close to that of the present field direction (assuming a geocentric dipole). However, the Clauchlands sheet is an early Tertiary intrusion

Table 22.

Natural Remanent Magnetization of the Clauchlands Sheet

Horizon (feet)	Sample	D	I	J_n 10^{-3} Oe	How Measured
+9	A/C/3/14	N 215	-64	-	Block
+3	A/C/3/13	N 192	-61	2.32	Mean of 3 cylinders
Top	A/C/3/12	N 228	-64	-	Block
127	A/C/3/15	N 201	-51	1.52	Mean of 6 cylinders
121	A/C/3/16	N 229	-01	-	Block
116	A/C/3/17	N 161	-15	-	Block
110	A/C/3/18	N 161	-50	1.01	Mean of 2 cylinders
108	A/C/4/30	N 60	+39	0.29	1 cylinder
102	A/C/3/19	N 118	-38	1.02	Mean of 2 cylinders
102*	A/C/3/20	N 153	-48	-	Block
102	A/C/3/21	N 150	-54	-	Block
99	A/C/3/22	N 177	-07	-	Block
95	A/C/3/23	N 343	+75	-	Block
92	A/C/3/24	N 171	-11	-	Block
88	A/C/3/31	N 191	-20	-	Block
84	A/C/3/32	N 196	-20	0.16	1 cylinder
76	A/C/3/33	N 323	+71	-	Block
68	A/C/3/34	N 243	-42	0.36	Mean of 6 cylinders
54	A/C/4/27	N 103	-13	0.22	1 cylinder
50	A/C/3/38	N 169	-44	-	Block
42	A/C/3/40	N 32	+26	-	Block
42	A/C/4/26	N 54	+61	-	Block
32	A/C/3/42	N 199	-55	0.39	Mean of 5 cylinders
30	A/C/4/25	N 102	+76	0.51	Mean of 3 cylinders
19	A/C/2/08	N 210	-47	-	Block
12	A/C/1/06	N 72	+09	-	Block
9	A/C/1/05	N 352	+61	-	Block
6	A/C/1/04	N 172	-10	1.33	Mean of 2 cylinders
3	A/C/1/03	N 216	-20	-	Block
½	A/C/1/01	N 215	- 53	-	Block

* Basalt dyke cutting the sheet.

Figure 31.

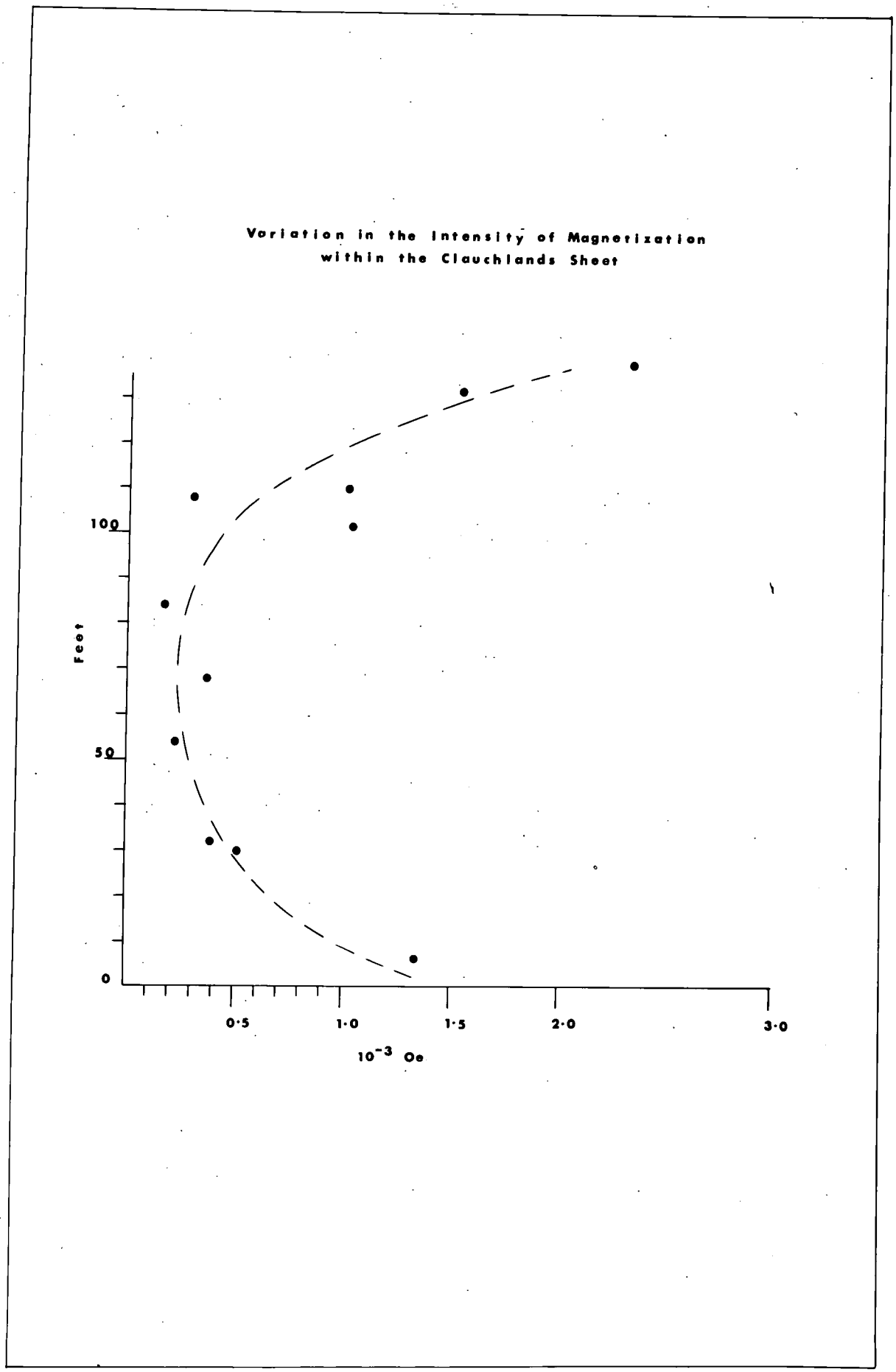
Variation in the Intensity of Magnetization
within the Clauchlands Sheet
100
50
0
Feet
0·5
1·0
1·5
2·0
3·0
10⁻³ Oe

Figure 31.

Variation of the intensity of magnetization
in a vertical section of the Clauchlands Sheet.

(Chapter III), and it is known that the direction of the geomagnetic field has changed but little since Tertiary times (Cox and Doell 1960), so that normally magnetized samples, if genuine, would be expected to approximate to the present direction.

The results on the stereogram would suggest that the normal magnetizations are not the true NRM but that they are directions resulting from an unstable magnetization, originally reversed, which has tended towards the present field direction, along planes defined by the two great circles shown. Examples of such 'streaking' along great circles connecting the ancient geomagnetic field with the present field direction have often been reported. (Runcorn 1956; Creer 1957; Kawai and Kume 1953). Hence it is concluded that the Clauchlands sheet is reversely magnetized and that samples having normal magnetization are unstable, such instability possibly being due to weathering (Nairn 1957).

The following discussions, therefore, are in terms only of the reversely magnetized samples. These directions are shown in Figure 33, without the normally magnetized directions, and the mean direction has been included.

The mean direction has a declination of N 184° and an inclination of -41°. The best estimate of the precision parameter is very low, $k = 5.8$ and α_{95} is fairly large at 12.4°, both these values indicating the wide scatter of the directions. The data and computation of the mean are given in Table 23 (see Appendix 4 for definitions of these quantities).

Nevertheless, despite the wide scatter of directions, the computed mean is in good agreement with results obtained from lavas in this Tertiary igneous province except that the inclination is some 20° shallower. These results, taken from Cox and Doell (1960) are shown in Figure 34 for comparison.

Figure 35 shows the direction of the NRM in rocks from the contacts of

Figure 32.

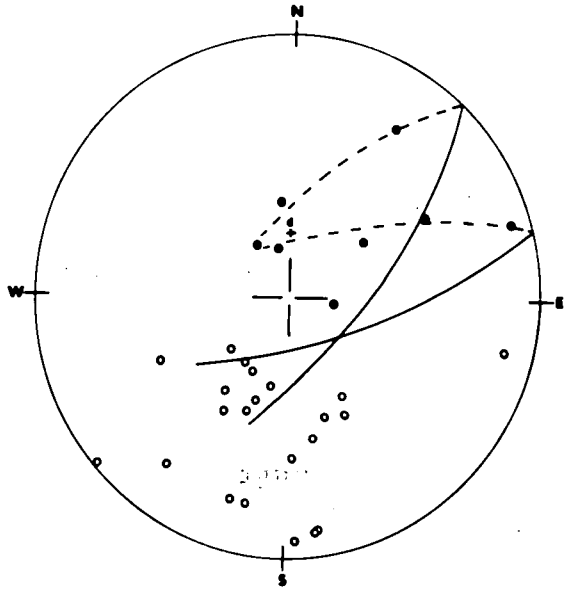

Figure 33.

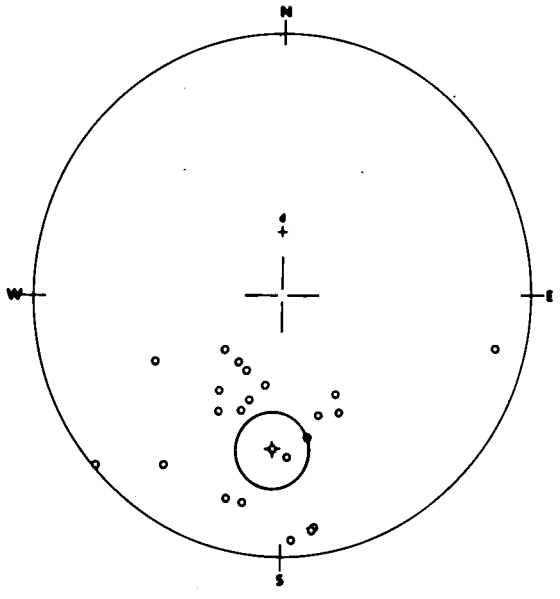

Figure 34.

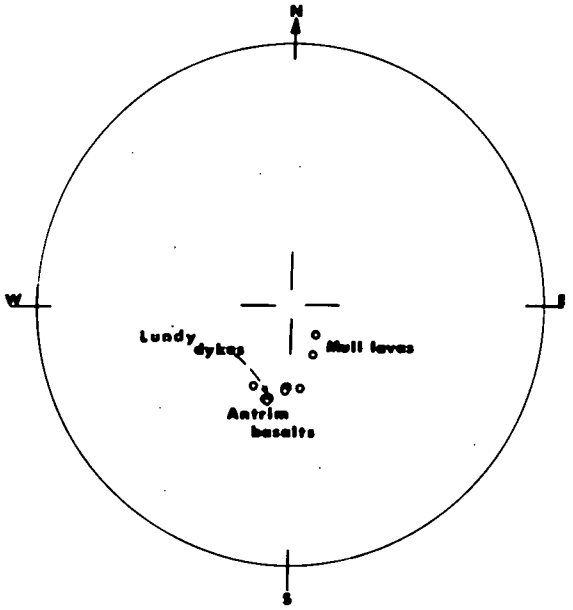

Figure 35.

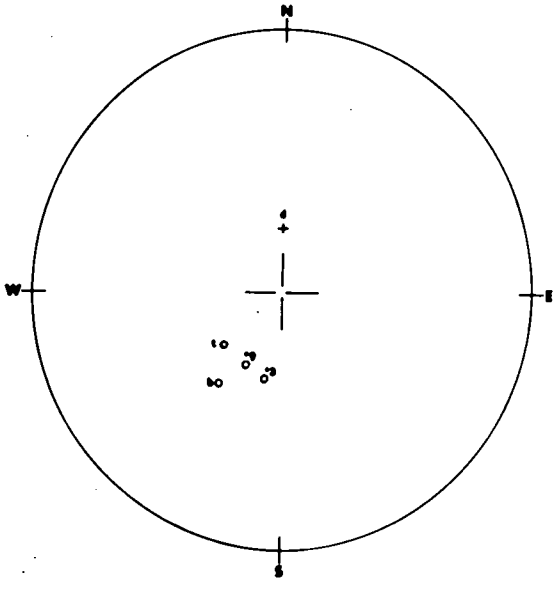

Figure 32.

Directions of NRM in the Clauchlands Sheet - equal area projection.

Figure 33.

Reverse directions only of NRM in the Clauchlands Sheet - equal area projection.

Figure 34.

Reverse directions of NRM in Tertiary lavas of comparable age to the Clauchlands Sheet and from the same igneous province. (after Cox and Doell 1960).

Figure 35.

Directions of NRM in the contact rocks of the Clauchlands Sheet.

Table 23.

I	D	sinI	cosI	sinD	cosD	cosIcosD	cosIsinD
-64	215	0.8988	0.4384	-0.5736	-0.8191	-0.3591	-0.2515
-61	192	0.8746	0.4848	-0.2079	-0.9781	-0.4742	-0.1008
-64	228	0.8988	0.4384	-0.7431	-0.6691	-0.2933	-0.3258
-51	201	0.7771	0.6293	-0.3584	-0.9336	-0.5875	-0.2255
-01	229	0.0174	0.9998	-0.7547	-0.6561	-0.6560	-0.7545
-15	161	0.2588	0.9659	+0.3256	-0.9455	-0.9132	+0.3145
-50	161	0.7660	0.6428	+0.3256	-0.9455	-0.6078	+0.2093
-38	118	0.6157	0.7880	+0.8829	-0.4695	-0.3670	+0.6957
-48	153	0.7431	0.6691	+0.4540	-0.8910	-0.5962	+0.3038
-54	150	0.8090	0.5878	+0.5000	-0.8660	-0.5090	+0.2939
-07	177	0.1219	0.9925	+0.0523	-0.9986	-0.9911	+0.0519
-11	171	0.1908	0.9816	+0.1564	-0.9877	-0.9695	+0.1535
-20	191	0.3420	0.9397	-0.1908	-0.9816	-0.9224	-0.1793
-20	196	0.3420	0.9397	-0.2756	-0.9613	-0.9033	-0.2590
-42	243	0.6691	0.7431	-0.8910	-0.4540	-0.3374	-0.6621
-13	103	0.2249	0.9744	+0.9744	-0.2249	-0.2191	+0.9494
-44	169	0.6947	0.7193	+0.1908	-0.9816	-0.7061	+0.1372
-55	199	0.8191	0.5736	-0.3256	-0.9455	-0.5423	-0.1868
-47	210	0.7313	0.6820	-0.5000	-0.8660	-0.5906	-0.3410
-10	172	0.1736	0.9848	+0.1392	-0.9903	-0.9752	+0.1371
-20	216	0.3420	0.9397	-0.5878	-0.8090	-0.7602	-0.5523
-53	215	0.7986	0.6018	-0.5736	-0.8191	-0.4929	-0.3452
N = 22		12.1093				-13.7734	-0.9375
		Z				X	Y

Calculation of the Mean Direction of Magnetization.

$$R = (X^2 + Y^2 + Z^2)^{\frac{1}{2}} = 18.3629$$

$\sin I = Z/R = 0.6594 \quad I = -41°$

$\tan D = Y/X = -0.0681 \quad D = 184°$

$$k = \frac{N - 1}{N - R} = 5.77$$

$$\alpha_{95} = \frac{140}{kN} = 12.4°$$

the Glauchlands sheet. One sample has been measured from the top contact, one from the bottom contact 130 ft. below, and two have been measured from the sandstones 3 ft. and 9 ft. above the intrusion. These samples have acquired their magnetization rapidly due to chilling of the magma at each margin and hence have much the same direction of NRM.

It is also noticable that these directions are essentially the same as those found in the Antrim basalts and Lundy dykes in Figure 34. Hence, the direction of magnetization in these contact rocks is probably more truly representative of the geomagnetic field direction at the time of intrusion than is the computed mean.

The computed mean, however, has not been obtained from a population of random samples, as is usually the case in palaeomagnetic investigations, but on the contrary, it has been obtained from a collection in which the element of time is important, the marginal samples having become magnetized before those at the centre of the intrusion. Therefore, secular variation may account for the scatter of the NRM's and the computed mean may be the average dipole field during the time the intrusion was cooling.

Jaeger (1957a) has shown that after injection of a sill the margins cool rapidly to about 665°C and thereafter, cooling proceeds slowly. Figure 36 shows his results for a sheet of dolerite D metres thick assuming that the magma was intruded at 1000°C and crystallized in the temperature range 1000°C - 800°C. These curves show the temperatures T at various points within the sheet plotted as functions of time after intrusion. The numbers on the curves are the distances from the centre of the sheet measured as fractions of the thickness so that 0 corresponds to the centre of the sheet, 0.5 corresponds to the contacts, and values greater than 0.5 correspond to

Figure 36.

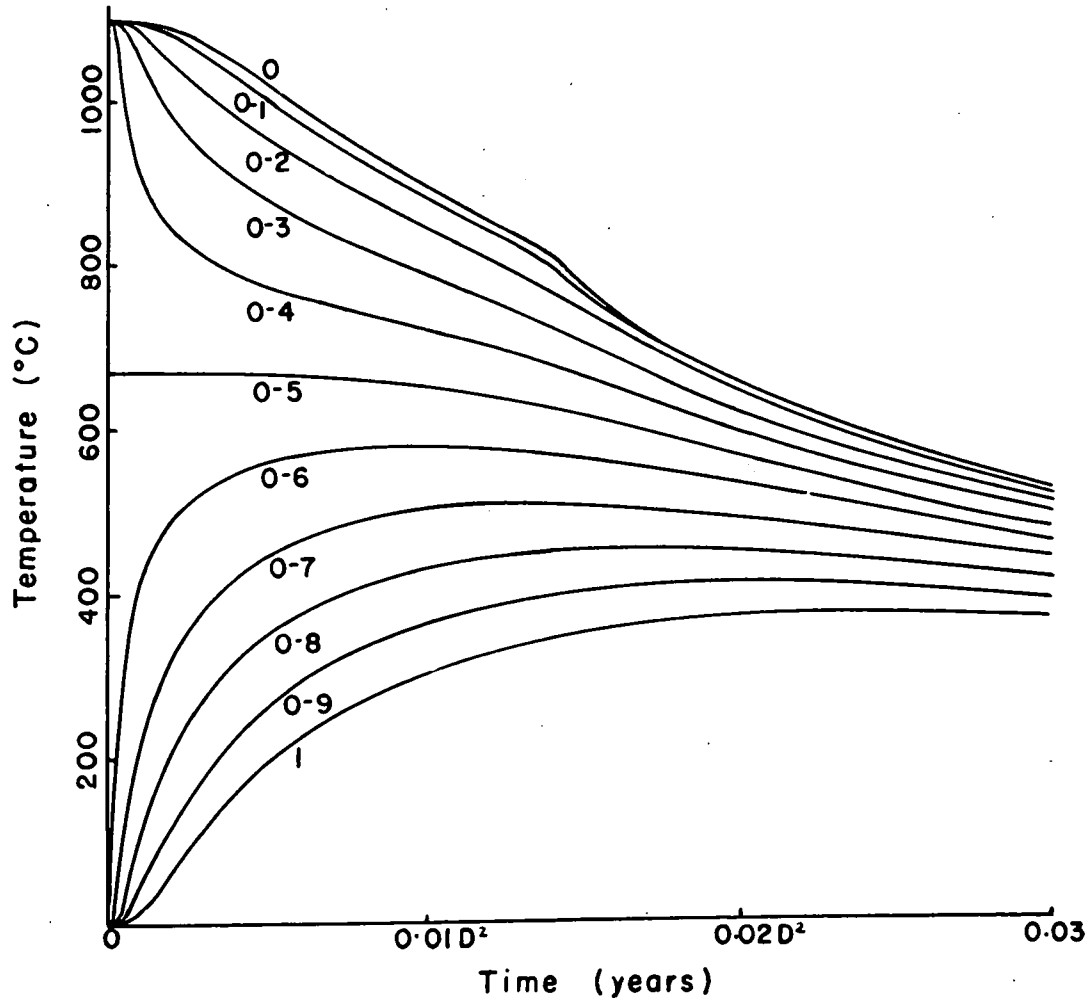
Temperature (°C)
1000
800
600
400
200
0
0·01D²
0·02D²
0·03
Time (years)
0
0·1
0·2
0·3
0·4
0·5
0·6
0·7
0·8
0·9
1

Figure 36.

Cooling curves for dolerite sheets intruded at 1100°C. (after Jaeger 1957).

temperatures within the adjacent country rock.

These results should be applicable to the Clauchlands sheet because the microcrystalline nature of the contact rocks and absence of phenocrysts (Chapter II) indicates that the magma was almost entirely liquid at the time of intrusion, and therefore was probably at a temperature of over 1100°C (Turner and Verhoogen 1960 p55).

Taking the Curie point as about 500°C, these curves show that the contact takes about $0.027D^2$ years to fall to this temperature and that the Curie point isotherm then takes a further $0.006D^2$ years to progress to the centre of the sheet. Taking the thickness of the Clauchlands sheet as approximately 40 meters these values become respectively 43 yrs and 10 yrs, and hence the intrusion may be expected to have acquired more than 90% of its thermoremanent magnetization in a very short time. This being the case then secular variation cannot account for the scattered directions of the NRM.

However, the Curie-points have been found to decrease away from the margins of the Clauchlands sheet (Chapter V) and towards the centre of the intrusion they fall below 400°C. Thus the intrusion probably acquired its magnetization over a much longer period, of the order of 100 yrs or more. Yet even such an interval is short in the geological time scale and it, therefore, seems improbable that secular variation has influenced the directions of the NRM.

However, the scatter of the NRM's is not random as can be seen in Figure 37. This curve shows how the inclination varies through the intrusion. It is steepest at the contacts, -64° at the top and -53° at the bottom, and then flattens abruptly in the marginal rocks reaching minimum values of about -2° 15 ft. below the top and about -8° 10 ft. above the bottom. Away

Figure 37.

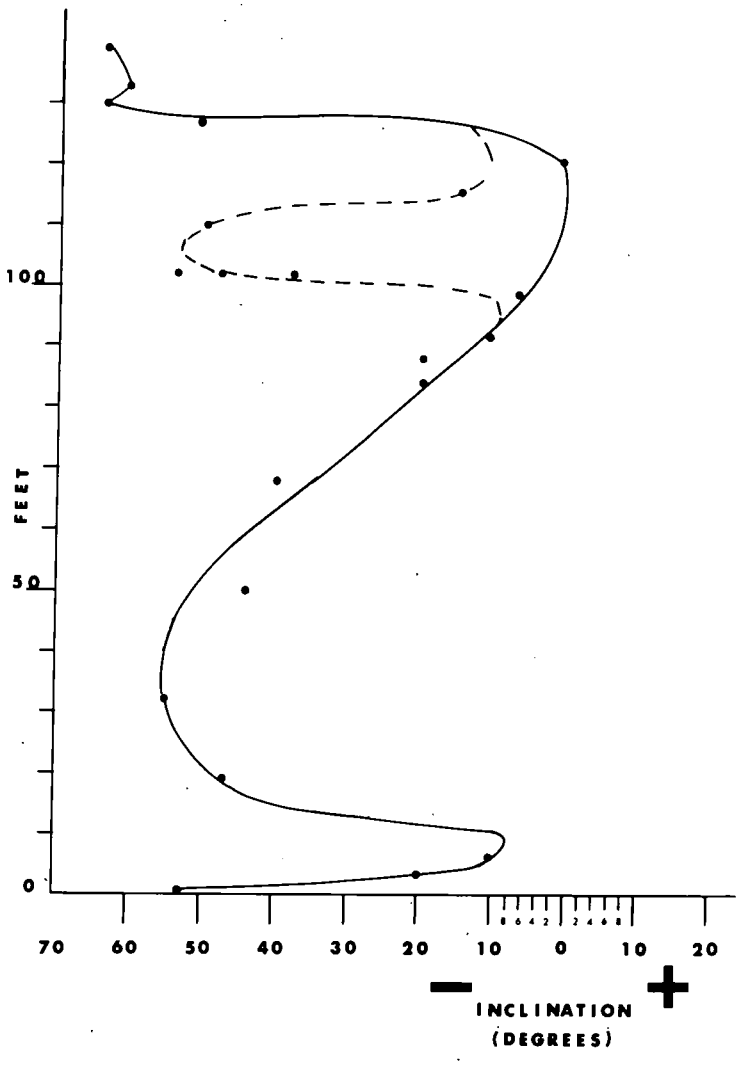

Figure 38.

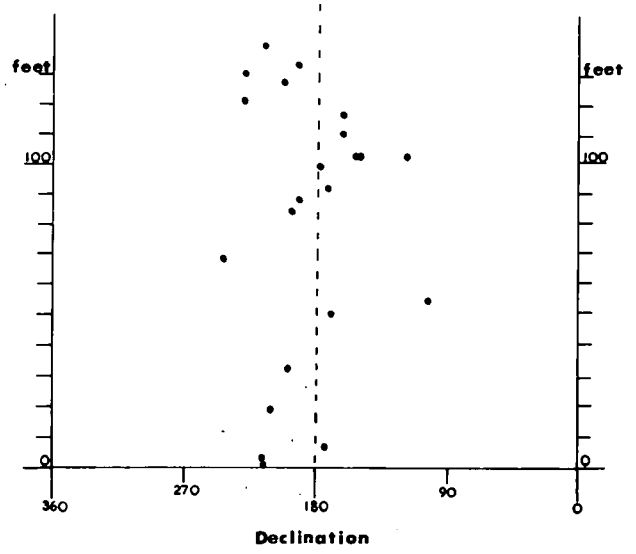

Figure 37.

Variation of the inclination in a vertical section of the Clauchlands Sheet.

Figure 38.

Variation of the declination in a vertical section of the Clauchlands Sheet.

from the margins it steepens gradually and reaches a maximum of about -55° 30 ft. above the base, so that this central part of the curve is markedly asymmetric.

The explanation of this variation may be related to the history of the intrusion, for this is well known from the exposures at Clauchlands point (Chapter I). Thus, the existance of connate xenoliths of 'basalt' in the lower parts of the sheet indicates that the intrusion is multiple, later pulses of magma having dislodged parts of the marginal rocks, and the existence of segregations of dolerite-pegmatite, limited to an horizon 30-40 ft. above the base, shows that solidification last took place at this height.

Petrographic examination (Chapter II) has also shown that the intrusion cooled asymmetrically, most of the heat having been lost from the upper surface, and it is because of this that the final solidification occurred below the central part of the sheet. Thus, by the same token, the Curie-point isotherms must have passed asymmetrically through the intrusion, progressing more rapidly from the top margin than from the bottom and finally converging about 30 ft. above the base.

These isotherms would pass through the contact rocks relatively quickly, and this would occur more or less simultaneously at both margins so that these rocks would acquire the same direction of NRM. However, shortly after the marginal rocks had become magnetized, further intrusion of magma must have occurred. The force of this intrusion was sufficient to dislodge parts of the lower margin (although not the actual contact rock) and also to deflect the TRM away from the field direction and towards the horizontal thus producing the observed 'edge-effect' in Figure 37.

Very little is known about the effects of stress on the direction of

TRM so that the mechanism responsible for this 'edge-effect' is uncertain. However, Hall and Neale (1960) have reported the rotation of TRM under stress. Using samples of a Tertiary dolerite dyke from Skye they have shown that the moment of the TRM acquired under the influence of uniaxial pressure is rotated systematically towards the plane normal to the vertical stress axis by up to 2.5°. Néel also considers that TRM may be deflected under stress and, on theoretical grounds, has deduced that for a directed stress of 500 Kg/cm^2 the rotation of the moment should be about 8° (Nagata 1961).

However, the deflections observed in the Clauchlands sheet are much greater than these values, and, therefore, although stress may have contributed to the 'edge-effect', it seems probable that actual rotation of the magnetite crystals has also occurred.

The central part of the inclination curve may also be interpreted in terms of multiple injection of magma. These later pulses would tend to penetrate the internal regions of the sheet where the rock was hotter and, therefore, less rigid than near the margins. It would also seem reasonable to envisage each succeeding pulse as being weaker than the earlier ones and therefore less effective in deflecting the TRM.

Thus, as cooling continued, and the rocks towards the centre of the sheet became magnetized, the direction of the TRM would approach more closely the direction of the ambient field, this direction being given approximately in the samples from the ontacts. Therefore, the inclination would tend to steepen towards the centre of the sheet, and since the Curie-point isotherms were moving asymmetrically through the intrusion the actual trend followed by the steepening inclinations would also be asymmetric, and the steepest values would be reached where the rock had solidified last.

This explanation may therefore account for the general form of the inclination curve shown in Figure 37. However, a number of the inclinations deviate markedly from this curve as indicated by the dashed line.

These samples have been collected from and adjacent to a basalt dyke intruded into the sheet. The effect of this intrusion would be to cause localised heating of the surrounding dolerite, and if the temperature rose above the Curie-point then a new TRM would be acquired on cooling which would be in the direction of the ambient field.

The Curie-point in the neighbourhood of the dyke is about 470°C (Chapter V) and it seems probable that the rocks in the immediate vicinity would reach this temperature and, therefore, acquire a new TRM with a direction roughly parallel to that in the dyke. However, these effects would be extremely local and rocks further from the dyke would not reach their Curie-points. Nevertheless, such rocks would become remagnetized in varying degrees, by acquiring a partial TRM.

Partial TRM is acquired during weak-field cooling through only a limited temperature range. When this temperature range extends from the Curie-point down to atmospheric temperatures then total TRM is acquired. The addition law of partial TRM says that the total TRM is the sum of the partial TRM's and, further, that the partial TRM produced by weak-field cooling through a limited temperature range T is independent of the magnetization produced by field-cooling through other temperature intervals. (Nagata 1961).

Thus rocks close to the dyke, where T is greatest, would be remagnetized more effectively than those further away and hence should show a larger deviation from the inclination curve.

This mechanism, therefore, can account satisfactorily for the observed

deviations of the inclination shown in Figure 37. The horizon within the sheet, at which these deviations occur is purely fortuitous, and it is anticipated that similar phenomena may occur wherever a dyke cuts the sheet.

Figure 38 shows how the declination varies through the intrusion. It is essentially the same at the contacts, being about N 210° at both top and bottom, but in the marginal rocks it has rotated eastwards and this change may be correlated with the 'edge-effect' observed for the inclination. The trend of the declination within the centre of the sheet is not clear, however, so that further discussion is not justified.

Nevertheless, it is clear that the inclination has been affected more than the declination, and this result may be explained in terms of the emplacement of the sheet.

The Clauchlands sheet is part of a cone-sheet (Chapter I), and therefore was probably emplaced in response to strong directed pressures radiating from a central magma source. These forces would act more or less parallel to the margins of the intrusion and would therefore have a greater effect on the vertical component of the magnetization than on the horizontal.

C. Summary

The NRM of the Clauchlands sheet has been investigated by measuring samples which represent a vertical section through the intrusion.

The intrusion has been found to be reversely magnetized except for a number of normally magnetized samples. These latter samples are considered to be unstable because they 'streak' along two great circles connecting the ancient field directions with that of the present geomagnetic field.

The intensity of magnetization has been found to decrease systematically

away from the margins of the intrusion and this trend may be correlated with a decrease in the content of 'magnetite' towards the centre of the sheet.

The directions of magnetization at the top and bottom contacts of the intrusion have been found to be similar and to agree closely with directions reported for the Antrim basalts and Lundy dykes of known Tertiary age.

The NRM's throughout the intrusion, however, show a wide scatter of directions and their computed mean is some 20° shallower than the inclinations recorded at the contacts. Since the samples became magnetized in a known sequence the possibility that secular variation has influenced the directions has been investigated. This is not considered likely since it can be estimated that the sheet acquired its magnetization over a period of little more than 100 years.

The inclination of the NRM has been found to vary systematically through the intrusion and to exhibit an 'edge-effect'. These variations have been explained in terms of the known history of the intrusion.

However, a number of the inclinations deviate from the general trend. These deviations have been explained as the effects of partial remagnetization of the dolerite where it has been cut by a basalt dyke.

The declination of the NRM has also been found to vary through the intrusion and may be correlated with the variation of the inclination. The trends shown by the declination, however, are less clear than with the inclination.

Chapter VIII. Discussion of the Reversed Magnetization

A. Introduction

There are apparently two possible explanations of the occurrence of a reversely magnetized rock formation. Either the Earth's magnetic field was reversed when the rock became magnetized, or the magnetic minerals in the rock have a "self-reversing" property which makes them assume a magnetization opposed to the applied field.

B. Reversal of the Earth's Magnetic Field

A large number of rock formations from all over the world are known to have a reversed NRM (Blackett et al 1960), and sedimentary as well as igneous rocks exhibit this phenomenon. It, therefore, seems improbable that the reversed directions in such a wide variety of rocks, which have acquired their magnetization by different methods, can in all cases be attributed to a self-reversal mechanism, and hence it seems likely that reversals of the geomagnetic field have occurred in past ages.

The latest epoch from which reversely magnetized rocks have been recorded is late Pliocene - early Pleistocene. Reversed rocks of this age have been reported on a world wide scale, from Iceland (Hospers 1953, 1954; Einarsson and Sigurgeirsson 1955), France (Roche 1956), Japan (Nagata et al 1957 a,b), Russia (Khramov 1957), Australia (Irving and Green 1957), South America (Creer 1958), New Zealand (Coombs and Hatherton 1959) and from Africa (Nairn priv. comm. to Nagata 1961). The global distribution of this so-called Plio-Pleistocene reversal would indicate the reality of geomagnetic field reversals, and this conclusion is supported by the conspicuous absence of reversely magnetized rocks of Permian age which in Australia, Europe and North America are magnetized

in a direction consistent with a field of one polarity. (Runcorn 1962).

Wilson (1962) has discussed the relationships between the NRM of igneous rocks and the baked contact rocks. If N represents normal magnetization and R represents a reversed magnetization, then there are four permutations of N and R, between the igneous rock and its contact:-

Igneous Rock	Baked Rock
N	N
R	R
N	R
R	N

Thus if field-reversals are common then the baked contacts should show the same polarity as the igneous rock and thus the relationship NN or RR should be predominant. If, however, field-reversals are rare (or non-existant) and self-reversal is common, then there should be no preferred relationship between the polarities of the independent igneous and baked rocks and the contacts should equally be NR or RN as well as NN or RR because normal and reversed rocks are known to occur with about equal likelihood.

Of the 52 baked contacts considered by Wilson, 48 show agreement between the polarities in the igneous and baked rocks, 14 being NN and 34 being RR, and this preponderance of agreement strongly suggests the reality of past reversals of the geomagnetic field.

C. Self-Reversal Mechanisms

Self-reversal mechanisms may be grouped into three categories (Nagata 1961):-

1. Two-constituent mechanisms involving magnetostatic interaction.

2. Two-constituent mechanisms involving exchange interaction.

3. One-constituent mechanisms.

Two-constituent mechanisms involving magnetostatic interaction require the development of a secondary magnetic phase during geological time. This phase will become magnetized under the influence of the demagnetizing field of the original magnetic phase and if its intensity of magnetization is large enough it may cause a reversal.

Artificial assemblages of interleaved magnetite and pyrrhotite have been found to be self-reversing in this way (Grabovsky and Pushkov 1954; Uyeda 1958), and Kwai, Kume and Sasajima (1956) have suggested that the intimate intergrowths formed by exsolution of a titaniferous magnetite into magnetite-rich and ulvöspinel-rich components might be natural examples of such an assemblage. It has also been suggested (Graham 1952) that the partial oxidation of magnetite, in magnetite-ilmenite intergrowths, might result in a reversal of the magnetization due to magnetostatic interaction between the secondary maghemite and the residual magnetite.

Two-constituent mechanisms involving exchange interaction are very similar to those involving magnetostatic interaction except that the interaction occurs at the molecular level. Such mechanisms therefore require not only that the two phases be intergrown but also that their crystal lattices be intimately bound together.

It seems probable that the intergrowths formed by exsolution of titaniferous magnetite would fit this category rather better than the category of magnetostatic interaction and such a mechanism may be more likely to cause self-reversal of the magnetization in view of the powerful forces acting at the molecular level

as compared to those acting at the microscopic level.

However, for such mechanisms to operate it is necessary that the two phases have Curie points rather far apart so that the first component may have acquired most of its magnetization before the second one becomes magnetized.

Uyeda (1958) has suggested that the self-reversing property of the rhombohedral ore-mineral component found in the Haruna dacite, may be explained in terms of exchange interaction. He envisages the interaction as taking place between ordered and disordered regions of the mineral, with the Curie point of the ordered phase being higher than that of the disordered phase. Carmichael (1961) has also found examples of self-reversing 'ilmenites' which he interprates in terms of order-disorder relationships.

Detailed discussions of two-constituent mechanisms have been given by Néel (1952, 1953, 1955) and also by Grabovsky and Pushkov (1954) and Uyeda (1958). Such discussions are largely theoretical, but Nagata, Uyeda and Ozima (1957) have reported on the experimental investigation of the magnetic interactions between ferromagnetic minerals in rocks. They conclude that such interactions are negative when the two ferromagnetic constituents form fine laminar intergrowths. If however, one of the constituents is non-ferromagnetic, then this simply results in an intensification of the TRM which seems to be related to an increase in the coercive force of the sample.

It seems, therefore, that the exsolution phenomena among the iron-titanium oxide minerals may, under suitable conditions, result in a two-constituent mineral assemblage with self-reversing properties. However, it is not known whether such assemblages are common in rocks or whether they can be correlated with the magnetization.

Much of the data of palaeomagnetism has been obtained from extrusive

volcanic rocks, mainly basalt lavas, and in such rocks the ore minerals are generally homogeneous titaniferous magnetites. Therefore, two-constituent mechanisms cannot account for the reversed magnetization of such rocks. However, a number of self-reversal mechanisms have been proposed which do not require the coexistence of two magnetic phases but which depend upon chemical inhomogeneity within a single phase.

Néel (1948) first suggested that some ferrites might exhibit an unusual variation of the spontaneous magnetization with temperature such that when the temperature passed through a critical point the direction of the magnetization reversed. Examples of this N-type variation were subsequently discovered in the mixed ferrites $Li_{0.5}Fe_{2.5-a}Cr_aO_4$ for values of a between 1.00 and 1.70 (Gorter and Schulkes 1953) and for a group of rare earth ferrites $Fe_2M_2O_6$ where M is the rare earth Gd, Er or Dy Guiot-Guillain, Pauthenet and Forestier 1954).

When such substance are heated, the spontaneous magnetization decreases normally and disappears for the first time at a temperature θ_c but then begins to increase again, reaches a maximum and then finally disappears at the Curie point θ_p. θ_c is not a Curie point but only the temperature at which the spontaneous magnetization changes sign. Below θ_c the spontaneous magnetization J_a of sub-lattice A (see Chapter V), say, is greater than that of sublattice B, while above θ_c the reverse is true. θ_c is known as the compensation temperature, and at this point the spontaneous magnetizations of the two sublattices are equal. Thus, if such a substance is cooled to room temperature from above its Curie point it will acquire a TRM opposite to the sense of the field to which it is due. However no natural 'magnetites' are known to show this type of thermal variation of the spontaneous magnetizations.

Néel (1955) has also suggested that reversal may occur through annealing, and this mechanisms has been demonstrated experimentally with nickel ferrite $NiFe_2O_4$. (Garter 1954). Nickel ferrite is an inverse spinel and has the cation distribution:-

$$\underset{A}{Fe^{3+}} \quad \underset{B}{Ni^{2+}Fe^{3+}} \quad O_4$$

When Al^{3+} replaces some of the Fe^{3+} so that the formula becomes $NiFe_{2-m}Al_mO_4$, the Al^{3+} ions are known to prefer the B-sites in the equilibrium state (Verwey and Heilmann 1947). If the equilibrium distribution is realised at all times, then the spontaneous magnetization should decrease as m increases, become zero when $m = 0.4$ and then reappear in the reverse direction for $m > 0.4$. However if the samples are quenched from high temperatures so that there is a disordered distribution of the cations then there will be no reversal of the spontaneous magnetization with increase in m. If on the other hand, a sample with $m > 0.4$ is annealed then it may be made to reverse on the laboratory time scale, owing to diffusion of Al^{3+} ions onto the B sites. To produce the inversion in the laboratory several hours at 400°C are needed, but the same effect would probably occur at ordinary temperatures in some millions of years (Néel 1955).

Although similar effects may exist in natural magnetites it is unlikely that they could be observed experimentally. The reason that they are observed in nickel ferrites is because the magnetic moments of the two sublattices A and B are very close, $5\mu_B$ and $7\mu_B$ so that it is much easier for the A sublattice to have a greater moment than the B than in magnetite, where the moments of the two sublattices are $5\mu_B$ and $9\mu_B$ and thus much less close.

Verhoogen (1956) has extended this argument to the case of the natural substituted magnetites on the basis that ordering may take place during

geological time and thus cause a reversal of the spontaneous magnetization. His calculations show that for a magnetite of formula $Fe_a^{2+} . Fe_b^{3+} M_c O_4$ self-reversal may be expected if $c > 0.75$ provided that M stands for a non-magnetic impurity with a greater affinity for B-sites than either Fe^{2+} or Fe^{3+}. On the other hand, the mineral must remain electrically neutral and, therefore, Verhoogen has suggested that the most likely impurities that may cause self-reversal are an appropriate combination of Al^{3+}, Ti^{4+}, Mg^{2+} and vacancies such that $c > 0.75$.

Unfortunately, little is known about the detailed compositions of natural magnetites, and even less about their relations to the magnetization of the host rocks. However, Verhoogen has listed several instances of magnetites whose compositions suggested that they may be self-reversing. In particular these magnetites contain appreciable amounts of Al^{3+} and Mg^{2+} as well as Ti^{4+}.

In order that the mechanism outlined by Verhoogen may operate, it is necessary that the crystal should retain a considerable degree of disorder at the temperature at which it acquires its magnetization, and hence the rate of ordering must be slow in comparison to the rate of cooling. It seems probable that this condition will be satisfied in rapidly cooled lavas and also in hypabbysal intrusions.

Verhoogen has estimated that an impure magnetite with inherent self-reversal properties could not reverse in less than about 10^5 to 10^6 years. This may be the reason why no modern lavas have been found to have a reversed magnetization.

Self-reversing mechanisms of this type, of course, cannot be demonstrated experimentally but it does seem likely that many magnetites have compositions

such that the mechanism could operate. This problem could best be settled by the long term accumulation of data on the detailed chemical composition of natural magnetites and also on the directions of magnetization of the rocks containing these analyzed minerals.

D. Applications to the Clauchlands Sheet

It seems probable that the directions of magnetization in the Clauchlands sheet are due to a genuine reversal of the Earth's magnetic field during the early Tertiary, since the baked sandstones above the intrusion have the same reversed polarity as the igneous contact.

Microscopic examination of the sandstones (Chapter III) has shown 'hematite' to be the predominant ore mineral with only minor amounts of 'magnetite'. However, the Curie point and intense magnetization of these rocks would indicate that the NRM is due to the 'magnetite' rather than the 'hematite'.

The unaltered rocks above the intrusion are dull-red flaggy sandstones and, therefore, it is presumed that the 'hematite', in the baked rocks is an original constituent. This 'hematite' occurs as complex recrystallised aggregates and the grains often have a core of 'magnetite'. Similar relationships are known to occur in hematite ores that have been sintered at 1100°C to 1300°C (see Chapter III), and on the basis of the petrographic evidence (Chapter II) it is thought that the Clauchlands sheet also was intruded initially at a temperature of about 1100°C so that the 'magnetite' in the baked sandstones has probably formed by dissociation of 'hematite'.

If this is the case, then the fact that these rocks have the same reversed magnetization as the igneous contact must strongly indicate that the Earth's field was reversed when they became magnetized. It seems

improbable that a self-reversal mechanism could have operated in both the 'magnetite' that crystallised from the magma and the 'magnetite' formed by dissociation of the 'hematite' in the sandstone so as to give the same direction of magnetization in both rocks.

The results of the present investigation have provided no positive evidence to indicate that self-reversal has occurred in the Clauchlands sheet. However, the accumulated data has indicated that the magnetic minerals are 'impure magnetites' and hence they may intrinsically be capable of self-reversal by the type of ordering mechanism outlined by Verhoogen (1956).

Recently, Ade-Hall and Wilson (1963) have suggested that there may be a connection between reversely magnetized igneous rocks and the occurrence of 'magnetite'-'ilmenite' intergrowths. They found that in the Mull lavas the normally magnetized rocks contain homogeneous pale brown magnetites whereas the reversely magnetized rocks contain oriented 'magnetite'-'ilmenite' intergrowths in which the 'ilmenite' forms up to 20-30% by volume of the crystals.

At present there is not sufficient information properly to assess such a correlation, but in the case of the Clauchlands intrusion it should be noted that the intergrown 'ilmenite' contains about 10 - 20 mol% Fe_2O_3, and that according to Chevallier, Mathieu and Bolfa (1955), such ilmenite is ferromagnetic with Curie points of about 200°C.

Although the results of thermomagnetic analysis have shown only the high Curie points associated with the 'magnetites', this may be because the analyses have been carried out in relatively large magnetic fields of about 1000 Oe, and analyses in weaker fields might have shown the ilmenites

to be magnetic. Therefore, the possibility of a two-constituent self-reversal mechanism cannot be ignored.

PART II

The Design of an Instrument for the Measurement of the Curie Point of Ferromagnetic Minerals

Plate XVIII

General View of the Thermomagnetic Balance

The balance is housed in the turreted box at right centre. The recording systems are grouped at the left of the photograph and the motor driven variac is visible at the right of the photograph. The rheostat, seen at the far left, controls the current to the electromagnet which is indicated on the meter situated to the left of the turret. The furnace current is indicated by the meter on the right of the turret.

Introduction

The instrument described in the following pages is a horizontal magnetic balance adapted for the measurement of the Curie points of small samples of ferromagnetic minerals and rock fragments (Plate XVIII). The basic principles governing the design of the instrument are simple and complications in the actual instrumentation are necessitated mainly by problems associated with making the measuring process automatic.

The principle of the magnetic balance is illustrated in Figures 39 and 40. A ferromagnetic sample placed at point p (Figure 39) so that it lies on the axis between the poles of a magnet, takes on a magnetic moment M parallel to the field direction H and experiences a force F_x along the axis such that:-

$$F_x = M \frac{dH}{dx} \qquad \text{.....1)}$$

$$= v.J.H \frac{dH}{dx} \qquad \text{.....2)}$$

where v is the volume of the sample and J its intensity of magnetization.

In Figure 40 the sample at p is shown attached to a rigid mobile system which is suspended at S by a length of fine wire. Under the influence of the field H the sample experiences a force F_x which causes a torsional deflection of the suspended system. If, however, the sample is surrounded by an electric furnace and heated, then at the Curie point the spontaneous magnetization becomes zero, F_x dissappears and the suspended system returns to its equilibrium position. Such a system, therefore, provides a sensitive means of detecting the Curie point and, suitably modified, can be used for its accurate measurement.

Figure 39.

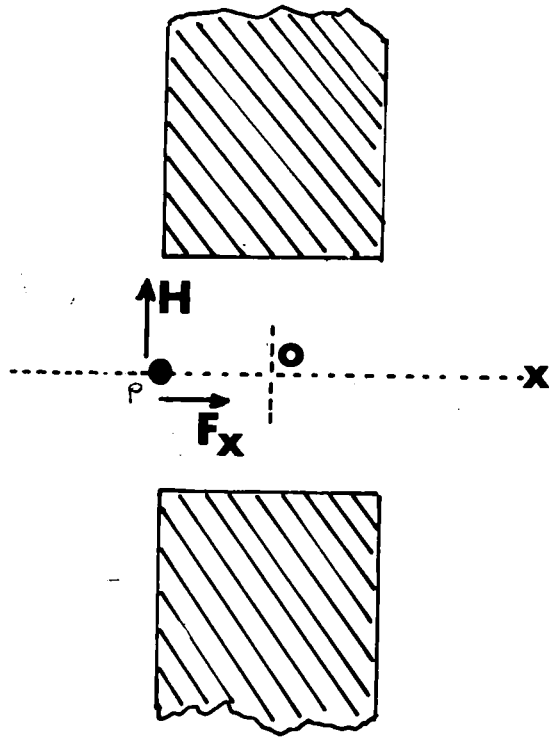

Figure 40.

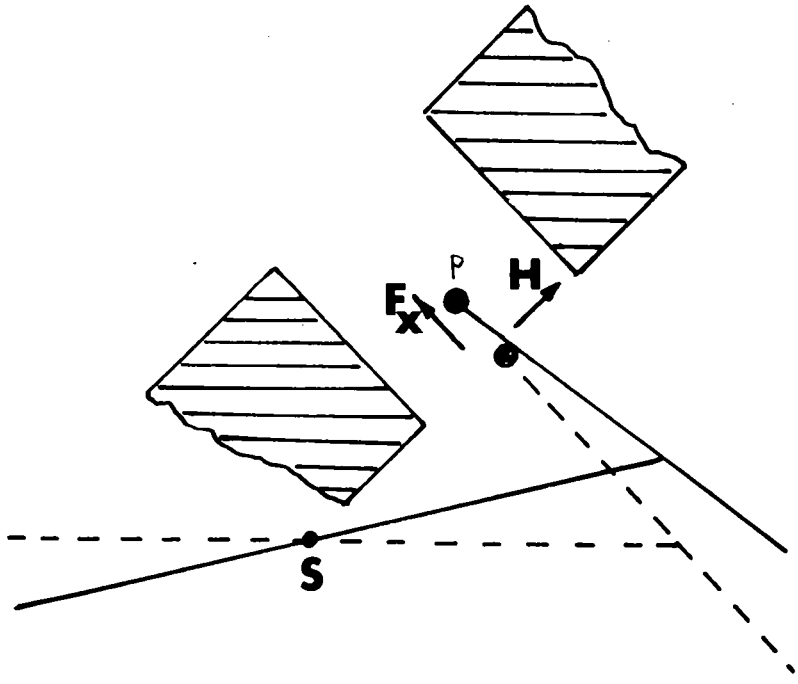

Figure 39.
Principle of the magnetic balance

Figure 40.
Principle of the magnetic balance

Plate XIX

View of the Recording Systems of the Thermomagnetic Balance

The controls for the 'Temperature Recording System' are aeen in the left hand frame above the Ether 'Transitrol' Controller. The scale on the Ether galvanometer is arbitrary and not ^{o}C as shown. The chart recorder is housed at top right with the stabilised power supply below it. The transistors of the 'Photo-electric Recording Unit' plug into the small box at the right of the photograph which contains the Wheatstone's bridge circuit. The output of the transistors can be indicated on the milliameter in this box when making preliminary adjustments before starting anaanalysis, and then switched to the Recorder.


EXCITOR LAMP CONTROL
TEMPERATURE
OFF
TEMP. DECREASE
STEP-RELAY INDICATOR
L1
L2
32V STABILIZED
24V
FUSE
°C
0
50
100
150
200

A magnetic balance working on the torsion principle was originally employed by P. Curie (1895) in order to measure paramagnetic susceptibilities. Subsequently this principle has been adapted in order to measure the Curie points of ferromagnetic substances and an instrument of this type has been described by Chevallier and Pierre (1932).

Chevallier and Pierre used an optical system to detect movements of the torsion balance and the instrument traced a record of the thermomagnetic curve on a photographic plate. Temperatures were indicated by breaks in this curve made at intervals of about 100°C (see for example Chevallier, Mathieu and Vincent 1954).

Larochelle (1961) has described an improved version of this instrument in which the thermomagnetic curve is traced out by a chart recorder. The temperature is measured by means of a potentiometer and indicated on the side of the chart at any desired interval. This, however, requires the constant attention of the operator.

In the present instrument the torsional deflection is detected photo-electrically and automatically recorded on a "Record" Graphic Recording Milliammeter. At the same time the temperature is measured by a chromel-alumel thermocouple and this is translated into an intermittent record on the chart via a marker pen. In this way a permanent thermomagnetic curve is obtained from which the Curie point may be determined.

Five basic units combine to make the complete instrument, and these are described in the following order:-

1. The Suspended System.
2. The Electromagnet.
3. The Photo-electric Recording System.
4. The Electric Furnace.

5. The Temperature Recording System.

Finally, instructions are given for the preparation of the instrument, its operation and the interpretation of the thermomagnetic record.

1) The Suspended System

Since the instrument is intended to analyse small samples, weighed in milligrammes, the torsion beam has to be light and have a low moment of inertia so that it may respond rapidly to the forces acting on the sample. The actual dimensions of the beam are not critical but it has to be constructed of non-magnetic material and housed in a non-magnetic structure.

The beam itself is in two parts as shown in Figure 41. A fused silica tube AB, 2mm in external diameter and approximately 15cms long is set at an angle of 45° to the beam CD, which is a dural tube 25 cms long and 4mm in external diameter. A brass bolt screwed into the end of the dural tube holds the silica beam in position such that the distance SD is 10cms. S is a shallow trough formed of silver foil and is approximately 1cm long. It is attached to the silica beam and acts as a holder for the samples. Silver is used for this purpose because of its high melting point ($960.8^{\circ}C$) and chemical stability and especially because of its large thermal conductivity (0.992 cols/sec/cm^3/$^{\circ}C$ $100^{\circ}C$) which ensures a rapid transfer of heat to the sample.

Silica is used for the beam AB because this part of the structure extends into the pole gap of the electromagnet, M; commercial dural tubing may contain ferromagnetic impurities in sufficient concentration to influence the deflection of the system if it were used in this position.

The beam CD, however, is well away from the magnet and it is therefore constructed of dural which is light and yet has the necessary strength that this structure needs in order that it may carry the suspension and other components of the system.

Figure 41.

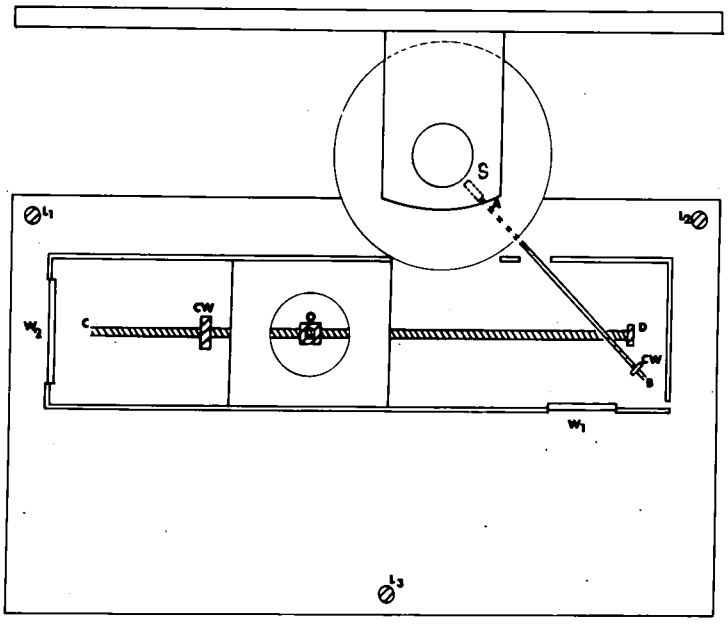

Figure 42.

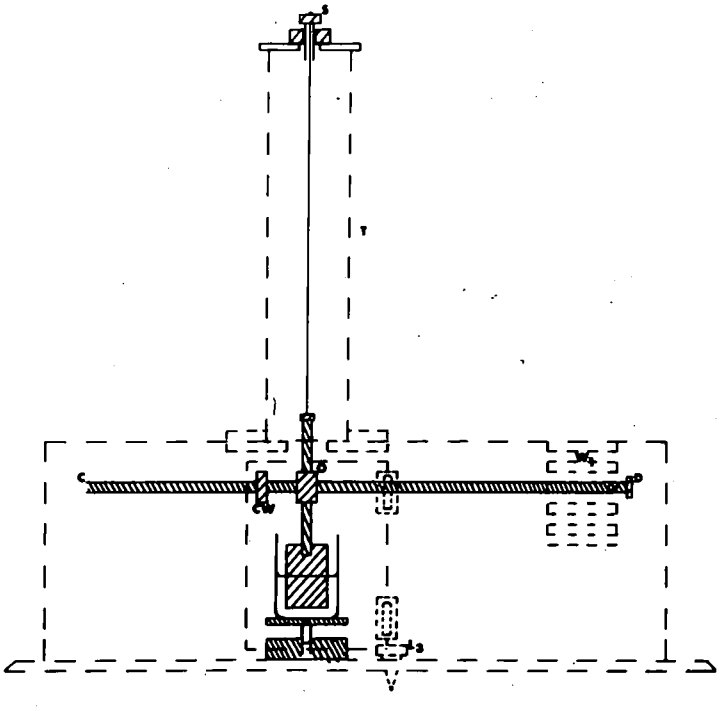

Figure 41.
Planeview of the beam

Figure 42.
Elevation view of the beam

The point of suspension is at O and is 14cms from D so that the angle OSD is 90°. Point S therefore lies on the tangent to a circle of radius OS. With these dimensions and an angular rotation of about 4° about O, the point S moves along the tangent for about 1cm without diverging sensibly from the straight line.

At O, the beam carries a brass collar (Figure 42). A 4cm length of dural tubing is screwed vertically into the top of this collar and a brass bolt, inserted into the top of this tube, acts as a base to which is soldered a length of SWG 36 copper wire. This is the suspension wire and is approximately 30cms long. The wire is soldered at its upper end to a brass screw s by means of which the height of the suspension can be varied over a range of 3cms.

Another 4cm length of dural tubing is screwed in vertically below the brass collar at O and this carries a brass damping plate which dips into a beaker of thin machine oil. The beaker stands on an adjustable platform which can be raised or lowered so that final settings of the damping can be controlled. The horizontal attitude of the suspended system is determined by the two brass counterweights CW.

The torsion beam is housed in a non-magnetic structure the walls of which are constructed of aluminium sheeting. A small door situated below the suspension turret permits easy access to the damper and to the interior in general.

The suspension turret T is formed of a tube of opaque black plastic 30cms long and 6 cms in internal diameter. It is supported on a wooden base securely bolted to the aluminium frame. (NB. The turret is omitted from Figure 41 and only the base is shown).

A small perspex window W_1 has been provided in the side of the frame

and carries horizontal lines engraved at 1cm intervals. This window is used for checking the horizontal attitude of the suspended system. Another perspex window W_2 has been inserted in the rear wall of the frame and this is engraved with rectilinear lines at $\frac{1}{2}$ cm intervals. This window is connected with the photoelectric recording system and need only be used when initially setting up the instrument.

The housing for the torsion beam stands on a wooden base which may be levelled by means of three brass levelling screws L_1 L_2 and L_3. A non-magnetic clamp links the suspension turret to the base board of the magnet (which is vertical) and ensures that the whole housing is firmly secured in position.

A general view of the suspended system is shown in Plate XX.

Plate XX

View of the Suspension System (with cover removed) the Furnace and the Magnet

The torsion beam is seen in position within the furnace. Movements of the beam are damped by the damping plate which is shown immersed in machine oil in the small beaker. The beaker stands on a metal table the height of which can be adjusted by rotating the disc. The furnace is supported on a slide that can move horizontally in the pole gap of the magnet. Cooling coils cover the pole tips to remove heat radiated from the furnace.

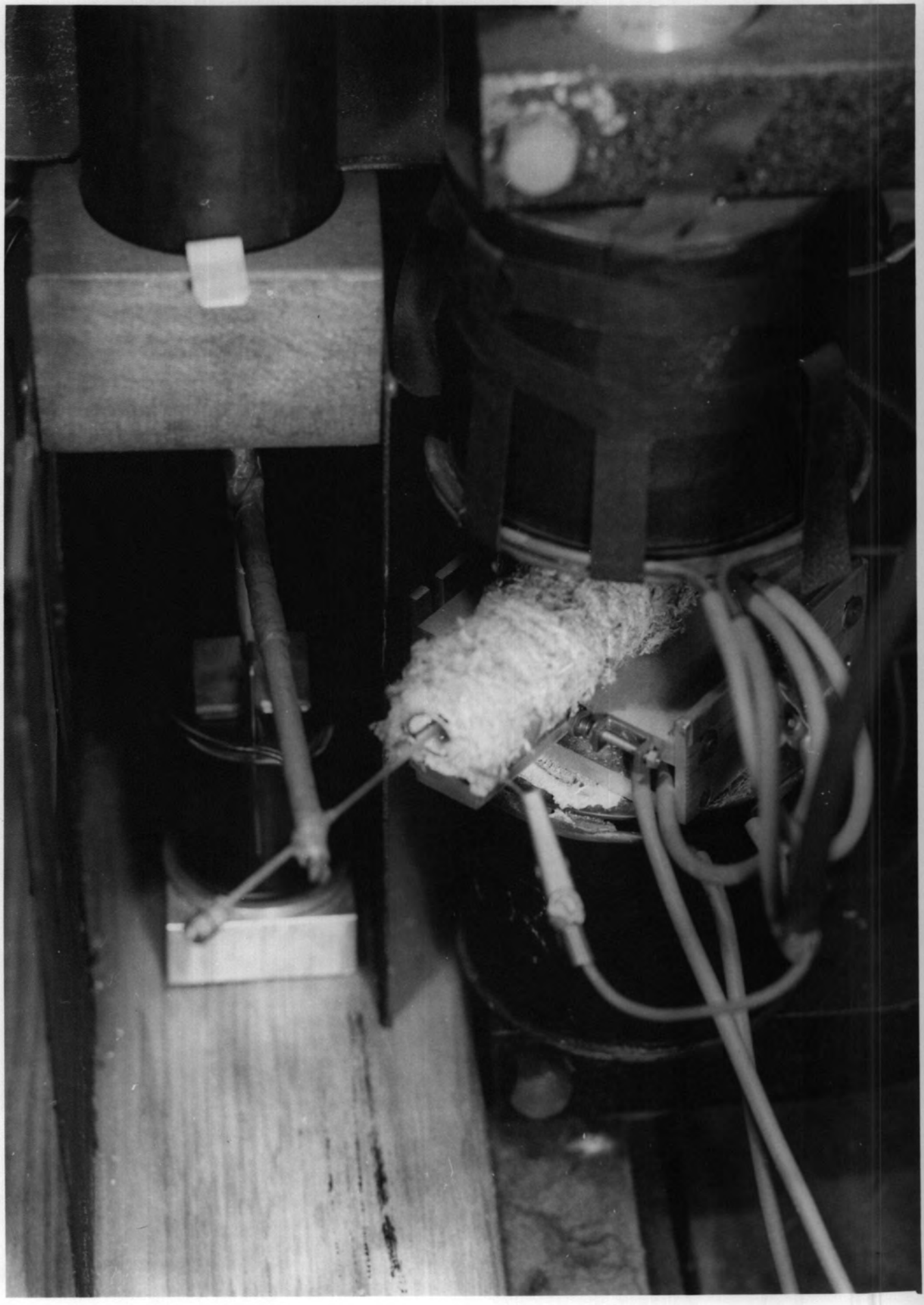

2) The Electromagnet

The coils of the electromagnet are wound in series and have a total resistance of about 12 ohms. They operate from a 24V DC supply and the current can be varied by means of a rheostat.

The field strength has been investigated using a search coil formed of 100 turns of SWG 36 copper wire. The dimensions of the search coil are:-

Inner diameter = 1.395cms	..... r_i	= 0.680cms
Outer diameter = 1.510cms	..... r_o	= 0.705cms
Cross-sectional Area	..... a_i	= 1.45 cm^2
	..... a_o	= 1.56 cm^2
Mean cross-sectional Area	..... a	= 1.50 cm^2

A Cambridge fluxmeter has been used to measure the field. This instrument is calibrated such that a deflection θ of one scale division equals 15,000 maxwell-turns. Therefore the field strength, H oersted, is given by:-

$$H = \frac{15000\ \theta}{N\ a} \qquad \ldots\ldots\ldots 3)$$

where N equals the number of turns on the search coil. For the present coil this gives:-

$$H = 100\ ^{\theta} \text{oe.}$$

The field strength has been measured as a function of the current in the magnet coils and the results are summarized in Table 24 and shown graphically in Figure 43.

These results, however, apply for a pole-gap of 4cms. A pole-gap of

Table 24.

Calibration Data for the Electromagnet
(Pole Gap = 4cms)

Magnet Current I amps	Fluxmeter Deflection θ divisions	Field Strength H oersteds
0.25	2.0	200
0.50	3.1	310
0.75	5.3	530
1.00	7.1	710
1.50	8.5	850
2.00	14.7	1470
2.25	15.8	1580

Figure 43.

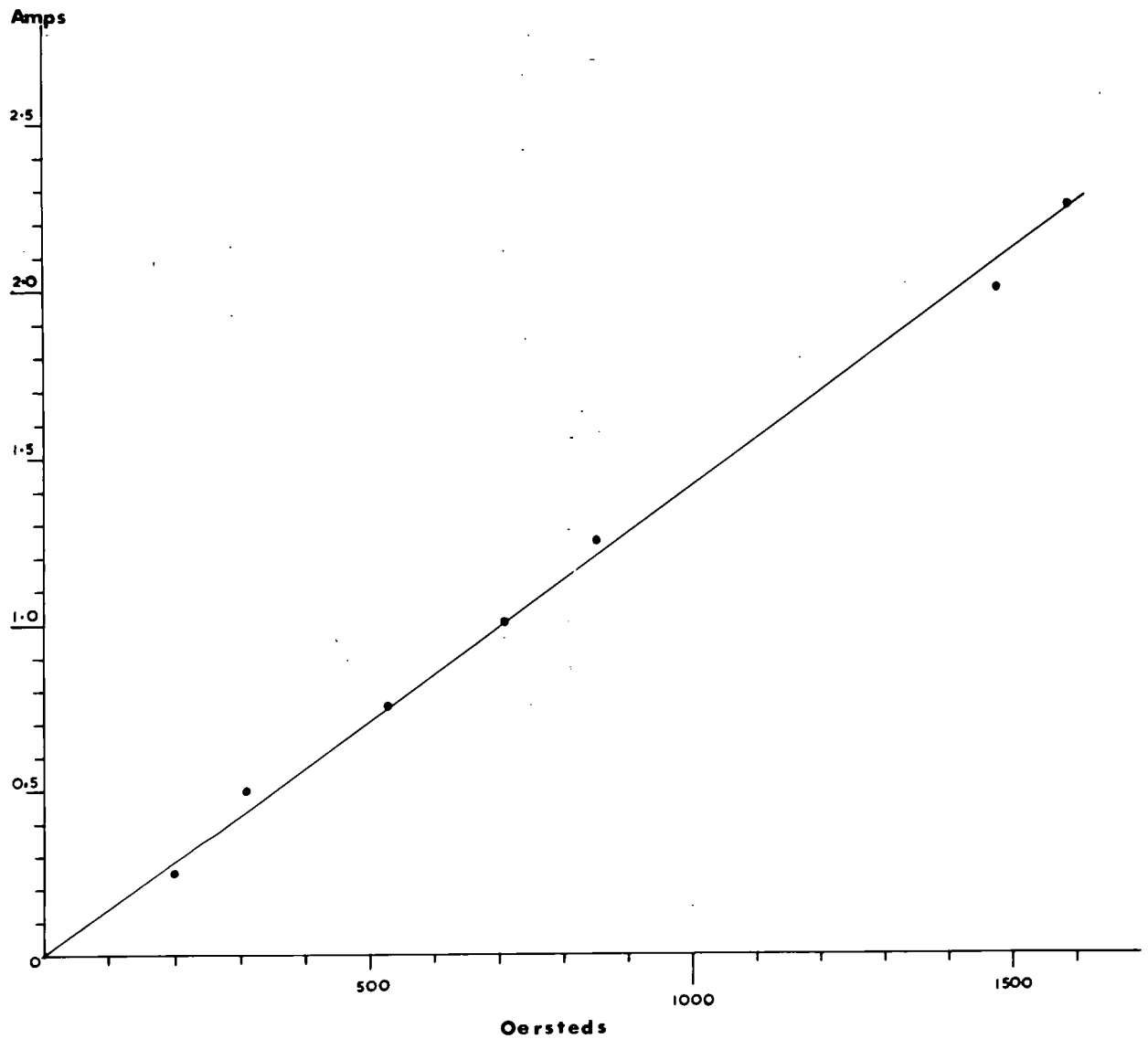

Figure 43.

Field strength of the electromagnet as a function of current.

5cms has been adopted in the final instrument and, therefore, the maximum field strength will be less than indicated in Figure 43 and is likely to be about 1000 oe.

The poles are cylinders 48mm in diameter with the faces machined to the form shown in Figure 44. This optimum shape has been chosen after concluding the series of analogue field mapping experiments described below.

It is necessary that the sample should experience a uniform force F_x when it is in the pole gap and that this force should remain constant over that region of the pole-gap in which the sample is able to move. In equation 2 (page 121) the values of v and J are constant for a given sample so that the equation may be rewritten:-

$$F_x = k.H \frac{dH}{dx} \qquad \ldots\ldots\ldots 4)$$

and thus the necessary conditions are satisfied when $H\frac{dH}{dx}$ is constant. This also requires that:-

$$\frac{dH^2}{dx} = K \quad \text{since} \quad \int \frac{dH^2}{dx} = 2H \frac{dH}{dx}$$

and this can be rewritten:-

$$dH^2 = K.dx \qquad \ldots\ldots\ldots 5)$$

Integrating 5) gives:-

$$H^2 = Kx + C \qquad \ldots\ldots\ldots 6)$$

where C is a constant. Thus $H\frac{dH}{dx}$ is constant when equation 6) is satisfied.

In Figure 45 are shown lines of equal voltage which may be determined by analogue field mapping. The lines a and b are equidistant from the axis

Figure 44.

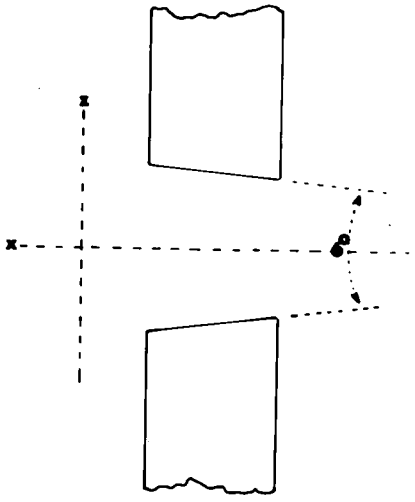

Figure 45.

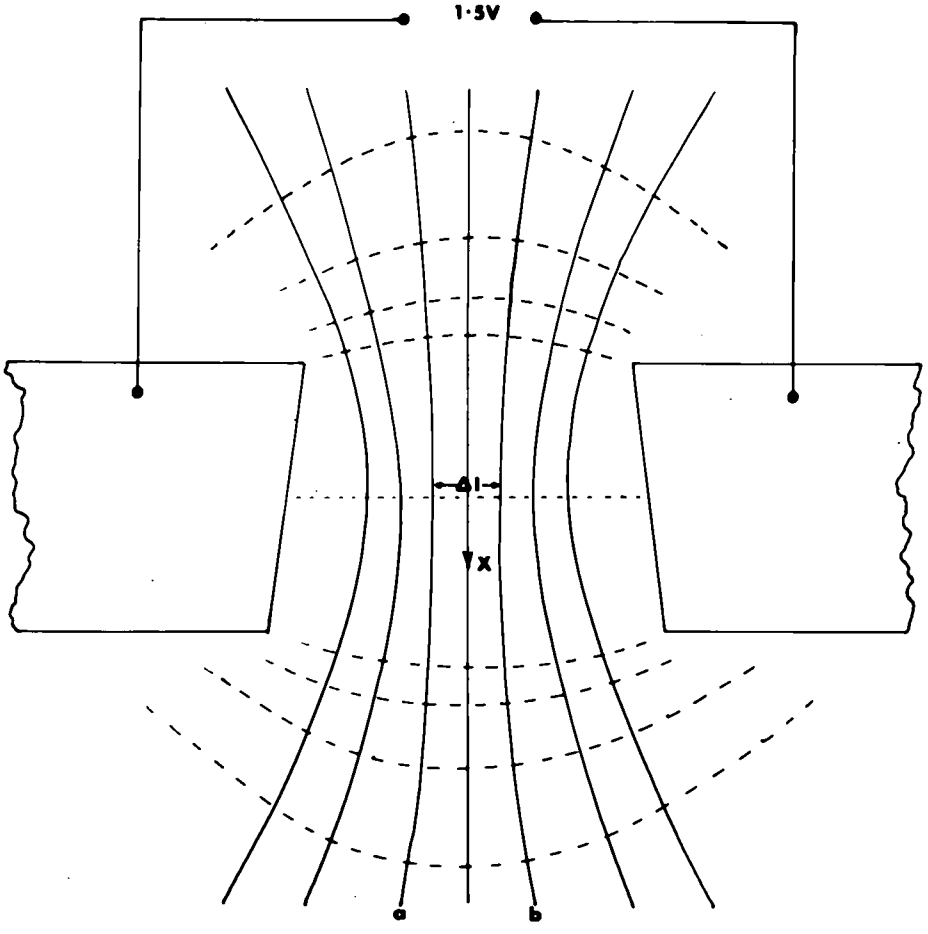

Figure 44.

Shape of the pole tips.

Figure 45.

Diagram illustrating the principle of analogue field mapping and showing lines of equal voltage.

and a distance Δl apart. Lines of magnetic equipotential run perpendicular to the voltage lines and the magnetic potential between a and b is given by:-

$$\Delta\Omega = \int_a^b H.dl$$

This equation can be rewritten:-

$$H = \Delta\Omega / \int_a^b dl$$

and integrating this gives:-

$$H = \frac{\Delta\Omega}{\Delta l} \qquad \ldots\ldots\ldots 7)$$

Hence equation 6) will be satisfied when a plot of $\left(\frac{1}{\Delta l}\right)^2$ against x is a straight line.

In analogue field mapping an electrical model is used to simulate the magnetic circuit and the required information is derived by analogy. Teledeltos facsimile recording paper has been used as a conducting sheet in these experiments and its use is described in the following extract taken from an article published by the Western Union Telegraph Company, USA.

"Teledeltos facsimile recording paper can be used as a conducting sheet for analogue field mapping in two dimensions, as a substitute for an electrolytic tank, sandbed or metallic conducting sheet. The useful part of the material is the black carbon-filled paper which is the base for the recording coating. Neither the electrosensitive layer nor the aluminium lacquer coating on the black surface of the paper enters into the field mapping process since each of these coatings is relatively non-conducting. The aluminium protective coating is quite thin, however, and is more easily penetrated by probes or by fixed electrical connections than the recording coating. In field mapping

applications it is customary to apply the required connections to the aluminium surface with silver conducting paint using acetone or methyl-ethyl ketone as the solvent, either one usually penetrating the coating sufficiently to make contact possible between the silver solids and the black paper. Where desired, the aluminium coating may be readily washed off with any good lacquer solvent at the site of the connection.

Mapping on Teledeltos paper should be performed with relatively low voltages and moderate currents. A maximum of about one third watt per square inch dissipation is desirable to reduce heating. Although the paper can tolerate temperatures well above 100°C without physical damage. The resistance change with drying is the significant factor here.

Probing is best accomplished by a null method using a potentiometer to determine the voltage line to be drawn....."

Electrolytic iron has been used in the present experiments since silver was not available. The iron was suspended in acetone and the required pole shape painted full size onto a large sheet of Teledeltos paper. A potential difference of 1.5V was applied across the electrodes using a torch battery, and a potentiometer was used to determine the voltage lines. A mounted zoological needle served as a probe, and in order that probing should be systematic a centimeter grid was drawn on a sheet of tracing paper and this placed over the electrodes. Probing was accomplished by pricking through to the carbon layer and in this way a pattern of voltage determinations built up from which the voltage lines could be drawn.

Data are presented for the following electrode shapes:-

a) The pole faces parallel and 5cms apart.

b) The pole faces diverging at 6° and a minimum distance of 5cms apart.

c) The pole faces diverging at 10° and a minimum distance of 5 cms apart.

d) The pole faces diverging at 40° and a minimum distance of 5cms apart.

Only one pair of voltage lines has been considered for each case, and these have been drawn so that Δl (the separation at the centre of the pole-gap) is 30mm and hence the results are directly comparable.

The relations between $\left(\frac{1}{\Delta l}\right)^2$ and x (the distance from the centre of the gap measured along the axis) have been plotted from which it is clear that the optimum pole shape is given by case B). Figure 46.

A minimum pole gap of 5cms has been adopted in the final instrument, and as the furnace occupies much of the available space, water-cooled copper discs have been attached to the pole tips to keep them cool. (see Plate XX)

Figure 46.

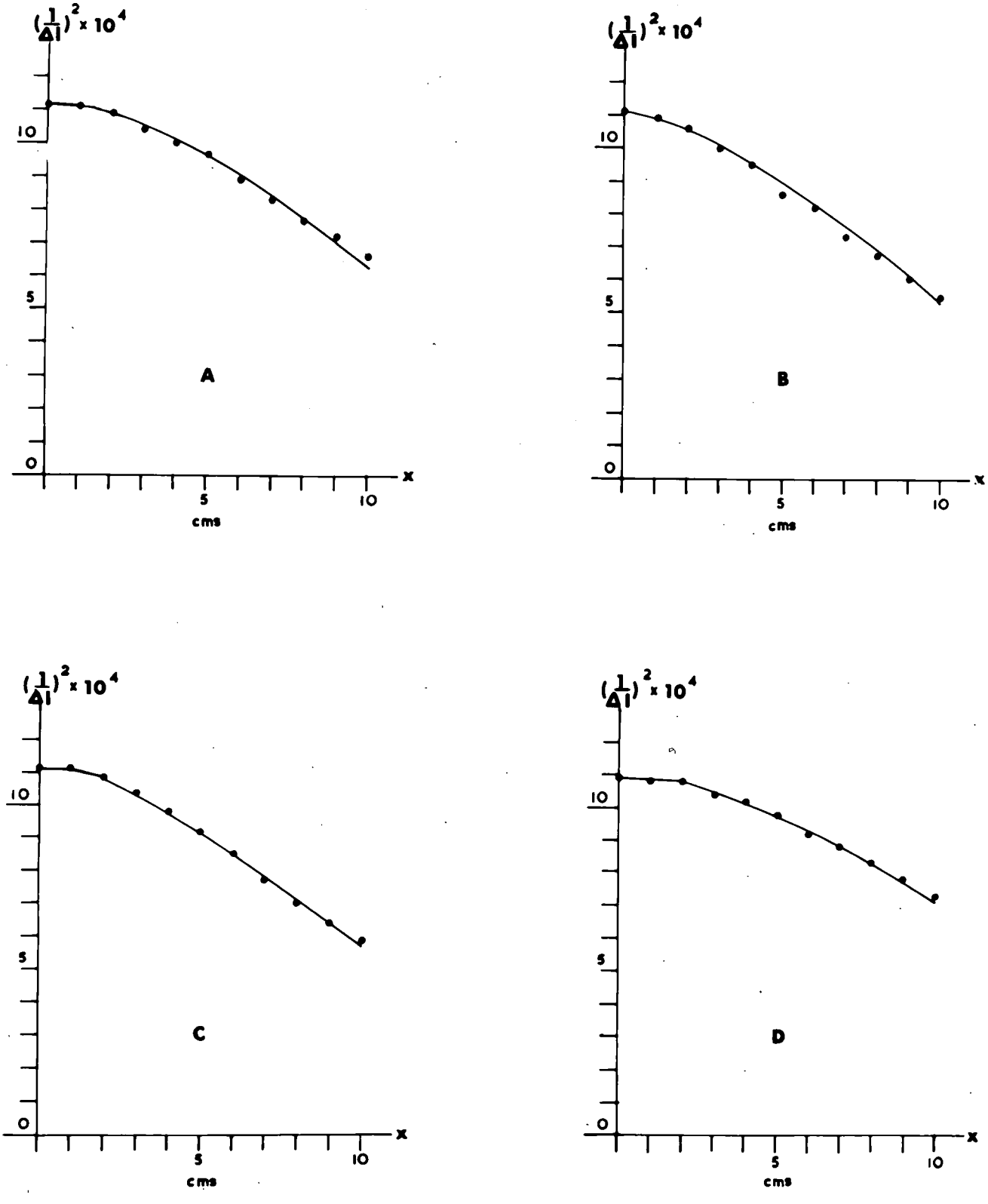
$(\frac{1}{\Delta l})^2 \times 10^4$
10
5
0
A
x
5
10
cms
$(\frac{1}{\Delta l})^2 \times 10^4$
10
5
0
B
x
5
10
cms
$(\frac{1}{\Delta l})^2 \times 10^4$
10
5
0
C
x
5
10
cms
$(\frac{1}{\Delta l})^2 \times 10^4$
10
5
0
D
x
5
10
cms

Figure 46.

Results of the analogue field mapping for different pole tip shapes expressed by plotting $(1/\Delta l)^2$ against x.

A) Faces parallel.

B) Faces diverging at 6°.

C) Faces diverging at 10°.

D) Faces diverging at 40°.

3) The Photo-electric Recording System

The deflection of the torsion beam is detected photo-electrically as follows. An aluminium flag, A, is fixed vertically to the torsion beam as shown in Figure 47. This flag is free to pass between an excitor lamp, L, located at the base of the suspension turret, and a pair of Mullard OCP71 photo-transistors, mounted as shown in Figure 48. A screen, Sc, placed directly in front of the transistors has two holes 1mm in diameter drilled through it which only allow light to fall on the sensitive areas of the individual transistors.

The transistor marked D in Figure 48 is used to detect movements of the torsion beam since the emitted current varies according to the position of the flag. The transistor marked, S in Figure 48 is constantly illuminated and its function is to compensate for any variations in emitted current that may occur if the temperature of the transistors changes. This is acheived by including the two transistors in opposition as part of the Wheatstone's bridge circuit shown in Figure 49, so that any changes in one transistor are cancelled out by equal and opposite changes in the other.

The output from the transistors is measured by a "Record" Graphic Recording Milliammeter reading from 0 to 5 mA or it may be switched to an ordinary milliammeter of the same range which is used during the preliminary stages of an analysis. The output from the transistors may be adjusted by means of a potentiometer which is located in a control unit.

This control unit houses the circuit for the photo-electric recording system, but for convenience the transistors have been separated from it and have to be plugged in before use. It is important that this plug be removed when the instrument is not in use so as to prolong the life of the battery.

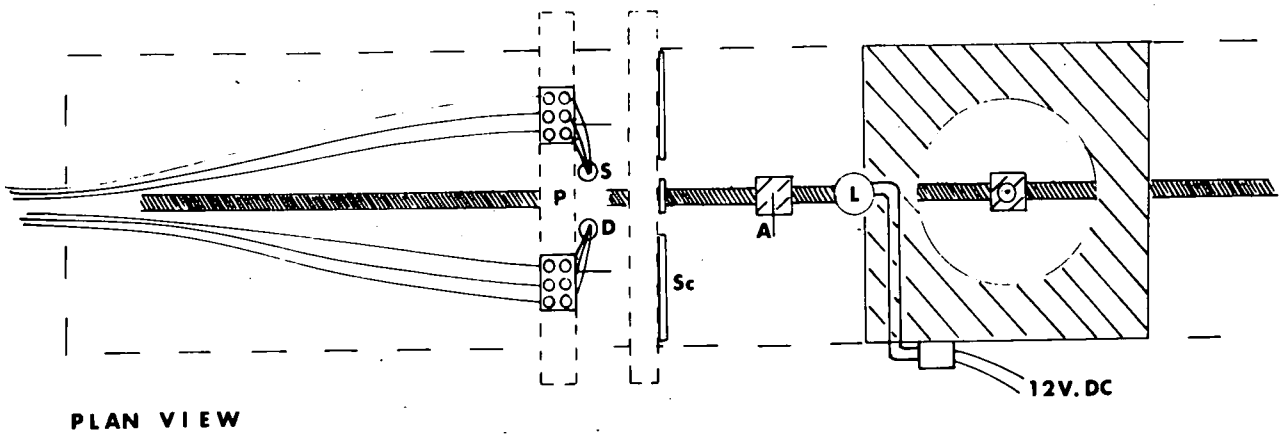

PLAN VIEW

Figure 47.

THE
PHOTOELECTRIC RECORDING SYSTEM

Figure 48.

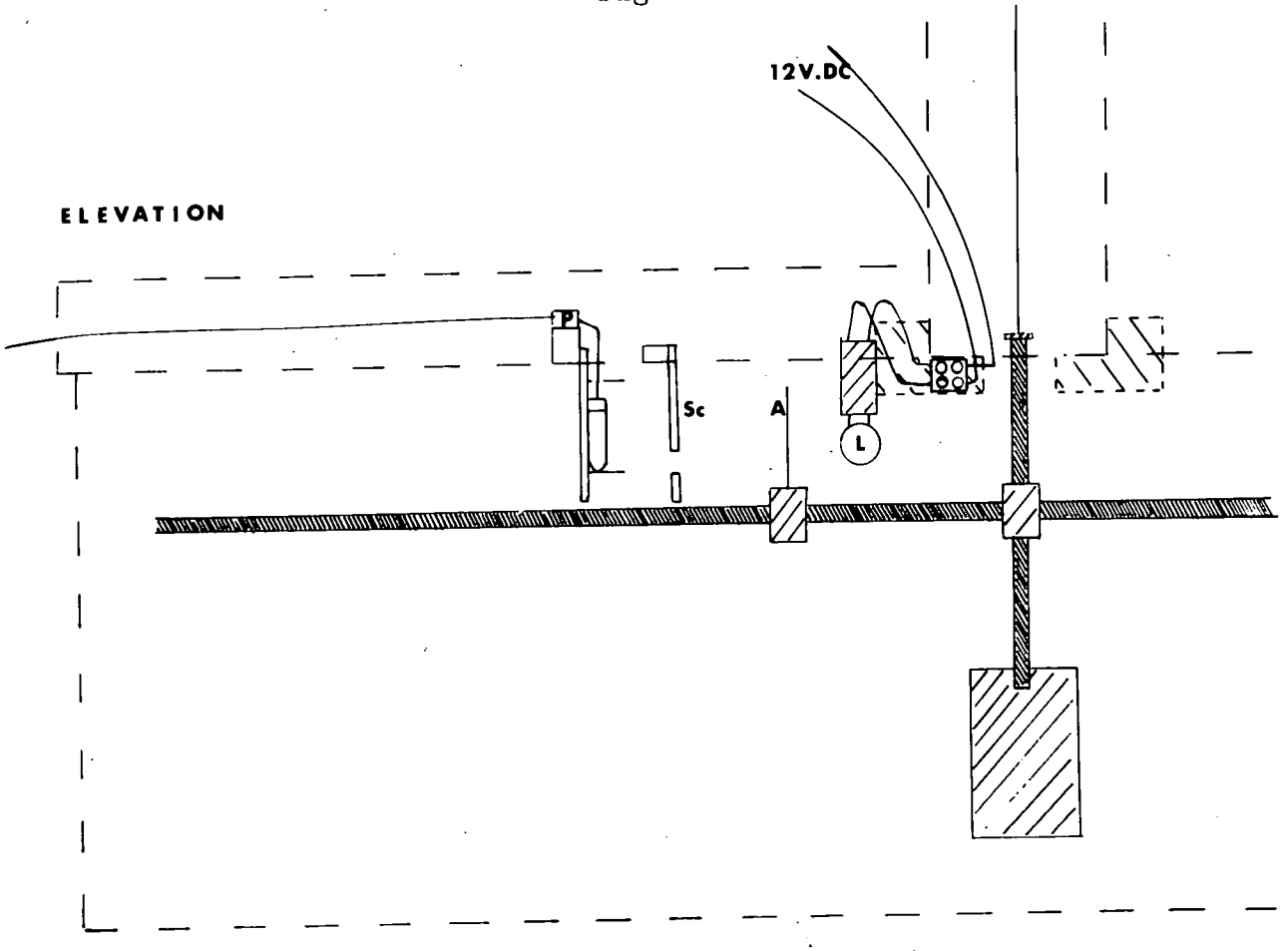

Figure 47.

Plan view of the photoelectric recording system;

Figure 48.

Elevation view of the photoelectric recording system.

Figure 49.

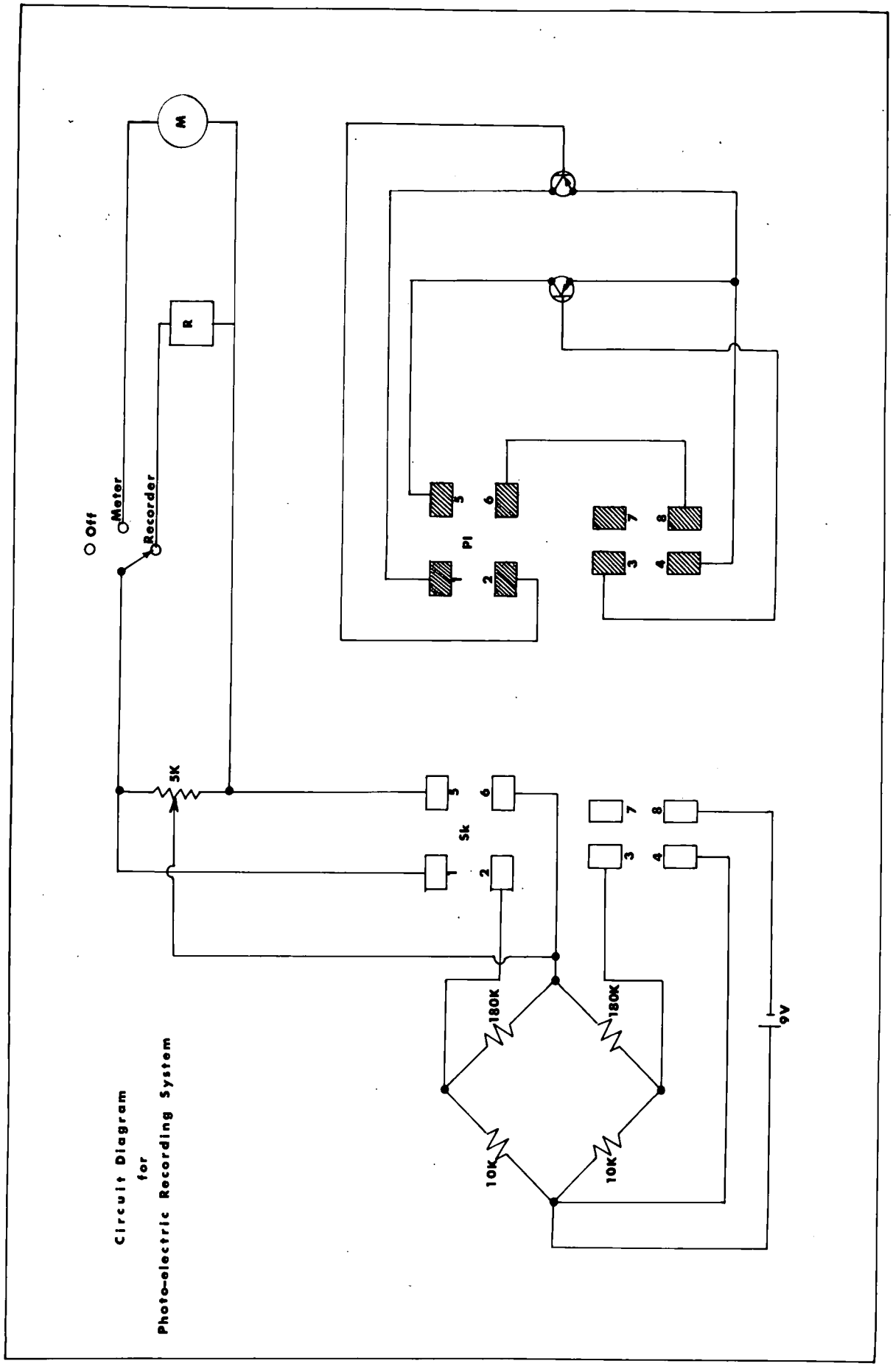
M
R
Off
Meter
Recorder
5K
5k
180K
180K
10K
10K
9V
P1
1
2
3
4
5
6
7
8
Circuit Diagram
for
Photo-electric Recording System

Figure 49.

Wheatstone's bridge circuit for the photoelectric recording system.

The battery may be replaced by removing the back cover of the control unit.

The transistor unit and the screen can be moved horizontally along the torsion beam housing and the aluminium flag can be moved along the torsion beam itself so that the sensitivity of the system can be varied over a wide range. This sensitivity increase as the transistor unit moves further away from the flag but is accompanied by a fall in the output of the transistors as the intensity of illumination decreases. However, the output can be increased by means of the potentiometer control so that to some extent this effect is compensated.

The preferred direction of mounting for a transistor is such that the incident light is perpendicular to the plane of the leads and on the side of the bulb bearing the type number.

The leads from the transistors pass through a polythene connector strip so that an individual transistor is easily replaced.

The excitor lamp is a 12V 6W car headlamp bulb and is located at the base of the suspension turret. It may be reached via the door in the torsion beam housing. The bulb operates from a 32V DC stabilized supply and an equivalent bulb and a 100 ohm potentiometer are included in series with it so that it does not burn out. The intensity of illumination may be varied within narrow limits by means of the potentiometer, and the second bulb, which is mounted above the Temperature Recording Unit, provides a useful indication of this intensity.

4) The Electric Furnace

The furnace consists of a thin walled silica tube onto which has been wound Eureka wire. The wire is held in position by alumina cement and thermal insulation has been provided largely by asbestos string (see Plate XX).

The silica tube is 80mm long, has an internal diameter of 10mm and a wall thickness of 0.9mm. A short length of narrower silica tubing, only 9mm in external diameter, has been fused into one end of the furnace tube (Figure 50). This acts as a collar and supports a length of twin-bore silica thermocouple tubing such that it lies on the axis of the furnace. This tubing carries a chromel-alumel thermocouple and supports the thermocouple head at a point 2.5cms from the back of the furnace. This point has been found to be the hottest part of the furnace.

The heating element consists of a single winding of SWG20 Eureka wire. It has a resistance of 3.5 ohms and a current of 5 amps is sufficient to maintain the furnace temperature at about 700°C. The wire has been wound directly onto the silica and is held in position by alumina cement. This is a refractory cement and after application it has been dried out at 1000°C. A layer of asbestos paper coated with alumina cement covers the windings, but most of the thermal insulation has been provided by winding on thin asbestos string. The final diameter of the furnace is approximately 30mm.

Internally, the furnace has been lined with a tube of brass 50mm long, 10mm in external diameter and having a wall thickness of 1mm. This promotes a more uniform distribution of heat through the furnace and this has been further improved by adding an inner lining of silver foil 0.12mm thick. The actual temperature gradient within the furnace has been investigated and the results are described later in this section.

Figure 50.

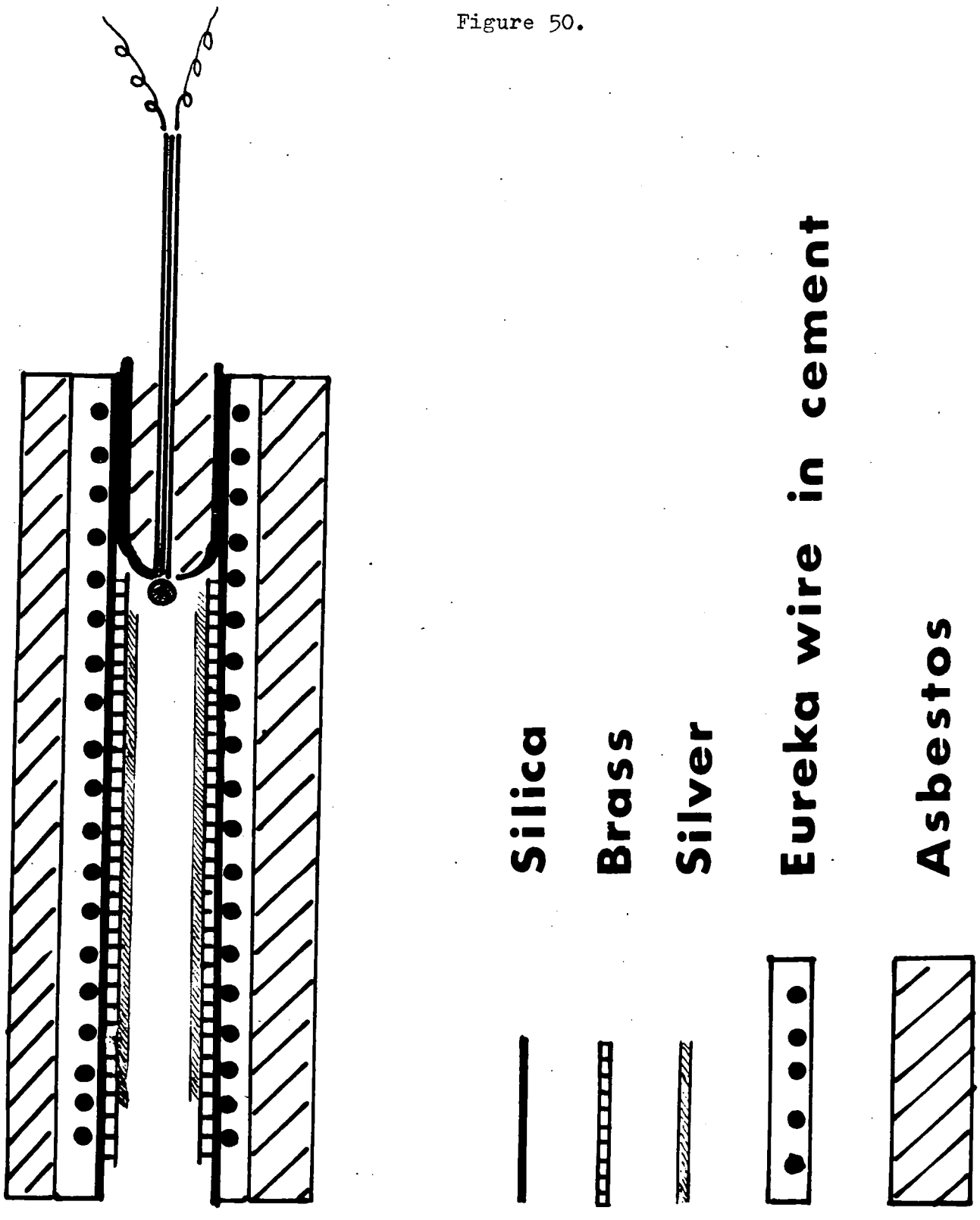

Figure 50.
Diagram of the furnace.

The thermocouple has been calibrated in position within the furnace by comparison with a mercury thermometer:-

A 360°C thermometer was inserted horizontally along the furnace until the bulb touched the back. It was then eased slightly from this position so as to remain close to the head of the thermocouple but not in contact with the silica. The thermocouple was connected to a potentiometer and the furnace heated, by passing a constant current. When the potentiometer readings became constant the thermometer temperature was taken. Readings have been taken at three temperatures. The thermometer has been read to $\pm \frac{1}{2}^{\circ}$ C and the thermoelectric emf is accurate to ±0.003mV.

The results are summarized in Table 25 and are shown graphically in Figure 57. The values of temperature v emf obtained from this straight line relationship agreed closely with those given in international tables of physical constants and hence it is concluded that such tabulated values may be taken safely as a measure of the temperature when using this thermocouple.

The thermocouple, however, occupies a fixed position in the furnace whereas the sample on the torsion beam is free to move over a distance of about 10mm along the axis of the furnace. Therefore, in order that the thermocouple should measure the temperature of the sample it is necessary that the furnace temperature should remain constant within this distance of the thermocouple head.

The temperature gradient within the furnace has been investigated as follows:-

A chromel-alumel thermocouple supported by a length of twin-bore silica tubing, was inserted horizontally along the axis of the furnace until it touched the back. It was then eased slightly from this position so as to

Table 25.

Thermocouple Calibration Data

Temperature °C	Thermoelectric voltage mV
66.5	2.550
66.5	2.545
66.5	2.545
167.0	6.910
167.0	6.910
167.0	6.910
293.0	12.150
293.0	12.155
293.0	12.155

Figure 51.

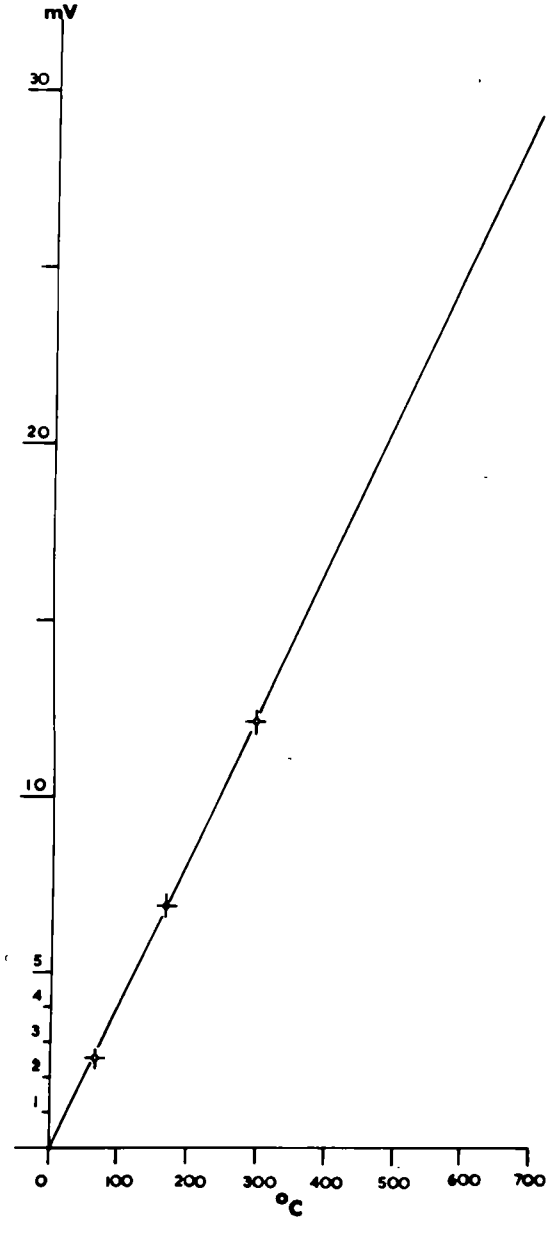

Figure 52.

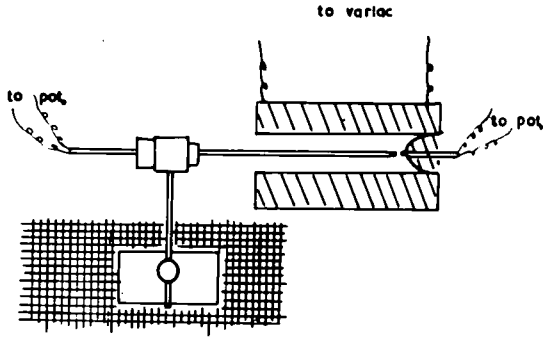

Figure 51.

Calibration curve for the thermocouple.

Figure 52.

Experimental arrangement for measuring the thermal gradients in the furnace.

remain close to the thermocouple head but not touching the silica. The twin-bore tube extended beyond the mouth of the furnace (Figure 52) and passed through a rubber bung held in a clamp. The clamp stand rested on a sheet of centimeter graph paper which acted as a graduated surface so that the thermocouple could be moved in and out of the furnace by measurable amounts.

The leads from both thermocouples were taken to two separate circuits of a potentiometer by means of which it was possible to measure the emf's separately and rapidly. The furnace was heated by passing a constant current. When the furnace thermocouple gave a constant reading the furnace temperature was steady. This reading was noted and compared with the reading of the exploring thermocouple. The exploring thermocouple was then withdrawn from the furnace in steps of 2mm intervals and at each position the two emf's compared. The reading of the furnace thermocouple was always taken first to allow the exploring thermocouple to adjust to any change in temperature.

Measurements were taken up to a distance of 18mm from the furnace thermocouple and then the process repeated whilst bringing the exploring thermocouple back into the furnace, until it was back to its initial position. In this way average readings were obtained for each position. Measurements were not made at more than 18 mm from the furnace thermocouple since the temperature gradient was by then appreciable.

Measurements have been made at three furnace temperatures:

192°C, 395°C and 647°C and the results are summarized in Tables 26, 27 and 28. In the fourth column of these tables the differences in voltage have been calculated and in the fifth column these values have been converted to differences in temperature. In the sixth columnthe mean temperature

Table 26.

Temperature Variation in the Furnace

Furnace temperature approx. 192°C (7.84mV).

Position of eT/C mm	Thermocouple Readings fT/C mV	eT/C	ΔE mV	ΔT °C	$\overline{\Delta T}$ °C
0	7.80	7.82	+0.02	+0.50	+0.25
2	7.85	7.82	-0.03	-0.75	-0.62
4	7.88	7.83	-0.05	-1.25	-0.87
6	7.88	7.82	-0.06	-1.50	-1.00
8	7.90	7.81	-0.09	-2.25	-1.37
10	7.90	7.82	-0.08	-2.00	-1.37
12	7.90	7.81	-0.09	-2.25	-1.87
14	7.89	7.79	-0.10	-2.50	-2.25
16	7.88	7.79	-0.09	-2.25	-2.62
18	7.88	7.75	-0.13	-3.25	-3.25
16	7.86	7.74	-0.12	-3.00	
14	7.84	7.76	-0.08	-2.00	
12	7.83	7.77	-0.06	-1.50	
10	7.82	7.79	-0.03	-0.75	
8	7.81	7.79	-0.02	-0.50	
6	7.81	7.79	-0.02	-0.50	
4	7.81	7.79	-0.02	-0.50	
2	7.81	7.79	-0.02	-0.50	
0	7.80	7.80	0.00	0.00	

Table 27.

Temperature Variation in the Furnace

Furnace temperature approx. 395°C (16.30mV).

Position of eT/C	Thermocouple Readings fT/C	eT/C	ΔE	Δ T	$\Delta \overline{T}$
mm	mV		mV	°C	°C
0	16.45	16.40	-0.05	-1.25	-1.50
2	16.45	16.40	-0.05	-1.25	-1.50
4	16.44	16.38	-0.06	-1.50	-1.62
6	16.44*	16.30*	-0.14	-3.50	-2.37
8	16.44*	16.29*	-0.15	-3.75	-2.25
10	16.41*	16.30*	-0.11	-2.75	-2.75
12	16.39*	16.25*	-0.14	-3.50	-2.00
14	16.36*	16.16*	-0.20	-5.00	-2.50
16	16.33*	16.10*	-0.23	-5.75	-3.37
18	16.34	16.28	-0.06	-1.50	
16	16.34	16.30	-0.04	-1.00	
14	16.34	16.34	-0.00	-0.00	
12	16.35	16.33	-0.02	-0.50	
10	16.32	16.32	-0.00	-0.00	
8	16.30	16.27	-0.03	-0.75	
6	16.25	16.20	-0.05	-1.25	
4	16.20	16.13	-0.07	-1.75	
2	16.16	16.09	-0.07	-1.75	
0	16.16	16.09	-0.07	-1.75	

* NB. The ice at the thermocouple cold junction melted at some time during these measurements and had to be replenished.

Table 28.

Temperature Variation in the Furnace

Furnace temperature approx. 647°C (26.81mV).

Position of eT/C mm	Thermocouple Readings fT/C mV	eT/C mV	ΔE mV	ΔT °C	$\overline{\Delta T}$ °C
0	26.87	26.90	+0.03	+0.75	-0.75
2	26.92	26.92	0.00	0.00	-0.87
4	26.94	26.95	+0.01	+0.25	-1.12
6	26.94	26.89	-0.05	-1.25	-1.25
8	26.92	26.86	-0.06	-1.50	-1.87
10	26.93	26.82	-0.11	-2.75	-2.62
12	26.90	26.77	-0.13	-3.25	-3.25
14	26.90	26.70	-0.20	-5.00	-5.62
16	26.88	26.68	-0.20	-5.00	-6.25
18	26.87	26.59	-0.28	-7.00	-7.00
16	26.84	26.54	-0.30	-7.50	
14	26.81	26.56	-0.25	-6.25	
12	-	-	-	-	-
10	26.80	26.70	-0.10	-2.50	
8	26.83	26.74	-0.09	-2.25	
6	26.80	26.75	-0.05	-1.25	
4	26.81	26.71	-0.10	-2.50	
2	26.77	26.70	-0.07	-1.75	
0	26.75	26.66	-0.09	-2.25	

differences have been calculated and these values are shown graphically in Figure 53.

Figure 53 shows that no appreciable temperature gradient exists along the axis of the furnace for a distance of about 10mm at these temperatures. However, the results also appear to indicate that the furnace temperature, as measured by the exploring thermocouple (eT/C) is lower than that indicated by the furnace thermocouple (fT/C). But these results have been obtained by measuring the thermoelectric emf's of the two thermocouples and converting these to temperatures. These conversions have been made on the assumption that 0.04mV corresponds to 1°C which is correct for the furnace thermocouple, which has been calibrated, but which may not be correct for the exploring thermocouple which has not been calibrated. Thus the apparent lower temperature within the furnace is probably an expression of the fact that at the same temperature the emf of the exploring thermocouple is less than that of the furnace thermocouple. If, therefore, it is assumed that when the exploring thermocouple is at 0mm it is at the same temperature as the furnace thermocouple, then corrections may be applied to the curves shown in Figure 53 so that $\Delta\overline{T}$ is zero at 0mm.

These new curves are shown in Figure 54 and it can be seen that the temperature of a sample moving in the region 0 to 10mm can be measured to within 2°C at a furnace temperature well beyond that of the Curie point of magnetite (585°C) and approaching that of the Curie point of hematite (675°C). Thus for most of the analyses involving titaniferous magnetites the sample temperature may be expected to be accurate to within 1°C whilst for analyses involving titaniferous hematites with Curie points higher than about 600°C an accuracy of about 2°C is more reasonable.

The current to the furnace is controlled by a motor driven variac.

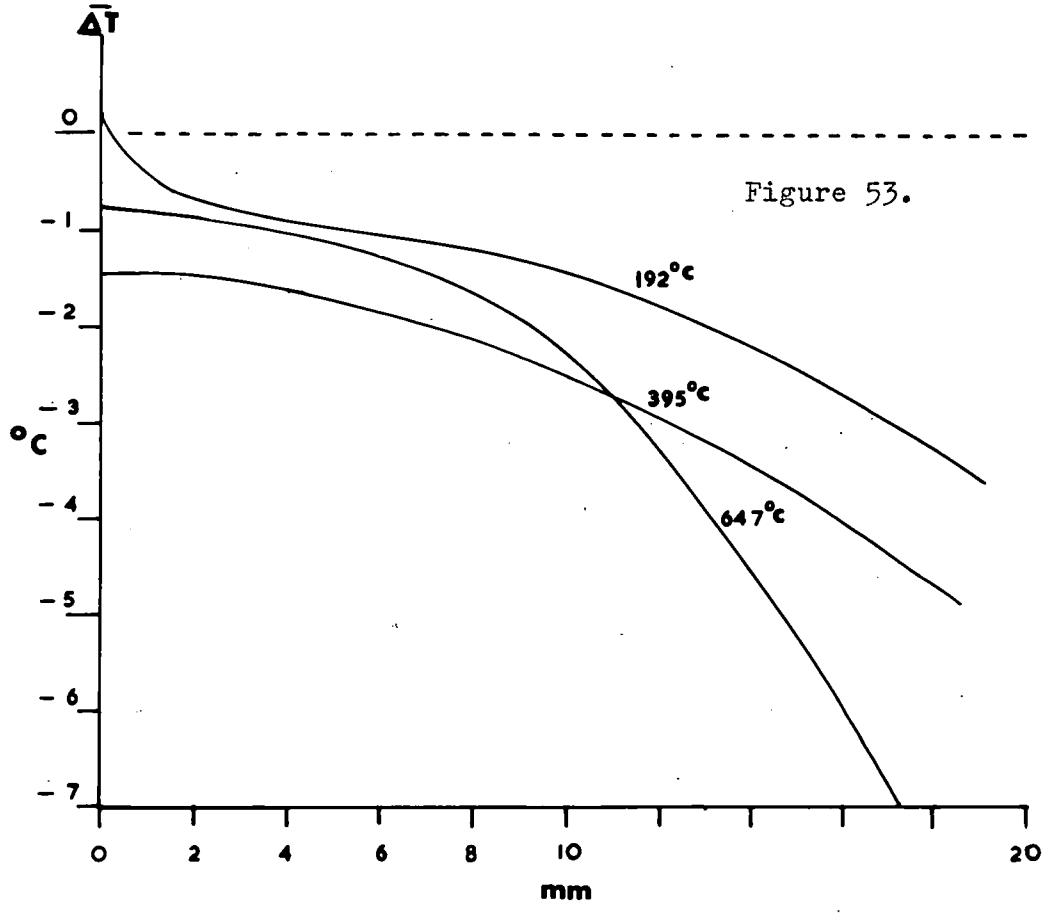

Figure 53.

Position of eT/c

mm

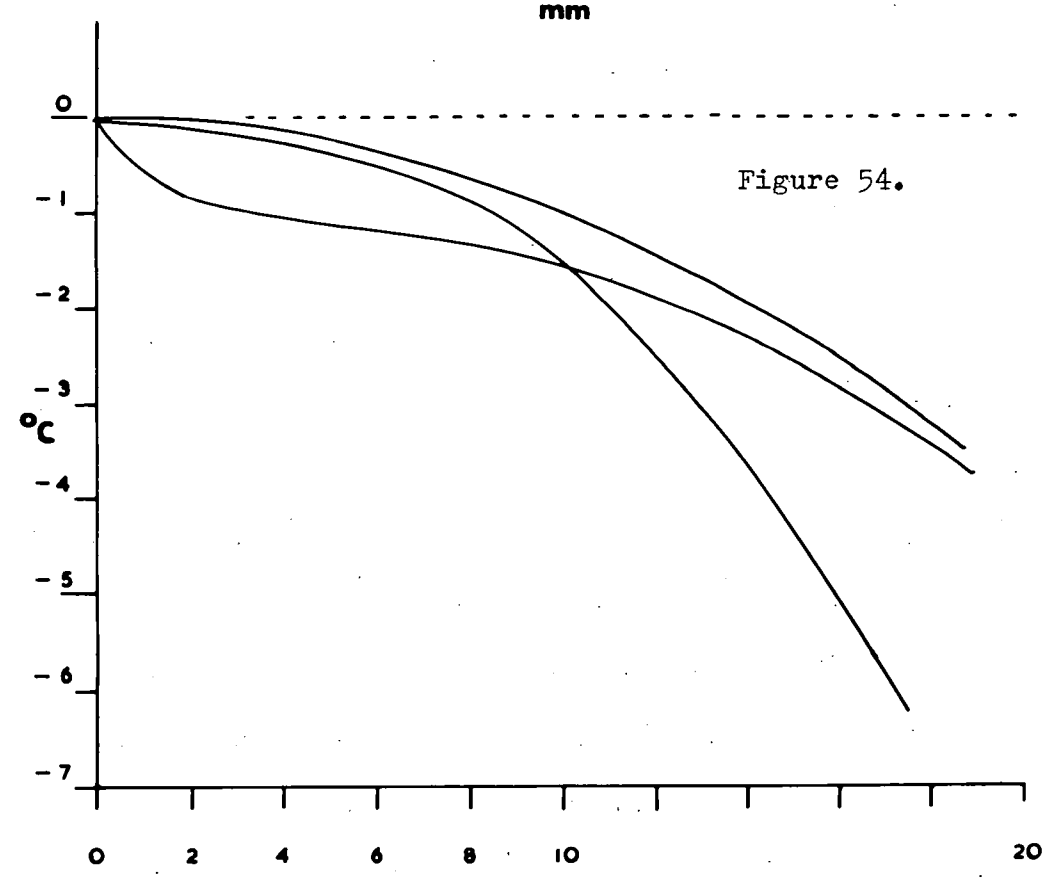

Figure 54.

Figure 53.
Thermal gradients in the furnace at different operating temperatures - uncorrected.

Figure 54
Thermal gradients in the furnace at different operating temperatures - corrected to allow for the different readings of the two thermocouples at the same temperature.

The motor completes one revolution in 57 minutes and via a 2:1 gear ratio drives the variac control at half this speed. Limit switches are provided externally at the maximum and minimum settings and are adjustable. They function only to switch off the motor drive at each end of its run and do not turn off the current to the furnace. A reversing switch is provided so that both heating and cooling cycles may be controlled. AC current is employed as this is non-inducting.

A heating and cooling rate of about 15°C per. min. has been adopted and a complete cycle is shown in Figure 55 drawn from the data summarized in Table 29. This rate of change of temperature is preferred because it limits the duration of a complete analysis to about 2 hrs. In this way the sample is not kept at elevated temperatures for a long time as this might cause changes of composition when analysing solid-solution minerals.

The furnace is supported in the pole-gap of the electromagnet on a sliding support constructed of dural and its position can be adjusted horizontally along the x-axis of the magnet.

Table 29.

Data for a Complete Heating/Cooling Cycle of the Furnace

Time mins	mV	Temp °C	Time mins	mV	Temp °C	Time mins	mV	Temp °C
0	0.81	20.25	42	30.68	736.75	84	8.53	207.5
1	1.40	35.0	43	31.00	744.5	85	7.84	192.75
2	2.10	52.0	44	31.08	746.5	86	7.32	179.75
3	2.74	67.5	45	31.06	746.0	87	6.82	167.25
4	3.30	81.0	46	30.96	743.5	88	6.36	155.75
5	3.88	94.75	47	30.78	739.25	89	5.94	145.25
6	4.54	110.75	48	30.56	734.0	90	5.55	135.5
7	5.19	126.5	49	30.28	727.25	91	5.19	126.5
8	5.83	142.5	50	29.94	719.25	92	4.85	118.25
9	6.48	158.75	51	29.48	708.25	93	4.55	111.0
10	7.11	174.5	52	29.05	698.0	94	4.26	104.0
11	7.80	191.75	53	28.56	686.25	95	4.00	97.75
12	8.49	208.75	54	28.06	674.5	96	3.76	92.0
13	9.20	226.5	55	27.54	662.0	97	3.55	86.75
14	9.96	245.25	56	27.10	651.5	98	3.35	82.0
15	10.64	261.75	57	26.63	640.5	99	3.16	77.5
16	11.36	279.5	58	25.85	622.0	100	2.99	73.5
17	12.04	295.75	59	25.23	607.5	101	2.84	69.75
18	12.75	313.0	60	24.60	592.75	102	2.69	66.25
19	13.46	330.0	61	23.96	577.75	103	2.56	63.0
20	14.20	347.75	62	23.42	565.0	104	2.45	60.5
21	14.94	365.5	63	22.84	551.5	105	2.34	57.75
22	15.70	383.5	64	22.22	537.0	106	2.23	55.0
23	16.45	401.25	65	21.65	523.5	107	2.12	52.5
24	17.21	419.25	66	21.03	509.0	108	2.03	50.25
25	18.00	437.75	67	missed		109	1.94	48.0
26	18.78	456.25	68	19.86	481.5	110	1.86	46.25
27	19.61	475.75	69	19.22	466.5	111	1.80	44.75
28	20.40	494.25	70	18.60	452.0	112	1.71	42.5
29	21.17	512.25	71	17.98	437.5	113	1.64	40.75
30	21.96	530.75	72	17.35	422.5	114	1.58	39.25
31	22.74	549.25	73	16.72	407.5	115	1.51	37.5
32	23.52	567.5	74	16.12	393.5	116	1.42	35.5
33	24.32	586.25	75	15.50	378.75	117	1.39	34.75
34	25.14	605.5	76	14.90	364.5	118	1.35	33.75
35	25.94	624.25	77	14.33	350.75	119	1.30	32.5
36	26.74	643.0	motor stopped switched off variac.					
37	27.29	656.25						
motor stopped			78	13.44	329.5			
38	28.40	682.5	79	12.31	302.25			
39	29.12	699.5	80	11.36	279.5			
40	29.70	713.5	81	10.53	259.25			
reversed motor			82	9.78	240.75			
41	30.20	725.5	83	9.09	223.75			

Figure 55.

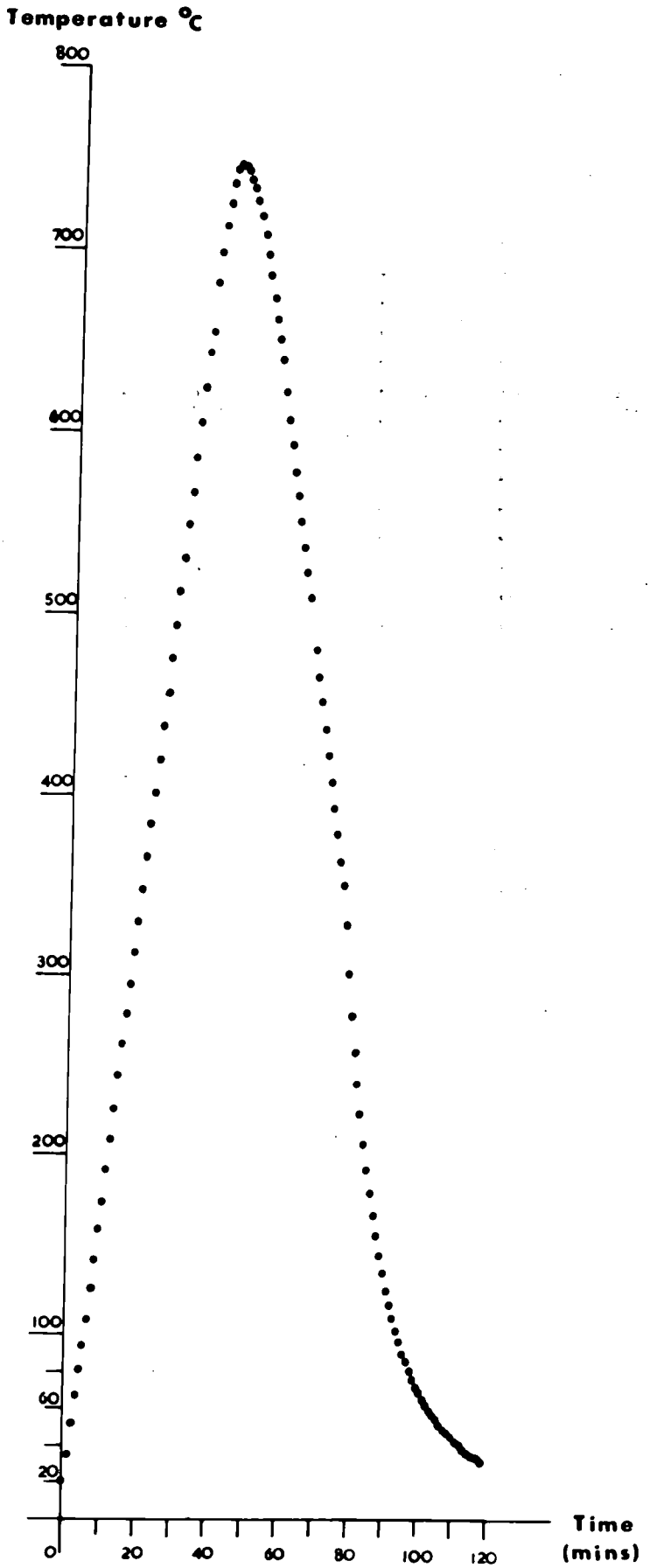
Temperature °C
800
700
600
500
400
300
200
100
60
20
0
20
40
60
80
100
120
Time
(mins)

Figure 55.

Complete heating-cooling cycle of the furnace.

5) The Temperature Recording System

The temperature recording system functions in such a way that a marker-pen, operating on a $\frac{1}{4}$" strip at the side of the recorder chart, is made to indicate successive changes in the furnace temperature of about 15°C, during both the heating and cooling cycles. The system has been calibrated so that each successive mark corresponds to an accurately known temperature.

Figure 56 illustrates the principle on which the system works. At a temperature of about 700°C a chromel-alumel thermocouple generates a thermo-electric emf of about 29mV, and changes in temperature of about 15°C result in changes in the emf of about 0.6mV; therefore, in order to record the changes in furnace temperature at intervals of about 15°C as it is heated from room temperature to about 700°C it is necessary to measure the thermo-electric emf as it increases by increments of about 0.6mV. This is done by applying a voltage of, say 1.2mV, to the galvanometer G thus causing a deflection of the instrument. The thermocouple is connected to the same galvanometer but in opposition to the applied voltage so that as the temperature rises a backing-off emf appears which reduces the deflection of the galvanometer so that there will be zero deflection when the thermoelectric emf reaches 1.2mV. At this point the galvanometer operates a photoelectric system which automatically operates the marker-pen on the recorder and at the same time increase the applied voltage to the galvanometer by a further 0.6mV so that the process starts again.

A step, or ratchet, relay is used to increase the applied voltage by the required increments. It functions so that each time the galvanometer G reads zero, a contact K is automatically stepped on one unit along a chain

Figure 56.

Principle
of the
Temperature Recording System

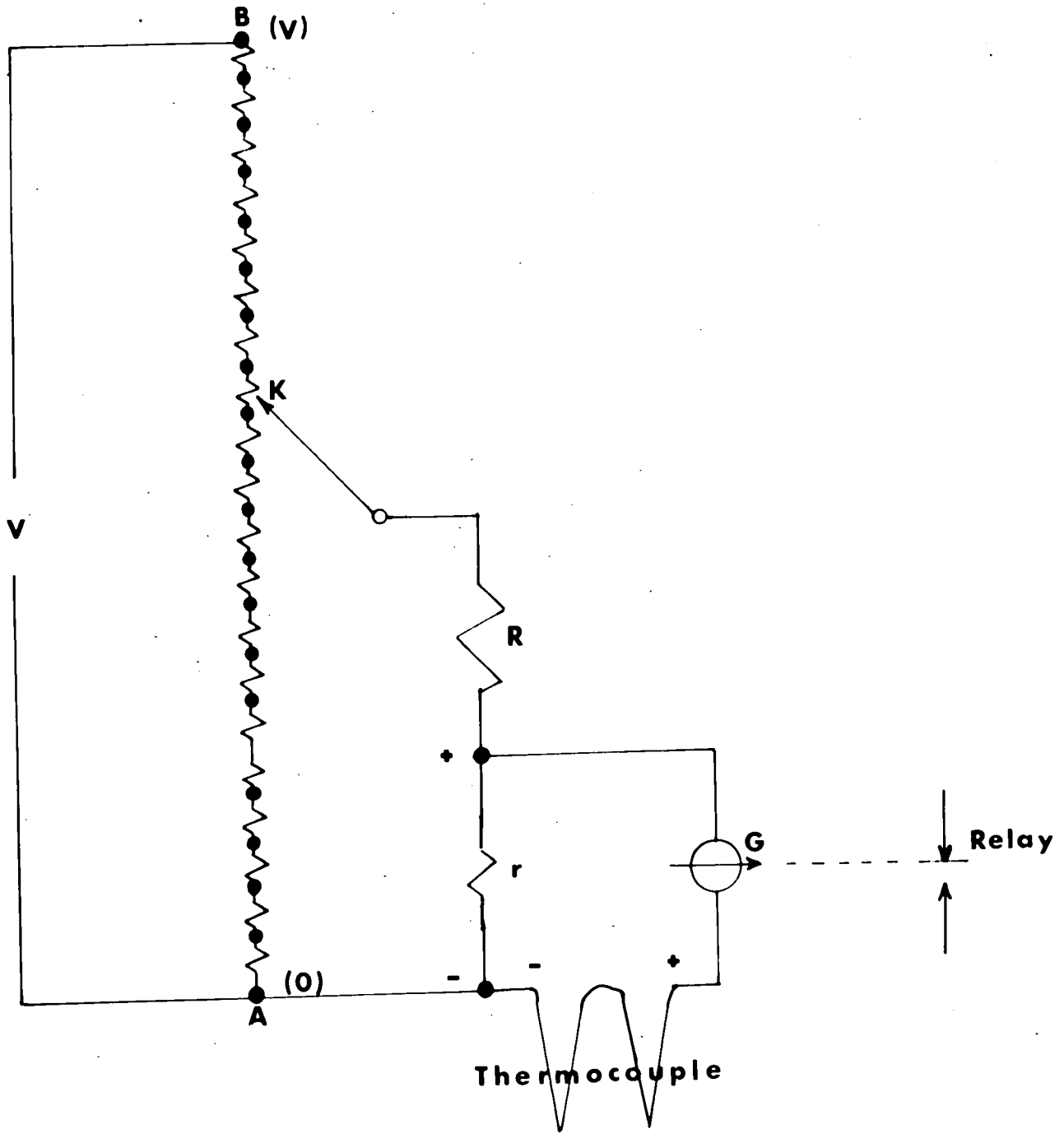

Figure 56.

Principle of the temperature recording system.

of resistors, A-B. By choosing the right value of the voltage V applied to the chain and the right value for the individual resistors, it is possible to arrange that the voltage to the galvanometer increases by the required increments of 0.6mV. However, contact potentials may be a source of serious error if the voltage is increased by such small amounts directly, and therefore it is arranged that the resistors in the chain and the voltage applied to the chain are such as to give comparatively large changes for each step and this is then divided to reduce it to the required voltage at the galvanometer connections. For example, with a chain of fifty 10 ohms resistors and a voltage of 50V, the voltage drop across each resistor would be 1V, and then this would have to be divided by about 1000 before reaching the galvanometer.

The full details of the system are shown in Figure 57. The resistence chain is formed of 47 high stability 10 ohm resistors and a further three 10 ohm resistors are included in series with the chain so that when the wiper is at the beginning of the chain the resistance is 40 ohms and not 10 ohms. This means that the wiper cannot step on to the next resistor until the thermocouple has reached a temperature of about 45°C, ie, well above room temperature. A stabilized voltage of 32V DC is applied to the chain and this, together with the potential divider shown, gives a voltage range from about 2mV to 29mV rising by increments of about 0.6mV.

The galvanometer is part of an Ether Transitrol Controller Type 990. This instrument includes a built-in photoelectric system which is used to operate the marker-pen and the step-relay. An arbitrary zero position is set by a red pointer on the instrument scale and the instrument has been supplied without the normal cold-junction compensation so that this zero remains steady. (NB. The cold-junction compensation unit is a bimetallic strip which, in the standard instrument, controls the position of the red

Figure 57.

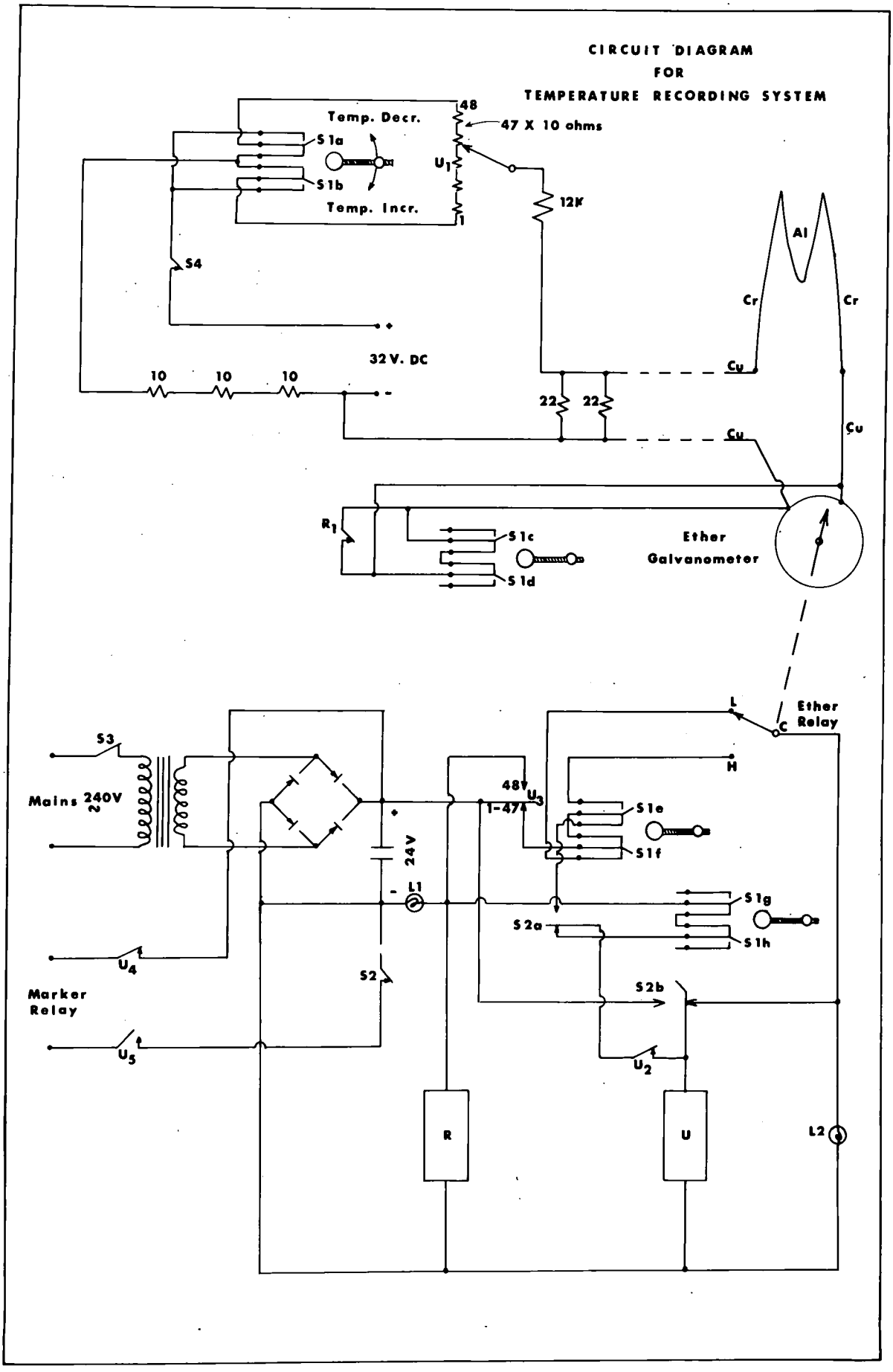
CIRCUIT DIAGRAM
FOR
TEMPERATURE RECORDING SYSTEM
Temp. Decr.
S 1a
S 1b
Temp. Incr.
48
47 X 10 ohms
U1
12K
S4
32 V. DC
10
10
10
22
22
Al
Cr
Cr
Cu
Cu
Cu
R1
S 1c
S 1d
Ether
Galvanometer
L
C
Ether
Relay
H
S3
Mains 240V
48V
U3
1-47K
S 1e
S 1f
24V
L1
S 1g
S 2a
S 1h
U4
S2
S2b
Marker
Relay
U5
U2
R
U
L2

Figure 57.

Circuit diagram for the temperature recording system.

pointer so that it moves according to the ambient room temperature).

The step-relay is basically a rotary switch and the wiper moves in one direction only. Therefore, when recording a cooling cycle, provision has to be made to reverse the polarity of the resistor chain and also to reverse the connections to the relay in the Ether Controller. The necessary switches are shown in Figure 57. The circuit also includes warning pilot lights, L_1 to indicate the end of the sequence and L_2 to indicate a failure in the system. The galvanometer is protected by shorting out at the end of the sequence and this also occurs in case of failure.

The basic components of the system are as follows:-

S1... Muirhead key switch: four double banks of c.o contacts.

Function:- Temperature Increasing
Off
Temperature Decreasing

S2... Post office key switch: biassed from both sides.

Function:- Step-on
Operate
Reset to start

S3... 24V supply On/Off

S4... 32V supply On/Off

L1... Red pilot light

Function:- Indicates end of travel of the wiper.

L2... Red pilot light

Function:- Indicates that the Ether relay has stuck.

R.... Ether relay

U.... Step-relay

The circuit is built on an aluminium chassis and the step-relay is mounted so that the position of the wiper can be seen on a dial set into the front panel. This dial carries 48 radial lines corresponding to the

48 contacts of the rotary-switch part of the relay. An arrow indicates the first step of the chain and every twelth step is indicated in red.

The system is operated as follows:-

1) Switch on the Ether Controller at the mains thus bringing the photoelectric system into operation. Switch on the 24V supply (S3) and the 32V supply (S4).

2) Depress S2 and hold down until the wiper has moved round to the end of its travel. L1 then lights up.

3) Set S1 to "Temperature Increasing". The wiper steps onto the first step and L1 goes out. The galvanometer deflects to the left of the set zero.

4) Switch on the furnace.

5) The first step occurs at about 45°C and this completes an external marker circuit through U/4, U/5 and S2. At every 12th step U/4 is opened mechanically by a cam on the step-relay and therefore no mark is made. In this way successive groups can be readily identified on the chart.

6) When the wiper reaches the end of its travel U/3 operates and shorts out the galvanometer via R/1. This prevents further steps (which would jump back to the starting position) by removing the 24V supply from S1f. L1 then lights up to show that the sequence is completed.

7) Reset S1 to Off. U then receives an extra pulse via S1g, S1h, S2a and U/3(48) which resets to the start position. U/3 is thus reset and the cycle can recommence.

8) Now set S1 to "Temperature Decreasing". This reverses the polarity of the chain U/1 and exchanges the connections to the Ether relay. U then steps when the furnace temperature is too cold, and the

backing-off emf is gradually reduced. When room temperature is reached, U/3 operates as before L1 lights up and the galvanometer is shorted out via R/1.

9) If it is desired to start from any position other than the first step, U can be stepped on one division at a time by successively lifting S2.

10) NB. If at any time the Ether relay fails to operate, a warning light L2 lights up. However, this light always appears momentarily during each step of U and in this case it does not indicate a fault.

The thermocouple is not connected directly to the galvanometer. Instead, the chromel leads are soldered to copper leads which are then taken to the galvanometer. In this way the two chromel-copper junctions can be immersed in melting ice and thus they have no effect on the thermoelectric emf of the chromel-alumel thermocouple.

The system has been calibrated by measuring the applied voltage after each step of the cycle using a potentiometer, and this data is given in Table 30. The thermocouple was not, of course, in the circuit during these measurements.

Table 30.

Calibration Data - Temperature Recording System

	Step Number	Temp.Inc. mV	Temp.Inc. °C	Temp.Dec. mV	Temp.Dec. °C	
	1	1.76	43.75	29.46	707.75	
	2	2.35	58.0	28.85	693.75	
	3	2.94	72.25	28.245	678.75	
	4	3.505	85.75	27.64	664.5	
	5	4.095	99.75	27.03	650.0	
	6	4.68	114.0	26.41	635.25	
	7	5.26	128.25	25.80	620.75	
	8	5.85	143.0	25.20	606.75	
	9	6.44	157.75	24.60	592.75	
	10	7.01	172.0	23.995	578.5	
absent	11	7.60	186.75	23.39	564.25	absent
	12	8.19	201.5	22.80	550.5	
	13	8.76	215.5	22.21	536.75	
	14	9.34	230.0	21.62	522.75	
	15	9.92	244.25	21.04	509.25	
	16	10.50	258.5	20.445	495.25	
	17	11.09	272.75	19.85	481.25	
	18	11.66	286.75	19.26	467.5	
	19	12.24	300.75	18.675	453.75	
	20	12.80	314.25	18.095	440.0	
	21	13.38	328.25	17.51	426.25	
	22	13.96	342.0	16.92	412.25	
absent	23	14.55	356.0	16.34	398.75	absent
	24	15.14	370.25	15.75	384.75	
	25	15.71	383.75	15.155	370.5	
	26	16.30	397.75	14.57	356.5	
	27	16.90	411.75	13.99	342.75	
	28	17.49	425.75	13.40	328.5	
	29	18.06	439.25	12.84	315.25	
	30	18.65	453.25	12.25	301.0	
	31	19.245	467.0	11.68	287.25	
	32	19.83	480.75	11.10	273.0	
	33	20.425	494.75	10.51	258.75	
	34	21.02	508.75	9.94	244.75	
absent	35	21.60	522.5	9.35	230.25	absent
	36	22.20	536.5	8.77	215.75	
	37	22.79	550.25	8.19	201.5	
	38	23.39	564.25	7.605	186.75	
	39	23.99	578.5	7.02	172.25	
	40	24.59	592.5	6.44	157.75	
	41	25.19	606.5	5.85	143.0	
	42	25.80	620.75	5.26	128.25	
	43	26.40	635.0	4.68	114.0	
	44	27.01	649.5	4.095	99.75	
	45	27.64	664.5	3.505	85.75	
	46	28.245	678.75	2.94	72.5	
	47	28.85	693.75	2.35	58.0	

Applied voltage - 32V. Pot.div. - one 12K and two 22 ohms in parallel.

Operating Instructions

1) Preparation of the Instrument

Ensure:-

That the base board is level.

That the suspension turret is vertical and that the torsion beam is free to rotate.

That the torsion beam is horizontal and that it is correctly aligned in relation to the furnace tube so as to be free to move inside it.

Adjust:-

The level of the damping fluid until the torsion beam has a period of oscillation of about 10 seconds.

Ensure:-

That the aluminium flag is vertical and free to move between the excitor lamp and the transistors.

That the excitor lamp is at its optimum height so that the transistors receive maximum illumination.

Set:-

The arbitray zero on the Ether galvanometer so that the Ether relay is just on the point of operating when the galvanometer pointer moves to the right.

Ensure:-

That the stabilized voltage is 32V.

That the marker-pen and the recorder-pen are coincident on the chart and that the chart speed is 6" per hour.

Check:-

The ink supplies to both pens and inspect the supply to the marker

pen daily.

Ensure:-

That the initial furnace current is about 1.8 amps.

2) Preparation of the Sample

Powdered samples should be fine-grained but need not be especially pure since the magnetic analysis does not take into account the paramagnetic and diamagnetic constituents. Alternatively rock fragments about 2-3mm in size may be analysed provided they contain sufficient ferromagnetic material to be attracted by the magnet.

Powders should be introduced into small silica sample tubes and compressed so as to occupy about 1-2mm of the available space, using a fine glass rod. The sample tubes may be prepared from fine silica tubing (1mm diameter), by fusion in an oxygen-gas flame, and should be about 5mm long.

3) Starting the Analysis

Remove the covers on the instrument housing to reveal the torsion beam and the photoelectric unit.

Slide the furnace back into the pole gap so as to expose the silver holder for the sample tube or rock fragment. Using a pair of fine tweezers place the sample onto the holder. If a powdered sample is used then the sample tube should be placed with its closed end towards the magnet so that the material is not pulled out.

Switch on the excitor lamp at the mains and set it to maximum illumination by means of the control located above the temperature indication unit. (NB. Switching on this also energises the Temperature Recording

System, but this does not operate whilst in the Off position).

By rotating the brass screw on top of the suspension turret adjust the position of the torsion beam until the shadow cast by the flag just covers the left hand hole in the screen as viewed from the light source.

Slide the furnace forward until the sample is about 1cm from the back of the tube. (NB. there is a spring loaded catch on the slide).

Plug in the transistors to the control box and switch to M so that the output appears on the ammeter. Check that the shadow of the flag still covers the left-hand hole and then adjust the current to about 1.5mA.

Make final adjustments to the position of the torsion beam so that light is just able to pass through the hole. At the correct position the ammeter should be wavering slightly indicating that the photoelectric system is responding to slight movements of the beam.

Switch on the electromagnet at minimum current and increase this until maximum deflection of the torsion beam is indicated on the ammeter. At this stage it will propably be found that the shadow cast by the flag has rotated beyond the limits of the hole. If this is the case then slide the furnace forward so as to push the beam back until the shadow of the flag just cuts the hole. If this is not the case then simply slide the furnace forward until it touches the beam.

Reduce the current to the magnet until the magnetic field is just strong enough to hold the torsion beam at the back of the furnace. The rotation of the torsion beam is now limited so that the shadow cast by the flag cannot rotate beyond the limits of the hole. If such a limit were not put on the position of the beam then it would tend to rotate further into the pole-gap during heating, due to the Hopkinson effect (increase in magnetization with elevation in temperature up to just below the Curie

point - Nagata 1961).

Replace the covers on the instrument housing so as to exclude draughts and then switch on the Temperature Recording System as follows:-

1) The mains supply has already been switched on at the same time as the excitor lamp.

2) Switch on the 24V and 32V supplies.

3) Depress the post office switch to "reset" and hold down until the step relay has reached the end of its travel and L1 lights up. Set to "Temperature Increasing" and release the post office switch. Lift the post office switch to "step-on" one so that the galvanometer deflects to the left and L1 goes out.

4) Place melting ice around the cold junction of the thermocouple.

To bring the instrument into operation, turn on the water supply to the cooling coils of the magnet, switch on the furnace at the mains, switch on the motor driven variac, setting the switch to H, and switch on the Recorder-Clock at the mains. Finally, switch from M to R on the control unit so as to transfer the transistor output to the Recorder.

4) The Analysis

The analytical process is automatic, but after about 45 minutes the furnace temperature reaches 700°C which is the maximum that can be recorded and the warning light L1 appears on the Temperature Recording Unit, to indicate that the heating cycle is complete.

In order to analyse during the cooling cycle, switch the variac motor drive to C and set the Temperature Recording Unit to "Temp. Decreasing". At the end of the cyle L1 lights up.

The motor drive controlling the furnace current has limit switches

at both ends of its movement which cut off the motor after 37 minutes. At the end of the cooling cycle the furnace current should be switched off at the mains as soon as the motor stops so that the furnace can cool to room temperature.

It is not necessary to use the complete temperature range of the equipment if this is not required. Changes from heating to cooling can be made at any temperature. In such a case, however, before switching to "Temp. Decreasing", it is necessary to ensure that the "Step-Relay Indicator" (on the dial) is at least the same number of divisions beyond the starting position (indicated by the arrow), measured anticlockwise, as it was in front of the starting position when the heating was stopped. This may be done as follows.

Switch the motor drive to C and set the Temperature Recording Unit to Off. Note the number of divisions remaining on the "Step-Relay Indicator" and then reset to the starting position by depressing the post office switch until L1 lights up. Release the switch and then step-on one division at a time by lifting the switch until the same number of divisions have been passed. However, owing to thermal hysteresis the furnace will probably be hotter than when it was switched over to cooling and therefore it will probably be necessary to step-on two or three divisions beyond this point.

Finally, set the Temperature Recording Unit to "Temp. Decreasing" and make sure that the Ether galvanometer deflects to the <u>right</u> of the set zero so that as the backing off emf falls the step-relay is moved on. If the galvanometer does not deflect to the right then set the Temperature Recording Unit to Off once again and step-on one or two more divisions until deflection to the right is obtained. After this has been set the cooling process is automatic.

5) Interpretation of the Thermomagnetic Record

On the heating curve, the point of inflection at which the attraction on the sample suddenly dissappears is taken as the Curie point. On the cooling curve the point of inflection at which the attraction on the sample suddenly appears is taken as the Curie point.

The temperature at which these inflections occur is measured with reference to the temperature marks on the side of the chart. Each of these marks corresponds to an accurately known temperature (Table 30) and it is possible to measure the Curie point to $\pm 1.5^{\circ}C$.

If more than one magnetic phase is present in the sample then the thermomagnetic record will contain more than one inflection whilst if the composition of the magnetic phase varies more or less continuously over a range of solid solution then the thermomagnetic record will show a gradual change of slope limited by the Curie points of the end members (Figure 19).

Examples of thermomagnetic records showing these features are shown in Figure 23.

6) Accuracy

The instrument has been calibrated using samples of pure synthetic Fe_3O_4 prepared by M. Guillaud at Bellevue, France. An X-ray powder photograph of this material showed it to have a unit cell edge of 8.396_2Å (cp 8.3963Å Basta 1953; 1957). The X-ray data are summarized in Tables 31 and 32.

Four samples of this material have been analysed thermomagnetically and gave the following values for the Curie Point:- 589°C, 585°C, 586°C, 586°C. The mean value is 586.5°C which may be compared with the value given by Brailsford (1960) who records the Curie point of $FeFe_2O_4$ as 585°C.

Table 31.

X-ray Powder Data for Pure Synthetic Fe_3O_4. (Guillaud)

CoK_α radiation. Camera diameter 114cm. Straumannis mounting.

θ	d	I	hkl
10.78	4.80	mw	111
17.75	2.94	s	220
20.93	2.505	vvs	311
21.82	2.409	vvw	222
25.42	2.086	ms	400
31.67	1.705	mw	422
33.86	1.607	s	511/333
37.30	1.477	vs	440
42.65	1.321	vw	620
44.58	1.275	wm	533
45.21	1.261	vw	622
50.14	1.165 α_1	vw	-
52.09	1.134 α_1	vvw	-
52.94	1.121 α_1	vw	642
54.99	1.092 α_1	mw	800
67.24	0.970 α_1	mw	752/555
72.36	0.939 α_1	wm	840

Table 32.

Data used to Extrapolate to a_o of the Fe_3O_4 Sample

θ	$\sin^2\theta$	N	hkl	cosec θ	$\sqrt{N}\frac{\lambda}{2}$	a	$\frac{1}{2}\left(\frac{\cos^2\theta}{\theta}+\frac{\sin^2\theta}{\sin\theta}\right)$
52.94	0.6368	56	642	1.2532	6.693451	8.38823	0.425
54.99	0.6709	59	731, 553	1.2210	6.870401	8.38876	0.372
67.24	0.8503	75	751, 555	1.0845	7.746164	8.40071	0.146
72.36	0.9082	80	840	1.0493	8.000204	8.39461	0.084

$a = \text{cosec}\,\theta\sqrt{N}\,\frac{\lambda}{2}$.

$a_o = 8.396_2$ Å

Thus analyses involving titaniferous magnetites should be accurate to $\pm 1^{\circ}C$ since the error of $1.5^{\circ}C$ at a temperature of nearly $600^{\circ}C$ may be expected to be reduced at the lower Curie points.

PART III

The Design of an Instrument for the Measurement of the Saturation Magnetization of Ferromagnetic Minerals at Room Temperature

Introduction

The instrument described in Part II is a horizontal magnetic balance in which the force acting on the ferromagnetic sample causes the balance to rotate about a point of suspension. This system is well suited to the measurement of Curie points since the small torsional deflection of the balance can be readily detected and recorded.

There is, however, an alternative arrangement for a horizontal magnetic balance in which the force acting on the sample causes a translational movement of the balance (Figure 58). This system has been adopted in order to measure the saturation magnetization of small samples of ferromagnetic powders following a null method essentially similar to that described by Chevallier and Mathieu (1943).

The principle of the method is to measure the translational force exerted on the sample in an inhomogeneous magnetic field H. Under the influence of this field, the sample takes on a magnetic moment M parallel to H and experiences a force F (see Part II. Introduction) given by:-

$$F_x = M \frac{dH}{dx} \qquad \ldots\ldots\ldots\ldots\ldots 1)$$

The specific intensity of magnetization is then obtained from:-

$$\sigma = \frac{M}{m} \qquad \ldots\ldots\ldots\ldots\ldots 2)$$

where M is in emu and m is the mass of the sample in grammes. If the magnetic field H is large enough to saturate the sample then the ratio M/m gives the value of the specific intensity of saturation magnetization σ_s.

Figure 59.

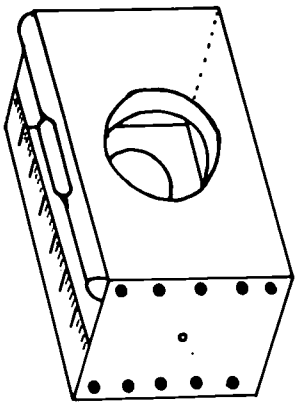

Figure 58.

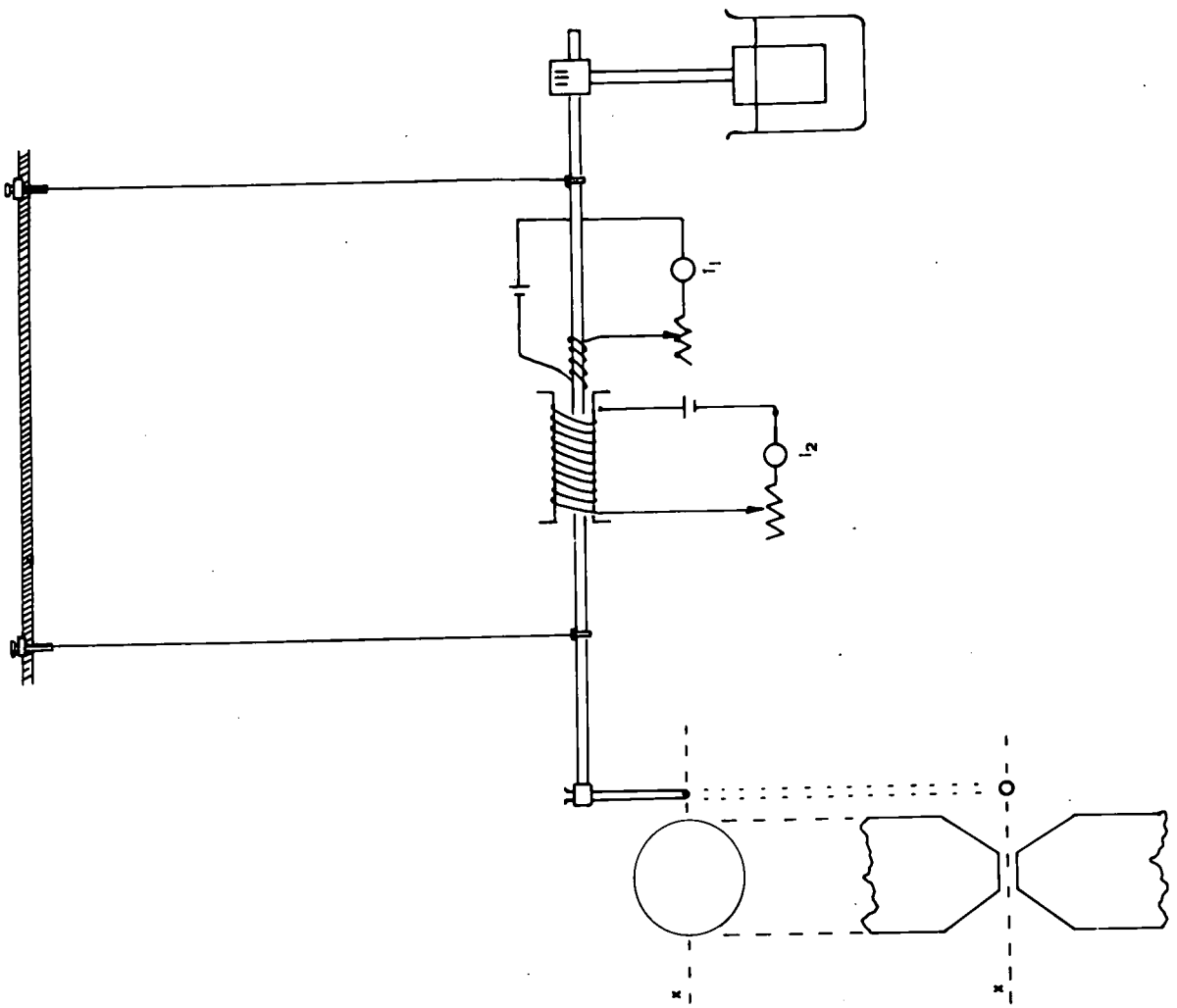

Figure 58.

Diagram of equipment for measuring saturation magnetization at room temperature.

Figure 59.

Box attachment for the magnet; used for positioning a sample in the pole gap.

Chevallier, Mathieu and Vincent (1954) have found that titaniferous magnetites are essentially saturated in a magnetic field of 6500 Oe, and in the present equipment field strengths exceeding this value have been readily obtained using a small electromagnet.

The force F_x acting on the sample may be measured by applying an equal and opposite force to the translation beam. This may be done by passing currents through two coaxial solenoids one of which is fixed to the beam (Figure 58). The force acting between these solenoids is given by:-

$$F = k\ i_1 \cdot i_2 \qquad \ldots\ldots\ldots\ldots\ldots 3)$$

where i_1 and i_2 are the currents and k is an experimentally determined constant.

The instrument described in the following pages, therefore, comprises:-

1) A translation beam.
2) An electromagnet.
3) Two solenoids and accessory equipment for measuring the force acting on the beam.
4) A microscope for measuring the position of the beam.

1. The Translation Beam

The translation beam is shown in Figure 58 and is of very simple construction. It consists of a length of dural tubing (4mm external diameter) 30 cms long. A dural ring, 5 mm in internal diameter, is inset into one end of the beam and a glass tube containing the sample slots into this. The other end of the beam carries a dural damping plate immersed in thin machine oil. The plate is attached to the beam by way of a dural collar and its

position may be adjusted laterally along the beam. A mm scale has been attached to the collar and this is viewed through a microscope.

The beam is suspended horisontally beneath an aluminium frame by two Cu wires 23 cms long. These wires are soldered into brass screws inset into the beam at a distance of 8 cms from each end. At their upper ends the wires are soldered to brass adjusting screws (3 cms long) so that the height and attitude of the beam can be set. Two cotton threads are attached to the beam at the sample end and these pass to the sides of the aluminium frame. These threads prevent lateral movement of the beam.

The aluminium frame is attached to a wooden base board, which also carries the magnet. This board may be levelled by three brass levelling screws. In order that the laboratory bench is not damaged these screws are supported on brass pads which separate the screws from the bench.

2. The Electromagnet

a) Introduction

The magnet is a Newport electromagnet having 1.5" diameter poles with conical pole tips. It works from a 150V DC supply and, according to the manufacturers, produces a field of 16,500 Oe with a pole gap of 5 mm. This field, of course, is at the centre of the pole gap and may be expected to fall off rapidly away from this point.

In the present equipment it is required to know the field H and the gradient $\frac{dH}{dx}$ at a given point on the axis of the pole gap for different values of current in the magnet coils. H has been measured using a search coil and the gradient has been determined by measuring the force acting on a paramagnetic sample of known susceptibility (χ) and applying the relationship:-

$$F_x = m\chi H \frac{dH}{dx} \qquad \text{.....4)}$$

where m is the mass of the sample.

These measurements require a means of defining a selected position on the axis of the pole gap. This has been done by attaching a box-like structure to the poles of the magnet as shown in Figure 59. This structure is constructed of aluminium held together by brass screws. It consists of two rectangular side plates (60 x 80 x 10 mm) and two end plates (60 x 40 x 2 mm). The side plates are pierced centrally by holes 1.5" in diameter so that they fit snugly over the pole pieces, and the end plates are pierced centrally by pin-holes.

A light source consisting of a 1.5V,0.3W bulb is attached to the outside of one of the end plates so that a narrow beam of light can pass through. When the box is horizontal and symmetrically disposed between the pole tips then this beam of light defines the horizontal axis of the pole gap. A spirit level attached to one of the side plates indicates when the beam is horizontal. Therefore, by this means, it is possible to locate a sample on the axis since at this height it is illuminated.

The magnet moves horizontally on runners attached to the base board and it is thus possible to adjust the position of a sample along the axis. This position may be measured by means of a plastic mm scale attached to the other side plate.

b) Measurement of the Field Strength

A small search coil has been constructed consisting of 200 turns of SWG42 copper wire. It has the dimensions:-

Inner diameter 0.36cms .....r_i = 0.180 cms

Outer diameter 0.63cms .....r_o = 0.315 cms

Cross-sectional Area	a_i	=	0.1017 cm^2
	a_o	=	0.3117 cm^2
Mean cross-sectional area	a	=	0.2607 cm^2

A Cambridge fluxmeter has been used to measure the field. This instrument is calibrated such that a deflection θ of one scale division equals 15,000 maxwell-turns. Therefore, the field strength H oersted is given by:-

$$H = \frac{15000}{N\,a}\,\theta \qquad \ldots\ldots\ldots 5)$$

where N equals the number of turns on the search coil. For the present coil this gives:-

$$H = 362.8\,\theta$$

The field has been measured by holding the search coil in a clamp such that it lies on the horizontal axis of the pole gap and at a known distance from the centre of the gap. When the magnet was switched on the fluxmeter deflection was noted and converted to oersteds. The error in these measurements is bout 100 Oe since the fluxmeter deflections have been read to $\pm$ 0.25 scale-division.

The field has been measured for magnet currents in the range 0.4 - 1.6 amps at positions 1.0cms, 1.2cms, 1.5cms and 2.0cms from the centre of the pole gap. These results are summarized in Tables 33, 34, 35 and 36 and shown graphically in Figure 60. They show that fields in excess of the required 6500 Oe may be achieved 1.0cms from the centre of the gap.

Table 33.

Calibration Data for the Electromagnet

Magnetic field at x = 1.0 cms.

Magnet Current I amps.	Fluxmeter Deflection θ divisions		Mean	Field H Oe
0.4	17.5		17.5	6349
0.5	18.5	18.25	18.37	6665
0.6	19.25	19.0	19.12	6936
0.7	19.75	19.5	19.62	7119
0.8	20.25	20.0	20.12	7300
0.9	20.75	20.5	20.62	7482
1.0	21.25	21.0	21.12	7663
1.1	21.75	21.5	21.62	7845
1.2	22.0	21.75	21.87	7936
1.3	22.5	22.0	22.25	8074
1.4	22.5	22.25	22.37	8117
1.5	23.0	22.5**	22.75	8254
1.6	23.25*	***	23.25	8435

* First reading. **Last reading.

***Initial current not attainable due to heating of the magnet's coils.

Table 34.

Calibration Data for the Electromagnet

Magnetic field at x = 1.2 cms.

Magnet Current I amps.	Fluxmeter Deflection θ divisions		Mean	Field H Oe
0.4	14.25		14.25	5170
0.5	15.25	15.0	15.12	5487
0.6	16.0	15.5	15.75	5715
0.7	16.5	16.25	16.37	5939
0.8	16.76	16.5	16.62	6030
0.9	17.25	17.0	17.12	6212
1.0	17.5	17.25	17.37	6301
1.1	18.0	17.5	17.75	6440
1.2	18.25	18.0	18.12	6575
1.3	18.5	18.25	18.37	6665
1.4	18.75	18.5	18.62	6753
1.5	19.0	18.75**	18.87	6847
1.6	19.5*	***	19.5	7074

* First reading. **Last reading.

***Initial current not attainable due to heating of the magnet's coils.

Table 35.

Calibration Data for the Electromagnet

Magnetic field at x = 1.5 cms.

Magnet Current I amps.	Fluxmeter Deflection θ divisions		Mean	Field H Oe
0.4	11.25		11.25	4082
0.5	11.75	11.75	11.75	4264
0.6	12.5	12.25	12.37	4487
0.7	12.75	12.75	12.75	4626
0.8	13.0	13.0	13.0	4717
0.9	13.5	13.25	13.37	4852
1.0	13.75	13.75	13.75	4989
1.1	14.0	13.75	13.87	5034
1.2	14.25	14.0	14.12	5123
1.3	14.5	14.25	14.37	5213
1.4	14.75	14.5	14.62	5306
1.5	15.0	14.75**	14.87	5396
1.6	15.25*	***	15.25	5533

* First reading. **Last reading.

***Initial current not attainable due to heating of the magnet's coils.

Table 36.

Calibration Data for the Electromagnet

Magnetic field at x = 2.0 cms.

Magnet Current I amps.	Fluxmeter Deflection θ divisions		Mean	Field H Oe
0.4	7.5		7.5	2721
0.5	7.75	7.75	7.75	2812
0.6	8.25	8.25	8.25	2993
0.7	8.5	8.5	8.5	3084
0.8	8.75	8.75	8.75	3175
0.9	9.25	9.0	9.12	3309
1.0	9.25	9.25	9.25	3356
1.1	9.5	9.5	9.5	3446
1.2	9.75	9.75	9.75	3538
1.3	9.75	10.0	9.87	3581
1.4	10.0	10.0	10.0	3622
1.5	10.0	10.0**	10.0	3622
1.6	10.25*	***		

* First reading. **Last reading.

***Initial current not attainable due to heating of the magnet's coils.

Figure 61.

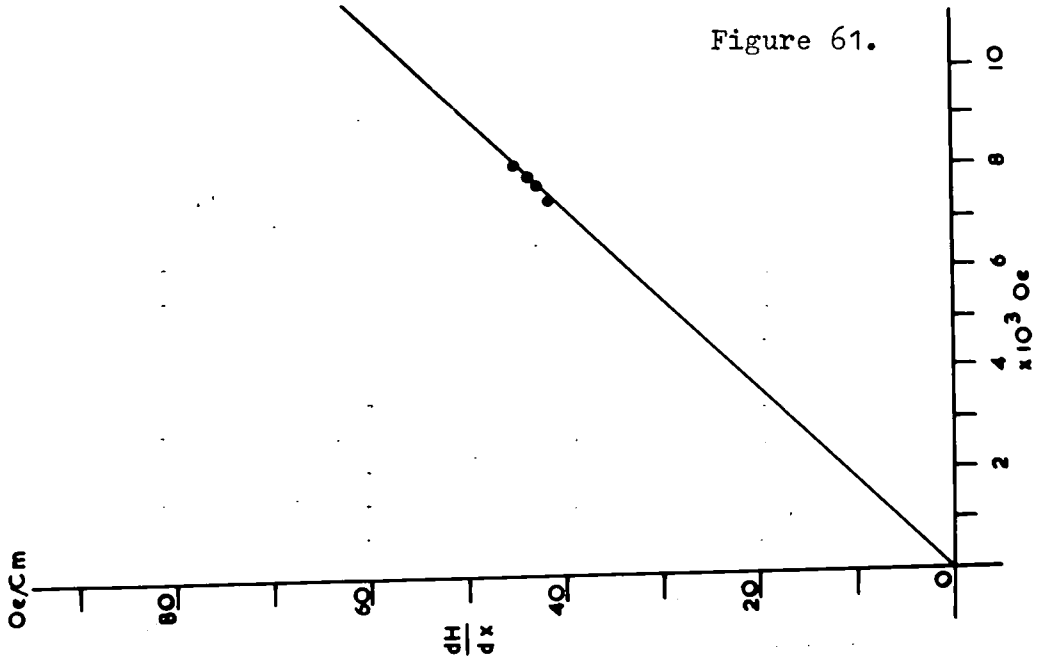

Figure 60.

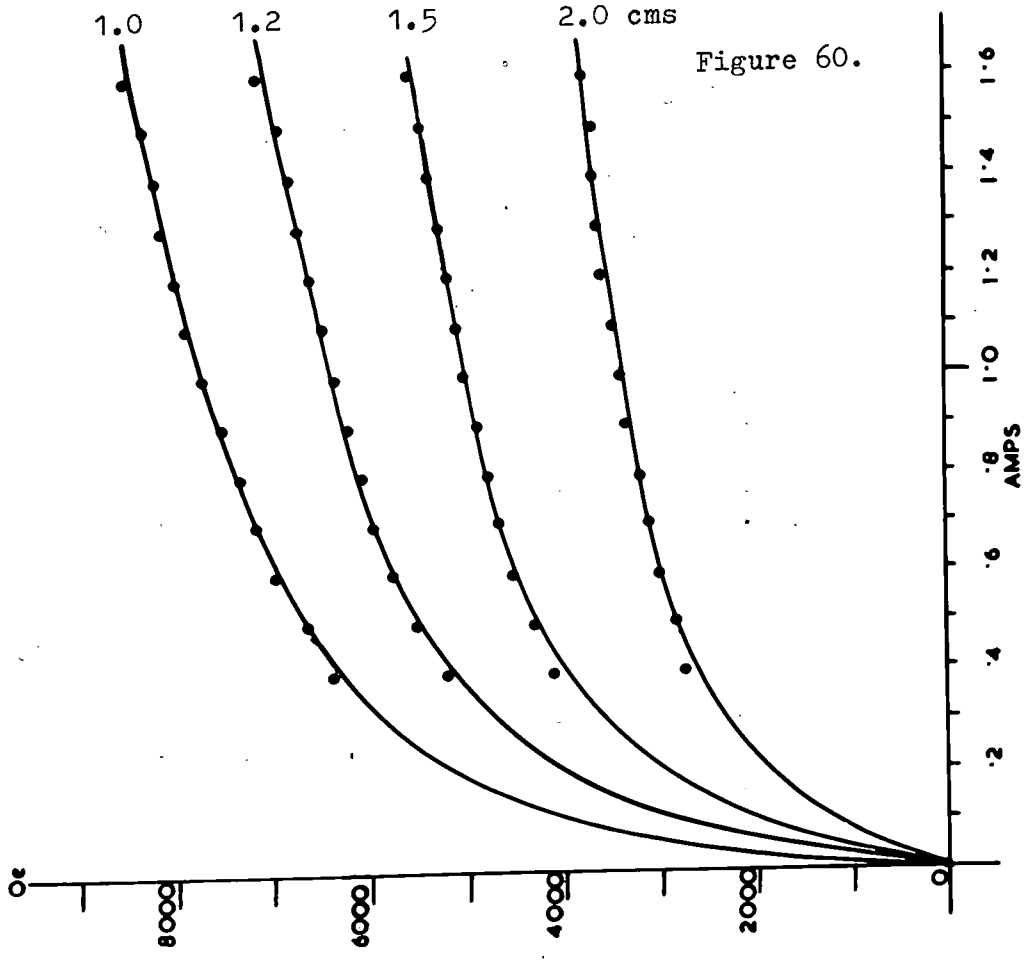

Figure 60.

Field strength of the magnet at different positions on the axis as a function of current.

Figure 61.

Calibration curve for determining the gradient dH/dX.

c) Measurement of the Magnetic Gradient

The magnetic gradient at the point 1.0cms from the centre of the pole gap has been determined by measuring the force acting on samples of $MnSO_4$ ($\chi = 88.5\ 10^{-6}$ at 24°C) and $MnCl_2$ ($\chi = 107.0\ 10^{-6}$ at 24°C). These samples (carefully dehydrated) were contained in small glass tubes which slotted firmly into the sample holder on the translation beam. The force acting on them for different values of H was measured by applying an equal restoring force by means of the coaxial solenoids. The calibration data for these solenoids is described later.

The results of these measurements are summarized in Table 37. They show a fair agreement between the gradients determined with $MnSO_4$ and those measured with $MnCl_2$. However, the mean values have been taken as the best estimates of the gradients and these have been plotted in Figure 61. These values fall on a straight line through the origin as required by Equation 4. Therefore, using this curve it is possible to determine the field gradient for any value of H.

3. Calibration of the Restoring Forces due to the Solenoids

The force created between two coaxial solenoids carrying currents i_1 and i_2 is proportional to the product $i_1 i_2$ (Chevallier et Mathieu 1943). In the present system a small coil consisting of 120 turns of enamelled SWG48 copper wire has been wound onto the translation beam. This coil takes current from a 24V DC mains supply controlled by a rheostat, and since it has a low resistance (about 2 ohms) it can carry up to 4 amps without over heating. The current (i_1) is measured on a 0 - 5 amp ammeter and is known to an accuracy probably better than 0.01 amp.

Table 37.

Determination of the Magnetic Gradient at x = 1.0 cms.

1) $MnSO_4$: m = 0.0501g. Temp. = 23.2°C. χ = 88.5 10^{-6} at 24°C.

I amps.	H Oe	i_1	i_2 amps	$i_1 i_2$	F dynes	$\frac{dH}{dx}$ * Oe/cm
0.8	7440	2	0.228	0.456	1.30	39.92
1.0	7740	2	0.253	0.506	1.42	41.30
1.2	7970	2	0.261	0.522	1.48	41.80
1.4	8180	2	0.277	0.554	1.56	42.92

2) $MnCl_2$; m = 0.0274g. Temp. = 23.2°C. χ = 107.0 10^{-6} at 24°C.

I amps.	H Oe	i_1	i_2 amps	$i_1 i_2$	F dynes	$\frac{dH}{dx}$ * Oe/cm
0.8	7440	2	0.166	0.332	0.95	43.54
1.0	7740	2	0.178	0.356	1.00	44.05
1.2	7970	2	0.189	0.378	1.07	46.01
1.4	8180	2	0.200	0.400	1.12	46.89

3) Mean gradients, from 1) and 2).

H Oe	$\frac{dH}{dx}$ Oe/cm
7440	41.43
7740	42.67
7970	43.90
8180	44.90

* $\frac{dH}{dx} = \frac{F}{m\chi H}$

Figure 63.

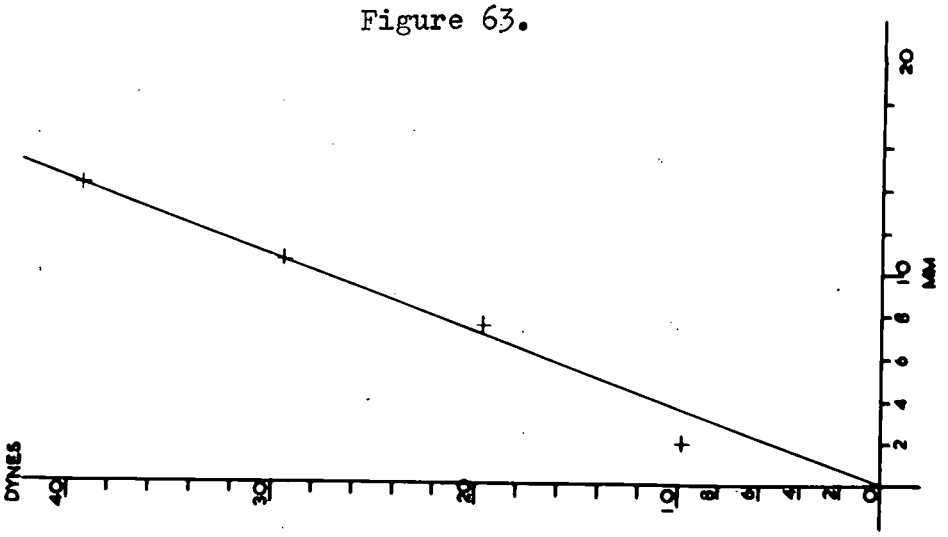

Figure 62.

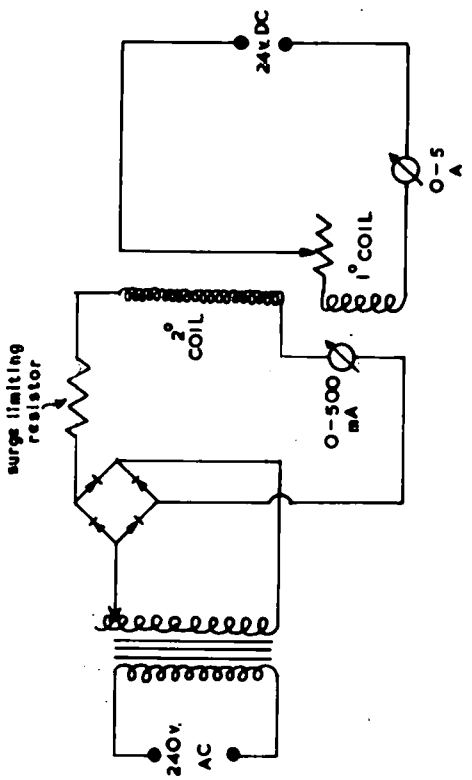

Figure 64.

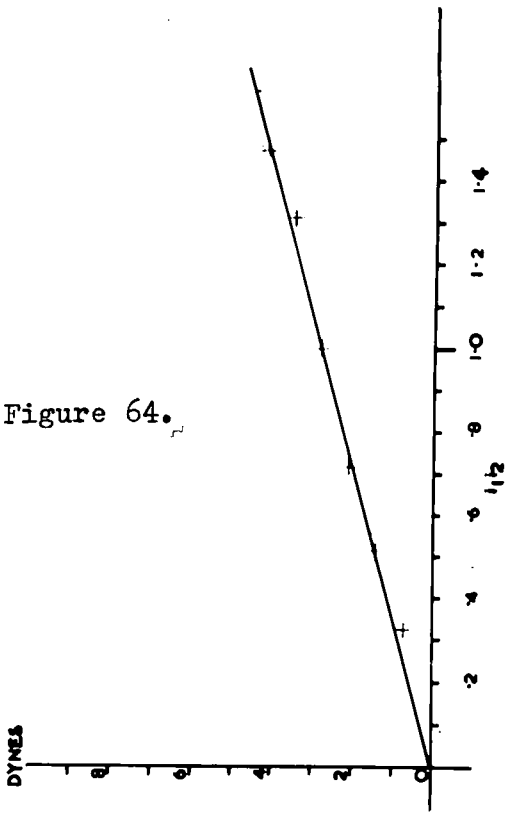

Figure 62.

Circuit diagram for the restoring system.

Figure 63.

Calibration curve for the spring coil.

Figure 64.

Restoring force due to the solenoids as a function of the currents ($i_1 i_2$) passing through them.

A much larger coil consisting of 3000 turns of SWG36 copper wire has been wound onto an aluminium former which is fixed to the frame of the apparatus so as to be coaxial with the translation beam and the attached primary coil. This coil takes current from a 240V AC mains supply which is controlled by a variac and then rectified before passing through the coil. Since this coil has a high resistance (65 ohms) it carries currents less than 0.5 amp but as these are measured on a 0 - 500mA ammeter their values (i_2) are known to an accuracy of $\pm$0.001 amp. The circuit diagram for the whole system is shown in Figure 62.

A calibration curve relating the value of $i_1 i_2$ to the force exerted has been obtained by measuring the extension of a calibrated spring coil. This coil was made by winding a length of fine copper wire round a glass rod. The coil was then housed in a glass tube and one end attached to a stopper inserted in one end of the tube. The other end of the coil passed through a light plastic cap and was glued firmly to it. This cap ensured that the unloaded spring had a constant extension.

The spring was calibrated by clamping it vertically and measuring the extension caused by adding small balance weights. This data is summarized in Table 38 and the calibration curve is shown in Figure 63. This curve is a straight line through the origin.

The spring was next clamped horizontally and the free end attached to the translation balance. Its position was adjusted so as to be in line with the translation beam and also so that the extension of the spring corresponded to the unloaded state. The extension of the spring was then measured for various values of $i_1 i_2$ using the microscope and scale to measure this to the nearest 0.25mm. These results are summarized in Table 39 and the calibration curve is shown in Figure 64. This curve relates the

Table 38.

Extension of the Spring Coil

Mass (grms)	Force (dynes)	Extension (mm)
0.00	0.00	0.0
0.01	9.81	2.0
0.02	19.68	7.0
0.03	29.52	10.5
0.04	39.36	14.0

Table 39.

Calibration of the Coaxial Solenoids against the Spring Coil

Extension of spring	Force	i_1	i_2	i_2	i_2	i_2	$i_1 i_2$
mm	dynes	amps	amps			mean	
0.0	0.0	0	0	0	0	0	0
0.25	0.70	2	0.162	0.170	0.155	0.162	0.324
0.5	1.41	2	0.260	0.260	0.252	0.257	0.514
0.75	2.11	2	0.362	0.348	0.360	0.357	0.714
1.0	2.82	3	0.336	0.338	0.330	0.335	1.005
1.25	3.52	3	0.430	0.442	0.440	0.437	1.311
1.5	4.23	3	0.490	0.490	0.490	0.490	1.470

force exerted to the value of the product $i_1 i_2$.

4. Measurement of the Position of the Translation Beam

The force F_x acting due to the magnetic moment M of a sample attached to the translation beam, is measured by applying an equal and opposite force to bring the beam back to its equilibrium position. This position is measured by focussing a microscope with a low power objective onto an illuminated mm scale attached to the beam. An old petrographic microscope having cross wires engraved on the ocular has proved quite suitable for this purpose, with the stage and substage attachments removed.

5. Measuring Procedure, for Ferromagnetic Samples

The following measuring procedure is recommended:

a) It is essential to use small quantities of material as the forces acting on large samples may be too great to measure, and in any case, large forces should be avoided as they tend to distort the movement of the beam.

Samples weighing between 0.0003g and 0.002g should be used the larger amounts being required for material with relatively small magnetic moments. Generally, however, 0.001g will be adequate. It is essential, however, that these weights be known accurately. Using a Mettler balance Type H16 it is possible to weigh the sample to $\pm$0.00001g.

Such small quantities of powder are conveniently contained in the fine silica tubes used in the thermomagnetic balance. Their weight is determined as the difference between the weight of the tube empty and containing the sample.

The sample tube should be placed in a small test tube approximately 50mm long and 5mm in external diameter. These tubes just slot into the

holder on the translation balance. The sample may be held firmly in place at the bottom of the test tube by inserting a wad of soft tissue-paper.

b) The position of the sample in the pole gap can be adjusted vertically by means of the suspension wires until it is illuminated by the light beam defining the x axis. This adjustment, once made, should apply to all subsequent samples.

The position of the sample in the pole gap can be adjusted horizontally by moving the magnet. It should be set so as to be 1.0cms from the centre of the gap. This setting also should apply to subsequent samples.

c) Using the microscope, focus on the illuminated scale on the translation beam and set the cross-wires against an arbitrary reference mark. This setting marks the equilibrium position of the beam.

d) The magnetic moment of the sample may be determined by measuring the force acting on it for different values of $\frac{dH}{dx}$ and plotting the relationship between them. Provided the field H is large enough to saturate the sample then this relationship should be a straight line with slope M (Equation 1).

With a pole gap of 5mm and the sample 1.0cms from the centre of the gap a field of 7000 Oe is created when the magnet current is 0.6 amps. (Figure 60), and the field gradient at this point is 38.6 Oe/cm (Figure 61). This field, therefore, is sufficient to saturate the sample.

Measurements may be made with magnet currents of 0.6 0.8,1.0, 1.2, and 1.4 amps. These fixed points have been chosen for convenience and the corresponding values of H and $\frac{dH}{dx}$ determined from Figures 60 and 61 are summarized in Table 40. Other settings may be used if preferred.

In measuring the restoring force it is generally convenient to set the current in the primary coil (i_1) to a fixed value, usually 2 or 3 amps,

Table 40.

The Magnetic Gradients used in the Measurement of Saturation Magnetization

I amps.	H Oe	$\frac{dH}{dx}$
0.6	7000	38.6
0.8	7440	41.4
1.0	7740	42.7
1.2	7970	43.9
1.4	8180	44.9

and vary the current (i_2) in the secondary coil using the variac for this purpose. Two or three readings should be taken at each setting, checking the equilibrium position between each reading, and a mean value taken. Normally the values of i_2 do not differ by more than 0.004 amp.

Knowing i_1 and i_2 the force may be determined from the product $i_1 i_2$ and referring to Figure 64. This value is plotted against the gradient, and the slope of the curve is taken as M knowing the mass of the sample and the value of M it is thus a simple matter to calculate σ from Equation 2.

It is recommended that two independent measurements be made on separate samples of the same material and the mean value of σ be adopted. This serves as a useful mutual check on the result.

6. Accuracy of the Results

Samples of pure synthetic Fe_3O_4 prepared by M. Guillaud at Bellevue, France have been measured. The saturation magnetization of Fe_3O_4 is 92 - 93 emu/grm (Nagata 1961). The results of the present measurements are summarized in Table 41. They give a mean value of 94.58 emu/grm for σ_∞. Taking the true value as being 92.5 emu/grm this indicates an error of 2.08 in 92.5 or about 2%

Table 41.

The Saturation Magnetization of Pure Fe_3O_4

I	H	i_1	i_2	$i_1 i_2$	F	$\frac{dH}{dx}$
amps.	Oe	amps.	amps.		dynes	Oe/cm
Sample 1.	m = 0.00030g.		Temperature = 20°C.			
0.6	7000	2	0.202	0.404	1.12	38.6
0.8	7440	2	0.210	0.420	1.20	41.4
1.0	7740	2	0.210	0.420	1.20	42.7
1.2	7970	2	0.215	0.430	1.22	43.9
1.4	8180	2	0.220	0.440	1.26	44.9
Sample 2.	m = 0.00088g.		Temperature = 20°C.			
0.6	7000	3	0.393	1.179	3.30	38.6
0.8	7440	3	0.406	1.218	3.42	41.4
1.0	7740	3	0.417	1.251	3.50	42.7
1.2	7970	3	0.428	1.284	3.60	43.9
1.4	8180	3	0.439	1.317	3.70	44.9

Results :-

Sample 1. M = 0.0288. $\sigma_\infty = \frac{M}{m} = 96.00$ emu/g

Sample 2. M = 0.0820. $\sigma_\infty = \frac{M}{m} = 93.17$ emu/g

Mean value = 94.58 emu/g

APPENDICES.

Appendix 1.

Separation of the Ferromagnetic Minerals

The following procedure has been adopted in order to separate the ferromagnetic minerals from the parent rock:-

1) A hand sized sample has been split into small fragments using a hydraulic jack manufactured by Slayhi Limited, London. These fragments have then been crushed using a Spex Mixer Mill manufactured by Spex Industries Inc., the fragments being contained in a tungsten carbide container during this process, thus avoiding the contamination by iron, which might have occurred if a steel container had been used.

2) About 140grms (a full 4oz bottle) of the inhomogeneous powder have been crudely fractionated using an elutriating tube similar to that described by Frost (1959). The powder was introduced into the elutriating tube as a slurry and was found that the addition of ammonia solution to the slurry prevented coagulation of the powder. Separation took about 45 minutes and yielded three fractions.

(a) A heavy, coarse grained, fraction at the bottom of the tube.

(b) A medium grained fraction concentrated in the lower levels of the tube.

(c) A fine, clayey, fraction left as a residue at the top of the tube and in the overflow.

3) The fine fraction was found to contain hardly any ferromagnetic minerals and was rejected.

4) The coarse fraction consisted of a random mixture of coarse grains of low density (felspar etc.) and smaller grains of higher density (magnetite etc.). The fraction was first washed with water to remove residual clay

material, although much of this was removed in the elutriating tube. It was then dried for about an hour at about 100°C in an electric oven. The dry powder was then crushed using an agate pestle and mortar and then graded by seiving into the following fractions: 100-110 mesh, 110-200 mesh, 200-250 mesh and less than 250 mesh. Each grade was then passed through a Cooke magnetic separator and the magnetic fraction retained.

5) The medium grained fraction contained most of the ferromagnetic minerals. It was washed and dried as in the case of the coarse grained fraction and then graded and passed through the magnetic separator.

6) The magnetic fraction obtained from both the coarse and medium grained rock powders was then crushed again using an agate pestle and mortar, until it formed a very fine powder that was smooth to the touch. This powder was then slowly passed through the magnetic separator and the magnetic fraction collected.

7) The final yield was about 1-3grms of ferromagnetic mineral, the highest yields being obtained from samples close to the margins of the Clauchlands sheet, which contain the highest content of opaque minerals (see Chapter II), whilst samples towards the centre of the sheet yielded less ferromagnetic mineral.

Appendix 2.

Data used for Determining the Lattice Parameters of the Separate 'Ilmenites'.

The lattice parameters have been determined from the powder photographs by a method of successive extrapolations, using the basic equations:-

$$a_o = \frac{\lambda}{2\sin\theta}\sqrt{\frac{4}{3}s + \left(\frac{a}{c}\right)^2 . l^2} \quad \ldots\ldots 1$$

$$c_o = \frac{\lambda}{2\sin\theta}\sqrt{\frac{4}{3}\left(\frac{c}{a}\right)^2 . s + l^2} \quad \ldots\ldots 2$$

where $s = (h^2 + hk + l^2)$.

In each case, calculations leading to the first extrapolation have been made using the values:-

$$\left(\frac{a}{c}\right)^2 = 0.12911. \qquad \left(\frac{c}{a}\right)^2 = 7.74492.$$

these values having been determined from the lattice parameters given on ASTM card 3-0799 which are:

$$a_o = 5.0791 \text{ Å}. \qquad c_o = 14.1350 \text{ Å}.$$

Subsequent calculations have then been made on the newly obtained axial ratios.

The values of $\sin\theta$ and $\cos\theta$ have been obtained from nine figure tables and have been read to the 5th decimal place.

Calculations have been made using a Madas electrically operated calculator and square roots have been determined using 5-figure logs.

Sample A/C/3/42. Film : 5947.

θ	$\cos^2\theta$	$\sin\theta$	hk.l	$\frac{4}{3}s$	$(\frac{a}{c})^2 l^2$	a_o
20.811	0.87	0.35529	11.0	4	0	5.0387
37.790	0.62	0.61277	30.0	12	0	5.0600
50.782	0.40	0.77474	31.4	17.3	2.066	5.0897
				Extrapolated value		5.130

				$\frac{4}{3}(\frac{c}{a})^2 s$	l^2	c_o
23.819	0.84	0.40385	11.3	30.979	9	14.0140
31.479	0.73	0.52219	11.6	30.979	36	14.0282
53.318	0.36	0.80196	22.6	123.92	36	14.1147
				1st Extrapolated value		14.167
"	"	"	"	30.505	9	13.9300
"	"	"	"	30.505	36	13.9786
"	"	"	"	122.02	36	14.0304
				2nd Extrapolated value		14.120
"	"	"	"	30.303	9	13.8950
"	"	"	"	30.303	36	13.9573
"	"	"	"	121.21	36	13.9946
				3d Extrapolated value		14.090
"	"	"	"	30.175	9	13.8724
"	"	"	"	30.175	36	13.9442
"	"	"	"	120.700	36	13.9717
				4th Extrapolated value		14.076
"	"	"	"	30.115	9	13.8616
"	"	"	"	30.115	36	13.9446
"	"	"	"	120.46	36	13.9610
				5th Extrapolated value		14.076

Result :- a_o = 5.130 Å

c_o = 14.076 Å

.....

Sample A/C/3/39. Film : 5937.

θ	$\cos^2\theta$	$\sin\theta$	hk.l	$\frac{4}{3}s$	$(\frac{a}{c})^2 l^2$	a_o
20.728	0.87	0.35393	11.0	4	0	5.0580
37.720	0.62	0.61180	30.0	12	0	5.0680
50.878	0.40	0.77580	31.4	17.3°	2.066	5.0817
				Extrapolated value		5.100(5)

				$\frac{4}{3}(\frac{c}{a})^2$	s	l^2	a_o
23.732	0.84	0.40246	11.3	30.979	9		14.0623
31.392	0.73	0.52089	11.6	30.979	36		14.0618
53.201	0.36	0.80074	22.6	123.92	36		14.1362
			1st Extrapolated value				14.182
"	"	"	"	30.926	9		14.0532
"	"	"	"	30.926	36		14.0581
"	"	"	"	123.70	36		14.1264
			2nd Extrapolated value				14.173
"	"	"	"	30.885	9		14.0459
"	"	"	"	30.885	36		14.0538
"	"	"	"	123.54	36		14.1191
			3d Extrapolated value				14.170
"	"	"	"	30.872	9		14.0436
"	"	"	"	30.872	36		14.0522
"	"	"	"	123.488	36		14.1169
			4th Extrapolated value				14.170

Result :- a_o = 5.100(5) Å

c_o = 14.170 Å

.....

Sample S36. Film : 5935.

θ	$\cos^2\theta$	$\sin\theta$	hk.l	$\frac{4}{3}s$	$(\frac{a}{c})^2 l^2$	a_o
37.776	0.62	0.61258	30.0	12	0	5.06159
45.000	0.50	0.70711	22.0	16	0	5.06343
68.404	0.13	0.92180	41.0	28	0	5.09354
				Extrapolated value		5.1034

				$\frac{4}{3}(\frac{c}{a})^2 s$	l^2	c_o
50.946	0.40	0.77655	31.4	134.24	16	14.1180
53.203	0.36	0.80076	22.6	123.92	36	14.1312
63.111	0.20	0.89188	31.8	134.24	64	14.1411
				1st Extrapolated value		14.1685
"	"	"	"	133.60	16	14.0982
"	"	"	"	123.324	36	14.1091
"	"	"	"	133.60	64	14.1077
				2nd Extrapolated value		14.1235
"	"	"	"	132.75	16	14.0582
"	"	"	"	122.54	36	14.0747
"	"	"	"	132.75	64	14.0771
				3d Extrapolated value		14.1035
"	"	"	"	132.38	16	14.0408
"	"	"	"	122.19	36	14.0592
"	"	"	"	132.38	64	14.0643
				4th Extrapolated value		14.0956
"	"	"	"	132.04	16	14.0247
"	"	"	"	121.88	36	14.0452
"	"	"	"	132.04	64	14.0519
				5th Extrapolated value		14.0730
"	"	"	"	131.81	16	14.0137
"	"	"	"	121.67	36	14.0365
"	"	"	"	131.81	64	14.0435
				6th Extrapolated value		14.073

Result :- a_o = 5.1034 Å

c_o = 14.073 Å

.....

Sample S34. Film : 5936.

θ	$\cos^2\theta$	$\sin\theta$	hk.l	$\frac{4}{3}s$	$(\frac{a}{c})^2 l^2$	a_o
20.969	0.87	0.35786	11.0	4	0	5.002
37.755	0.62	0.61229	30.0	12	0	5.006
50.700	0.40	0.77384	31.4	17.336	2.066	5.095
				1st Extrapolated value		5.150
"	"	"	"	"	0	5.002
"	"	"	"	"	0	5.006
"	"	"	"	"	2.110	5.100
				2nd Extrapolated value		5.119
"	"	"	"	"	0	5.002
"	"	"	"	"	0	5.006
"	"	"	"	"	2.093	5.098
				3d Extrapolated value		5.123

a_o taken as mean of 2nd and 3d extrapolations = 5.121

				$\frac{4}{3}(\frac{c}{a})^2 s$	l^2	c_o
23.877	0.84	0.40493	11.3	30.979	9	13.9769
31.541	0.73	0.52311	11.6	30.979	36	14.0039
53.197	0.36	0.80070	22.6	123.92	36	14.1369
				1st Extrapolated value		14.180
"	"	"	"	30.324	9	13.8618
"	"	"	"	30.324	36	13.9350
"	"	"	"	121.30	36	14.0204
				2nd Extrapolated value		14.152
"	"	"	"	30.572	9	13.9050
"	"	"	"	30.572	36	13.9610
"	"	"	"	122.29	36	14.0645
				3d Extrapolated value		14.152
"	"	"	"	30.548	9	13.9012
"	"	"	"	30.548	36	13.9585
"	"	"	"	122.19	36	14.0601
				4th Extrapolated value		14.150

Result :- a_o = 5.121Å

c_o = 14.150Å

.....

Appendix 3.

Numerical Data used for Determining Saturation Magnetization.

I^{Magnet} amps	H Oe	i_1 amps	i_2 amps	$i_1 i_2$	F dynes	$\frac{dH}{dX}$ Oe/cm
1. Pure Fe_3O_4 (Guillaud). m = 0.00030g. Temp. = 20°C.						
0.6	7000	2	0.202	0.404	1.12	38.6
0.8	7440	2	0.210	0.420	1.20	41.4
1.0	7740	2	0.210	0.420	1.20	42.7
1.2	7970	2	0.215	0.430	1.22	43.9
1.4	8180	2	0.220	0.440	1.26	44.9
		M = 0.0288.	σ= 96.00 emu/g.			
2. Pure Fe_3O_4 (Guillaud). m = 0.00088g. Temp. = 20°C.						
.	.	3	0.393	1.179	3.30	.
.	.	3	0.406	1.218	3.42	.
as above		3	0.417	1.251	3.50	as above
.	.	3	0.428	1.284	3.60	.
.	.	3	0.439	1.317	3.70	.
		M = 0.0820.	σ= 93.17 emu/g.			
1. Sample S2.			m = 0.00136g.	Temp. = 26°C.		
.	.	2	0.330	0.660	1.86	.
.	.	2	0.348	0.696	1.98	.
as above		2	0.361	0.722	2.02	as above
.	.	2	0.370	0.740	2.10	.
.	.	2	0.382	0.764	2.14	.
		M = 0.0424.	σ= 31.18 emu/g.			
2. Sample S2.			m = 0.00114g.	Temp. = 26°C.		
.	.	2	0.274	0.548	1.56	.
.	.	2	0.287	0.574	1.62	.
as above		2	0.300	0.600	1.70	as above
.	.	2	0.306	0.612	1.72	.
.	.	2	0.313	0.626	1.78	.
		M = 0.0368.	σ= 32.28 emu/g.			
1. Sample S4.			m = 0.00072g.	Temp. = 23°C.		
.	.	2	0.143	0.286	0.80	.
.	.	2	0.148	0.296	0.84	.
as above		2	0.152	0.304	0.88	as above
.	.	2	0.156	0.312	0.90	.
.	.	2	0.164	0.328	0.94	.
		M = 0.0186.	σ = 25.83 emu/g.			

I	H	i_1	i_2	$i_1 i_2$	F	$\frac{dH}{dX}$
2. Sample S4.			m = 0.00090g. Temp. = 23°C.			
n	. .	2	0.203	0.406	1.16	.
	. .	2	0.210	0.420	1.20	.
	as above	2	0.218	0.436	1.22	as above
	. .	2	0.221	0.442	1.24	.
	. .	2	0.228	0.456	1.26	.
		M = 0.0185.		σ = 20.55 emu/g.		
1. Sample S9.			m = 0.00192g. Temp. = 24°C.			
	. .	2	0.319	0.638	1.80	.
	. .	2	0.332	0.664	1.86	.
	as above	2	0.345	0.690	1.94	as above
	. .	2	0.355	0.710	2.00	.
	. .	2	0.366	0.732	2.06	.
		M = 0.0454.		σ = 23.64 emu/g.		
2. Sample S9.			m = 0.00161g. Temp. = 25°C.			
	. .	2	0.233	0.466	1.32	.
	. .	2	0.243	0.486	1.38	.
	as above	2	0.252	0.504	1.42	as above
	. .	2	0.262	0.524	1.48	.
	. .	2	0.268	0.536	1.52	.
		M = 0.0338.		σ = 20.99 emu/g.		
1. Sample S11.			m = 0.00251g. Temp. = 25°C.			
	. .	2	0.319	0.638	1.80	.
	. .	2	0.333	0.666	1.88	.
	as above	2	0.343	0.686	1.94	as above
	. .	2	0.355	0.710	2.00	.
	. .	2	0.365	0.730	2.06	.
		M = 0.0458.		σ = 18.25 emu/g.		
2. Sample S11.			m = 0.00163g. Temp. = 25°C.			
	. .	2	0.260	0.520	1.48	.
	. .	2	0.273	0.546	1.54	.
	as above	2	0.282	0.564	1.60	as above
	. .	2	0.290	0.580	1.64	.
	. .	2	0.296	0.592	1.66	.
		M = 0.0314.		σ = 19.26 emu/g.		
1. Sample S31.			m = 0.00198g. Temp. = 25°C.			
	. .	2	0.240	0.480	1.36	.
	. .	2	0.249	0.498	1.42	.
	as above	2	0.257	0.514	1.44	as above
	. .	2	0.263	0.526	1.48	.
	. .	2	0.271	0.542	1.52	.
		M = 0.0240.		σ = 12.12 emu/g.		

I	H	i_1	i_2	$i_1 i_2$	F	$\frac{dH}{dX}$
2. Sample S 31.		m = 0.00196g. Temp. = 26°C.				
.	.	2	0.210	0.420	1.20	.
.	.	2	0.218	0.436	1.24	.
as above		2	0.222	0.444	1.26	as above
.	.	2	0.228	0.456	1.28	.
.	.	2	0.237	0.474	1.34	.
		M = 0.222. σ = 11.32 emu/g.				
1. Sample S40.		m = 0.00074g. Temp. = 19°C.				
.	.	2	0.224	0.448	1.28	.
.	.	2	0.232	0.464	1.30	.
as above		2	0.240	0.480	1.36	as above
.	.	2	0.250	0.500	1.40	.
.	.	2	0.250	0.500	1.40	.
		M = 0.032. σ = 43.24 emu/g.				
2. Sample S40.		m = 0.00105g. Temp. = 21°C.				
.	.	2	0.400	0.800	2.24	.
.	.	2	0.418	0.836	2.36	.
as above		2	0.432	0.864	2.42	as above
.	.	2	0.447	0.894	2.50	.
.	.	2	0.450	0.900	2.52	.
		M = 0.0454. σ = 43.24 emu/g.				
1. Sample S43.		m = 0.00102g. Temp. = 18°C.				
.	.	2	0.289	0.578	1.64	.
.	.	2	0.302	0.604	1.70	.
as above		2	0.305	0.610	1.74	as above
.	.	2	0.312	0.624	1.76	.
.	.	2	0.318	0.636	1.80	.
		M = 0.0254. σ = 24.90 emu/g.				
2. Sample S43.		m = 0.00152g. Temp. = 19°C.				
.	.	2	0.430	0.860	2.42	.
.	.	2	0.439	0.878	2.48	.
as above		2	0.458	0.916	2.58	as above
.	.	2	0.465	0.930	2.62	.
.	.	2	0.478	0.956	2.70	.
		M = 0.0604. σ = 39.74 emu/g.				
1. Sample S47.		m = 0.00113g. Temp. = 20°C.				
.	.	2	0.288	0.576	1.64	.
.	.	2	0.299	0.598	1.70	.
as above		2	0.305	0.610	1.72	as above
.	.	2	0.312	0.624	1.76	.
.	.	2	0.322	0.644	1.80	.
		M = 0.0284. σ = 25.13 emu/g.				

I	H	i_1	i_2	$i_1 i_2$	F	$\frac{dH}{dX}$
2. Sample S47.			m = 0.00106g. Temp. = 20°C.			
.	.	2	0.270	0.540	1.54	.
.	.	2	0.276	0.552	1.56	.
as above		2	0.286	0.572	1.60	as above
.	.	2	0.292	0.584	1.64	.
.	.	2	0.298	0.596	1.70	.
		M = 0.0298. σ = 28.11 emu/g.				

N.B. Since measurements have been made with magnet currents of 0.6, 0.8, 1.0, 1.2 and 1.4 amps (see page 159), these fixed values of I and the corresponding values of H and $\frac{dH}{dX}$ are only listed at the beginning of the above table.

Appendix 4.

The Measurement and Representation of Palaeomagnetic Directions

Techniques

1. Collection of Samples

Oriented rock samples have been collected using a Brunton compass and the simple instrument illustrated in Figure 65. This instrument, designed by Dr. R.W. Girdler, consists of a triangular table of perspex having a spirit level inset parallel to the base, and standing on three brass screws of equal length.

The sample is first hammered out of the rock and then carefully replaced in its original orientation. The triangle is then placed on the sample and its position adjusted until the spirit level is horizontal. In this position the base of the triangle defines a unique direction on the surface of the sample. This direction is marked on the sample and, using the compass, its bearing is taken. The slope of the table in a direction at right angles to the horizontal datum is also measured and recorded on the surface of the sample and finally the orientation of the table is defined by marking the positions of the legs on the surface.

The markings on a field sample are illustrated in Figure 66 where the arrow indicates the bearing of the horizontal datum line and the short line at right angles to this is the direction of slope.

2. Measurement of the NRM.

The directions of the NRM have been measured using an astatic magnetometer. In this instrument the magnetic field caused by the sample deflects a

Figure 65.

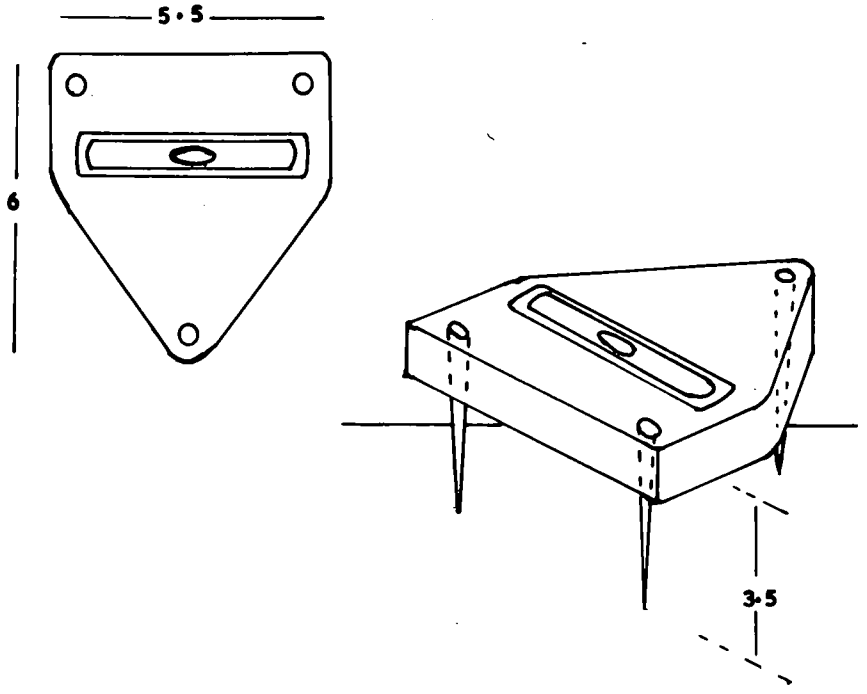

Figure 66.

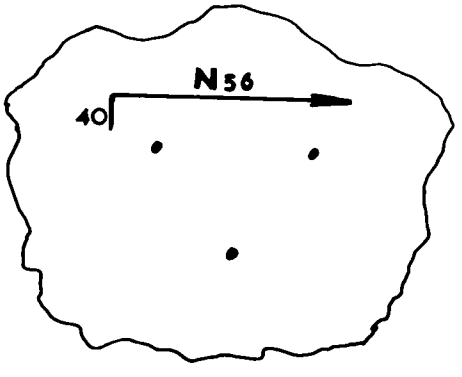

Figure 65.

Triangle used for obtaining oriented samples.

Figure 66.

Orientation marks on a sample. - Diagrammatic.

a sensitive magnet system hanging on a weak fibre. By measuring the deflections with the sample in different positions the declination (D) and inclination (I) of the magnetization can be determined, and by considering the amplitude of these deflections the intensity (J_n) can be determined.

A comprehensive discussion of the astatic magnetometer has been given by Blackett (1952) and Collinson, Creer, Irving and Runcorn (1957). Briefly, however, the condition for equilibrium of an astatic magnetometer in which two magnets of nearly the same magnetic moment P_1 and P_2 are set horizontally and antiparallel to each other (Figure 67) is given by:-

$$(P_1H_1 - P_2H_2)\sin\theta = (P_1 - P_2)H\sin\theta = \tau(\theta - \theta).$$

where θ = the angle between the axis of the magnet and the horizontal direction of the magnetic field.

H = the horizontal component of the geomagnetic field.

τ = the torsional constant of the suspension wire.

If the additional magnetic field, h, due to the magnetization of the sample is perpendicular to H, and affects only the P_1 - magnet, then the sensitivity of the system is given by:-

$$\frac{d\theta}{dh} = \frac{P_1 \cos\theta}{(P_1 - P_2)H\cos\theta + P_1 h \sin\theta + \tau}$$

and when $\theta \simeq 0$, then:-

$$\frac{d\theta}{dh} = \frac{1}{\left(1 - \frac{P_2}{P_1}\right)H + \frac{\tau}{P_1}}$$

Thus when $P_1 = P_2$ the sensitivity $d\theta/dh$ becomes P_1/τ and provided that H is uniform in the neighbourhood of the P_1 - and P_2- magnets then the

Figure 67.

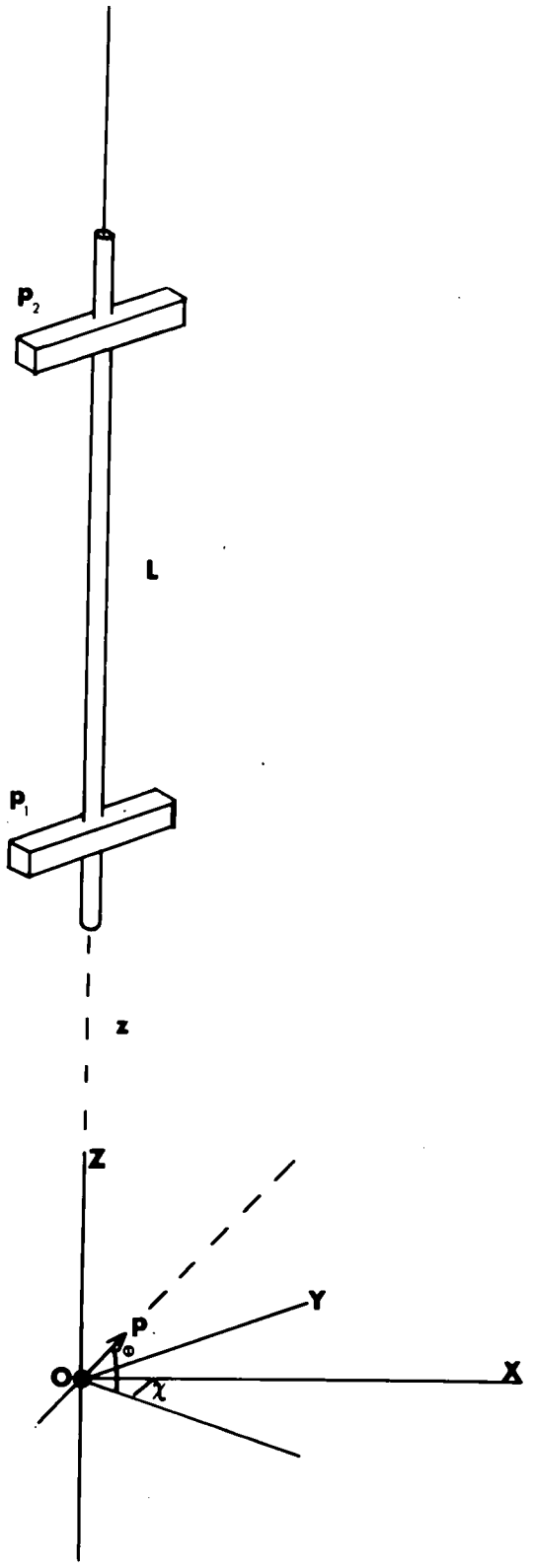

Figure 67.

The elements of an astatic magnetometer. (after Blackett 1952).

equilibrium state of the suspended system is not influenced by fluctuations in H.

In practice, however, fluctuations in H do tend to disturb the magnetometer. These fluctuations are usually of a heterogeneous nature and their effects can generally be ignored when measuring the NRM of strongly magnetized rocks. However, when measuring weakly magnetized sedimentary rocks, this noise can be a serious complication and special precautions are required to eliminate its effects.

If the size of the sample is small compared with the distance z from the lower magnet (P_1) of the astatic pair, then the magnetic field of the sample at the magnetometer can be represented by the field of a point dipole, p.

Let p lie on the axis of the magnetometer and at a distance z below the lower magnet, and let the distance between the two magnets L, be large compared with z so that only the lower magnet need be considered.

If the dipole p makes an angle φ with the horizontal, then its horizontal component will be $p_x = p\cos\varphi$ and the horizontal component at P_1 will be:-

$$H_x = \left(\frac{P}{z^3}x\right)\cos\chi$$

where χ is the angle with Ox made by the projection of p on the xOy plane.

If the dipole p is rotated in azimuth about the vertical axis, then the deflecting field at P_1 will be a simple harmonic function of azimuth, and from the amplitude of the measured field, together with the value of z and the measured sensitivity of the magnetometer, the value of p_x can be determined. In this way both the direction and magnitude of p_x can be determined, and similarly, by reorientating the sample beneath the magnetometer,

the components p_y and p_z can be determined.

Two magnetometers have been used during the present investigation, one at the Department of Physics, The University, Newcastle and the other at the Department of Geology, Durham.

Samples measured with the Newcastle magnetometer were first machined to the form of equidimensional cylinders 2.5cms high and 2.5cms in diameter, care being taken to preserve the field orientation marks (Collinson and Nairn 1960).

The direction of magnetization of a cylinder can be determined by rotating it, first about a vertical axis until maximum deflection is obtained and then about an horizontal axis, parallel to the magnetic axis of the system, until zero deflection is obtained. The magnetization vector is then vertical and its direction with respect to the orientation lines on the sample can be read directly. (Collinson et al 1957). It is then a simple matter to obtain the direction of the vector with respect to the present north and the horizontal plane.

The intensity of magnetization may be determined by comparing the deflection due to the cylinder with that caused by a field of known intensity, produced by a solenoid having the same dimensions as the cylinder. For a short solenoid, the magnetic field at the centre is given by:-

$$H = 4\pi ni \left(1 - \frac{a^2}{2l^2}\right)$$

where a = radius. l = half the length. n = number of turns and i = current. The standard coil used consisted of 9 turns of copper wire wound onto a perspex cylinder 2.5 cms high and 2.5 cms in diameter. Thus a = l and therefore the above expression reduces to:-

$$H = 2\pi ni$$

and for i = 5mA the field H is $2.828\ 10^{-2}$ Oe.

In general two or three cylinders have been cored from each field sample and the mean values of D,I and J_n taken.

The Durham magnetometer was constructed by Dr. R.W. Girdler, and is designed to measure the average NRM of the field sample without the need for coring.

Ideally the samples should be spheres so that the magnetometer always 'sees' the same cross-section irrespective of the orientation of the sample; further they should be small (hand-sized) and z (Figure 67) should be as large as possible so that the magnetization can be reduced to the effects of a dipole at the centre.

In practice, the sample is trimmed so as to be roughly equidimensional and then mounted in plaster of paris in such a way that it is approximately at the centre of a cube (Figure 68).

The sample is mounted so that the horizontal datum line obtained in the field is once again horizontal and is parallel to one side of the cubic mount. It is not necessary to restore the original slope at this stage however since this can be introduced into the calculations following the measurements.

The faces of the plaster cube are identified by the following, arbitrary, convention:

Face I..... is the uppermost face and contains the exposed surface of the sample (Figure 68)

Face II..... is the bottom of the cube.

Face III..... are the sides of the cube and are labelled

IV..... in clockwise rotation, taking Face III as

Figure 68.

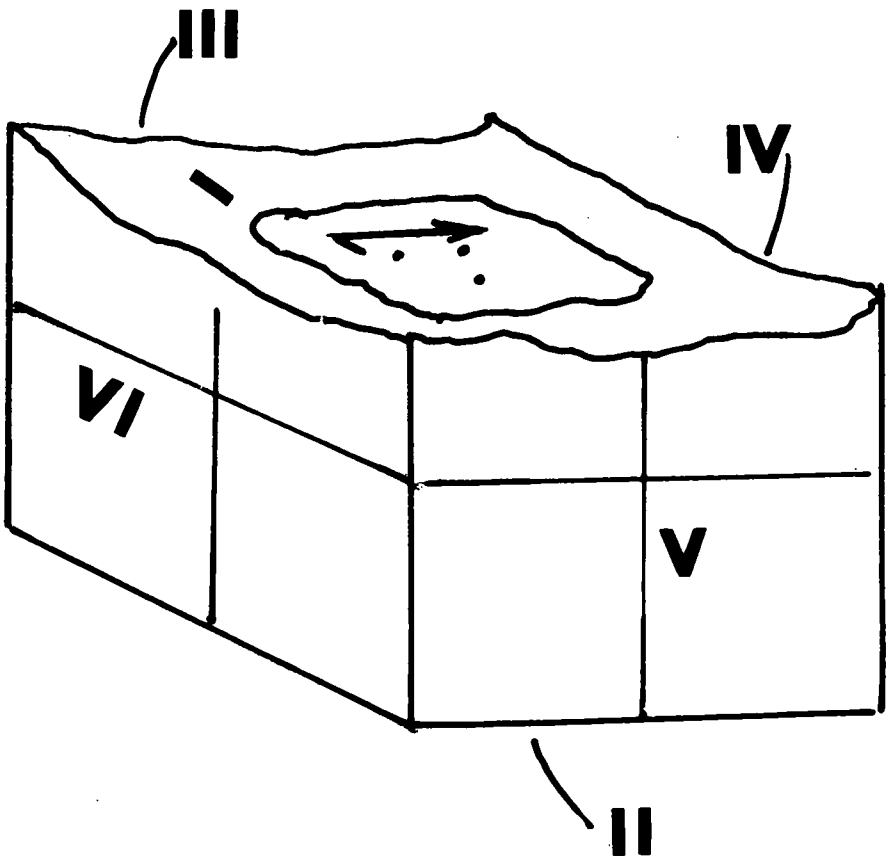

Figure 68.

An oriented sample mounted in plaster of paris.
- Diagrammatic.

V..... that one parallel to the horizontal datum

VI..... line and with the slope of the sample away from it.

The orientation of the dipole in relation to any one of these faces may be determined by placing this face uppermost beneath the magnetometer and rotating the sample about the vertical axis. This causes the deflections of the magnetometer to follow a sine curve e.g.:-

Azimuth	Measured Deflection		Corrected Deflection	
0	+40 mm		+40 mm	+
90	+44 mm	(+1)	+45 mm	+
180	+10 mm	(+3)	+13 mm	-
270	+ 3 mm	(+5)	+ 8 mm	-
0	+33 mm	(+7)	+40 mm	

The above magnetometer deflections have been amplified optically and measured on a centre-zero galvanometer scale placed about 5m from the instrument. The sign of these deflections has been taken, arbitrarily, as +ve when to the right of the scale zero and -ve when to the left, and the effects of drift, which have been assumed to be linear during the measuring period, have been eliminated by obtaining the deflection of the magnetometer with the sample at zero azimuth both at the beginning and end of the measuring sequence and then applying the appropriate correction factors.

If the face under investigation is visualized in terms of four quadrants, it can be seen that their are four possible deflection patterns for the magnetometer, according as to which quadrant contains the dipole, and that these patterns may be represented symbollically as:-

Azimuth				
0	+	-	-	+
90	+	+	-	-

Azimuth				
180	-	+	+	-
270	-	-	+	+

Thus, knowing the orientation of the lower magnet of the astatic pair at equilibrium, it is possible to decide into which quadrant the dipole is directed, and by considering the amplitudes of the deflections it is possible to determine the angular orientation of the dipole with respect to the face in question.

It is a simple matter, therefore, to construct a table relating the pattern of deflections obtained for a given face to the orientation of the dipole with respect to that face, and the data applicable to the present instrument are summarized in Table 42.

The deflection patterns for face II have been omitted from this table because this data cannot be obtained in practice owing to the irregular surface of face I.

The use of this table can best be explained by considering a specific example.

Figure 69 shows a sample oriented beneath the magnetometer with face I uppermost and in the position of zero azimuth. By definition, the zero azimuth for this face is taken as that position in which face III is parallel to the geo-magnetic north-south direction and facing towards the east. By convention, north is considered as the +X direction, east as the +Y direction and +Z as vertically upwards.

Figure 69 also shows the orientation of the lower magnet of the astatic pair and the orientation of the dipole. Therefore, with the sample in this position, the magnetometer will give a +ve deflection on the scale. If

Table 42.

Deflection Patterns for the Astatic Magnetometer.

	Azimuth				
Face I	0	+	-	-	+
dy/dx	90	+	+	-	-
	180	-	+	+	-
	270	-	-	+	+
		NE	SE	SW	NW
Face III	0	+	+	-	-
dz/dx	90	+	-	-	+
	180	-	-	+	+
	270	-	+	+	-
		ND	NU	SU	SD
Face IV	0	+	+	-	-
dz/dy	90	+	-	-	+
	180	-	-	+	+
	270	-	+	+	-
		ED	EU	WU	WD
Face V	0	+	+	-	-
dz/dx	90	+	-	-	+
	180	-	-	+	+
	270	-	+	+	-
		SD	SU	NU	ND
Face VI	0	+	+	-	-
dz/dy	90	+	-	-	+
	180	-	-	+	+
	270	-	+	+	-
		WD	WU	EU	ED

Figure 69.

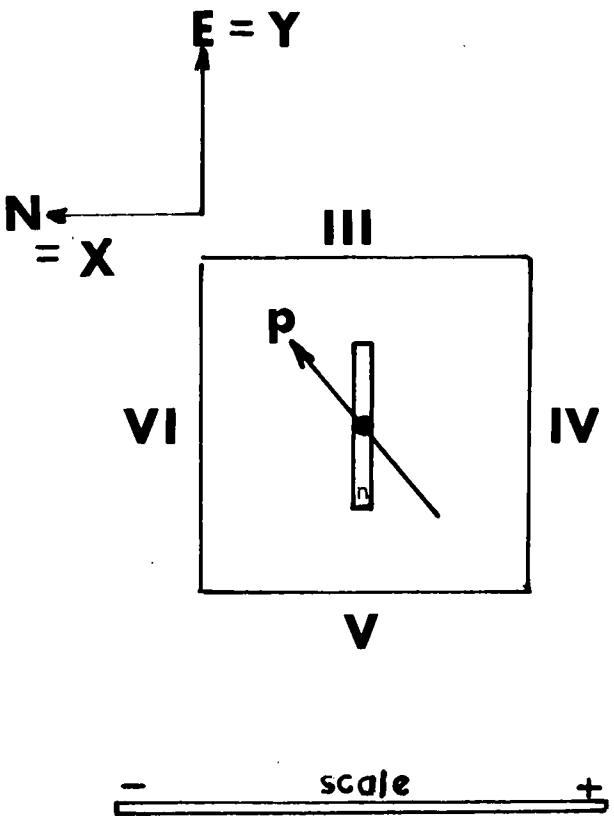

Figure 70.

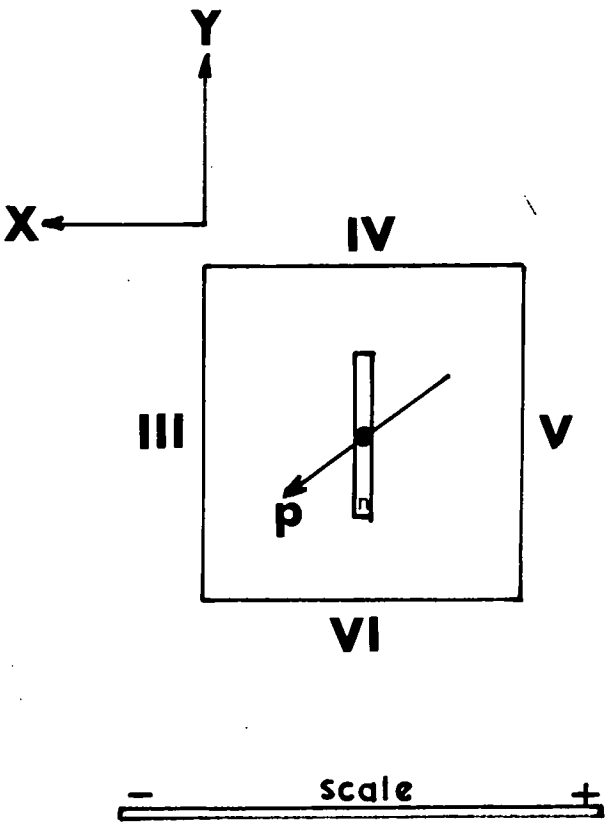

Figure 71.

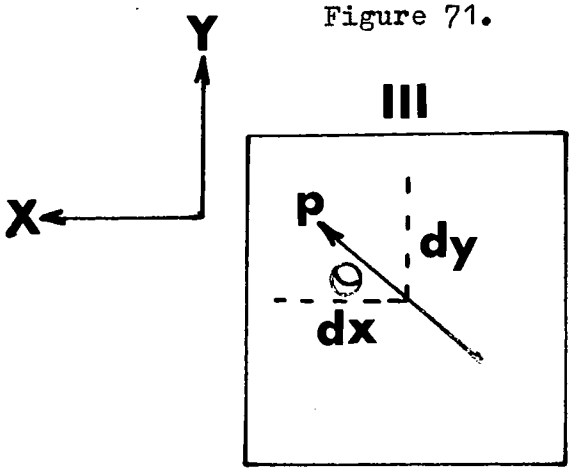

Figure 69.

An oriented sample seen vertically beneath the magnetometer and at zero azimuth.

Figure 70.

An oriented sample seen vertically beneath the magnetometer and at 90° azimuth.

Figure 71.

The angular orientation of the dipole in the sample - Diagrammatic.

the sample is rotated 90° anticlockwise (Figure 70), the magnetometer will still give a +ve deflection, but clearly, -ve deflections will be obtained for the remaining two measurements, so that the deflection pattern will be:

Azimuth	Deflection
0	+
90	+
180	-
270	-

thus showing that the dipole is directed into the north-east quadrant.

The angular orientation of the dipole within this quadrant is given by:

$$dy/dx = \tan \theta$$

where dy is the algebraic difference between the deflections obtained at 90° and those obtained at 270°, and dx is the algebraic difference between the deflections at 0° and 180° (Figure 71).

One component of the vector is thus identified but it is not known whether it points up out of the sample or down below it. This can be determined, however, by measuring its orientation with respect to the sides of the cube, i.e. faces III to VI.

The procedure adopted for these faces is the same as for face I, except that the position of zero azimuth is defined as that position in which the exposed sample (face I) faces towards the west. Each face is measured by rotating it anticlockwise beneath the magnetometer and noting the pattern

and magnitude of the deflections produced. These deflections show whether the dipole is pointing up or down towards the north or up or down towards the south (faces III and V) and whether it is directed up, or down to the east or up or down to the west (faces IV and VI). The angular relations are given by dz/dx for faces III and V, and by dz/dy for faces IV and VI, where dz is the algebraic difference between the deflections at 90° and 270° and dx and dy are the algebraic differences between the deflections at 0° and 180°.

The orientation of the dipole with respect to the whole sample is defined by the co-ordinates Δx, Δy and Δz where these represent the sums of dx, dy and dz respectively, obtained for each face.

By convention:

North = +X = + x.

South = -X = - x

East = +Y = + y

West = -Y = - y

Up = +Z = + z

Down = -Z = - z

Thus, $\Delta y/\Delta x = \tan\theta$ = declination whilst $\Delta z/\Delta x = \tan\varphi_1$ and $\Delta z/\Delta y = \tan\varphi_2$ together define the inclination. These angular relationships are shown stereographically in Figure 72. They do not, however, give the palaeomagnetic direction but must be adjusted in relation to the field orientation of the sample.

In the simplest case, the arrow on the horizontal datum line will already point north when face I is at the zero azimuth position and in this case the angle $\Delta y/\Delta x = \tan\theta$ needs no correction for it is measured from magnetic

Figure 72.

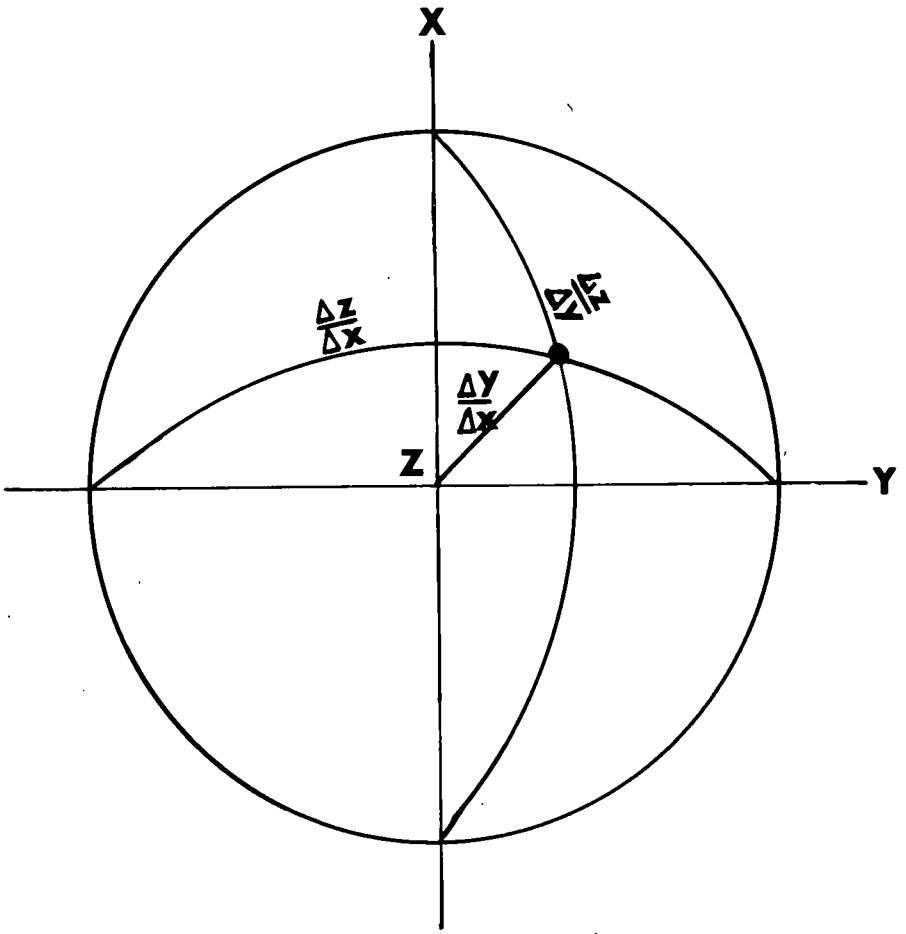
X
Y
Z
$\frac{\Delta z}{\Delta x}$
$\frac{\Delta z}{\Delta y}$
$\frac{\Delta y}{\Delta x}$

Figure 72.

Stereographic representation of the angular orientation of a dipole.

Figure 73.

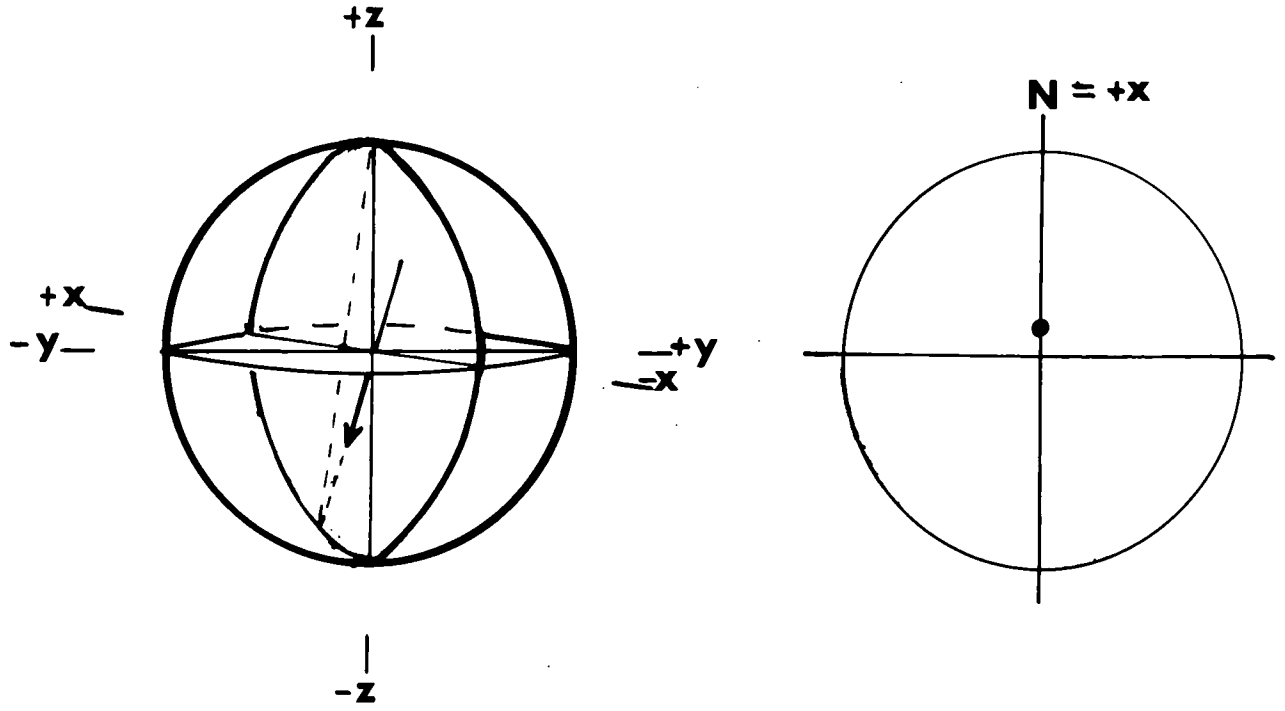

Figure 74.

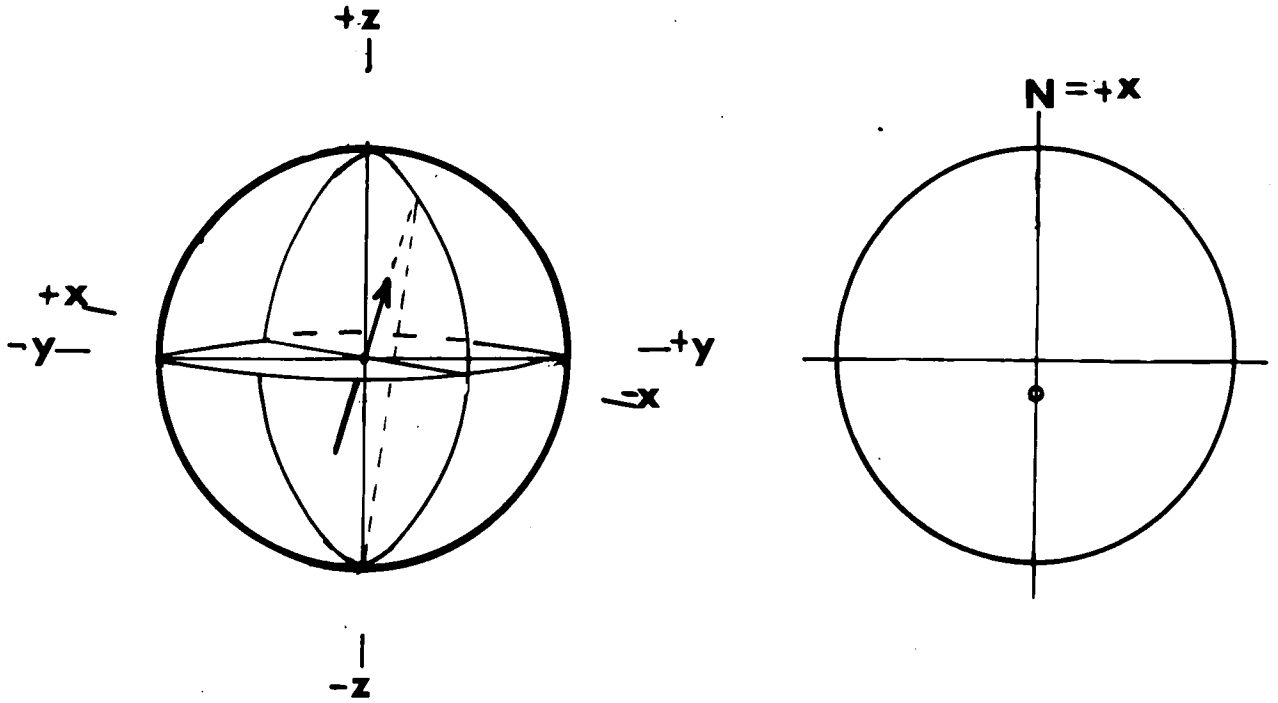

Figure 73.

Stereographic representation of normal magnetization.

Figure 74.

Stereographic representation of reverse magnetization.

north. If, however, the arrow points south then this angle must be adjusted by 180° in order to refer to magnetic north, or possibly the datum line will be at some small angle to the north-south direction when face I is at 0° in which case a different correction will be needed.

It is also most unlikely that the slope of the mounted sample is that of the original field orientation, and hence even when the declination is corrected as above it will not give the true palaeomagnetic direction. The true declination and inclination must be obtained by rotating the sample about the horizontal datum line as axis so that the original slope is restored, and then relating the magnetic vector to this new orientation.

This may be done stereographically (see Phillips 1954) by moving the vector along a small circle perpendicular to the bearing of the datum line, the number of degrees moved being the difference between the slope of the sample as mounted in plaster and the original slope as measured in the field. When this is done a new vector is defined which is the true direction of the NRM, the co-ordinates being related to the present magnetic north and to the horizontal.

3. Representation of the NRM.

The direction of the NRM of a sample may be represented as a point on a stereogram. Since the interpretation of palaeomagnetic directions depends on the grouping of many such sample directions, however, the simple Wulff, or equal-angle, projection (commonly employed in crystallography) is not generally used because it is not area-true. Instead the Lambert equal-area projection (Schmidt net) is customarily employed.

The device of stereographic projection is a very ancient one, already in use in Greece by the second century B.C., which has been developed primarily

by crystallographers. (Phillips 1954). Only in recent times has this technique been adopted by structural geologists and others.

By convention, crystallographers use the projection in terms of an upper hemisphere; however, it has been found that in most geological problems it is preferable to project in terms of the lower hemisphere and this convention has become firmly established both in the fields of structural geology and structural petrology.

The direction of NRM, however, differs from those elements handled by crystallographers and structural geologists alike in that it is a vector, which is always considered in terms of its north-seeking pole. Hence the stereographic projection of NRM may be obtained either from the upper or the lower hemisphere depending on the direction of this pole.

Thus, if the north-seeking pole is directed downwards (Figure 73) then its projection is obtained from the lower hemisphere, and by convention, is represented as a solid circle. If, however, the north-seeking pole is directed above the horizontal then its projection is obtained from the upper hemisphere and is represented by an open circle. (Figure 74).

A fair representation of the earth's magnetic field may be obtained by assuming it to be due to a magnet at the centre with the magnetic poles where the axis intersects the earth's surface. On this basis it can be seen that, at the present time, the magnetic vector points below the horizontal in the northern hemisphere and above it in the southern hemisphere. This condition is defined as normal.

Hence, if the NRM of rocks collected from the northern hemisphere is directed below the horizontal then the rocks are said to be Normally Magnetized and may be represented as solid circles on the stereogram. However, many rocks have been found to have directions of magnetization above the horizontal

and these are, therefore, said to be Reversely Magnetized and are represented by open circles on the stereogram.

4. Analysis of the Direction of NRM

Fisher (1953) has developed a method for the statistical interpretation of palaeomagnetic data. In this method each direction is given unit weight and there is no weighting in favour of more intensely magnetized samples.

In order rigorously to justify the use of Fisher statistics the population from which the sample is drawn must satisfy two conditions:

1. The vectors in the population must be distributed with axial symmetry about their mean direction.

2. The density of the vectors in the population must decrease with increasing angular displacement from the main direction according to the probability density function -

$$P = \frac{k}{4\pi \sinh k} \cdot \exp(K \cos \psi)$$

where k describes the tightness of the group of vectors and is called the precision parameter. High values of k indicate tight groups and k=0 corresponds to a population uniformly distributed over the entire surface of the unit sphere.

Provided these conditions are satisfied Fisher has shown that the best estimate of the true mean direction of the population is given by the direction of the vector sum of the N unit vectors.

If the i^{th} unit vector has declination D_i east of north and inclination I_i below the horizontal, then the mean direction may be calculated from

the relations:

$$Z = \sum_{i=1}^{N} \sin I_i \qquad \text{(Downward component)}$$

$$X = \sum_{i=1}^{N} \cos I_i \cos D_i \qquad \text{(North component)}$$

$$Y = \sum_{i=1}^{N} \cos I_i \sin D_i \qquad \text{(East component)}$$

$$R = (X^2 + Y^2 + Z^2)^{1/2}$$

$$\sin I_R = \frac{Z}{R}$$

$$\tan D_R = \frac{Y}{X}$$

where Z,X and Y are the components of the resultant vector, R its unit length and D_R and I_R its declination and inclination respectively.

The best estimate of the precision parameter is given by:

$$k = \frac{N - 1}{N - R} \qquad \text{for } k > 3$$

and the true mean direction of the population, at a probability level of (1 - P), lies within a circular cone about the resultant vector R with a semivertical angle $\alpha_{(1-P)}$, given for $k > 3$, by:-

$$\cos\alpha_{(1-P)} = 1 - \frac{N - R}{R}\left[\left(\frac{1}{P}\right)^{\frac{1}{N-1}} - 1\right]$$

In palaeomagnetic analysis P is usually taken as 0.05, which means

that there is 1 chance in 20 that the true mean direction of the population lies outside the "cone of confidence" specified by α_{95} and the direction of R.

The following approximate relationships are valid for small values of α :

$$\alpha_{50} = \frac{67.5^{\circ}}{kN} \qquad (P = 0.05)$$

$$\alpha_{95} = \frac{140^{\circ}}{kN} \qquad (P = 0.05)$$

Bibliography

Ade-Hall J. and Wilson R.L.	1963	Petrology and the Natural Remanence of the Mull Lavas. Nature 198 p.659.
Akimoto S.	1954	Thermomagnetic Studies of Ferromagnetic Minerals Contained in Igneous Rocks. J. Geomagn. Geoelect., Kyoto. VI. pp.1-14.
	1955	Magnetic Properties of Ferromagnetic Minerals Contained in Igneous Rocks. Jap. J. Geophys. 1 No.2.
	1957	Magnetic Properties of Ferromagnetic Oxide Minerals as a Basis of Rock Magnetism. Adv. Phys. 6 No.23. pp.288-98.
	1962	Magnetic Properties of $FeO-Fe_2O_3-TiO_2$ System as a Basis of Rock Magnetism. J. Phys. Soc. Japan. 17. Suppl. B-I.
Akimoto S. and Katsura T.	1959	Magnetochemical Study of the Generalized Titanomagnetite in Volcanic Rocks. J. Geomagn. Geoelect. Kyoto 10 pp.69-90.
Akimoto S., Katsura T. and Yoshida M.	1957	Magnetic Properties of the $TiFe_2O_4-Fe_3O_4$ System and their Change with Oxidation. J. Geomagn. Geoelect. Kyoto IX. No.4 pp.165-78.
Akimoto S. and Kushiro I.	1960	J. Geomagn. Geoelect. Kyoto 11 p.94.
Almond M., Clegg J.A. and Jaeger J.C.	1956	Remanent Magnetism of some Dolerites, Basalts and Volcanic Tuffs from Tasmania. Phil. Mag. Ser. 8 1 pp.771-82.
Anderson E.M.	1935	The Dynamics of the Formation of Cone-sheets, Ring-dykes and Cauldron-subsidences. Proc. roy. Soc. Edinb. LVI. p.128.
Anderson P.W.	1950	Phys. Rev. 79 p.350.
Bailey E.B. et al.	1924	Tertiary and Post-Tertiary Geology of Mull. Loch Aline and Oban. Mem. geol. Surv. U.K.

Barringer A.R. 1953 The Preparation of Polished Sections of Ores and Mill Products using Diamond Abrasives, and their Quantitative Study by Point Counting Methods. Institut. Min. Met. Trans. 63 pp.21-41.

Barth T.W.F. and Posnjak E. 1932 Spinel Structures: with and without Variate Atom Equipoints. Z. Kristallogr. 82. p.325.

Basta E.Z. 1953 Mineralogical Aspects of the System $FeO-Fe_2O_3-TiO_2$. Ph.D. thesis. Bristol University.

1957 Accurate Determination of the Cell Dimensions of Magnetite. Miner. Mag. 31 p.431.

1959 Some Mineralogical Relationships in the System $Fe_2O_3-Fe_3O_4$ and the Composition of Titanomaghemite. Econ.Geol. 54 p.698.

1960 Natural and Synthetic Titanomaghemites. (The System $Fe_3O_4-Fe_2TiO_4-FeTiO_3$). Neues. Jb. Miner. Abt. 94 p.1017.

Bastin E.S. 1950 Interpretation of Ore Textures. Mem. geol. Soc. Amer. 45.

Benard J. and Chaudron G. 1937 Preparation de Ferrites par Substitution des Ions Ferraux dans la Magnetite. C.R. Acad. Sci. Paris. 204. p.766.

Berry L.G. and Thompson R.M. 1962 X-Ray Powder Data for Ore Minerals. The Peacock Atlas. Mem.geol.Soc.Amer. 85.

Blackett P.M.S. 1952 A Negative Experiment Relating to Magnetism and the Earth's Rotation. Phil.Trans. ser.A. 245. pp.303-70.

Blackett P.M.S., Clegg J.A. and Stubbs P.H.S. 1960 An Analysis of Rock Magnetic Data. Proc. roy.Soc. ser.A. 256 pp.291-322.

Bowie S.H.U. and Taylor K. 1958 A System of Ore Mineral Identification. Min. Mag. pp.2-23.

Bragg W.H. 1915 The Structure of the Spinel Group. Phil.Mag. 30.

Brailsford F.	1960	Magnetic Materials. Methuen. London. 181 pp.
Cameron E.N.	1959	The Study of Opaque Minerals in Reflected Light. Preprint A.S.T.M.
Carmichael C.W.	1961	The Magnetic Properties of Ilmenite-Haematite Crystals. Proc.roy.Soc. Ser.A. 263. pp.508-30.
Chevallier R., Bolfa J., et Mathieu S.	1955	Titanomagnetites et Ilmenites Ferromagnetiques. Bull.Soc.franc. Miner. LXXVIII. pp.307-46.
Chevallier R. et Girard J.	1950	Synthese des Titanomagnetites Bull.Soc.chim. Paris. nos.5-6.
Chevallier R. et Mathieu S.	1943	Proprietes Magnetiques des Poudres d/Hematites. Ann.Phys. ser. 11. 18-19.
Chevallier R., Mathieu S. and Vincent E.A.	1954	Iron-titanium Oxide Minerals in Layered Gabbros of the Skaergaard Intrusion, East Greenland. Pt.II - Magnetic Properties. Geochim. et Cosmoch. Acta. 6 pp.27-34.
Collinson D.W., Creer K.M., Irving E., and Runcorn S.K.	1957	The Measurement of the Permanent Magnetization of Rocks. Phil. Trans. Ser. A. 250 p.73.
Collinson D.W. and Nairn A.E.M.	1960	A Survey of Palaeomagnetism. O.G.S. Miner. Resources Div. H.M.S.O. London.
Coombs D.S. and Hatherton T.	1959	Palaeomagnetic Studies of Cenozoic Volcanic Rocks in New Zealand. Nature 184 p.883.
Corliss L.M., Hastings J.M. and Brockman F.G.	1953	A Neutron Diffraction Study of Magnesium Ferrite. Phys. Rev. 90 p.1013.
Cox A. and Doell R.R.	1960	Review of Palaeomagnetism. Bull. geol.Soc.Amer. 71 pp.645-768.
Creer K.M.	1957	Palaeomagnetic Investigations in Great Britain: V. The Remanent Magnetism of Unstable Keuper Marls. Phil.Trans. Ser. A. no.974. 250 pp.130-43.

Creer K.M.	1958	Preliminary Palaeomagnetic Measurements from South America. Ann. Geophys. 14. pp.373-90.
Creer K.M., Irving and Nairn A.E.M.	1959	Palaeomagnetism of the Great Whin Sill. Geophys. J. roy. Astron. Soc. 2 No.4 pp.306-23.
Clark G.L., Ally A. and Badger A.E.	1931	The Lattice Dimensions of Spinels. Amer.J.Sci. 22 pp.539-46.
Deer W.A., Howie R.A. and Zussman J.	1962	Rock Forming Minerals Vol. 5 - Non-silicates. Longmans. London.
Deutsch E.R.D., Radakrishnamurty C. and Sahasrabudhe P.W.	1958a	The Remanent Magnetism of some Lavas in the Deccan Traps. Phil. Mag. 3 No.26. p.170.
	1958b	Remanent Magnetism of the Rajmahal Traps of North-east India. Nature 181 pp.830-31.
Edwards A.B.	1938	Some Ilmenite Microstructures and their Interpretation. Australian Instit. Min. Met. Proc. 110 pp.39-58.
	1947	Textures of the Ore Minerals and their Significance. Melbourne. (Australian Instit. Min. Met. Inc.).
Einarsson T. and Sigurgeirsson T.	1955	Rock Magnetism in Iceland. Nature 175 p.892.
Ernst T.	1943	Z.Angew. Min. 4. p.349.
Everrit C.W.F.	1960	Rock Magnetism and the Origin of the Midlands Basalt. Geophys. J. roy. Astron.Soc. 3 No.2. pp.203-10.
Fisher R.A.	1953	Dispersion on a Sphere. Proc. roy.Soc. ser.A. 217 pp.295-305.
Ford W.E.	1958	Dana's Textbook of Mineralogy 4th Edit. Wiley. London.
Frost I.C.	1959	An Elutriating Tube for the Specific Gravity Separation of Minerals. Amer. Min. 44. pp.886-90.

Fuller M.D.	1960	Anisotropy of Susceptibility and the Natural Remanent Magnetization of some Welsh Slates. Nature. 186 p.791.
Goldschmidt I.M.	1954	Geochemistry: Oxford Clarendon Press.
Gorter E.W.	1957	Chemistry and Magnetic Properties of some Ferrimagnetic Oxides like those occurring in Nature. Adv.Phys. 6 pp.336-361.
Gorter E.W. and Schulkes J.A.	1953	Phys. Rev. 89 p.487.
Grabovsky M.A. and Pushkov A.H.	1954	Izvest. Akad.Nauk. SSSR. ser. geofiz. 320.
Graham J.W.	1952	J.geophys. Res. 57 p.429.
	1953	Changes of Ferromagnetic Minerals and their Bearing on the Magnetic Properties of Rocks. J.geophys. Res. 58 pp.243-60.
Gray I.M. and Millman A.B.	1962	Reflection Characteristics of Ore Minerals. Econ.Geol. 57 pp.325-49.
Greenwald S., Pickart S.J. and Grannis F.H.	1954	Cation Distribution and g Factors in Certain Spinels Containing Ni^{++}, Mn^{++}, Co^{++}, Al^{+++}, Ga^{+++} and Fe^{+++}. J.chem.Phys. 22 pp.1597-1600.
Guiot-Guillain G., Pauthenet R. and Forestier H.	1954	Etude Thermomagnetique des Ferrites de Dysprosium et d'Erbium. C.R. Acad.Sci. Paris. 239 p.155.
Hägg G.	1935	Die Kristallstruktur des magnetischen Ferrioxyds γ-Fe_2O_3 and γ-Al_2O_3. Z.phys.Chem. 29B p.95.
Haigh G.	1958	The Process of Magnetization by Chemical Change. Phil.Mag. 3 pp.267-86.
Hall J.M. and Neale R.N.	1960	Stress Effects of Thermoremanent Magnetization. Nature 188. pp.805-6;843.
Harker A.	1904	The Tertiary Igneous Rocks of Skye. Mem.geol.Surv.U.K.

Hastings J.M. and Corliss L.M. 1953 Neutron Diffraction Studies of Zinc Ferrite and Nickel Ferrite. Rev.Mod.Phys. 25 p.114.

Henry N.F.M., Lipson H. and Wooster W.H. 1951 The Interpretation of X-Ray Diffraction Photographs. MacMillan. London.

Hospers J. 1953-1954 Reversals of the Main Geomagnetic Field: Koninkl. Nederlandse Akad. Wetensch Proc. of Section on Sciences, ser.B. Phys. Sci. Part I and II (1953) 56. pp.426-76; 477-91. Part III (1954) 57. pp.112-21.

Howie R.A. 1955 The Geochemistry of the Charnockite Series of Madras, India. Trans. roy.Soc. Edinb. 62 p.725.

Irving E. and Green R. 1957 The Palaeomagnetism of the Kainozoic Basalts of Victoria. Roy.Astron.Soc.Monthly Notices. geophys.Suppl. 7. pp.347-59.

Ishikawa I. and Akimoto S. 1957 Magnetic Properties of the $FeTiO_3$-Fe_2O_3 Solid Solution Series. J. phys.Soc.Japan. 12 p.1083.

1958 Magnetic Properties and Crystal Chemistry Ilmenite ($MeTiO_3$) and Hematite (Fe_2O_3) System. I. Crystal Chemistry. J.phys.Soc.Japan 13 pp.1110;1298.

Jacobson R.R.E., MacLeod W.N. and Black R. 1958 Ring Complexes in the Younger Granite Province of Northern Nigeria. Mem.geol.Soc.London. no.1.

Jaeger J.C. 1957 The Temperature in the Neighbourhood of a Cooling Intrusive Sheet. Amer. J.Sci. 255 pp.306-318.

Johansson K. 1928 Mineralogische Mitteilungen. Z.Kristallogr. 68 p.87.

Katsura T. and Kushiro I. 1961 Titanomaghemite in Igneous Rocks. Amer. Min. 46 p.134.

Kawai N. and Kume S. 1953 J.Geomagn. Geoelect., Kyoto. 5 p.67.

Kawai N, Kume S. and Sasajima S.	1956	Proc.imp.Acad.Japan. 32 p.459.
Kawai N. and Yong-Ho Kang	1962	Magnetism of Black Shales and Red Sandstones in Japan. J. Geomagn. Geoelect. Kyoto XIII. pp.80-83.
Khramov A.W.	1957	Palaeomagnetism - the Basis of a New Method of Correlation and Subdivision of Sedimentary Strata. Akad. Nauk.SSSR. Dokadly ser.geol. 112 pp.849-52 (in Russian). (English Translation - Consultants Bureau Inc. 1958).
Klug H.P. and Alexander L.E.	1954	X-Ray Diffraction Procedures for Polycrystalline and Amorphous Materials. Wiley. N.Y.
Kobayashi K.	1961	J. Geomagn. Geoelect. Kyoto. 12 p.148.
Königsberger J.G.	1938	Terr.Mag. 43 pp.119-229.
Larochelle A.	1961	Design of a Curie Point Meter. Bull.geol.Surv.Canada. 69.
Lindsley D.H.	1962	Investigations in the System $FeO-Fe_2O_3-TiO_2$. Ann.rep. Director Geophys. Lab. Carnegie Instit. Washington.
Mason B.	1943	Geol.Fören. Förhandl. 65 p.95.
Mehl R.F. and Barret C.S.	1930	Studies upon Widmanstätten Structure. Amer. Instit. Min. and Mech. Eng. Tech. Publ. 353.
Michel A. and Chaudron G.	1935	C.R. Acad. Sci.Paris. 201 p.1191.
Millman A.P.	1957	Reflection Microscopy of Ferro-magnetic Minerals. Phil.Mag. Suppl. 6 no.23. p.323.
Miller J.A. and Harland W.B.	1963	Ages and Some Tertiary Intrusive Rocks in Arran. Miner. Mag. 33 pp.521-3.
Mogensen F.	1946	A Ferro-orthotitanate Ore from Södra Ulvon. Geol. fören. Stockholm Förh. 68 p.578-88.
Nagata T.	1943	Bull.Earthquake Research Instit. 21 pl.

Nagata T.	1961	Rock Magnetism. Maruzen. Tokyo. Japan. 331pp.
Nagata T., Akimoto S. and Uyeda S.	1953	J. Geomagn. Geoelect. Kyoto. 5 p.168.
Nagata T., Akimoto S., Uyeda S., Shimizu Y., Ozima M., Kobayashi K. and Kuno H.	1957	Palaeomagnetic Studies in a Quaternary Volcanic Region in Japan. J. Geomagn. Geoelect. Kyoto. 9. pp.23-41.
Nagata T., Uyeda S. and Ozima M.	1957	Magnetic Interaction between Ferromagnetic Minerals Contained in Rocks. Adv.Phys. 6 no.23. pp.264-87.
Nagata T. and Yama-ai M.	1961	Antarctic Record Japan no.11. p.945.
Nairn A.E.M.	1957	Palaeomagnetic Collections from Britain and South Africa Illustrating Two Problems of Weathering. Adv.Phys. 6 pp.162-8.
Néel L.	1948	Ann.Phys. 3 p.137.
	1949	Ann.Geophys. 5 p.99.
	1951	L'Inversion de L'Aimantation Permanente des Roches. Ann.Geophys. 7. pp.90-102.
	1952	Confirmation Experimentale d'un Mecanisme d'Inversion de l'Aimantation Thermoremanente. C.R. Acad.Sci. Paris. 234 p.1991.
	1953	Some New Results on Antiferromagnetism and Ferromagnetism. Rev.mod.Phys. 25 p.58.
	1955	Some Theoretical Aspects of Rock Magnetism. Adv.Phys. 4. pp.191-243.
Néel L. and Pauthenet R.	1952	Etude Thermomagnetique d'un Monocristal de Fe_2O_3. C.R. Acad.Sci. Paris. 234 pp.2172-74.
Newhouse W.H.	1936	Opaque Oxides and Sulphides in Common Igneous Rocks. Bull. geol.Soc.Amer. 47 pp.1-52.

Newhouse W.H. and Glass J.J.	1936	Some Physical Properties of Certain Iron Oxides. Econ.Geol. 31 p.699.
Nicholls G.D.	1955	The Mineralogy of Rock Magnetism. Adv. Phys. 4 pp.113-90.
Nicholl I.	1962	A Study of some Opaque Manganese Minerals. Ph.D thesis University of Durham.
" Ödman O.H.	1932	Mineragraphic Study of the Opaque Minerals in the Lavas from Mt. Elgon, British East Africa. - Geol.Fören.Förhandl. 54 p.285-304.
Palache C.	1910	Contributions to the Mineralogy of Franklin Furnace N.J. Amer.J.Sci. 4th ser. 29. p.177.
Peiser H.S., Rooksby H.P. and Wilson A.J.C.	1955	X-Ray Diffraction by Polycrystalline Materials. Instit. Phys.
Phillips F.C.	1954	The Use of Stereographic Projection in Structural Geology. Edward Arnold Ltd. London 73pp.
Posnjak E. and Barth T.W.F.	1934	Notes on Some Structures of the Ilmenite Type. ZKristallogr. 88 p.271.
Pouillard E.	1950	Sur le Comportment de l'Alumine et de l'Oxyde de Titane-Vis-a-Vis des Oxydes de Fer. Ann.Chim. 5 p.164.
Pouillard E. et Michel A.	1949	Etudes des Composes Defines et des Solutions Solides que Peuvent Former l'Oxyd de Titane TiO_2 et les Oxydes de Fer. C.R. Acad.Sci.Paris 288 p.1232.
Radtke A.S.	1962	Coulsonite FeV_2O_4. A Spinel - type Mineral from Lovelock, Nevada. Amer.Min. 47. pp1284-9
Ramdohr P.	1953	Ulvöspinel and its Significance in the Titaniferous Iron Ores. Econ.Geol. 48 no.81. pp677-88.

Richey J.E. et al	1930	The Geology of Ardnamurchan, North-west Mull and Coll. Mem.geol. Surv.U.K.
Roche A.	1956	Sur la Date de la Derniere Inversion du Champ Magnetique Terrestiere. C.R. Acad.Sci.Paris 243 pp.812-14.
Runcorn S.K.	1956	Palaeomagnetic Survey in Arizona and Utah: Preliminary Results. Bull.geol.Soc.Amer. 67 pp.301-316.
	1962	Palaeomagnetic Evidence for Geomagnetic Field Reversals and Continental Drift. J. Geomagn. Geoelect.Kyoto. XIII. pp.84-5.
Schmahl N.G. and Meyer G.	1959	Uber Eisentitanate in Bereicht direkt messbarer Sauerstoffdrucke. Metall. 13 p.1114.
Schwartz G.M.	1931	Textures due to Unmixing of Solid Solutions, Econ.Geol. 26. pp.739-63.
	1951	Classification and Definition of Textures and Mineral Structures in Ores. Econ.Geol. 46 p.578.
Shirane G., Pickart S., Nathan R. and Ishikawa Y.	1959	J. phys.Chem.Solids 10 p.35.
Shull C.G., Wollan E.O. and Koehler W.C.	1951	Neutron Scattering and Polarization by Ferromagnetic Materials. Phys. Rev. 84 p.912.
Soren R.K.	1960	X-Ray Diffraction Technique for Small Samples. Amer. Min. 45 p.1104.
Stacey F.D.	1958	Thermoremanent Magnetization (TRM) of Multidomain Grains in Igneous Rocks. Phil.Mag. ser.8. 3 p.1391.
Takeuchi T. and Nambu N.	1958	Maghemite from Takonokura mine, Fukushima Prefecture. J. Miner. Soc. Japan. 3 p.486.
Taylor R.W.	1961	An Experimental Study of the System $FeO-Fe_2O_3-TiO_2$, and its Bearing on Mineralogical Problems. Ph.D thesis. Penn. State Univ.

Teall J.J.H. 1888 British Petrography. Dulau and Sons. London.

Tomkeieff S.I. 1961 Isle of Arran. Geol.Assoc. Guide No.32.

Tomkeieff S.I. and Longstaff M. 1960 The Magmatic Complex at Kingscross Point, Isle of Arran. Trans.geol. Soc.Edinb. XVIII. pp.194-201.

Tschermak G. 1869 Die Porphyrgesteine Österreich Wien. (quoted in Teall 1888, p.359).

Turner F.J. and Verhoogen J. 1961 Igneous and Metamorphic Petrology 2nd Edit. McGraw-Hill 672pp.

Tyrrel G.W. 1928 The Geology of Arran. Mem.geol.Surv. U.K.

Uyeda S. 1958 Thermo-remanent Magnetism as a Medium of Palaeomagnetism, with Special Reference to Reverse Thermo-remanent Magnetism. Jap.J.Geophys. 2 pp.1-123.

Uytenbogaardt W. 1951 Tables for Microscopic Identification of Ore Minerals. Princeton Univ. Press.

Van Vleck J.H. 1945 A Survey of the Theory of Ferromagnetism. Rev.mod.Phys. 17 p.27.

Verhoogen J. 1956 Ionic Ordering and Self-Reversal of Magnetization of Impure Magnetites. J.geophys.Res. 61 pp.201-9.

1959 The Origin of Thermoremanent Magnetization. J.geophys.Res. 64 pp.2441-2449.

1962 Oxidation of Iron-titanium Oxides in Igneous Rocks. J.Geol. 70 no.2.

Verwey E.J.W. 1935 The Crystal Structure of γ-Fe_2O_3 and γ-Al_2O_3. Z.Kristallogr. 91 p.65.

Verwey E.J.W. and Heilmann F.L. 1947 Physical Properties and Cation Arrangement of Oxides with Spinel Structures.
I - Cation Arrangement in Spinels. J.chem.Phys. 15 p.174.

Vincent E.A. 1960 Ulvöspinel in the Skaergaard Intrusion East Greenland. Neues. Jb. Miner. Abt. 94 p.993.

Vincent E.A. and Phillips R. 1954 Iron-titanium Oxide Minerals in Layered Gabbros of the Skaergaard Intrusion, East Greenland. Geochim. et cosmoch. Acta 6 pp.1-26.

Vincent E.A., Wright J.B., Chevallier R. and Mathieu S. 1957 Heating Experiments in some Natural Titaniferous Magnetites. Miner. Mag. 31 p.624.

Walker F. 1953 Notes on the Classification of Scottish and Moravian Teschenites. Geol. Mag. LX. pp242-8.

Walker T.L. 1923 Trevorite, a Distinct Mineral Species. Univ.Toronto Stud. Geol. Ser. no. 16. p.53.

Webster A.H. and Bright N.F.H. 1961 The System Iron-Titanium-Oxygen at 1200°C and Oxygen Partial Pressures between 1 atm. and 2.10^{-14} atm. Amer. ceram.Soc.J. 44 110.

Wilkinson J.F.G. 1955 The Terms Teschenite and Crinanite. Geol.Mag. 92 pp282-9.

1957 Titanomagnetites from a Differentiated Teschenite Sill. Miner.Mag. 31 p.443.

1961 Some Aspects of the Calciferous Amphiboles, Oxyhornblende, Kaersutite and Barkevikite. Amer. Min. 46 pp340-54.

Wilson R.L. 1962 The Palaeomagnetism of Baked Contact Rocks and Reversals of the Earth's Magnetic Field. Geophys.J.astron. Soc. 7 no.2. pp194-202.

Wright J.B. 1959 Some Further Heating Experiments on Natural Titaniferous Magnetites. Miner. Mag. 32 No.244. p.32.

1961 Solid-solution Relationships in some Titaniferous Iron Oxide Ores of Basic Igneous Rocks. Miner. Mag. 32 No.253. p.718.

Wyckoff R.W.G. 1949 Electron Microscopy - Technique and Applications. Interscience Publ. N.Y.

Yoder H.S. and Tilley C.E. 1962 The Origin of Basalt Magmas: An Experimental Study of Natural and Synthetic Rock Systems. J. Pet. 3 pp.342-532.